Genome and epigenome approaches in human assisted reproduction

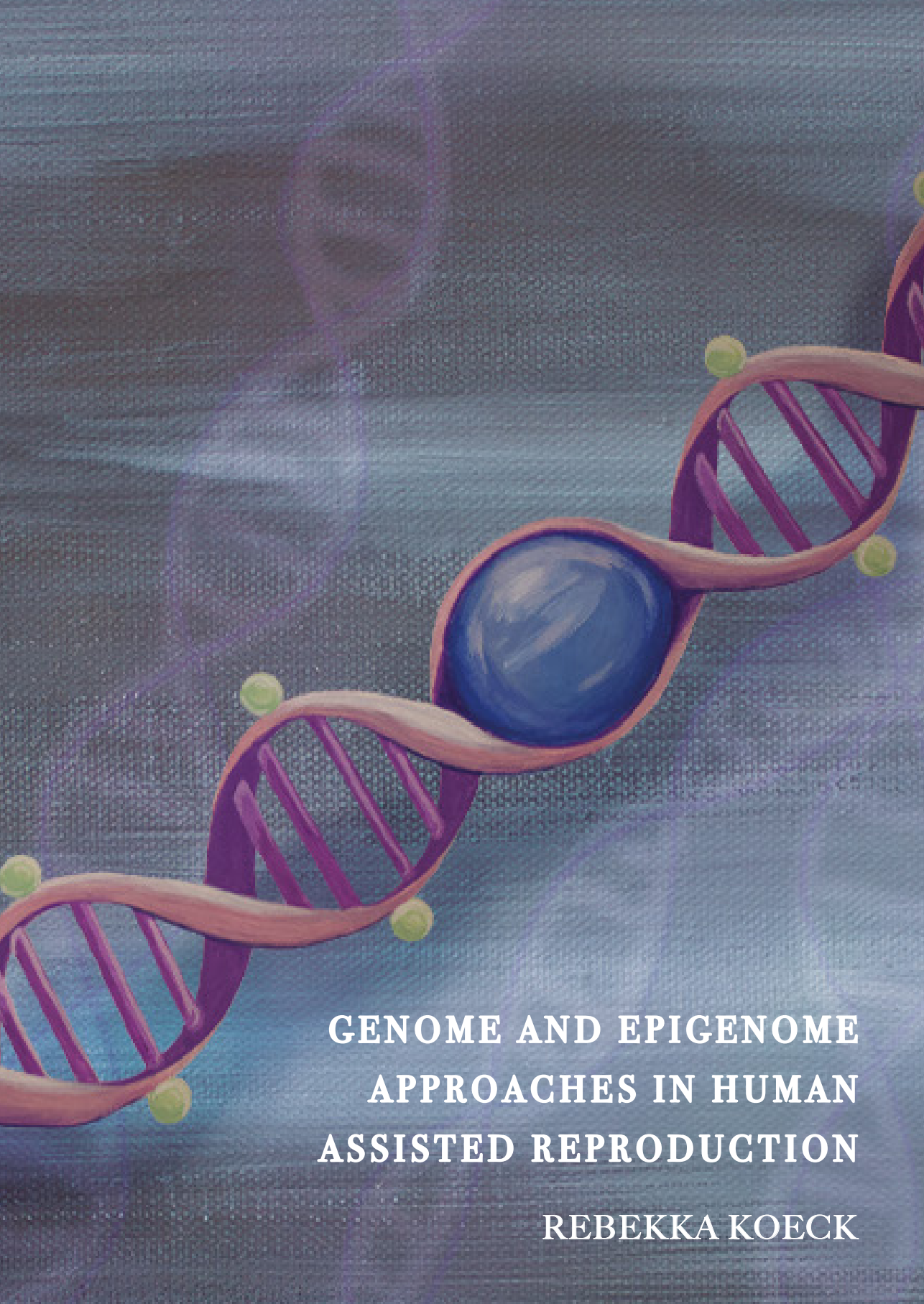

GENOME AND EPIGENOME APPROACHES IN HUMAN ASSISTED REPRODUCTION

REBEKKA KOECK

Genome and epigenome approaches in human assisted reproduction

Rebekka Maria Koeck

ISBN: 978-94-6496-051-8

Cover: Elena Barnett
Layout: Ilse Modder (www.ilsemodder.nl)
Printed by: Gildeprint Enschede (www.gildeprint.nl)

Genome and epigenome approaches in human assisted reproduction

Dissertation

to obtain the degree of Doctor at Maastricht University,
on the authority of the Rector Magnificus, Prof. dr. Pamela Habibović
in accordance with the decision of the Board of Deans,
to be defended in public on
Wednesday 13th March 2024, at 13:00 hours

by

Rebekka Maria Koeck

Supervisors:
Prof. dr. H. Brunner
Dr. ir. M. Zamani Esteki

Co-supervisors:
Dr. M. Gielen
Dr. A.P.A. van Montfoort

Assessment Committee:
Prof. dr. M. van Engeland (chair)
Dr. ir. A. Derijck (Amsterdam University Medical Center, The Netherlands)
Prof. dr. D. van den Hove
Prof. dr. D. de Neubourg (University of Antwerp, Belgium)
Dr. E. Vrij

The research presented in this thesis was conducted at GROW-School for Oncology and Reproduction, Department Genetics and Cell Biology in the Cellular Genomic Medicine group of Maastricht University.

The work presented in this thesis was made possible by the financial support of the EVA (Erfelijkheid Voortplanting & Aanleg) specialty program (pillar 1, grant no. KP111513, Maastricht University Medical Centre), NPO support from FHML (Faculty of Health, Medicine and Life Sciences, Maastricht University), March of Dimes (6-FY13-153), the stichting fertility foundation, Horizon Europe (NESTOR, grant no. 101120075, European Commission) and the Horizon 2020 innovation (ERIN, grant no. EU952516) grants.

Contents

Chapter 1	Introduction	9
Chapter 2	Methylome-wide analysis of IVF neonates that underwent embryo culture in different media revealed no significant differences	21
Chapter 3	At age 9, the methylome of assisted reproductive technology children that underwent embryo culture in different media is not significantly different on a genome-wide scale	57
Chapter 4	Embryo tracking system for high-throughput sequencing-based preimplantation genetic testing	89
Chapter 5	Clinical whole-genome sequencing-based haplarithmisis enables simple, scalable, and universal preimplantation genetic testing	109
Chapter 6	The nature and prevalence of chromosomal alterations in first-trimester spontaneous pregnancy loss	145
Chapter 7	Liquid biopsy: state of reproductive medicine and beyond	187
Chapter 8	General Discussion & Summary	215
Appendices	Nederlandse samenvatting	230
	Impact Statement	232
	Acknowledgements	236
	About the author	238
	List of manuscripts	239

Chapter 1

Introduction

In the mere 45 years since the birth of the first ever "test-tube baby" in 1978[1], assisted reproductive technologies (ART), such as *in vitro* fertilisation (IVF), have become the cornerstone of infertility treatment. Year-on-year, an increase is seen in the number of ART treatment cycles carried out and globally more than 3 million cycles are now performed annually[2,3]. In fact, in countries like the Netherlands, 2.5% of babies born today are conceived through ART[2]. These numbers reflect changes in societal attitudes towards reproduction, where advancing parental age and an increased desire for reproductive autonomy (including the desire to have a healthy child) are key principles.

Human preimplantation embryo development

The first 5 days of human embryonic development, between fertilisation and implantation, are characterised by some of the most dramatic cellular and molecular developments that occur during our lifespan (**Fig. 1**). On a cellular level, the process begins with the fusion of an oocyte and a spermatozoon to generate a zygote: a single diploid cell, containing 23 chromosomes from each of the individual gametes, encompassed in the zona pellucida (ZP)[4]. Several rapid rounds of mitotic cleavage division follow, culminating in an 8-cell embryo by the third day post-fertilisation. The morula stage is reached once these cells have compacted[4]. Further rounds of mitotic cell division follow before cavitation begins on day 4 post-fertilisation, ultimately giving rise to the structure that is known as the blastocyst[4]. At this stage, the embryonic cells have already differentiated into two distinct lineages, namely inner cell mass (ICM), which will contribute to the future fetus, and the peripheral trophectoderm (TE) cells, which will develop into the placenta[4]. Continued expansion of the blastocyst eventually causes the blastocyst to hatch from the ZP, thereby exposing the TE to endometrial epithelial cells and in turn permitting the crosstalk between the embryo and the uterus that is essential for implantation and pregnancy establishment[4].

Genome-spanning molecular transformations occur in the genome, epigenome, and transcriptome of preimplantation embryos (**Fig. 1**). Although these molecular occurrences have been relatively well described in isolation, how and to what extent they interact with each other remains poorly understood due to the scarcity of human embryos for research, and the high level of heterogeneity between and within embryos. At the very beginning of their development, human embryos are transcriptionally silent, making them exclusively reliant on maternal transcripts that were already present in the oocyte. Upon zygotic genome activation (ZGA), which is initiated at the 4 to 8 cell transition, the embryo gains the capacity to generate transcripts from its own genome and subsequently the maternal transcripts are depleted[5,6].

Figure 1 | Overview of human preimplantation embryo development and ART

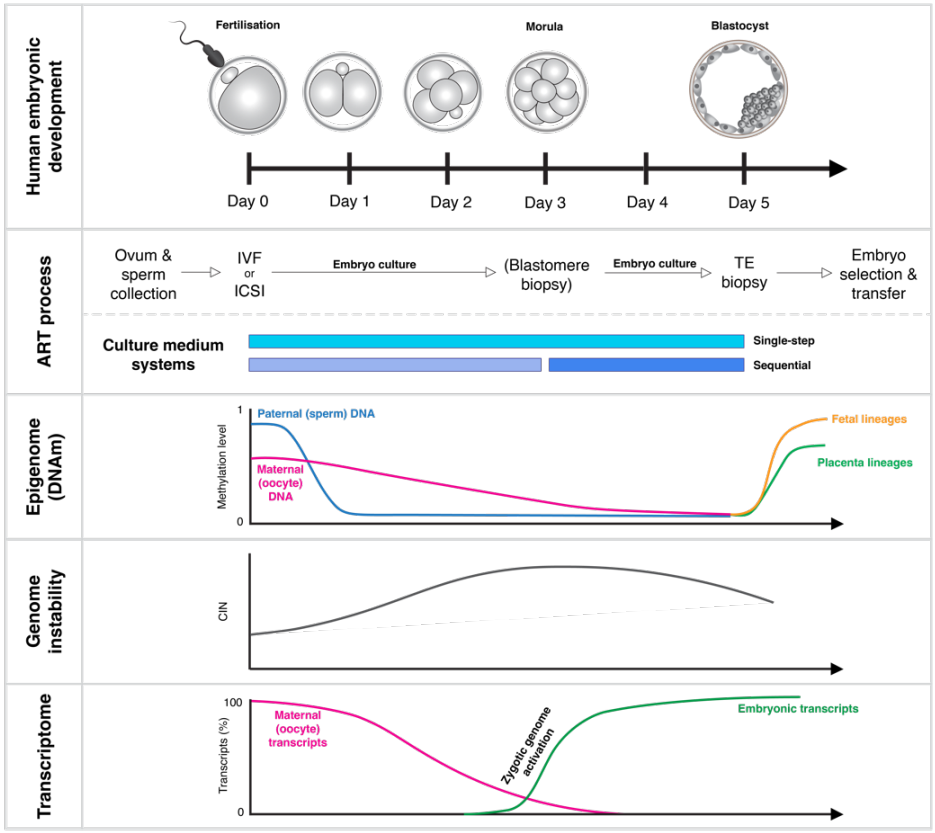

Schematic representation of the cellular and molecular changes occurring during preimplantation human embryo development and how these relate to the timing of ART procedures.
IVF = in vitro fertilisation, ICSI = intracytoplasmic sperm injection, TE = trophectoderm, DNAm = DNA methylation, CIN = chromosome instability

Concurrently, epigenetic reprogramming is occurring, involving virtually complete erasure and re-establishment of DNA methylation marks. Prior to fertilisation, the paternal genome within the spermatozoon is relatively hypermethylated compared to that of the unfertilized oocyte[7]. Fusion of the gametes triggers the extensive depletion of DNA methylation marks, which progresses more rapidly in the paternal genome so that by the 2-cell stage residual methylation of the maternal genome is already higher than that of the paternal genome[7]. Throughout the remainder of the preimplantation period the embryo exists in a relatively hypomethylated state, with re-methylation only occurring from the blastocyst stage onwards[8,9]. Re-methylation, however, is not a uniform process across all embryonic lineages; and although the differences are still small at the blastocyst stage[8], ultimately TE-derived lineages remain hypomethylated compared to

ICM-derived lineages[9,10]. DNA demethylation has been linked to chromosome instability (CIN) in oncological specimens,[11] and CIN is also commonly observed in early human embryos[12,13]. While precise estimates of the prevalence of aneuploidies in embryos at different stages vary, it is consistently described that at least half of preimplantation embryos harbour one or more aneuploid cells[9,14-16]. The majority of these aneuploidies arise during the first mitotic divisions, leading to embryos that are mosaic, i.e., containing cellular lineages with different chromosome states[14,16,17]. From approximately the third day post-fertilisation, the proportion of aneuploid cells begins to decline, allowing (partially) aneuploid embryos to develop into healthy, euploid fetuses[18]. While this demonstrates complete elimination of aneuploid cells from the fetal lineages, the occurrence of confined placental mosaicism suggests that the extraembryonic lineages are more tolerant of aneuploid cells[18-20].

ART procedures and preimplantation genetic testing

Assisted reproductive technologies are defined as treatments that involve the *in vitro* handling of oocytes or sperm cells[21] (**Fig. 1**). Most ART treatments commence with the administration of hormones to promote the maturation of multiple ovarian follicles, instead of the one that is typically matured during a natural menstrual cycle. Follicle maturation is monitored using ultrasonography to ensure that ovum pick-up is carried out at the optimal time. The retrieved oocytes are subsequently fertilised, either by being co-cultured with sperm cells or by direct injection of a single sperm into the cytoplasm of the oocyte, called intracytoplasmic sperm injection (ISCI). Subsequently, the resulting embryos are cultured *in vitro* for 3-6 days before a morphological assessment is undertaken to ascertain which embryos have good implantation potential. A single embryo is then selected for transfer to the woman's uterus, with the aim to implant and establish a viable pregnancy. Alternatively, *in vitro* generated embryos can be cryopreserved on day 5 or day 6, so that they can be transferred during subsequent natural or hormone-enhanced menstrual cycles.

Originally, ART was developed as a treatment for infertility, but the recent advances in few- and single-cell analysis methodologies have paved the way for a new application of ART, namely, to facilitate preimplantation genetic testing (PGT). PGT is offered to couples who are known to be carriers of heritable genetic mutations that have the potential to cause serious disease in their offspring. Eligible couples may be identified either because one of the potential parents is affected themselves; because they have previously had an affected child; because a condition is known to run in their family; or because they belong to a high-risk group. High risk groups include consanguineous couples or couples from any community where certain genetic abnormalities are

particularly prevalent. PGT is offered in several forms, specifically PGT for monogenic diseases (PGT-M), PGT for structural rearrangements (PGT-SR), PGT for aneuploidies (PGT-A) and PGT for mitochondrial disease (PGT-Mito). Embryonic material for genetic testing can either be retrieved by means of a single blastomere biopsy on day 3 or a 5- to 20-cell TE biopsy taken at the blastocyst stage. Depending on the indication, this material is then subjected to one of several laboratory and analysis protocols to ascertain a diagnosis. Chromosome-scale abnormalities, such as structural rearrangements and copy number variants (CNVs), i.e., PGT-A and PGT-SR, were initially analysed using targeted approaches such as fluorescence in-situ hybridisation (FISH), but are now commonly assessed using approaches such as array comparative genomic hybridization (aCGH) and shallow, approximately 1X, whole-genome next-generation sequencing (NGS)[22]. The most commonly used method for PGT-M has been short-tandem repeat (STR) marker-based PCR, which requires an individualised primer design and validation for each genetic indication[22]. This laborious method is gradually being superseded by approaches based on SNP arrays or reduced-representation genotyping by sequencing (GBS)[22-25], that facilitate genome-wide haplotyping with sophisticated methods such as Haplarithmisis[14], and therefore offer a universal solution for PGT-M indications. Despite the previously unparalleled resolution of GBS-based PGT-M, its limited genome coverage of approximately 10% means that certain indications and diagnoses remain a challenge. These include indications in centromeric or telomeric regions, indications within or adjacent to regions of loss of heterogeneity that are seen in consanguineous couples and when homologous recombination events occur in close proximity to the genetic indication.

Evaluating innovations in ART

Evaluating the impact of modifications to ART and its adjuncts on treatment outcomes is complicated by the lack of standardised reporting across studies: studies do not consistently report the same outcome measures. Some possible measures of success include (i) embryo development rate and quality scores, (ii) time to pregnancy, (iii) biochemical or clinical pregnancy rate (defined as detection of beta hCG in the blood or urine, or the presence of gestational sacs on ultrasonographic investigation, respectively), or (iv) live birth rate[21]. The latter two outcome measures could be presented per embryo that is transferred, per ART treatment cycle (which can involve transfer of more than one embryo), or cumulatively per couple across multiple treatment cycles.

One example of an innovation in ART where the choice of outcome measure has offered different insights, is in the modification of the embryo culture environment from atmospheric to physiological oxygen levels (from 20% to 5%). A meta-analysis of 21

studies assessing the impact of oxygen levels for human embryo culture only found a modest improvement in pregnancy and live birth rate (around 5%). However, the included studies did not consider the availability of good morphology blastocysts for cryopreservation, and therefore the possibility of further embryo transfers from the same oocyte aspiration cycle[26]. When this was taken into account, it was found that the number of embryos suitable for cryopreservation and the cumulative live birth rate for the aspiration cycle was significantly higher in the 5% oxygen group[27].

The embryo culture environment is further modifiable by using compositionally different culture media. Broadly, two different classes of culture medium are available (**Fig. 1**). The first type are the single-step media, which support embryo growth from fertilisation up to and including the blastocyst stage. The second type are the sequential media, which require a medium change on day 3, at the time point when embryo energy substrate requirements switch from pyruvate to glucose. Although sequential media are optimised to accommodate the changing requirements of a developing embryo, they necessitate additional embryo handling which may be detrimental. Additional handling may be detrimental through increasing the exposure to light and pipetting shear force, as well as exposure to potential temperature and oxygen level fluctuations caused when removing embryos from the incubator. In 2010, the first study emerged reporting that the choice of culture medium is indeed an important consideration and has the capacity to affect treatment outcomes[28]. Since then, several pairs of compositionally different culture media have been compared. However, cross-study comparisons are not possible as no two studies have compared the same media pairs and many of the studies are limited by sample size and study design[29]. Nonetheless, it is clear that culture medium composition has the capacity to affect ART treatment parameters including the quantity and quality of the generated embryos, implantation, pregnancy and live birth rates, as well as the growth of the resultant children both during the prenatal period and throughout childhood[29-34]. In line with the developmental origins of health and disease (DoHAD) hypothesis[35], the observed (birth) weight differences may be relevant for the continuing health of these children, especially when considering cardiometabolic outcomes[36,37]. Whether this is the case remains to be seen over the course of the next 50 or more years, as ART offspring reach the age where cardiometabolic diseases commonly present.

Another adjunct to ART procedures, introduced with the aim of improving success rates, was the routine application of PGT-A to ascertain mosaicism level, since aneuploidy is associated with both developmental arrest of preimplantation embryos[38,39] and early miscarriage[40]. However, the suitability of this approach relies on several contested assumptions. Firstly, that the abnormalities identified in embryos that are subsequently discarded are not compatible with pregnancy establishment or the birth of a healthy,

euploid child. While it has been shown that higher levels of mosaicism are associated with lower implantation and pregnancy rates, it has also been shown that mosaic embryos can establish pregnancies where the fetus is healthy and euploid[41,42]. Secondly, the TE biopsy from which the mosaicism level is determined should be representative of the whole embryo, and most importantly the fetal lineages. Evidence to the contrary comes from both animal and human studies, which show that aneuploid cells are eliminated from the fetal lineages by apoptosis, while this is not the case in placental lineages[18,43]. Instead, aneuploid cells can persist in the placental lineages, giving rise to confined placental mosaicism[19]. For these reasons, the validity of PGT-A for embryo selection is highly contested[44]. While large scale clinical trials and systematic reviews have found that using PGT-A to prioritise transfer of low-level mosaic or euploid embryos may reduce the time to pregnancy and miscarriage rate, it ultimately has not improved cumulative live birth rates in the general ART population and may lead to embryos with pregnancy potential being discarded[45-48]. For this reason, countries like the Netherlands have opted not to routinely apply PGT-A to determine mosaicism level.

Despite these ART modifications, data from European IVF centres show that for the last 10 years the live birth rate per embryo transferred has plateaued at approximately 25%[2]. As such, further research is crucial to better understand the impacts of past modifications so that these can guide future advances.

Aims and outline of the thesis

Furthering our understanding of genome and epigenome dynamics during early human embryogenesis may provide novel insights that allow us to further optimise ART procedures and embryo selection, thereby improving ART success rates. Additionally, state-of-the art omics principles should continually be integrated into and developed for the laboratory and bioinformatic PGT workflow, to facilitate embryonic genome characterisation and to ensure that PGT is reliable and readily accessible.

To achieve these aims, the following objectives have been addressed:

1. Examine how the use of different embryo culture media affects the methylomes of the resulting children, at multiple timepoints.
2. Develop and validate several novel laboratory and bioinformatic approaches for NGS-based PGT that improve reliability, scalability, and generalisability.
3. Explore the possibilities for future innovations in prenatal genetic testing.

In **chapters 2 and 3** we examine the impact of using compositionally different ART culture media on the methylomes of the resulting children (neonates and 9-year-olds). Clinical trials showed that the use of the four media in question affected both ART treatment outcomes and the growth of the resultant children, however the underlying mechanism of this relationship remains undetermined. A better understanding of the interplay between the *in vitro* environment and embryos would be beneficial to further optimise ART culture systems.

In **chapters 4 and 5** we describe the implementation and validation of improvements to current genetic testing methods based on embryo biopsy. In **chapter 4** we develop unique barcoded oligonucleotides for sample tracking that are compatible with genotyping-by-sequencing (GBS) workflows. We demonstrate that they can be safely implemented to reduce the reliance on the 4-eye principle and to prevent misdiagnoses related to sample switching or sample contamination while preserving the quality of the generated diagnostic data. In **chapter 5** we describe the first PGT approach based on whole genome sequencing (WGS). We portray how WGS-PGT facilitates a one-size-fits-all approach to PGT that can be used for not only all forms of PGT, (i) PGT-M, (ii) PGT-SR, (iii) PGT-A (with origin), but also for PGT for mitochondrial indications.

In **chapter 6** we characterize the chromosomal landscape of early miscarriages in different embryonic tissues by applying Haplarithmisis, on a genome-wide scale. From this work we have gained an in-depth insight into the contribution of chromosome copy-number abnormalities to sporadic and recurrent pregnancy loss, which has implications for the clinical management of pregnancy loss, as well as the interpretation of PGT-A findings.

In **chapter 7** we explore the future possibilities for prenatal genetic testing. We summarise the available methods for liquid biopsy-based diagnostics and their current applications in reproductive medicine. Furthermore, we contemplate how current methodological limitations could be overcome and hypothesise how the full potential of these methods might be harnessed for pre-implantation and prenatal genetic testing in the future.

References

1 Steptoe, P. C. & Edwards, R. G. Birth after the reimplantation of a human embryo. *Lancet* **2**, 366 (1978). https://doi.org:10.1016/s0140-6736(78)92957-4

2 Wyns, C. *et al.* ART in Europe, 2018: results generated from European registries by ESHRE. *Hum Reprod Open* **2022**, hoac022 (2022). https://doi.org:10.1093/hropen/hoac022

3 Adamson, G. D. *et al.* ICMART preliminary world report 2015. *Hum Reprod* **34** (2019). <https://academic.oup.com/humrep/article/34/Supplement_1/i1/5528444>.

4 Firmin, J. & Maître, J. L. Morphogenesis of the human preimplantation embryo: bringing mechanics to the clinics. *Semin Cell Dev Biol* **120**, 22-31 (2021). https://doi.org:10.1016/j.semcdb.2021.07.005

5 Petropoulos, S. *et al.* Single-Cell RNA-Seq Reveals Lineage and X Chromosome Dynamics in Human Preimplantation Embryos. *Cell* **167**, 285 (2016). https://doi.org:10.1016/j.cell.2016.08.009

6 Asami, M. *et al.* Human embryonic genome activation initiates at the one-cell stage. *Cell Stem Cell* **29**, 209-216.e204 (2022). https://doi.org:10.1016/j.stem.2021.11.012

7 Li, L. *et al.* Single-cell multi-omics sequencing of human early embryos. *Nat Cell Biol* **20**, 847-858 (2018). https://doi.org:10.1038/s41556-018-0123-2

8 Guo, H. *et al.* The DNA methylation landscape of human early embryos. *Nature* **511**, 606-610 (2014). https://doi.org:10.1038/nature13544

9 Zhu, P. *et al.* Single-cell DNA methylome sequencing of human preimplantation embryos. *Nat Genet* **50**, 12-19 (2018). https://doi.org:10.1038/s41588-017-0007-6

10 Yuan, V. *et al.* Cell-specific characterization of the placental methylome. *BMC Genomics* **22**, 6 (2021). https://doi.org:10.1186/s12864-020-07186-6

11 Rodriguez, J. *et al.* Chromosomal instability correlates with genome-wide DNA demethylation in human primary colorectal cancers. *Cancer Res* **66**, 8462-9468 (2006). https://doi.org:10.1158/0008-5472.Can-06-0293

12 Angell, R. R., Aitken, R. J., van Look, P. F., Lumsden, M. A. & Templeton, A. A. Chromosome abnormalities in human embryos after in vitro fertilization. *Nature* **303**, 336-338 (1983). https://doi.org:10.1038/303336a0

13 Vanneste, E. *et al.* Chromosome instability is common in human cleavage-stage embryos. *Nat Med* **15**, 577-583 (2009). https://doi.org:10.1038/nm.1924

14 Zamani Esteki, M. *et al.* Concurrent whole-genome haplotyping and copy-number profiling of single cells. *Am J Hum Genet* **96**, 894-912 (2015). https://doi.org:10.1016/j.ajhg.2015.04.011

15 Zhou, F. *et al.* Reconstituting the transcriptome and DNA methylome landscapes of human implantation. *Nature* **572**, 660-664 (2019). https://doi.org:10.1038/s41586-019-1500-0

16 Starostik, M. R., Sosina, O. A. & McCoy, R. C. Single-cell analysis of human embryos reveals diverse patterns of aneuploidy and mosaicism. *Genome Res* **30**, 814-825 (2020). https://doi.org:10.1101/gr.262774.120

17 Delhanty, J. D. *et al.* Detection of aneuploidy and chromosomal mosaicism in human embryos during preimplantation sex determination by fluorescent in situ hybridisation, (FISH). *Hum Mol Genet* **2**, 1183-1185 (1993). https://doi.org:10.1093/hmg/2.8.1183

18 Yang, M. *et al.* Depletion of aneuploid cells in human embryos and gastruloids. *Nat Cell Biol* **23**, 314-321 (2021). https://doi.org:10.1038/s41556-021-00660-7

19 Eggenhuizen, G. M., Go, A., Koster, M. P. H., Baart, E. B. & Galjaard, R. J. Confined placental mosaicism and the association with pregnancy outcome and fetal growth: a review of the literature. *Hum Reprod Update* **27**, 885-903 (2021). https://doi.org:10.1093/humupd/dmab009

20 Zamani Esteki, M. *et al.* In vitro fertilization does not increase the incidence of de novo copy number alterations in fetal and placental lineages. *Nat Med* **25**, 1699-1705 (2019). https://doi.org:10.1038/s41591-019-0620-2

21 Zegers-Hochschild, F. *et al.* The International Glossary on Infertility and Fertility Care, 2017. *Hum Reprod* **32**, 1786-1801 (2017). https://doi.org:10.1093/humrep/dex234

22 van Montfoort, A. *et al.* ESHRE PGT Consortium data collection XIX-XX: PGT analyses from 2016 to 2017. *Hum Reprod Open* **2021**, hoab024 (2021). https://doi.org:10.1093/hropen/hoab024

23 Masset, H. *et al.* Multi-centre evaluation of a comprehensive preimplantation genetic test through haplotyping-by-sequencing. *Hum Reprod* **34**, 1608-1619 (2019). https://doi.org:10.1093/humrep/dez106

24 De Witte, L. *et al.* GENType: all-in-one preimplantation genetic testing by pedigree haplotyping and copy number profiling suitable for third-party reproduction. *Hum Reprod* **37**, 1678-1691 (2022). https://doi.org:10.1093/humrep/deac088

25 Masset, H. *et al.* Single-cell genome-wide concurrent haplotyping and copy-number profiling through

genotyping-by-sequencing. *Nucleic Acids Res* **50**, e63 (2022). https://doi.org:10.1093/nar/gkac134

26 Nastri, C. O. *et al.* Low versus atmospheric oxygen tension for embryo culture in assisted reproduction: a systematic review and meta-analysis. *Fertil Steril* **106**, 95-104.e117 (2016). https://doi.org:10.1016/j.fertnstert.2016.02.037

27 Van Montfoort, A. P. A. *et al.* Reduced oxygen concentration during human IVF culture improves embryo utilization and cumulative pregnancy rates per cycle. *Hum Reprod Open* **2020**, hoz036 (2020). https://doi.org:10.1093/hropen/hoz036

28 Dumoulin, J. C. *et al.* Effect of in vitro culture of human embryos on birthweight of newborns. *Hum Reprod* **25**, 605-612 (2010). https://doi.org:10.1093/humrep/dep456

29 Youssef, M. M. *et al.* Culture media for human pre-implantation embryos in assisted reproductive technology cycles. *Cochrane Database Syst Rev*, Cd007876 (2015). https://doi.org:10.1002/14651858.CD007876.pub2

30 Kleijkers, S. H. *et al.* IVF culture medium affects post-natal weight in humans during the first 2 years of life. *Hum Reprod* **29**, 661-669 (2014). https://doi.org:10.1093/humrep/deu025

31 Nelissen, E. C. *et al.* IVF culture medium affects human intrauterine growth as early as the second trimester of pregnancy. *Hum Reprod* **28**, 2067-2074 (2013). https://doi.org:10.1093/humrep/det131

32 Kleijkers, S. H. *et al.* Influence of embryo culture medium (G5 and HTF) on pregnancy and perinatal outcome after IVF: a multicenter RCT. *Hum Reprod* **31**, 2219-2230 (2016). https://doi.org:10.1093/humrep/dew156

33 Zandstra, H., Van Montfoort, A. P. & Dumoulin, J. C. Does the type of culture medium used influence birthweight of children born after IVF? *Hum Reprod* **30**, 530-542 (2015). https://doi.org:10.1093/humrep/deu346

34 Zandstra, H. *et al.* Association of culture medium with growth, weight and cardiovascular development of IVF children at the age of 9 years. *Hum Reprod* **33**, 1645-1656 (2018). https://doi.org:10.1093/humrep/dey246

35 Barker, D. J. & Osmond, C. Infant mortality, childhood nutrition, and ischaemic heart disease in England and Wales. *Lancet* **1**, 1077-1081 (1986). https://doi.org:10.1016/s0140-6736(86)91340-1

36 Wadhwa, P. D., Buss, C., Entringer, S. & Swanson, J. M. Developmental origins of health and disease: brief history of the approach and current focus on epigenetic mechanisms. *Semin Reprod Med* **27**, 358-368 (2009). https://doi.org:10.1055/s-0029-1237424

37 Roseboom, T. J. Developmental plasticity and its relevance to assisted human reproduction. *Hum Reprod* **33**, 546-552 (2018). https://doi.org:10.1093/humrep/dey034

38 Qi, S. T., Liang, L. F., Xian, Y. X., Liu, J. Q. & Wang, W. Arrested human embryos are more likely to have abnormal chromosomes than developing embryos from women of advanced maternal age. *J Ovarian Res* **7**, 65 (2014). https://doi.org:10.1186/1757-2215-7-65

39 Maurer, M. *et al.* Chromosomal Aneuploidies and Early Embryonic Developmental Arrest. *Int J Fertil Steril* **9**, 346-353 (2015). https://doi.org:10.22074/ijfs.2015.4550

40 Popescu-Hobeanu, G. *et al.* Cytogenetic Analysis of Sporadic First-Trimester Miscarriage Specimens Using Karyotyping and QF-PCR: A Retrospective Romanian Cohort Study. *Genes (Basel)* **13** (2022). https://doi.org:10.3390/genes13122246

41 Zhang, Y. X. *et al.* The Pregnancy Outcome of Mosaic Embryo Transfer: A Prospective Multicenter Study and Meta-Analysis. *Genes (Basel)* **11** (2020). https://doi.org:10.3390/genes11090973

42 Greco, E., Minasi, M. G. & Fiorentino, F. Healthy Babies after Intrauterine Transfer of Mosaic Aneuploid Blastocysts. *N Engl J Med* **373**, 2089-2090 (2015). https://doi.org:10.1056/NEJMc1500421

43 Bolton, H. *et al.* Mouse model of chromosome mosaicism reveals lineage-specific depletion of aneuploid cells and normal developmental potential. *Nat Commun* **7**, 11165 (2016). https://doi.org:10.1038/ncomms11165

44 Mastenbroek, S., de Wert, G. & Adashi, E. Y. The Imperative of Responsible Innovation in Reproductive Medicine. *N Engl J Med* **385**, 2096-2100 (2021). https://doi.org:10.1056/NEJMsb2101718

45 Simopoulou, M. *et al.* PGT-A: who and when? A systematic review and network meta-analysis of RCTs. *J Assist Reprod Genet* **38**, 1939-1957 (2021). https://doi.org:10.1007/s10815-021-02227-9

46 Cornelisse, S. *et al.* Preimplantation genetic testing for aneuploidies (abnormal number of chromosomes) in in vitro fertilisation. *Cochrane Database Syst Rev* **9**, CD005291 (2020). https://doi.org:10.1002/14651858.CD005291.pub3

47 Mastenbroek, S. *et al.* In vitro fertilization with preimplantation genetic screening. *N Engl J Med* **357**, 9-17 (2007). https://doi.org:10.1056/NEJMoa067744

48 Yan, J. *et al.* Live Birth with or without Preimplantation Genetic Testing for Aneuploidy. *N Engl J Med* **385**, 2047-2058 (2021). https://doi.org:10.1056/NEJMoa2103613

Chapter 2

Methylome-wide analysis of IVF neonates that underwent embryo culture in different media revealed no significant differences

---

Rebekka M. Koeck, Florence Busato, Jorg Tost, Dimitri Consten, Jannie van Echten-Arends, Sebastiaan Mastenbroek, Yvonne Wurth, Sylvie Remy, Sabine Langie, Tim S. Nawrot, Michelle Plusquin, Rossella Alfano, Esmée M. Bijnens, Marij Gielen, Ron van Golde, John C. M. Dumoulin, Han Brunner, Aafke P. A. van Montfoort*, Masoud Zamani Esteki*

*** Joint last authors**

My contribution: all data processing, analysis, and visualisation as well as writing and editing the full text.

Adapted from R.M. Koeck, F. Busato, J. Tost, D. Consten, J. van Echten-Arends, S. Mastenbroek, Y. Wurth, S. Remy, S. Langie, T.S. Nawrot, M. Plusquin, R. Alfano, E.M. Bijnens, M. Gielen, R. van Golde, J.C.M. Dumoulin, H. Brunner, A.P. A. van Montfoort, M. Zamani Esteki. Methylome-wide analysis of IVF neonates that underwent embryo culture in different media revealed no significant differences. NPJ Genom Med. (2022) 7(1):39. https://doi.org/10.1038/s41525-022-00310-3

Abstract

A growing number of children born are conceived through in vitro fertilisation (IVF), which has been linked to an increased risk of adverse perinatal outcomes, as well as altered growth profiles and cardiometabolic differences in the resultant individuals. Some of these outcomes have also been shown to be influenced by the use of different IVF culture media and this effect is hypothesised to be mediated epigenetically, e.g. through the methylome. As such, we profiled the umbilical cord blood methylome of IVF neonates that underwent preimplantation embryo development in two different IVF culture media (G5 or HTF), using the Infinium Human Methylation EPIC BeadChip. We found no significant methylation differences between the two groups in terms of: (i) systematic differences at CpG sites or regions, (ii) imprinted sites/genes or birth weight-associated sites, (iii) stochastic differences presenting as DNA methylation outliers or differentially variable sites, and (iv) epigenetic gestational age acceleration.

Introduction

Since its first successful implementation in 1978, more than 8 million children[1] (~3% of all births in European countries) have been conceived through in vitro fertilisation (IVF)[2]. Although most of these children are born seemingly healthy, assisted reproductive technology (ART) singletons are at increased risk of adverse perinatal[3] and childhood[4,5] outcomes as compared to their naturally conceived counterparts. For instance, IVF neonates are at higher risk of preterm birth (<37 weeks, relative risk (RR) 1.4–2.0), low birth weight (<2500 g, RR 1.6–1.7), being small for gestational age (RR 1.5) and perinatal mortality (RR 1.7–2.0)[3]. Later life outcomes mainly relate to growth and weight, as well as disturbed cardiometabolic function, demonstrated by increased systolic blood pressure, suboptimal diastolic function, lower low-density lipoprotein and higher fasting insulin levels[4-6].

The IVF process involves 2–6 days of in vitro embryo culture, during which embryos are exposed to an artificial environment that is influenced by the culture medium, atmospheric conditions (oxygen levels) and laboratory plastics. Over the years, a variety of culture media have been used[7-11], which have been shown to affect short- and long-term health outcomes of the resultant offspring in both animal and human studies. In human studies culture medium composition has been linked to differences in birth weight[12-14], postnatal weight[15,16] and the childhood developmental profile[17]. Previously, we conducted a multi-centre randomised controlled trial (RCT) among six Dutch IVF centres to compare the effect of G5 (Vitrolife) and HTF (Lonza) media on pregnancy and neonatal outcomes. Of note is that the G5 medium contains amino acids[9,18], while HTF does not. While it was found that G5 led to lower fertilisation rates, it generated more embryos that were suitable for transfer and had a higher implantation rate, leading to a higher cumulative live birth rate[14]. At birth, G5 neonates were more likely to be born prematurely and with lower birth weights[14] even when birth weight was corrected for gestational age, indicating an additional effect of the culture medium on birth weight.

Although no causative mechanism for these differences in outcome has been established, the findings are consistent with the Developmental Origins of Health and Disease (DOHaD) paradigm. This paradigm suggests that adversity during early life, such as during the peri-conception period, makes the resultant offspring more vulnerable to disease in later life[19] and this effect may be mediated by the epigenome, and specifically DNA methylation[20]. In the context of IVF, the handling of gametes and embryos and exposure to the in vitro environment or the hormone-primed uterus represent environmental exposures that could contribute to the observed disease susceptibility[21]. Further evidence for the involvement of DNA methylation is that epigenetically regulated imprinting disorders, although still rare, are more common

after IVF[22]. Moreover, the period of in vitro embryo culture of IVF procedures coincides with the process of epigenetic reprogramming, during which DNA methylation marks are almost completely erased and re-established[23,24]. This process has been shown to be responsive to environmental cues[24].

Relatively few studies have used molecular assays to assess the effects of different IVF culture media on the resultant embryos and neonates. For instance, the methylome of IVF neonates from a culture medium trial has only been investigated in one prior study. As a follow-up to the aforementioned G5 versus HTF RCT, placental DNA methylation at selected imprinting control regions was compared in resultant singletons finding no significant differences within these regions[25]. In contrast, most other work so far has focused on comparing the placenta or umbilical cord blood (UCB) methylome of IVF neonates in general to their naturally conceived counterparts[26-32]. These studies were recently summarised in a systematic review and meta-analysis[30] which described that most sites or regions identified to be differentially methylated were inconsistent or contradictory between studies, likely due to differences in the methylome analysis methods, heterogeneity within the cohorts and due to sample size. The majority of included studies used targeted approaches to look at imprinting genes, and a meta-analysis of such studies conducted on the placenta and UCB samples revealed only significant differential methylation at the *PEG1/MEST* imprinting gene locus[30]. Methylation at the imprinted regions *KvDMR1*, *H19* CTCF3 and CTCF6 and *SNRPN* may also be perturbed in IVF placentas, but these did not reach statistical significance in the meta-analysis[30]. The epigenetic deregulation in these cases is thought to occur post-fertilisation as it involves both paternally and maternally methylated regions and the methylation levels differ only by a few percent, indicating that the loss or gain of methylation only affects a minority of alleles. The findings from genome-wide methylation studies on these tissues have been contradictory, with some studies identifying differential methylation, predominantly with small differences, and others not[29-31]. Interestingly, some studies report increased variation in DNA methylation in IVF offspring[28,29], suggesting a stochastic rather than a systematic universal effect of IVF on the methylome. This is substantiated by the reported increased rate of so-called methylation outliers (i.e. samples with an outlying methylation value at a given site or region) in the IVF group[25]. The contribution of different culture media to systematic or stochastic methylome differences on a genome-wide scale remains undetermined.

In this study, we investigated the effect of different IVF culture media on the DNA methylation of human IVF neonates on a genome-wide scale. To this end, we profiled the UCB methylome of IVF neonates that underwent embryo culture in G5 or HTF medium as part of a RCT. Additionally, the methylome profiles of this IVF cohort are compared to data from two reference birth cohorts of naturally conceived individuals (**Fig. 1a**).

Results

In the present study, we investigated genome-wide DNA methylation patterns of DNA samples derived from UCB collected at birth from 114 IVF neonates that had undergone embryo culture in G5 or HTF medium. 106 of the UCB samples ($n = 59$ G5, $n = 47$ HTF) yielded sufficient DNA for DNA methylation profiling using the EPIC array (**Fig. 1a**). Maternal characteristics, IVF treatment parameters and neonatal outcomes were comparable between the culture medium groups. In the G5 group, although not statistically significant, a higher percentage of pregnancies were complicated by hypertension and pre-eclampsia than in the HTF group (hypertension—14 vs. 6%, pre-eclampsia 7 vs. 2% for G5 and HTF pregnancies respectively). Delivery by caesarean section was lower (12%) in the G5 group compared to the HTF group (23%) (**Table 1** and **Supplementary Table 1**).

All of the 106 samples that underwent DNA methylation analysis by EPIC array met our QC criteria (Methods). One sample from the G5 group was excluded from our analyses based on a mismatch between the recorded and predicted sex (**Fig. 2a**). Of the approximately 850,000 CpG sites represented on the EPIC array, we retained 696,205 sites for our analyses and 689,139 of these represented complete observations with no missing values in any samples.

Global analysis of DNA methylation

Principal component analysis (PCA) did not reveal any separation of the culture medium groups within the first eight principal components (PCs) (**Figs. 1b, 2c**) that explain a total of 46.7% of the variance within our data (**Supplementary Table 2**), indicating that the culture media are not the main contributors to the variance of our data. Instead, the first eight PCs were significantly associated with sample characteristics including sex (PCs 5 and 8), gestational age (PC7), sample plate (PCs 1, 2, 4 and 6) as well as cellular composition of the samples (PCs 1–7) (**Fig. 2b, c**). Therefore, we corrected for these technical factors in our subsequent analyses, alongside potential confounders (sex, gestational age, maternal age, treatment centre and pregnancy complications) that were chosen a priori based on literature and expert opinion. The distribution of all beta values (all sites in all samples) was also similar between the culture medium groups (**Fig. 1d**).

Figure 1 | Genome-wide DNA methylation analysis of IVF neonates that underwent embryo culture in different media revealed no significant differences

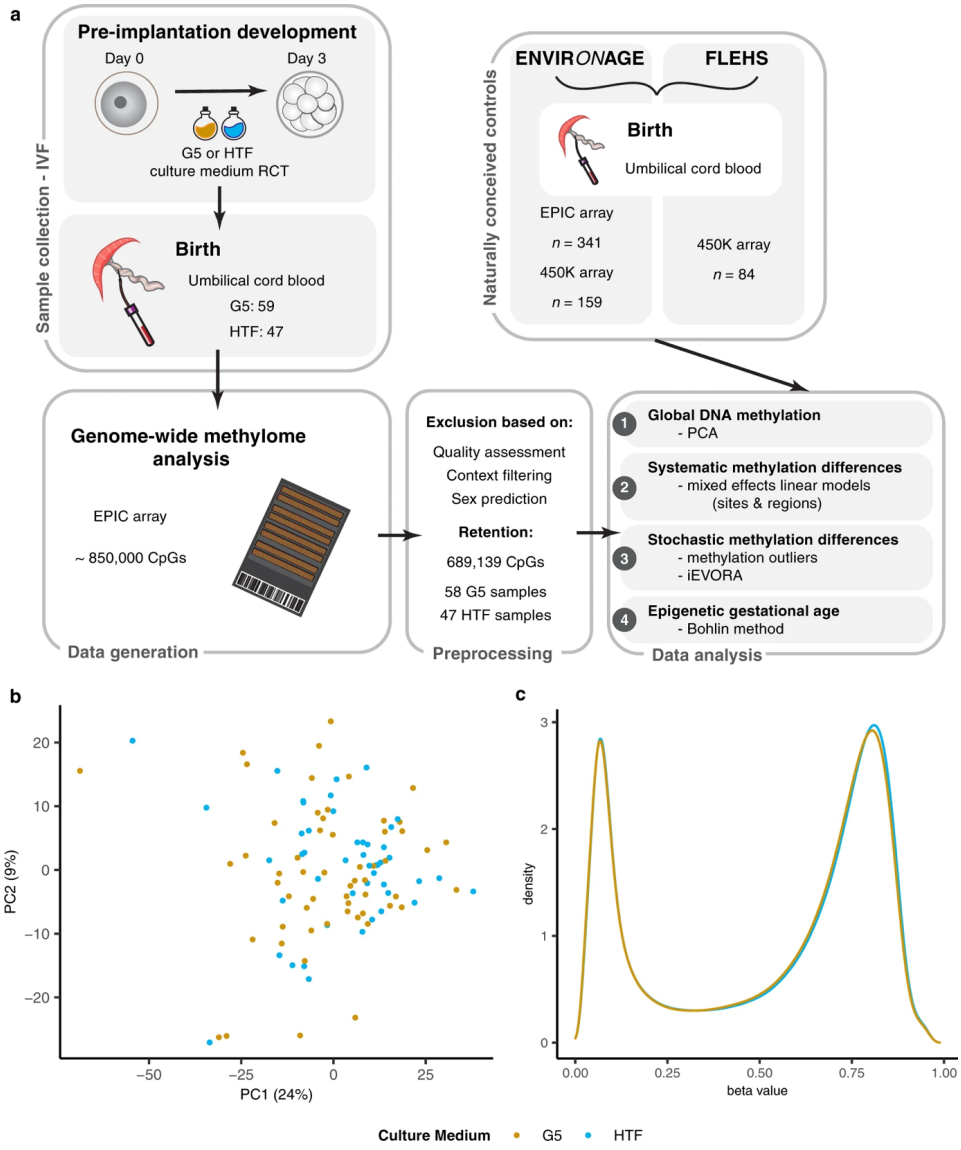

a *Schematic overview showing sample collection from IVF neonates from the G5 versus HTF RCT as well as the inclusion of naturally conceived neonates, genome-wide DNA methylation data generation, data processing and analyses included in this study.* ***b*** *PCA of all CpG sites passing our QC criteria in data from UCB samples of IVF neonates that underwent embryo culture in G5 (gold) or HTF (blue) medium.* ***c*** *Density plot showing the distribution of beta values from all sites and samples within each group (G5 = gold, HTF = blue).*

Table 1 | Maternal and neonatal characteristics (see also Supplementary Table 1)

Characteristic	Culture medium		*P* value
	G5 (*n* = 59)	HTF (*n* = 47)	
Maternal characteristics			
Age (years)	33.2 ± 3.6	33.1 ± 3.6	0.861
Nulliparous	43 (73)	35 (74)	1.000
Smoking before pregnancy (yes)	10 (17)	10 (21)	0.752
Smoking during pregnancy (yes)	2 (3)	3 (6)	0.794
Fertility treatment			
Indication for fertility treatment			0.630
Unexplained	8	8	
Female factor	14	8	
Male factor	35	31	
Treatment type			1.000
IVF	19 (33)	16 (34)	
ICSI	38 (67)	31 (66)	
Pregnancy characteristics			
Pregnancy complication			
Diabetes	2 (3)	1 (2)	1.000
Hypertension	8 (14)	3 (6)	0.362
Pre-eclampsia	4 (7)	1 (2)	0.496
Delivery by caesarean section	7 (12)	11 (23)	0.220
Neonatal outcomes			
Sex (female)	29 (49)	26 (55)	0.663
Gestational age at birth (weeks)	39.7 ± 1.2	39.3 ± 1.3	0.127
Birth weight (g)	3404.9 ± 459.7	3449.1 ± 432.5	0.672

Continuous variables are shown as mean ± SD and categorical variables are shown as n (%). Maternal age at the time of ovum pick-up is shown. ICSI = intracytoplasmic sperm injection.

Analysis of DNA methylation at individual CpG sites

Next, we investigated associations between the culture medium and DNA methylation at single CpG sites in an epigenome-wide analysis (EWAS) using linear mixed-effects models (**Methods**). Less than 0.01% of sites (37 sites in total) had a group mean difference of more than 10%, with the most extreme difference being 23.6%. After correcting for multiple testing, no statistically significant differentially methylated positions (DMPs) were found between the two culture medium groups (**Fig. 3a, b**). As pregnancy complications, such as gestational diabetes and pre-eclampsia, could affect or be affected by the methylome, we conducted the analyses twice, once with pregnancy complications included as a binary variable (yes/no) and once where all samples from complicated pregnancies ($n = 18$) were excluded. The results from this analysis were comparable to those of the first analysis (**Supplementary Fig. 1**).

Figure 2 | Preprocessing of umbilical cord blood (UCB) methylome data

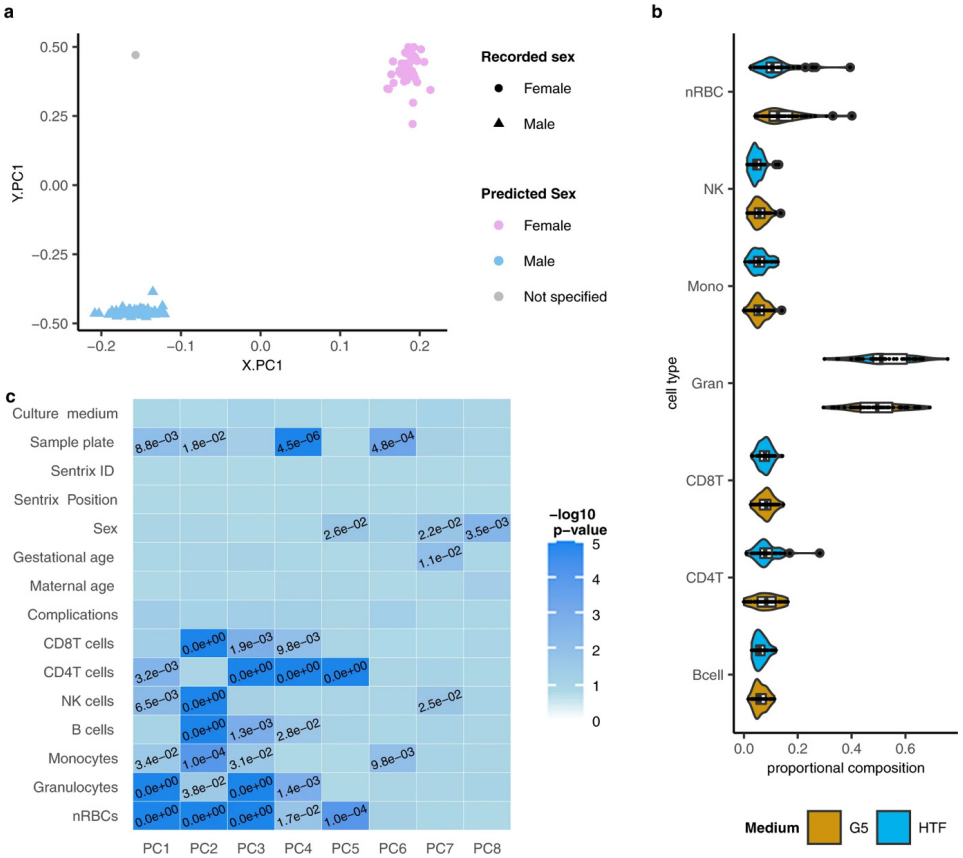

a *Scatter plot showing the projection of UCB samples (n = 105) into the PC space generated using reference data for sex prediction. The shape of the dots represents the recorded sex of the participants (circles = female, triangle = male), while the colour shows the predicted sex based on results from sEST (blue = male, pink = female, grey = not specified).* ***b*** *Violin plot showing the predicted cellular composition of the UCB samples, split by culture medium group (gold and blue represent G5 and HTF medium respectively). The violin plots are overlaid with boxplots where the horizontal lines represent the 25th percentile, median and 75th percentile respectively while the whiskers extend to the farthest data points that are no more than 1.5 times the IQR from the upper or lower quartile.* ***c*** *Heatmap showing associations between the principal components and biological/technical aspects of the samples. The colour gradient represents the –log10 of the p values. P values < 0.05 are shown. Significance of the correlation between age, maternal age, CD8-T cells, CD4T cells, NK cells, B cells, monocytes, granulocytes and nRBCs and the 8 PCs was tested using a permutation test with 10,000 permutations. The associations of the PCs with variables creating 2 groups (sample plate, sex, culture medium, pregnancy complication) and those creating three or more groups (Sentrix ID, Sentrix position) were tested using two-sided Wilcoxon rank tests and Kruskal–Wallis one-way analysis of variance respectively.*

To reduce the number of comparisons, we also chose to repeat the analyses with sites of potential interest only, namely sites within imprinted genes[33] and sites previously associated with birth weight[34]. After the data were pre-processed, 8726 sites within

imprinted genes were tested. The maximum group mean difference amongst the imprinted sites was 6.9% (**Fig. 3a**). None of the sites were found to be significantly differentially methylated between the culture medium groups. Of the 914 CpG sites consistently found to be associated with birth weight in the meta-analysis by Küpers et al.[34], 749 passed our quality control (QC) criteria and were included in the analysis. Amongst these sites, the maximal group mean difference was 3.0% and we did not find any of them to be statistically differentially methylated (**Fig. 3b**). Excluding the samples from complicated pregnancies did not change the result of either analysis (**Supplementary Fig. 1a, b**).

Figure 3 | Analysis of systematic methylation differences between G5 and HTF neonates: differentially methylated positions and regions

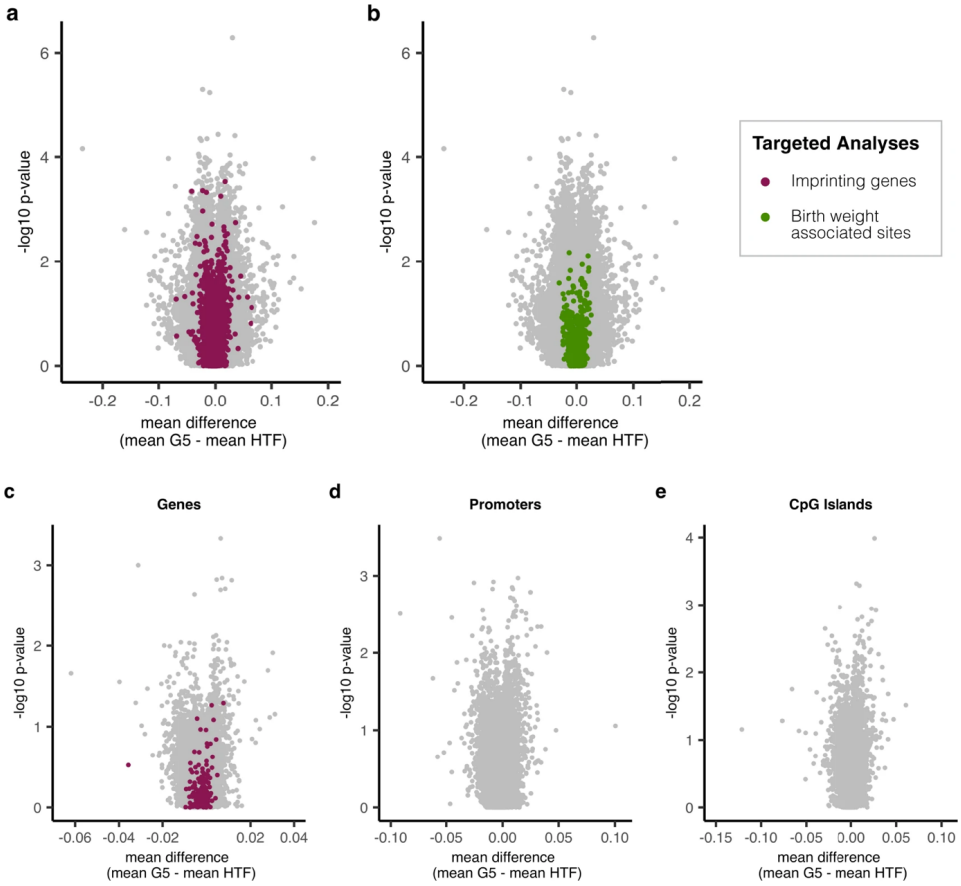

*Volcano plots showing differential methylation between G5 and HTF neonates where the grey dots represent all individual CpG sites (**a**, **b**) or multiple CpG sites aggregated into genomic regions, namely genes (**c**), promoters (**d**), CpG islands (**e**). Imprinted genes (**c**) and sites within them (**a**) are highlighted in purple while CpG sites associated with birth weight are shown in green (**b**). No significantly differentially methylation positions or regions (FDR adjusted p value < 0.1) were identified when comparing the two culture medium groups.*

Regional analysis of DNA methylation

After looking at the methylation levels of individual sites, we looked at methylation across larger genomic regions, namely whole genes, promoters, and CpG islands (CGIs). Our analyses included 28,009 genes, of which 207 were imprinted genes, 42,035 promoters and 25,238 CGIs. The maximal group mean difference of any gene was 8.1%. Imprinted genes showed even lower group mean differences than imprinted sites, with a maximal difference of 3.6%. No genes were found to be significantly differentially methylated between the G5 and HTF groups (**Fig. 3c**). The maximal group mean differences for promoters and CGIs were 10.0% and 12.1%, respectively (**Fig. 3d, e**) and no promoters or CGIs were found to be significantly differentially methylated between the culture medium groups. Excluding samples from pregnancies with complications did not affect the results (**Supplementary Fig. 2a-c**).

Differential DNA methylation variance in IVF samples

To assess the contribution of stochastic DNA methylation alterations to the observed phenotypes in our IVF cohorts, we assessed differential variance, using the iEVORA algorithm[35], and identified methylation outliers, using previously described thresholds[36], in all samples. Applying this threshold, we identified a total of 157,160 outliers within the 105 analysed samples, with a predominance of hypomethylation outliers (114,693 hypomethylation outliers and 42,467 hypermethylation outliers) (**Fig. 4**). The median number of all, both hypo- and hypermethylation, outliers in each G5 sample was 571 (567.5 IQR) and 536 (269 IQR) in each HTF sample (**Fig. 4**), which was not found to be significantly different ($p = 0.86$) between the culture medium groups. Furthermore, when considering hypomethylation and hypermethylation outliers separately, no significant difference was found between the culture medium groups. Outlier burden, the total number of outliers per sample, was not significantly associated with gestational age, birth weight or maternal age. Only technical features of our samples, including sample plate and cell composition, were significantly associated with outlier burden (**Supplementary Table 3**). An association between pregnancy complications and the total number of outliers was not tested statistically, but amongst the samples with very high numbers of outliers (above the upper quartile), only 1 was born after a pregnancy complicated by pre-eclampsia. The results were comparable when the samples taken from neonates that had experienced pregnancy complications were excluded (**Supplementary Fig. 3 and Supplementary Table 4**). When applied to the full cohort, the iEVORA algorithm identified 262 CpG sites with significantly different variances between the culture medium groups (**Supplementary Table 5, sheet 1**). Of these sites, 90% (235 sites) were more variable in the G5 group as compared to the HTF group. 202 of the 262 differentially variable CpG sites were annotated with a gene name and four genes, namely *FAM38A*, *MEF2C*, *OCA2* and *TNNT2,* each contained two differentially variable sites. Additionally, three of the differentially variable sites were located within

imprinting genes, namely *PEX10*, *MAGI2* and *OBSCN*. None of the differentially variable sites were amongst the birth weight-associated sites[37]. We then repeated the analysis excluding all participants who had experienced pregnancy complications which identified 105 differentially variable sites (**Supplementary Table 5, sheet 2**). Of these sites, 56% (50 sites) were more variable in the G5 group than the HTF group and 65 of the sites were the same as those identified in the analysis where all the participants were included. Seventy-nine of the sites were annotated with a gene name and multiple differentially variable sites were identified in two of the genes, namely two sites within the *TNNT2* gene and three sites within the *MOV10L1* gene. Furthermore, one site was found to be differentially variable in the imprinted gene *PEX10* and none of the identified sites were birth weight-associated sites. GO and KEGG enrichment analyses of the differentially variable sites identified by iEVORA did not identify any significantly enriched ontologies or pathways after multiple testing corrections (**Supplementary Table 5, sheets 4–7**).

Figure 4 | Methylation outliers

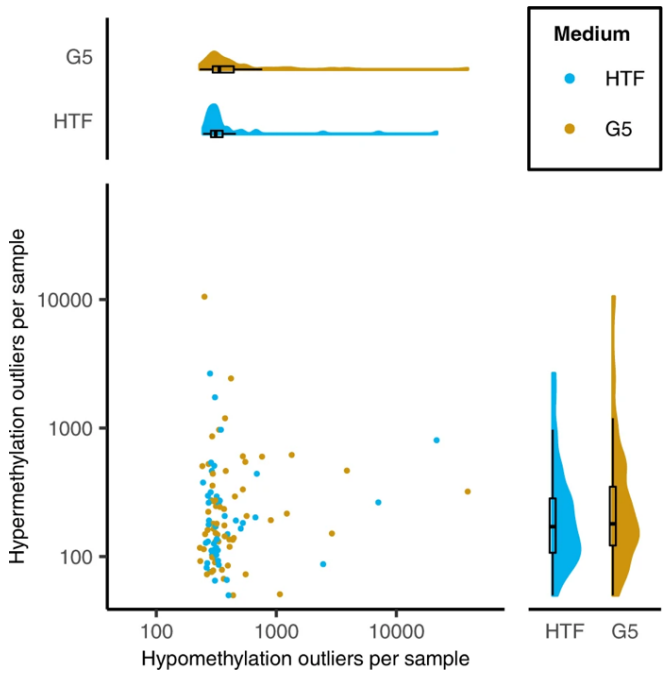

The main panel shows the number of hypomethylation (x-axis) and hypermethylation (y-axis) outliers per UCB sample (G5 = gold, HTF = blue). Distribution summaries, in the form of a density plot and boxplot, are shown for hypomethylation outliers and hypermethylation outliers in the top and right-side panels respectively. Lines of the boxplot represent the 25th percentile, median and 75th percentile respectively while the whiskers extend to the farthest data point that is no more than 1.5 times the IQR from the upper or lower quartile. The axes are shown on a log10 scale. The groups were not found to be significantly different (p value > 0.1).

Epigenetic gestational age as a marker of developmental maturity

Gestational age can be predicted from DNA methylation levels at certain CpG sites (epigenetic clock)[38,39]. Similar to birth weight, these have been used to comment on developmental maturity at birth and gestational age acceleration (GAA), i.e. when epigenetic gestational age (eGA) is more advanced than clinical gestational age (cGA), has been positively correlated with birth weight[37,39,40]. eGA estimates derived using the Bohlin prediction model[38] were more strongly correlated (Pearson correlation coefficient = 0.77) with our data and had a lower root mean squared error (RMSE = 1.29) than the estimates derived with the Knight prediction model[39] (Pearson correlation coefficient = 0.55, RMSE = 1.45), therefore only the results from the Bohlin epigenetic clock are shown. However, of note is that both prediction models were trained using data from the HumanMethylation450 (450K) array and of the 96 sites used for the Bohlin eGA prediction model, eight sites with coefficients ranging from −15.5 to 6.1 are no longer present on the EPIC array. We removed these sites from the prediction model. When applying the prediction model to 450K data from the ENVIR*ON*AGE study (n = 159), the omission of these eight CpG sites lead to a mean increase in the predicted gestational age by 0.73 weeks (range 0.17–1.10 weeks) (**Supplementary Fig. 4a**). Therefore, we cannot thoroughly evaluate absolute epigenetic gestational age, but we assume that all samples will be similarly affected by the missing sites and thus can compare the GAA between culture medium groups. GAA was calculated by regressing eGA on cGA while correcting for cell composition of the samples (Methods). In G5 samples the median GAA was 0.01 (0.64 IQR) and in HTF samples the median GAA was 0.03 (0.92 IQR), which was not significantly different (p = 0.42) (**Fig. 5**). Additionally, we found no significant correlation between GAA and birth weight (Pearson correlation = −0.17, p = 0.08). The results were comparable when participants who had experienced pregnancy complications were excluded from the analysis (**Supplementary Fig. 4b**).

Comparison of IVF neonates to naturally conceived neonates

Even though the main aim of this study was to investigate the effect of two different culture media on the methylome of IVF neonates, we also sought to compare the methylomes of the IVF neonates to those of naturally conceived neonates using previously published data from the FLEHS and ENVIR*ON*AGE longitudinal cohort studies. However, as these samples were not processed concurrently with the IVF samples it is not possible to correct for technical variation between the studies meaning that any effect of the IVF process cannot be differentiated from technical differences. These findings are demonstrated in the supplementary material (**Supplementary Table 6: participant demographics, Supplementary Fig. 5: processing of FLEHS and ENVIR*ON*AGE data, Supplementary Fig. 6: comparison of IVF and naturally conceived neonates**).

Figure 5 | Epigenetic gestational age acceleration

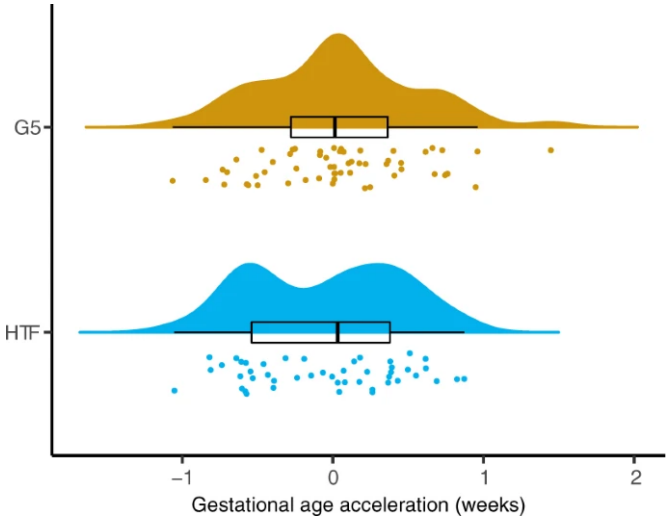

Raincloud plot showing the GAA of each UCB sample in each culture medium group. Points represent individual samples of the G5 (gold) and HTF (blue) groups. Above a density plot and boxplot is shown. Horizontal lines of the boxplot represent the 25th percentile, median and 75th percentile respectively while the whiskers extend to the farthest data point that is no more than 1.5 times the IQR from the upper or lower quartile. GAA is represented in weeks. The groups were not found to be significantly different (p value > 0.1).

Discussion

To the best of our knowledge, the genome-wide analysis of the influence of different IVF culture media on the methylome of human IVF neonates presented here is the largest cohort on which such a study has been conducted to date. Despite this, our sample size was insufficient to conduct sub-group analyses looking specifically at sex or treatment type (IVF vs. ICSI), which could reveal clinically relevant differences. We have investigated the impact of two compositionally different media, namely G5 from Vitrolife and HTF from Lonza, which were shown to influence IVF outcomes during the original RCT[14]. However, these phenotypic differences, e.g. in birth weight, were no longer significant in the sub-group of the original RCT that is presented here. We have found no evidence that these culture media lead to systematic or stochastic methylation differences in the resultant IVF neonates. To facilitate a comparison between different modes of conception, samples from well-matched naturally conceived individuals would have ideally been collected and processed alongside the IVF samples.

In line with findings from previous studies, examining the methylome of IVF children born after embryo culture in different media, we identified no differentially methylated positions or regions and only moderate group mean differences, largely less than 10%.

This was also seen when the methylation status of imprinting genes in the placenta of the same individuals was analysed[25]. Similarly, a comparison of IVF children (aged 7 or 8) born after embryo culture in a global medium (Life Global), or single-step medium (Irvine Scientific) found no evidence of differential methylation between the medium groups at imprinting genes, transposable elements or on a genome-wide scale[41,42].

The lack of differential methylation between G5 and HTF neonates may seem surprising given the stark differences in medium composition, which include the complete lack of amino acids in HTF medium, while G5 contains all amino acids except non-essential glutamate, glutamine and glycine[9], and the addition of hyaluronan and lipoic acid to G5 medium[14]. Although the direct interplay between these individual components and DNA methylation has not been investigated in human embryos, it seems plausible that amino acid availability may influence the functional capacity of DNA methylation establishment and maintenance machinery. The sensitivity of embryos to these environmental differences is further supported by the finding that gene expression differences exist between embryos cultured in G5 or HTF medium[43,44] and it is known that gene expression can be regulated by DNA methylation. However, the lack of differentially methylated sites or regions could be explained by a number of reasons. Firstly, dysregulated DNA methylation may be transient during in vitro embryogenesis and therefore not be detectable in neonates. Secondly, alternative epigenetic marks, such as histone modifications, may mediate the association between the culture media and the observed gene expression and phenotype differences. Additionally, in the sub-group of participants recruited for this follow-up study, phenotypic differences, such as birth weight, were less than in the full RCT cohort, which may have reduced the magnitude of any culture medium-induced effects. Finally, even though our study is the largest described methylome study after an IVF culture medium trial, we still lack the power to detect methylation differences with a magnitude of less than 10%. Although exact power estimates are challenging without the existence of prior data to establish the expected variance within our study population, simulation studies by Saffari et al.[45] and Tsai et al.[46] estimates that a sample size of 211 or more participants would be required to achieve 80% power to detect significant methylation differences with an effect size of 7% or less, respectively, using array-based assays such as the EPIC array[45,46]. However, it remains to be determined whether mean differences of less than 10%, representing methylation loss or gain at any site in just a small proportion of an individual's cells, represent clinically significant differences[47].

An alternative to the theory that peri-conception environmental differences induce systematic methylation differences, relates to the presence of stochastic epimutations that are either induced by the environment[48] or provide a survival benefit if selection pressure is applied by certain environmental conditions[49]. In placenta samples of

the same individuals as those described in this study, DNA methylation outliers were also identified in all samples without a difference in outlier burden between the culture medium groups[25]. Whether the number of outliers identified per individual is comparable between the two studies is difficult to assess due to the different thresholds used to define outliers and the different techniques used to analyse the methylome that differ vastly in their coverage of the genome. In the field of cancer biology, the iEVORA algorithm has been used to identify so-called field defects, which represent stochastic methylation alterations in normal pre-cancerous tissues that later undergo neoplastic transformation[35]. Frequently, sites identified as differentially variable in pre-cancerous samples become differentially methylated in tumour samples, suggesting that sites of this nature could be interesting biomarkers for disease with a later onset. In this study, such epimutations could be linked to later development of disease phenotypes, such as cardiometabolic diseases, although it should be noted that the differentially variable sites identified were not enriched in pathways relating to cardiovascular or metabolic function and it is not yet known whether there will be a difference in the prevalence of cardiometabolic disease between G5 and HTF offspring. Nonetheless, these sites warrant further clinical and molecular follow-up. Alternatively, differential variability at certain CpG sites could be driven by factors that are only experienced by a few individuals in the study population, such as pregnancy complications. Previously, DNA methylation differences associated with pre-eclampsia[50] and gestational diabetes[51-53] have been described when analysing UCB samples of neonates. According to our findings, there might be an association between culture medium, the number of differentially variable sites and pregnancy complications, but the design of this study does not allow to discuss the direction of causality (culture media, methylation and pregnancy complications).

Although studies comparing naturally conceived and IVF neonates have found some methylation differences, especially at imprinting genes[30], this has not been observed in this or other culture medium comparisons[25,41,42]. This may be due to the fact that the environmental discrepancy between two culture media is less severe than the difference between in vivo and in vitro embryo development, thus leading to a smaller or no effect on the methylome. The concurrent processing of samples from naturally conceived individuals would be required to assess this further.

The lack of difference we observed in GAA may relate to the fact that the eGA prediction tools were trained using the HumanMethylation450K array and eight of the 96 probes required for the prediction model are no longer present on the EPIC array. These probes were therefore excluded from the model leading to a consistent over-estimation of gestational age. The inclusion of these sites may be important to identify a relationship between GAA, birth weight[37,39,40] and potentially culture medium.

In conclusion, our genome-wide methylome analysis of IVF neonates that underwent embryo culture in G5 or HTF medium revealed no significant differences between the culture medium groups, suggesting that the use of either culture medium will establish a comparable DNA methylation signature, including at imprinting genes. However, we have observed some differentially variable sites between the culture medium groups, which seem associated with pregnancy complications, but the persistence and clinical significance of these findings should be assessed with further follow-up studies. To assess whether epigenetic reprogramming is transiently affected by differences in culture medium composition, epigenetic studies of embryos cultured in different media are required.

Methods

Ethical approval

This study was approved by the local medical ethical committee, Medische Ethische Commissie academisch ziekenhuis Maastricht/University of Maastricht (METC azM/UM) and registered in the Dutch Trial register (NTR 1979/NL1866). Both parents of all neonates gave written informed consent.

Study population and sample collection

Samples were collected as part of a culture medium comparison study[14], which was a multi-centre RCT, involving six IVF centres in the Netherlands. Specifically, couples undergoing IVF treatments were randomised to embryo culture either in HTF medium (Lonza, Verviers, Belgium) or Vitrolife G1™ Version 5 (G5, Göteborg, Sweden), while all other IVF-related procedures and conditions were kept the same. Of the 6 IVF centres, five participated in UCB sampling. In these five centres, the study resulted in 273 singleton live births that occurred after fresh (not frozen) embryo transfers. UCB samples were collected from as many resulting singleton pregnancies as possible, 115 in total, irrespective of birth weight, gestational age at birth and the presence of pregnancy complications. Within 30 min of delivery, UCB was collected by a gynaecologist, nurse or midwife according to a standardised protocol. The samples were sent to the Department of Obstetrics and Gynaecology at Maastricht University Medical Centre (MUMC+) and were stored at −80 °C until they were used.

DNA extraction

DNA was extracted from thawed UCB samples using the Gentra Puregene DNA purification kit (Qiagen Hilden, Germany) according to the manufacturer's instructions for 3 mL of human whole blood with minor modifications, namely, a smaller volume (8.5 mL) of red blood cell (RBC) lysis solution and longer centrifugation time (4 min

where 2 min are indicated and 8 min where 5 min are indicated).

Bisulfite conversion and methylome profiling by EPIC array

One microgram of DNA was bisulfite-treated using the EpiTect® Fast 96 DNA Bisulfite Kit (Qiagen Hilden, Germany) and analysed using the Infinium Human Methylation EPIC BeadChip Kit (Illumina, CA, USA) according to the manufacturer's protocol.

Data analysis

All data were analysed using R (version 3.6.3)[54]. The data were visualised using the ggplot2[55] and ComplexHeatmap[56] packages.

Baseline characteristics

Differences in baseline characteristics between the two culture medium groups were compared and evaluated using Student's *t*-tests for continuous variables and Pearson's chi-squared tests for categorical variables.

Quality control and preprocessing

We applied preprocessing functions from the RnBeads package[57] to normalise the data using subset-quantile within array normalisation (SWAN)[58], and to remove poor quality probes and samples using the greedycut algorithm with a detection *p* value threshold of 0.05. Subsequently, the following sites were removed: (i) sites on the sex chromosomes, (ii) sites in close proximity to single nucleotide polymorphisms (SNPs), (iii) sites with missing values in more than 5% of the samples, and (iv) sites not in a CpG context. Sites containing missing values in 0–5% of the samples were only used to calculate aggregated beta values for different regions, including genes, promoters and CpG islands (CGI), they were excluded in all analyses looking at individual sites. Unless indicated otherwise, we used methylation beta values, which are calculated for each individual, at each CpG site by dividing the methylated signal intensity by the sum of the methylated and unmethylated signal intensity. The sex of the samples was predicted by comparing the samples' sex chromosome methylation values and their respective detection *p* values to reference data using a clustering (PCA)-based approach, as implemented in the sEst package[59]. Correspondingly, each sample was assigned two predicted sexes based on the X-chromosome and Y-chromosome profiles respectively. If both matched, the sample was labelled as male or female, otherwise, it was labelled as "not specified". If a mismatch between the recorded and predicted sex was identified, the sample was removed from subsequent analyses ($n = 1$).

Cellular deconvolution of UCB samples

To estimate the cellular composition of the UCB samples, the reference-based method described by Gervin et al.[60] was implemented using the minfi package[61]. As recommended,

the algorithm was applied to data pre-processed with the *preprocessNoob* method[62] and deconvolution was carried out based on the IDOL optimised probes contained within the FlowSorted.CordBloodCombined.450k package[63]. The algorithm was used to estimate the proportion of natural killer cells, B cells, monocytes, granulocytes, nucleated red blood cells and CD4- and CD8-T cells within each sample.

Comparison of G5 and HTF IVF neonates

All high-quality CpG sites were used to conduct a PCA in which the beta values were centred but not scaled. Associations between the PCs and technical or demographic features of the samples were tested using: (i) permutation tests (with 10,000 permutations) to ascertain the significance of correlations (gestational age, maternal age, predicted cellular sample composition), (ii) a two-sided Wilcoxon rank test for categorical data where there are two groups (sex, culture medium, sample plate, pregnancy complication) or (iii) a Kruskal–Wallis one-way analysis of variance for categorical variables generating 3 or more groups (Sentrix ID, Sentrix position—array number and sample position respectively).

Methylation M-values, representing the log2 ratio of the methylated probe intensity compared to the unmethylated probe intensity[64], were used to test for an association between the culture medium and DNA methylation with mixed-effects linear models implemented using the variancePartition package[65]. The models were corrected for potential confounders, namely gestational age, sex, maternal age, pregnancy complications (included as a binary variable where the presence of gestational diabetes, hypertension and pre-eclampsia were encoded as "yes" and otherwise "no" was recorded) and the predicted cell compositions as fixed effects while the treatment centre and batch effects (sample plate) were included as random effects. As gestational diabetes, hypertension and pre-eclampsia represent pathophysiologically heterogeneous pregnancy complications, the analyses were repeated while excluding participants affected by any of the complications. The models were applied to individual CpG sites or aggregate (mean) values of multiple CpG sites within a region to identify differentially methylated positions (DMPs) or regions (DMRs) respectively. To examine DMRs, the M-values of all probes attributed to a specific gene, promoter or CGI were aggregated by calculating their mean. For the targeted analyses, the models described above were applied to (sites within) imprinted genes[33] and probes associated with birth weight[34]. All analyses were corrected for multiple testing using the Benjamini–Hochberg method[66], and an adjusted p value of <0.1 was considered significant.

DNA methylation outliers were defined as described previously[36]. In short, hypomethylation outliers were defined as beta values lower than three interquartile ranges (IQR) from the 25th percentile, while hypermethylation outliers were defined

as beta values greater than three times the IQR above the 75th percentile. The IQR and percentile values were calculated using all UCB samples. Subsequently, an association between the $\log_{10}$ transformed number of outliers and the culture medium was sought using the mixed-effects linear models as described above. To identify CpG sites with differential variance between the culture medium groups, we applied iEVORA[35] using the matrixTests package[67]. At each CpG site, iEVORA applies Bartlett's test, which is a parametric test for differential variance, as well as a Student's *t*-test. Thereafter, sites reaching significance in Bartlett's test after multiple testing correction (FDR corrected p value < 0.05) and nominal significance in the t-test (p value < 0.05 without multiple testing correction) are considered significant. As such, the output of Bartlett's test is regularised as it is usually overly sensitive to single outliers. Both DNA methylation outliers and iEVORA analyses were applied to the full cohort as well as the subset of participants that had not experienced pregnancy complications. Gene ontology (GO) and Kyoto Encyclopaedia of Genes and Genomes (KEGG) pathway enrichment analyses were conducted on differentially variable sites using functionality from the missMethyl package[68].

Estimation of epigenetic gestational age and gestational age acceleration

Epigenetic gestational age was calculated using methods described by Bohlin et al.[38] and Knight et al.[39]. The accuracy of the respective predictions was evaluated by calculating the Pearson's correlation and root mean squared error between eGA and cGA. The model described by Bohlin et al. generated more accurate predictions and was therefore used to calculate GAA as previously described[38]. The Bohlin eGA prediction model was applied exactly as described by Bohlin et al. Firstly, within array normalisation was carried out using the BMIQ method using the RnBeads package[57]. Subsequently, batch effects attributable to the sample plate were corrected using ComBat from the sva package[69]. There were no missing values in any samples at the required sites, apart from eight CpG sites of the prediction model that are not present on the EPIC array. These eight sites were therefore excluded from the prediction. GAA represents the residuals from regressing eGA on cGA corrected for sample cell composition. To determine whether there is an association between GAA and culture medium, we applied mixed-effects linear models correcting for sex and maternal age as fixed effects alongside IVF treatment centre as a random effect. Again, the analysis was carried out on the full cohort and repeated excluding those participants who had experienced pregnancy complications.

Comparison of IVF and naturally conceived neonates

Selection and processing of data from naturally conceived individuals

To compare the methylome of our IVF neonates to naturally conceived individuals, we used data from two geographically similar longitudinal birth cohorts, namely

the Flemish Environment and Health Study (FLEHS, Flanders Belgium)[70,71] and the Environmental Influence on Early Ageing study (ENVIR*ON*AGE)[72] that had both undertaken array-based methylome profiling. Samples were considered for inclusion if the neonates were born after at least 36 full weeks of gestation (comparable to the IVF neonates included in this study). A total of 85 individuals from the FLEHS cohort and 502 individuals from the ENIR*ON*AGE cohort were considered for inclusion based on this criterium. Methylation data in these studies were generated either with Illumina's EPIC or 450K arrays. Preprocessing of the data from the separate studies/arrays was conducted separately but in an identical fashion to the IVF data, with the exception of within-study batch effects, which were corrected using ComBat[69] as these could not be corrected for using the mixed-effects models. The sample inclusion and preprocessing steps of these two cohorts is summarised in Supplementary Fig. 5H. After study/data type-specific processing the data were combined, retaining only CpG sites present and passing the QC of all the array types included. Overall, 346,403 CpG sites were common to all platforms and studies.

To select only the data likely to be most similar to our IVF cohort, we generated a matched selection from the ENIR*ON*AGE neonates who had their methylome profiled using the EPIC array. We used nearest neighbour matching (Mahalanobis distance) based on sex, maternal age, birth weight and gestational age to select 105 neonates to compare to the IVF neonates. This matching was carried out using the MatchIt package[73].

Comparison of characteristics of matched IVF and naturally conceived individuals

The participant characteristics between IVF and matched naturally conceived individuals were compared and evaluated using Student's *t*-tests for continuous variables and Pearson's chi-squared tests for categorical variables. The *p* values obtained from this comparison are shown in **Supplementary Table 6**.

Statistical testing to compare naturally conceived and IVF neonates

Empirical Bayes moderated mixed effect linear models were used to ascertain associations between DNA methylation and mode of conception. These models were corrected for gestational age at birth, cell composition, sex, and maternal age as fixed effects and where relevant, array type as a random effect. Multiple testing correction was applied using the Benjamini–Hochberg method[66], and an adjusted p value of <0.05 was considered significant.

Data availability

The dataset generated during the current study, IVF samples, are available in the Gene Expression Omnibus (GEO) repository[74] under the accession number **GSE189531**. Data included from the FLEHS and ENVIR*ON*AGE cohorts are available from GEO under the

accession numbers GSE110128 and GSE151042 respectively.

Code availability

Custom R code used for the processing and analysis of the data described in this article are available at https://github.com/CellularGenomicMedicine/UCB_methylome.

Acknowledgements and funding

We thank the IVF couples who have agreed for their children to participate in this study. We thank all the employees of the IVF clinics and obstetrics departments involved in recruiting participants and collecting samples for this study. We thank E. Pishva for his consultation regarding data analysis and for the critical reading of the manuscript. This study was funded by March of Dimes (6-FY13-153). It was further supported by the stichting fertility foundation, EVA (Erfelijkheid Voortplanting & Aanleg) speciality programme (grant no. KP111513) of Maastricht University Medical Centre (MUMC+), and the Horizon 2020 innovation (ERIN) (grant no. EU952516) of the European Commission. We thank the FLEHS Supervisory Board for the provision of data. The FLEHS studies are commissioned, financed, and steered by the Flemish Government (Department of Economy, Science and Innovations, Agency for Care and Health and Department of Environment). The FLEHS dataset has been generated by the Flemish Center of Expertise on Environment and Health (FLEHS 2016–2020), funded by the Environment, Nature and Energy Department of the Flemish government. The views expressed in this manuscript are those of the author(s) and are not necessarily endorsed by the Flemish government.

Contributions

R.M.K., A.P.A.v.M. and M.Z.E. study design and conception. D.C., J.v.E.-A., S.M., Y.W., R.v.G., and J.C.M.D. were involved in sample collection for the IVF cohort. A.P.A.v.M. and F.B. carried out the lab work for the IVF samples. S.R., S.L., T.S.N., M.P., R.A. and E.M.B. were involved in sample collection and processing for the naturally conceived cohorts. R.M.K., F.B., J.T., A.P.A.v.M. and M.Z.E. were involved in the data analysis and interpretation. R.M.K. wrote the first draft of the manuscript. M.G., A.P.A.v.M. and M.Z.E. contributed to the writing of the manuscript. All authors provided textual comments and approved the manuscript. H.B., A.P.A.v.M. and M.Z.E. supervised the study.

References

1 Adamson, G. D. *et al.* ICMART preliminary world report 2015. *Hum Reprod* **34** (2019). <https://academic.oup.com/humrep/article/34/Supplement_1/i1/5528444>.

2 Wyns, C. *et al.* ART in Europe, 2018: results generated from European registries by ESHRE. *Hum Reprod Open* **2022**, hoac022 (2022). https://doi.org/10.1093/hropen/hoac022

3 Bernsten, S. *et al.* The health of children conceived by ART: 'the chicken or the egg?'. *Hum Reprod update* **25**, 137-158 (2019).

4 Ceelen, M. *et al.* Growth during infancy and early childhood in relation to blood pressure and body fat measures at age 8-18 years of IVF children and spontaneously conceived controls born to subfertile parents. *Hum Reprod* **24**, 2788-2795 (2009). https://doi.org/10.1093/humrep/dep273

5 Hann, M. *et al.* The growth of assisted reproductive treatment-conceived children from birth to 5 years: a national cohort study. *BMC Med* **16**, 224 (2018). https://doi.org/10.1186/s12916-018-1203-7

6 Guo, X. Y. *et al.* Cardiovascular and metabolic profiles of offspring conceived by assisted reproductive technologies: a systematic review and meta-analysis. *Fertil Steril* **107**, 622-631.e625 (2017). https://doi.org/10.1016/j.fertnstert.2016.12.007

7 Sunde, A. *et al.* Time to take human embryo culture seriously. *Hum Reprod* **31**, 2174-2182 (2016). https://doi.org/10.1093/humrep/dew157

8 Morbeck, D. E., Baumann, N. A. & Oglesbee, D. Composition of single-step media used for human embryo culture. *Fertil Steril* **107**, 1055-1060.e1051 (2017). https://doi.org/10.1016/j.fertnstert.2017.01.007

9 Morbeck, D. E. *et al.* Composition of commercial media used for human embryo culture. *Fertil Steril* **102**, 759-766.e759 (2014). https://doi.org/10.1016/j.fertnstert.2014.05.043

10 Mantikou, E. *et al.* Embryo culture media and IVF/ICSI success rates: a systematic review. *Hum Reprod Update* **19**, 210-220 (2013). https://doi.org/10.1093/humupd/dms061

11 Youssef, M. M. *et al.* Culture media for human pre-implantation embryos in assisted reproductive technology cycles. *Cochrane Database Syst Rev*, Cd007876 (2015). https://doi.org/10.1002/14651858.CD007876.pub2

12 Dumoulin, J. C. *et al.* Effect of in vitro culture of human embryos on birthweight of newborns. *Hum Reprod* **25**, 605-612 (2010). https://doi.org/10.1093/humrep/dep456

13 Zandstra, H., Van Montfoort, A. P. & Dumoulin, J. C. Does the type of culture medium used influence birthweight of children born after IVF? *Hum Reprod* **30**, 530-542 (2015). https://doi.org/10.1093/humrep/deu346

14 Kleijkers, S. H. *et al.* Influence of embryo culture medium (G5 and HTF) on pregnancy and perinatal outcome after IVF: a multicenter RCT. *Hum Reprod* **31**, 2219-2230 (2016). https://doi.org/10.1093/humrep/dew156

15 Kleijkers, S. H. *et al.* IVF culture medium affects post-natal weight in humans during the first 2 years of life. *Hum Reprod* **29**, 661-669 (2014). https://doi.org/10.1093/humrep/deu025

16 Zandstra, H. *et al.* Association of culture medium with growth, weight and cardiovascular development of IVF children at the age of 9 years. *Hum Reprod* **33**, 1645-1656 (2018). https://doi.org/10.1093/humrep/dey246

17 Bouillon, C. *et al.* Does Embryo Culture Medium Influence the Health and Development of Children Born after In Vitro Fertilization? *PLoS One* **11**, e0150857 (2016). https://doi.org/10.1371/journal.pone.0150857

18 Tarahomi, M. *et al.* The composition of human preimplantation embryo culture media and their stability during storage and culture. *Hum Reprod* **34**, 1450-1461 (2019). https://doi.org/10.1093/humrep/dez102

19 Wadhwa, P. D., Buss, C., Entringer, S. & Swanson, J. M. Developmental origins of health and disease: brief history of the approach and current focus on epigenetic mechanisms. *Semin Reprod Med* **27**, 358-368 (2009). https://doi.org/10.1055/s-0029-1237424

20 Felix, J. F. & Cecil, C. A. M. Population DNA methylation studies in the Developmental Origins of Health and Disease (DOHaD) framework. *J Dev Orig Health Dis* **10**, 306-313 (2019). https://doi.org/10.1017/S2040174418000442

21 Sullivan-Pyke, C. S., Senapati, S., Mainigi, M. A. & Barnhart, K. T. In Vitro fertilization and adverse obstetric and perinatal outcomes. *Semin Perinatol* **41**, 345-353 (2017). https://doi.org/10.1053/j.semperi.2017.07.001

22 DeAngelis, A. M., Martini, A. E. & Owen, C. M. Assisted Reproductive Technology and Epigenetics. *Semin Reprod Med* **36**, 221-232 (2018). https://doi.org/10.1055/s-0038-1675780

23 Li, L. *et al.* Single-cell multi-omics sequencing of human early embryos. *Nat Cell Biol* **20**, 847-858 (2018).

https://doi.org/10.1038/s41556-018-0123-2
24 Hanna, C. W., Demond, H. & Kelsey, G. Epigenetic regulation in development: is the mouse a good model for the human? *Hum Reprod Update* **24**, 556-576 (2018). https://doi.org/10.1093/humupd/dmy021
25 Mulder, C. L. *et al.* Comparison of DNA methylation patterns of parentally imprinted genes in placenta derived from IVF conceptions in two different culture media. *Hum Reprod* **35**, 516-528 (2020). https://doi.org/10.1093/humrep/deaa004
26 Mani, S. & Mainigi, M. Embryo Culture Conditions and the Epigenome. *Semin Reprod Med* **36**, 211-220 (2018). https://doi.org/10.1055/s-0038-1675777
27 Novakovic, B. *et al.* Assisted reproductive technologies are associated with limited epigenetic variation at birth that largely resolves by adulthood. *Nat Commun* **10**, 3922 (2019). https://doi.org/10.1038/s41467-019-11929-9
28 Turan, N. *et al.* Inter- and intra-individual variation in allele-specific DNA methylation and gene expression in children conceived using assisted reproductive technology. *PLoS Genet* **6**, e1001033 (2010). https://doi.org/10.1371/journal.pgen.1001033
29 Melamed, N., Choufani, S., Wilkins-Haug, L. E., Koren, G. & Weksberg, R. Comparison of genome-wide and gene-specific DNA methylation between ART and naturally conceived pregnancies. *Epigenetics* **10**, 474-483 (2015). https://doi.org/10.4161/15592294.2014.988041
30 Barberet, J. *et al.* DNA methylation profiles after ART during human lifespan: a systematic review and meta-analysis. *Hum Reprod Update* (2022). https://doi.org/10.1093/humupd/dmac010
31 El Hajj, N. *et al.* DNA methylation signatures in cord blood of ICSI children. *Hum Reprod* **32**, 1761-1769 (2017). https://doi.org/10.1093/humrep/dex209
32 Tierling, S. *et al.* Assisted reproductive technologies do not enhance the variability of DNA methylation imprints in human. *J Med Genet* **47**, 371-376 (2010). https://doi.org/10.1136/jmg.2009.073189
33 Ginjala , V. Gene imprinting gateway. *Genome Biol* **2** (2001). https://doi.org/https://doi.org/10.1186/gb-2001-2-8-reports2009
34 Küpers, L. K. *et al.* Meta-analysis of epigenome-wide association studies in neonates reveals widespread differential DNA methylation associated with birthweight. *Nat Commun* **10**, 1893 (2019). https://doi.org/10.1038/s41467-019-09671-3
35 Teschendorff, A. E., Jones, A. & Widschwendter, M. Stochastic epigenetic outliers can define field defects in cancer. *BMC Bioinformatics* **17**, 178 (2016). https://doi.org/10.1186/s12859-016-1056-z
36 Gentilini, D. *et al.* Stochastic epigenetic mutations (DNA methylation) increase exponentially in human aging and correlate with X chromosome inactivation skewing in females. *Aging (Albany NY)* **7**, 568-578 (2015). https://doi.org/10.18632/aging.100792
37 Khouja, J. N. *et al.* Epigenetic gestational age acceleration: a prospective cohort study investigating associations with familial, sociodemographic and birth characteristics. *Clin Epigenetics* **10**, 86 (2018). https://doi.org/10.1186/s13148-018-0520-1
38 Bohlin, J. *et al.* Prediction of gestational age based on genome-wide differentially methylated regions. *Genome Biol* **17**, 207 (2016). https://doi.org/10.1186/s13059-016-1063-4
39 Knight, A. K. *et al.* An epigenetic clock for gestational age at birth based on blood methylation data. *Genome Biol* **17**, 206 (2016). https://doi.org/10.1186/s13059-016-1068-z
40 Bright, H. D. *et al.* Epigenetic gestational age and trajectories of weight and height during childhood: a prospective cohort study. *Clin Epigenetics* **11**, 194 (2019). https://doi.org/10.1186/s13148-019-0761-7
41 Barberet, J. *et al.* Do assisted reproductive technologies and in vitro embryo culture influence the epigenetic control of imprinted genes and transposable elements in children? *Hum Reprod* **36**, 479-492 (2021). https://doi.org/10.1093/humrep/deaa310
42 Ducreux, B. *et al.* Genome-Wide Analysis of DNA Methylation in Buccal Cells of Children Conceived through IVF and ICSI. *Genes (Basel)* **12** (2021). https://doi.org/10.3390/genes12121912
43 Mantikou, E. *et al.* Factors affecting the gene expression of in vitro cultured human preimplantation embryos. *Hum Reprod* **31**, 298-311 (2016). https://doi.org/10.1093/humrep/dev306
44 Kleijkers, S. H. *et al.* Differences in gene expression profiles between human preimplantation embryos cultured in two different IVF culture media. *Hum Reprod* **30**, 2303-2311 (2015). https://doi.org/10.1093/humrep/dev179
45 Saffari, A. *et al.* Estimation of a significance threshold for epigenome-wide association studies. *Genet Epidemiol* **42**, 20-33 (2018). https://doi.org/10.1002/gepi.22086
46 Tsai, P. C. & Bell, J. T. Power and sample size estimation for epigenome-wide association scans to detect differential DNA methylation. *Int J Epidemiol* **44**, 1429-1441 (2015). https://doi.org/10.1093/ije/dyv041
47 Breton, C. V. *et al.* Small-Magnitude Effect Sizes in Epigenetic End Points are Important in Children's Environmental Health Studies: The Children's Environmental Health and Disease Prevention Research

Center's Epigenetics Working Group. *Environ Health Perspect* **125**, 511-526 (2017). https://doi.org/10.1289/EHP595

48 Gentilini, D. *et al.* Multifactorial analysis of the stochastic epigenetic variability in cord blood confirmed an impact of common behavioral and environmental factors but not of in vitro conception. *Clin Epigenetics* **10**, 77 (2018). https://doi.org/10.1186/s13148-018-0510-3

49 Tobi, E. W. *et al.* Selective Survival of Embryos Can Explain DNA Methylation Signatures of Adverse Prenatal Environments. *Cell Rep* **25**, 2660-2667.e2664 (2018). https://doi.org/10.1016/j.celrep.2018.11.023

50 Cirkovic, A. *et al.* Systematic review supports the role of DNA methylation in the pathophysiology of preeclampsia: a call for analytical and methodological standardization. *Biol Sex Differ* **11**, 36 (2020). https://doi.org/10.1186/s13293-020-00313-8

51 Elliott, H. R., Sharp, G. C., Relton, C. L. & Lawlor, D. A. Epigenetics and gestational diabetes: a review of epigenetic epidemiology studies and their use to explore epigenetic mediation and improve prediction. *Diabetologia* **62**, 2171-2178 (2019). https://doi.org/10.1007/s00125-019-05011-8

52 Awamleh, Z. *et al.* Exposure to Gestational Diabetes Mellitus (GDM) alters DNA methylation in placenta and fetal cord blood. *Diabetes Res Clin Pract* **174**, 108690 (2021). https://doi.org/10.1016/j.diabres.2021.108690

53 Howe, C. G. *et al.* Maternal Gestational Diabetes Mellitus and Newborn DNA Methylation: Findings From the Pregnancy and Childhood Epigenetics Consortium. *Diabetes Care* **43**, 98-105 (2020). https://doi.org/10.2337/dc19-0524

54 *R Core Team. R: A language and environment for statistical computing. R Foundation for Statistical Computing, Vienna, Austria. https://www.R-project.org/*, <URL https://www.R-project.org/> (2021).

55 Wickham, H. *ggplot2: Elegant Graphics for Data Analysis. Springer-Verlag New York. https://ggplot2.tidyverse.org*, <https://ggplot2.tidyverse.org> (2016).

56 Gu, Z., Eils, R. & Schlesner, M. Complex heatmaps reveal patterns and correlations in multidimensional genomic data. *Bioinformatics* **32**, 2847-2849 (2016). https://doi.org/10.1093/bioinformatics/btw313

57 Müller, F. *et al.* RnBeads 2.0: comprehensive analysis of DNA methylation data. *Genome Biol* **20**, 55 (2019). https://doi.org/10.1186/s13059-019-1664-9

58 Maksimovic, J., Gordon, L. & Oshlack, A. SWAN: Subset-quantile within array normalization for illumina infinium HumanMethylation450 BeadChips. *Genome Biol* **13**, R44 (2012). https://doi.org/10.1186/gb-2012-13-6-r44

59 Jung, C. H. *et al.* sEst: Accurate Sex-Estimation and Abnormality Detection in Methylation Microarray Data. *Int J Mol Sci* **19** (2018). https://doi.org/10.3390/ijms19103172

60 Gervin, K. *et al.* Systematic evaluation and validation of reference and library selection methods for deconvolution of cord blood DNA methylation data. *Clin Epigenetics* **11**, 125 (2019). https://doi.org/10.1186/s13148-019-0717-y

61 Aryee, M. J. *et al.* Minfi: a flexible and comprehensive Bioconductor package for the analysis of Infinium DNA methylation microarrays. *Bioinformatics* **30**, 1363-1369 (2014). https://doi.org/10.1093/bioinformatics/btu049

62 Triche, T. J., Weisenberger, D. J., Van Den Berg, D., Laird, P. W. & Siegmund, K. D. Low-level processing of Illumina Infinium DNA Methylation BeadArrays. *Nucleic Acids Res* **41**, e90 (2013). https://doi.org/10.1093/nar/gkt090

63 Jaffe, A. E. *FlowSorted.Blood.450k: Illumina HumanMethylation data on sorted blood cell population. https://bioconductor.org/packages/release/data/experiment/html/FlowSorted.Blood.450k.html*, <https://github.com/immunomethylomics/FlowSorted.CordBloodCombined.450k> (2018).

64 Du, P. *et al.* Comparison of Beta-value and M-value methods for quantifying methylation levels by microarray analysis. *BMC Bioinformatics* **11**, 587 (2010). https://doi.org/10.1186/1471-2105-11-587

65 Hoffman, G. E. & Schadt, E. E. variancePartition: interpreting drivers of variation in complex gene expression studies. *BMC Bioinformatics* **17**, 483 (2016). https://doi.org/10.1186/s12859-016-1323-z

66 Benjamini, Y. & Hochberg, Y. Controlling the false discovery rate: a practical and powerful approach to multiple testing. *J. Roy. Statist. Soc.* **Ser. B57**, 289-300 (1995).

67 Koncevičius, K. (2020).

68 Phipson, B., Maksimovic, J. & Oshlack, A. missMethyl: an R package for analyzing data from Illumina's HumanMethylation450 platform. *Bioinformatics* **32**, 286-288 (2016). https://doi.org/10.1093/bioinformatics/btv560

69 Leek, J. T., Johnson, W. E., Parker, H. S., Jaffe, A. E. & Storey, J. D. The sva package for removing batch effects and other unwanted variation in high-throughput experiments. *Bioinformatics* **28**, 882-883 (2012). https://doi.org/10.1093/bioinformatics/bts034

70 Van Den Heuvel, R. *et al.* Biobank@VITO: Biobanking the General Population in Flanders. *Front Med (Lausanne)* **7**, 37 (2020). https://doi.org/10.3389/fmed.2020.00037

71 Langie, S. A. S. *et al.* GLI2 promoter hypermethylation in saliva of children with a respiratory allergy. *Clin Epigenetics* **10**, 50 (2018). https://doi.org/10.1186/s13148-018-0484-1
72 Janssen, B. G. *et al.* Cohort Profile: The ENVIRonmental influence ON early AGEing (ENVIRONAGE): a birth cohort study. *Int J Epidemiol* **46**, 1386-1387m (2017). https://doi.org/10.1093/ije/dyw269
73 Ho, D. E., Imai, K., King, G. & Stuart, E. A. MatchIt: Nonparametric Preprocessing for Parametric Causal Inference. *Journal of Statistical Software* **42**, 1-28 (2011).
74 Edgar, R., Domrachev, M. & Lash, A. E. Gene Expression Omnibus: NCBI gene expression and hybridization array data repository. *Nucleic Acids Res* **30**, 207-210 (2002). https://doi.org/10.1093/nar/30.1.207

Supplementary Materials

Supplementary figure 1 | DNA methylation at individual CpG sites in participants without pregnancy complication

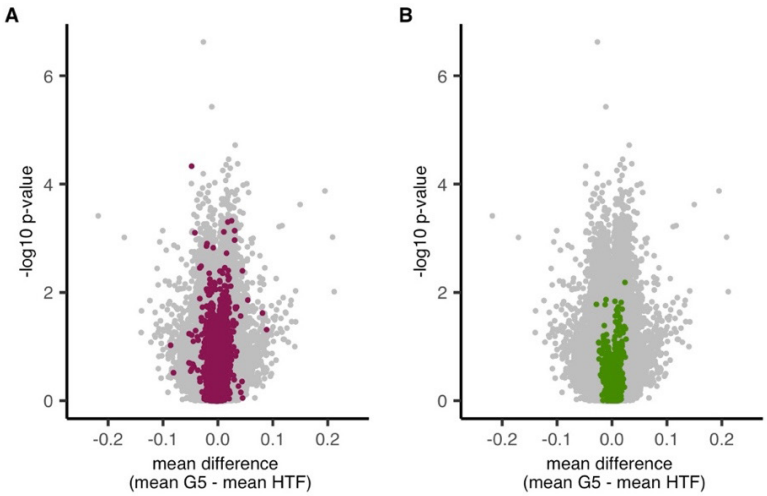

*Volcano plots showing differential methylation between G5 and HTF neonates at all individual CpG sites (grey dots, **A&B**). Samples from neonates whose were pregnancies complicated by gestational diabetes, hypertension or preeclampsia were excluded. Highlighted in purple are CpG sites within imprinted genes (**A**) and in green are birth weight associated CpG sites (**B**). No sites were significantly differentially methylated (false discovery rate (FDR) adjusted p-value <0.1) between the culture medium groups.*

Supplementary figure 2 | Regional DNA methylation in participants without pregnancy complications

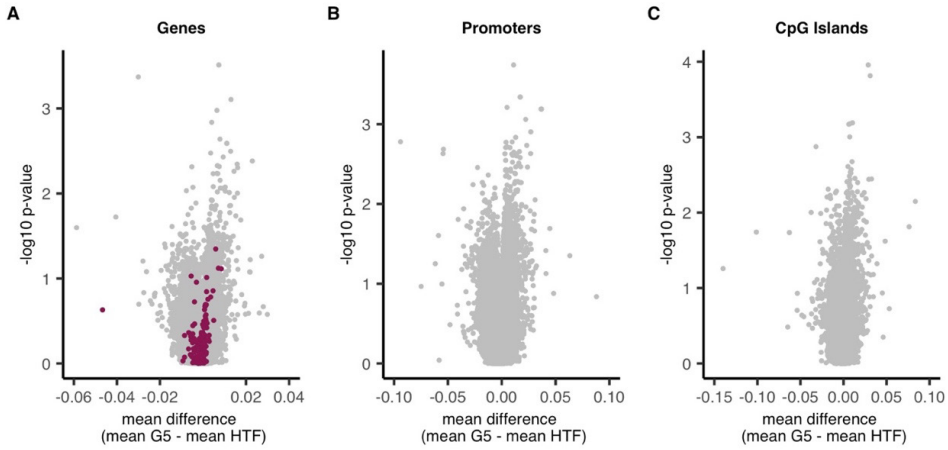

Volcano plots showing differential methylation between G5 and HTF neonates at multiple sites aggregated into regions: by gene (A), by allocation to distinct promoters (B) and by allocation to distinct CGIs (C). Samples from neonates whose were pregnancies complicated by gestational diabetes, hypertension or preeclampsia were excluded. Highlighted in purple are imprinted genes (A). No regions were significantly differentially methylated (false discovery rate (FDR) adjusted p-value <0.1) between the culture medium groups.

Supplementary figure 3 | Methylation outliers in samples without pregnancy complications

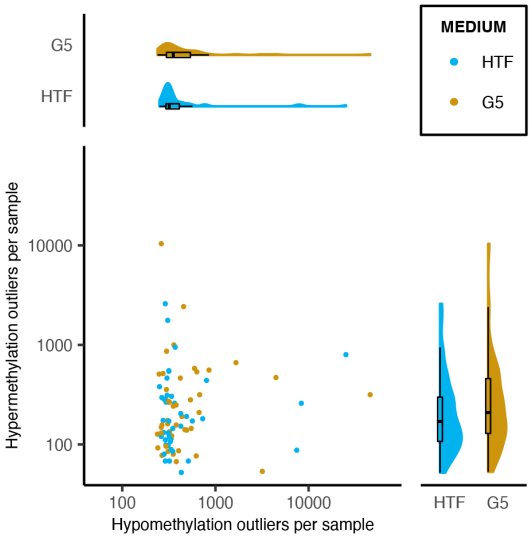

The main panel shows the number of hypomethylation (x-axis) and hypermethylation (y-axis) outliers per UCB sample (G5 = gold, HTF = blue). Distribution summaries, in the form of a density plot and boxplot, are shown for hypomethylation outliers and hypermethylation outliers in the top and right side-panels respectively. Lines of the boxplot represent the 25th percentile, median and 75th percentile respectively while the whiskers extend to the farthest data point that is no more than 1.5 times the IQR from the upper or lower quartile. The axes are shown on a log10 scale. The groups were not found to be significantly different (p-value >0.1).

Supplementary figure 4 | Epigenetic gestational age acceleration

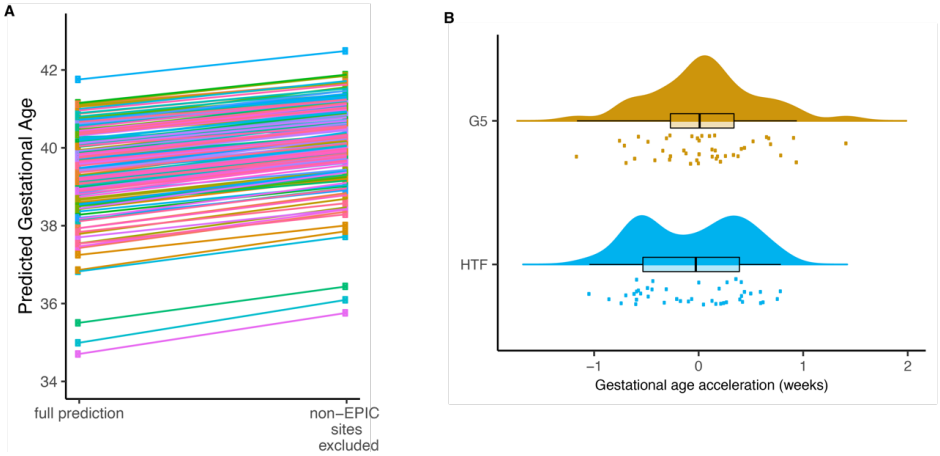

*(**A**) Prediction of epigenetic gestational age using the Bohlin method on 450K data from the ENVIRONAGE cohort (n = 159). Data points on the left show the prediction including all the specified sites, points on the right represent the predictions from the same samples when the 8 CpG sites that are not present on the EPIC array are excluded. (**B**) Raincloud plot showing the total number of outliers per umbilical cord blood (UCB) sample in each culture medium group when participants with pregnancy complications were excluded. Points represent individual samples of the G5 (gold) and HTF (blue) group. Above a density plot and boxplot is shown. Horizontal lines of the boxplot represent that 25th percentile, median and 75th percentile respectively while the whiskers extend to the farthest data point that is no more than 1.5 times the IQR from the upper or lower quartile. GAA is represented in weeks. The groups were not found to be significantly different (p-value >0.1).*

Supplementary figure 5 | Processing of UCB methylome data from naturally conceived neonates from the FLEHS and ENVIRONAGE cohorts

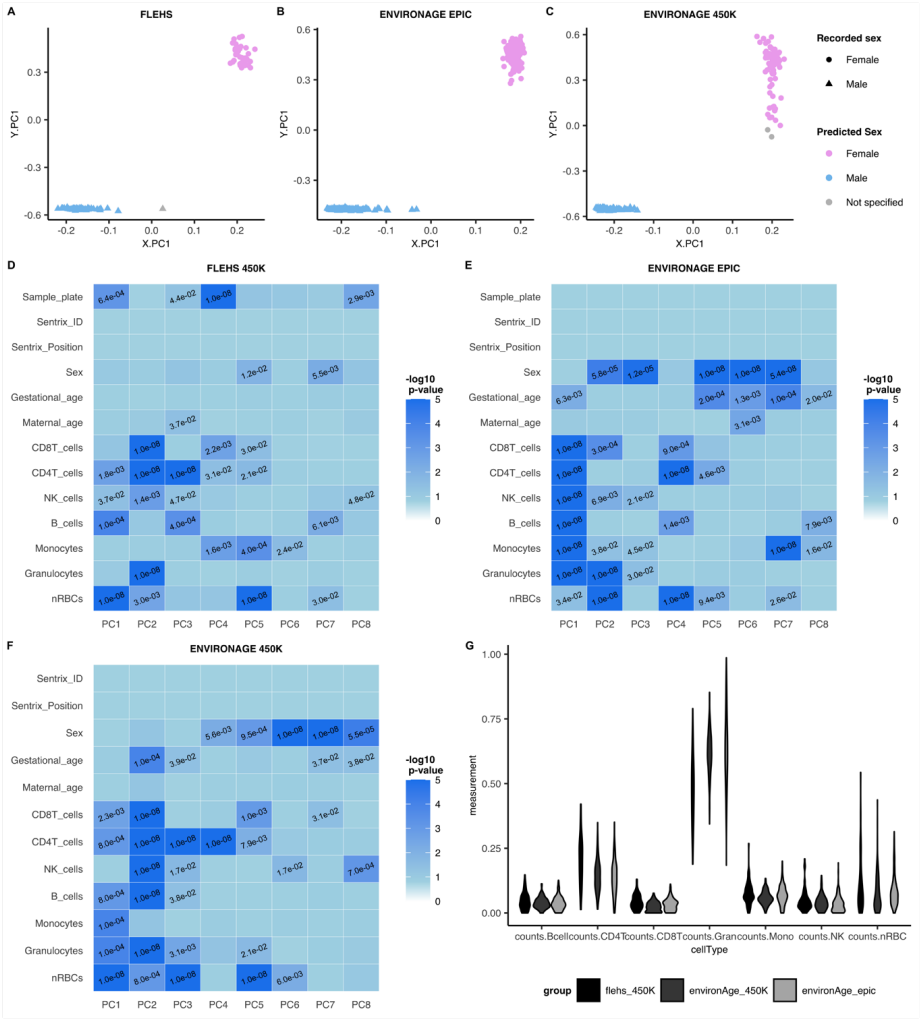

*(**A-C**) Scatter plots showing the projection of UCB samples (FLEHS 450K **(A)**, ENVIRONAGE 450K **(B)**, ENVIRONAGE EPIC **(C)**) into the principal component (PC) space generated using reference data for sex prediction. The shape of the dots represents the recorded sex of the participants (circles = female, triangle = male), while the colour shows the predicted sex based on results from sEST (blue = male, pink = female, grey = not specified). (**D-F**) Heatmaps showing associations between the principal components and biological/ technical aspects of the samples (FLEHS 450K **(D)**, ENVIRONAGE 450K **(E)**, ENVIRONAGE EPIC **(F)**). The*

*colour gradient represents the -log10 of the p-values. P-values that are <0.05 are shown. Significance of the correlation between continuous variables and the 8 principal components (PCs) was tested using a permutation test with 10,000 permutations. The associations of the PCs with variables creating 2 groups (and those creating 3 or more groups were tested using two-sided Wilcoxon rank tests and Kruskall-Wallis one-way analysis of variance respectively. (**G**) Violin plot showing the predicted cellular composition of the UCB samples, split by cohort and array type. (**H**) Overview of the data processing procedure showing the number of samples from each cohort excluded at each step, the batch effects that were pre-corrected using ComBat and the data included in the final dataset.*

Supplementary figure 6 | Comparison of IVF and naturally conceived individuals

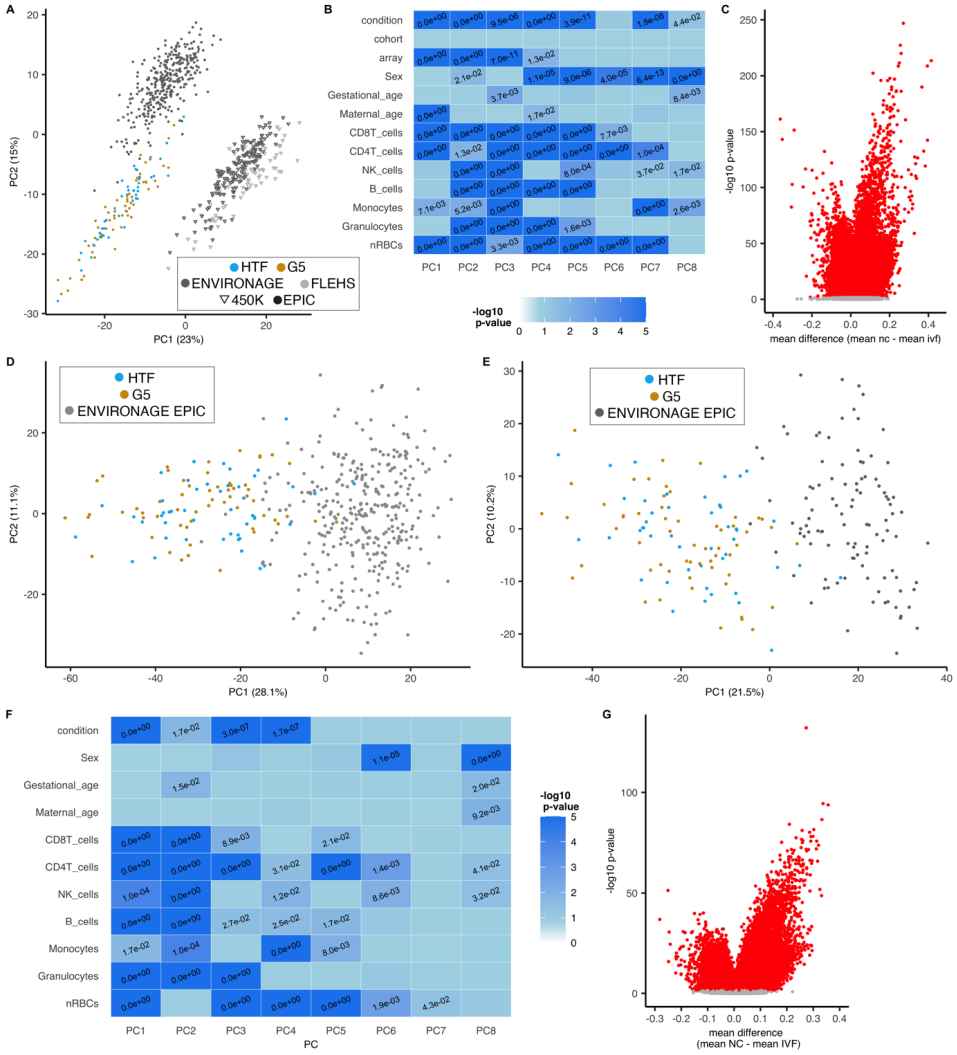

*(**A**) PCA including CpG sites that are present on the EPIC and 450K array and passed the QC criteria in all three studies that analysed the methylome of UCB samples: IVF study (G5 = gold, HTF = blue) and two studies that collected samples from naturally conceived neonates (ENVIRONAGE = dark grey, FLEHS = light grey). The shapes represent the array used to profile the samples (EPIC = dots, 450K = triangles). (**B**) Heatmap showing associations between the principal components and biological/technical aspects of the samples shown in **A** (n = 584 naturally conceived, n = 105 IVF). The colour gradient represents the -log10 of the p-values. P-values that are <0.05 are shown. Significance of the correlation between continuous variables and the 8 principal components (PCs) was tested using a permutation test with 10,000 permutations. The associations of the PCs with variables creating 2 groups and those creating 3 or more groups were tested using two-sided Wilcoxon rank tests and Kruskall-Wallis one-way analysis of variance respectively. (**C**) Volcano plots showing differential methylation between naturally conceived (n = 584) and IVF neonates (n = 105) at individual CpG sites (n = 346,403). (**D**) PCA including high quality CpG sites overlapping in IVF (n*

*= 105, blue and gold) and ENVIRONAGE EPIC (n = 341, grey) samples. (**E**) PCA including high quality CpG sites overlapping in IVF (n = 105, blue and gold) and matched ENVIRONAGE EPIC (n = 105, grey) samples. (**F**) Volcano plot showing differential methylation between IVF (n = 105) and matched naturally conceived (n = 105) neonates from the ENVIRONAGE study analysed with the EPIC array. Individual CpG sites (n = 671,145) are shown. All PCA plots show the first two PCs, with the variance explained by each shown in brackets. Volcano plots show significantly differentially methylated sites/regions (FDR adjusted p-value <0.05) in red and all other sites/regions in grey.*

Supplementary table 1 | Extended characteristics.

Characteristic	Culture Medium		P-value
	G5 (*n* = 59)	HTF (*n* = 47)	
Maternal characteristics			
Pre-pregnancy BMI	23.8 ± 3.5	24.5 ± 4.3	0.371
Paternal characteristics			
Age (years)	33.1 ± 3.6	33.1 ± 3.7	0.995
BMI	25.4 ± 3.3	26.0 ± 3.0	0.295
Fertility treatment			
IVF treatment centre			0.659
Amsterdam	4	5	
Groningen	6	5	
Maastricht	26	23	
Tilburg	9	3	
Eindhoven	14	11	
Egg donation (yes)	0	0	1.000
Sperm donation (yes)	1	0	1.000

Continuous variables shown as mean ± SD, categorical variables shown as n (%).

Supplementary table 2 | Variance explained by PCs 1-8 of global methylation PCA analysis

PC	Variance explained (%)
1	24.3
2	8.5
3	5.0
4	3.2
5	1.8
6	1.5
7	1.2
8	1.2
Total:	46.7

Supplementary table 3 | Association between number of outliers and sample features.

	Hypomethylation outliers		Hypermethylation outliers		Total number of outliers	
Feature	**Correlation**	**Significance**	**Correlation**	**Significance**	**Correlation**	**Significance**
Gestational age	-0.03	0.772	0.07	0.511	-0.01	0.900
Birth weight	0.01	0.942	-0.07	0.462	-0.01	0.911
Maternal age	0.03	0.783	-0.06	0.517	0.01	0.913
CD8T cells	**0.24**	**0.014**	0.12	0.120	**0.26**	**0.007**
CD4T cells	-0.13	0.167	0.03	0.756	-0.12	0.206
B cells	0.18	0.060	0.18	0.060	0.22	**0.019**
NK cells	**0.33**	**0.002**	**0.20**	**0.049**	**0.37**	**0.001**
Monocytes	0.17	0.067	0.06	0.567	0.19	0.054
Granulocytes	**-0.36**	**0.000**	-0.15	0.119	**-0.39**	**0.000**
nRBCs	0.05	0.567	-0.04	0.693	0.04	0.639
Sample plate*		**0.000**		**0.597**		**0.007**

NK = natural killer, nRBCs = nucleated red blood cells. Correlations shown are Pearson correlations and significance was tested with permutation tests (1000 permutation)
** significance tested with two-sided Wilcoxon rank test.*

Supplementary table 4 | Association between number of outliers and sample features in participants without pregnancy complications

	Hypomethylation outliers		Hypermethylation outliers		Total number of outliers	
Feature	**Correlation**	**Significance**	**Correlation**	**Significance**	**Correlation**	**Significance**
Gestational age	-0.03	0.75	0.05	0.65	-0.02	0.83
Birth weight	-0.01	0.90	-0.10	0.38	-0.03	0.77
Maternal age	0.04	0.71	-0.07	0.49	0.02	0.82
CD8T cells	**0.24**	**0.03**	0.12	0.26	**0.26**	**0.02**
CD4T cells	-0.16	0.10	0.04	0.70	-0.15	0.14
B cells	0.18	0.09	0.19	0.06	**0.22**	**0.03**
NK cells	**0.36**	**0.00**	**0.23**	**0.04**	**0.40**	**0.00**
Monocytes	0.17	0.11	0.04	0.72	0.17	0.10
Granulocytes	**-0.40**	**0.00**	-0.19	0.06	**-0.43**	**0.00**
nRBCs	0.13	0.19	-0.00	1.00	0.13	0.20
Sample plate*		**0.00**		0.73		**0.01**

NK = natural killer, nRBCs = nucleated red blood cells. Correlations shown are Pearson correlations and significance was tested with permutation tests (1000 permutation)
** significance tested with two-sided Wilcoxon rank test.*

Supplementary Table 5 | Differentially variable sites identified by iEVORA *(see the excel file in the online version of the article).*
*Differentially variable sites between the culture medium groups as identified by the iEVORA algorithm when applied to the full cohort (**Table sheet 1**) and when applied only on samples without pregnancy complications (**Table sheet 2**). Sites identified by both analyses are shown in **Table sheet 3**. Nominally significant GO enrichments for the iEVORA sites from the full cohort and the samples without pregnancy complications are shown in **Table sheet 4** and **Table sheet 5**, respectively. Nominally significantly enriched KEGG pathways for the iEVORA sites from the full cohort and the samples without pregnancy complications are shown in **Table sheet 6** and **Table sheet 7**, respectively.*

Supplementary Table 6 | Characteristics of naturally conceived and IVF neonates

Characteristic	FLEHS	ENVIRONAGE			IVF	Matched IVF-EPIC p-value
	450K (*n* = 84)	450K (*n* = 159)	EPIC (*n* = 341)	Matched EPIC (*n* = 105)	G5 & HTF (*n* = 105)	
Maternal characteristics						
Age (years)	28.8 ± 3.8	29.5 ± 4.5	30.2 ± 4.3	32.3 ± 3.5	33.1 ± 3.6	0.477
Nulliparous	54 (64)	80 (50)	179 (52)	46 (43.8)	77 (73.3)	**2.8e^{-06}**
Pregnancy characteristics						
Pregnancy complication						0.851
Diabetes	NA	4 (3)	16 (5)	10 (9.5)	3 (2.9)	
Hypertension	NA	13 (8)	10 (3)	4 (3.8)	10 (9.5)	
Preeclampsia	NA	3 (2)	4 (1)	2 (1.9)	5 (4.8)	
Neonatal outcomes						
Sex (female)	39 (46)	75 (47)	179 (52)	54 (51.4)	54 (51.4)	1.000
Gestational age at birth (completed weeks)	39.3 ± 1.1	39.3 ± 1.2	39.3 ± 1.2	39.2 ± 1.2	39.2 ± 1.3	0.957
Birth weight (g)	3391 ± 459	3433 ± 477	3430 ± 425	3425 ± 416	3426 ± 448	0.982

Continuous variables shown as mean ± SD, categorical variables shown as n (%).

Chapter 3

At age 9, the methylome of assisted reproductive technology children that underwent embryo culture in different media is not significantly different on a genome-wide scale

---

Rebekka M. Koeck, Florence Busato, Jorg Tost, Heleen Zandstra, Sylvie Remy, Sabine Langie, Marij Gielen, Ron van Golde, John C. M. Dumoulin, Han Brunner, Masoud Zamani Esteki*, Aafke P. A. van Montfoort*

*** Joint last authors**

My contribution: all data processing, analysis, and visualisation as well as writing and editing the full text.

Adapted from R.M. Koeck, F. Busato, J. Tost, H. Zandstra, S. Remy, S. Langie, M. Gielen, R. van Golde, J.C.M. Dumoulin, H.Brunner, M. Zamani Esteki, A.P.A. van Montfoort. At age 9, the methylome of assisted reproductive technology children that underwent embryo culture in different media is not significantly different on a genome-wide scale. Hum Reprod. (2022) 37(11):2709-2721. https://doi.org/10.1093/humrep/deac213

Abstract

Study question
Can we detect DNA methylation differences between ART children that underwent embryo culture in different media?

Summary answer
We identified no significant differences in site-specific or regional DNA methylation between the different culture medium groups.

What is known already
Embryo culture in G3 or K-SICM medium leads to differences in embryonic, neonatal and childhood outcomes, including growth and weight. The methylome may mediate this association as the period of in vitro culture of ART treatments coincides with epigenetic reprogramming.

Study design, size, duration
This study was conducted as a follow-up to a previous culture medium comparison study in which couples were pseudo-randomized to embryo culture in G3 or K-SICM medium. Of the resultant singletons, 120 (n = 65 G3, n = 55 K-SICM), were recruited at age 9.

Participants/materials, setting, methods
The ART children provided a saliva sample from which the methylome was analysed using the Infinium MethylationEPIC array. After quality and context filtering, 106 (n = 57 G3, n = 49 K-SICM) samples and 659708 sites were retained for the analyses. Differential methylation analyses were conducted using mixed effects linear models corrected for age, sex, sample plate and cell composition. These were applied to all cytosine-guanine dinucleotide (CpG) sites, various genomic regions (genes, promoters, CpG Islands (CGIs)) and as a targeted analysis of imprinted genes and birth weight-associated CpG sites. Differential variance was assessed using the improved epigenetic variable outliers for risk prediction analysis (iEVORA) algorithm and methylation outliers were identified using a previously defined threshold (upper or lower quartile plus or minus three times the interquartile range, respectively).

Main results and the role of chance
After correcting for multiple testing, we did not identify any significantly differentially methylated CpG sites, genes, promoters or CGIs between G3 and K-SICM children despite a lenient corrected P-value threshold of 0.1. Targeted analyses of (sites within) imprinted genes and birth weight-associated sites also did not identify any significant differences. The number of DNA methylation outliers per sample was comparable

between the culture medium groups. iEVORA identified 101 differentially variable CpG sites of which 94 were more variable in the G3 group.

Large scale data
Gene Expression Omnibus (GEO) GSE196432

Limitations, reasons for caution
To detect significant methylation differences with a magnitude of <10% between the groups many more participants would be necessary; however, the clinical relevance of such small differences is unclear.

Wider implications of the findings
The results of this study are reassuring, suggesting that if there is an effect of the culture medium on DNA methylation (and methylation-mediated diseases risk), it does not differ between the two media investigated here. The findings concur with other methylome studies of ART neonates and children that underwent embryo culture in different media, which also found no significant methylome differences.

Study funding/competing interest(s)
Study funded by March of Dimes (6-FY13-153), EVA (Erfelijkheid Voortplanting & Aanleg) specialty programme (grant no. KP111513) of Maastricht University Medical Centre (MUMC+) and the Horizon 2020 innovation (ERIN) (grant no. EU952516) of the European Commission. The authors do not report any conflicts of interest relevant to this study.

Trial registration number
Dutch Trial register—NL4083

Introduction

Year-on-year a worldwide increase in the number of ART procedures has led to the birth of more than 8 million babies[1] and currently, ~3% of births in European countries are conceived through ART[2]. Even though most ART children appear healthy at birth, follow-up studies have reliably shown that, compared to their naturally conceived counterparts, ART offspring are at increased risk of adverse perinatal[3], childhood and later life outcomes[4,5]. The perinatal risks include premature birth, low birth weight, being small for gestational age and perinatal mortality[3], while the later life outcomes relate mainly to cardiometabolic health, including weight[4-7]. Specifically, the affected cardiometabolic parameters include an increase in both systolic and diastolic blood pressure[6] and features of cardiovascular dysfunction, such as suboptimal cardiac diastolic function and increased blood vessel thickness[6]. Additionally, ART children have been shown to have significantly lower weights than their naturally conceived counterparts from birth until the age of 4[7]. These observations are in line with the developmental origins of health and disease (DOHaD) paradigm, which states that early life adversity predisposes an individual to disease in later life[8], therefore raising concerns about the impact of ART procedures on the resultant children.

During ART treatments, embryos undergo *in vitro* culture for 2–5 days prior to intrauterine transfer to establish a pregnancy. Throughout this time, embryos are exposed to an artificial *in vitro* environment consisting of the culture medium, the atmospheric conditions (oxygen levels) and laboratory-specific factors, such as laboratory plastics. Over time, a number of compositionally different culture media have been used for ART procedures[9-12] and these have been associated with differences in short- and long-term outcomes of the resultant offspring both in animal and human studies[13-17]. We previously conducted a culture medium trial, in which couples undergoing ART treatments in Maastricht were pseudo-randomized, by strict alternation, to embryo culture in G3 (Vitrolife) or Sydney IVF cleavage medium (K-SICM, Cook). Although several components of these culture media are known, their precise concentrations and composition are not fully disclosed by the manufacturers. However, a possible difference between G3 and K-SICM is that the version of K-SICM used for the treatments described in these studies, contained an unstable form of the amino acid glutamine (according to product inserts from the media in this period), while G3 contained a more stable dipeptide form of the same amino acid. Several studies have shown that ammonium accumulation during storage of media containing the unstable form of glutamine is significantly higher[18] and that an increased ammonium concentration in culture medium has an adverse effect on embryonic development[19,20]. Embryos cultured in G3 were found to have a greater number of cells, while their morphological grade was lower than K-SICM embryos[21]. Thereafter, implantation and pregnancy rates were higher

in the G3 group[21]. Interestingly, growth differences, namely increased growth in the G3 group, could already be detected by ultrasound in the second trimester[22], were evident at birth[21,23] and persisted at age 2 (weight)[24] and age 9[25]. At age 9, children from the G3 group remained heavier with higher waist circumferences and truncal adiposity than children from the K-SICM group[25]. Other markers of cardiovascular health, including blood pressure, lipid profile and endothelial function, were comparable between the culture medium groups[25]. Similarly, cognitive development was comparable between the culture medium groups[26].

To date, the molecular mechanisms mediating the relationship between culture medium composition and the observed outcomes are not fully understood. It has been suggested that the epigenome, and specifically DNA methylation in which a methyl (-CH_3) group is added to the cytosine base of cytosine-guanine dinucleotides (CpG), is sensitive to environmental perturbations and subsequently 'programs' an individual's disease susceptibility[27]. Furthermore, pre-implantation human embryos are undergoing epigenetic reprogramming, consisting of virtually complete erasure and re-establishment of DNA methylation marks[28,29], during which they may be especially sensitive to environmental regulation of the epigenome. DNA methylation-associated imprinting disorders, although still rare, are also more common amongst IVF children[30]. Consequently, methylome profiling of ART offspring born after culture medium trials has been carried out. For instance, our group examined DNA methylation in tissues collected at birth, namely the placenta[31] and umbilical cord blood[32], from neonates born after a multicentre randomized controlled trial comparing G5 (Vitrolife) and human tubal fluid (HTF, Lonza) media. Neither study identified any significant DNA methylation differences between the culture medium groups and the group mean differences at the sites analysed were small (largely <10%)[31,32]. Interestingly, we identified several CpG sites with differential variability between the culture medium groups[32]. These could relate to prenatal factors, such as the pregnancy complications, only experienced by some individuals in each group, alternatively, they could represent epigenetic marks indicative of disease that only some individuals will develop later in life. To investigate this further, later life or longitudinal methylome studies of ART offspring are required. Thus far, the methylome of ART children (age 7 or 8) has only been characterized in one cohort, in the context of a culture medium trial (global medium—LifeGlobal vs single-step medium—Irvine Scientific), finding no significant DNA methylation differences, and small intragroup differences (mostly <10%)[33,34].

Not in the context of culture media trials, the methylome has also been compared between ART and naturally conceived offspring and such studies were the focus of a recent meta-analysis[35]. In neonates, the meta-analysis only identified consistent differential methylation at the paternally expressed gene 1/mesoderm specific

transcript (*PEG1/MEST*) imprinting gene locus when including all targeted methylome studies of placenta and cord blood samples[35]. The findings from genome-wide analyses conducted on samples collected during the neonatal period have yielded contradictory result, with some studies identifying differentially methylated sites, while other studies found no differences[35-38]. In children, on the other hand, the meta-analysis of targeted methylation studies on blood and saliva samples, identified no significant differences between ART and naturally conceived individuals[35]. Similarly, genome-wide studies comparing ART and naturally conceived children[34,39], adolescents[40] or adults[41], found no or few significant differences. Although this suggests that any ART-associated methylation differences present at birth do not persist into adulthood, these results come from a small number of studies that have not been validated by other groups. Additionally, the studies lack a detailed description of the ART culture conditions that these individuals were exposed to, meaning that their effect on the methylome cannot be established. As already described, clinical differences are observed between ART offspring that were exposed to different culture environments, highlighting the need to specifically examine the methylomes of these ART sub-groups.

Here, we describe the saliva methylome of ART children (aged 9 or 10) that underwent embryo culture either in G3 (Vitrolife) or K-SICM (Cook) media. For this, we profiled DNA methylation on a genome-wide scale, using the EPIC array, in the largest cohort of its kind to date. Comparison to naturally conceived children was attempted using data from the Flemish Environment Health Study (FLEHS) (**Fig. 1A**).

Figure 1 | Genome-wide DNA methylation analysis of ART children that underwent embryo culture in different media revealed no significant differences

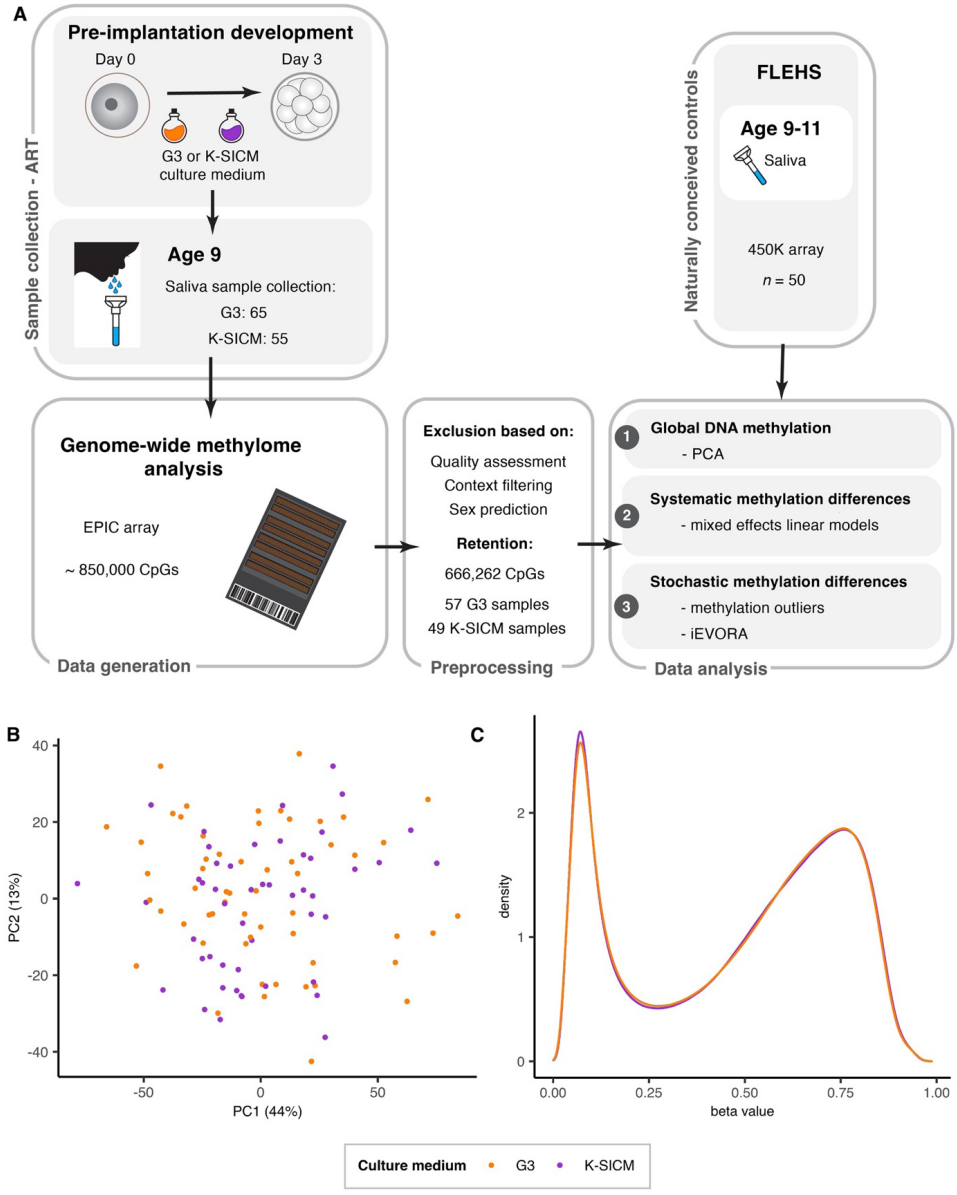

*(**A**) Schematic overview showing sample collection/inclusion of ART-conceived and naturally conceived children, methylome data generation alongside data processing and analyses included in this study. (**B**) Principal component analysis (PCA) of all cytosine-guanine dinucleotide (CpG) sites passing our quality control criteria in data from saliva samples of ART children that underwent embryo culture in G3 (orange) or Sydney IVF cleavage medium (K-SICM, purple) medium. (**C**) Density plot showing the distribution of beta values from all sites and samples within each group (G3 = orange, K-SICM = purple).*

Materials and methods

Ethical approval

This study was registered in the Dutch Trial register (trial number NL4083) and was approved by the ethical review board of the Maastricht University Medical Centre (MUMC+). Both parents of the children provided written, informed consent.

Study population and sample collection

Samples for methylome analysis were collected during medical follow-up of children born after a previously conducted culture medium comparison study[25]. Between July 2003 and December 2006, Vitrolife G1™ Version 3 (G3) (Göteborg, Sweden) and K-SICM from Cook (Brisbane, Australia) were used at MUMC+. Consecutive IVF treatments (with or without ICSI) were strictly alternated between the two media types, while all other ART procedures remained consistent[21,23]. Parents of all liveborn singletons from this study were approached for a follow-up investigation after the 9th birthday of the child. In addition to growth and cardiometabolic measurements, 2 ml of saliva were collected using the Saliva DNA Collection, Preservation and Isolation Kit (Norgen Biotek, Thorold, Canada). The saliva samples were collected after an overnight fast (necessary for blood glucose measurements) and after the children had rinsed their mouths with water. Subsequently, the preservation liquid was added to the tube and the samples were stored at room temperature, according to the manufacturer's instructions.

DNA extraction

DNA was extracted using the Saliva DNA Collection, Preservation and Isolation Kit (Norgen Biotek, Thorold, Canada) according to the manufacturer's instructions. Briefly, 2 ml of preserved saliva was mixed with 80 µl of proteinase K, 800 µl of Binding buffer B and 2.88 ml of isopropanol. After centrifugation, the resulting DNA pellet was washed in 70% ethanol and air-dried. The pellet was rehydrated in 300 µl of Tris–EDTA buffer. DNA quantity and quality were determined using a Nanodrop ND-1000 spectrophotometer (Nanodrop Technologies, Wilmington, USA).

Bisulfite conversion and DNA methylation profiling by EPIC array

Prior to DNA quantification, DNA samples containing precipitated material were heated to 65°C and centrifuged. Thereafter, 1 µg of DNA was bisulfite-treated using the EpiTect® Fast 96 DNA Bisulfite Kit (Qiagen Hilden, Germany) and analysed using the Infinium Human MethylationEPIC BeadChip Kit (Illumina, CA, USA) according to the manufacturer's protocol.

Data analysis

All data analysis was conducted using R (version 3.6.3)[42] and visualized using the ggplot2 and ComplexHeatmap packages[43]. Custom R code used for the processing

and analysis of the data described in this article are available at https://github.com/CellularGenomicMedicine/saliva_methylome.

Participant characteristics

The participant characteristics were compared for differences between the culture medium groups using Student's *t*-tests for continuous variables and Pearson's chi-squared tests for categorical variables.

Quality control and pre-processing

Data were pre-processed using pre-processing functions contained within the RnBeads package[44]. Data were normalized using the subset-quantile within array normalization (SWAN) method[45]. Poor quality probes and samples were removed using the greedycut algorithm with a detection *P*-value threshold of 0.05. Sites were further filtered out based on the following criteria: (i) if they were located on the sex chromosomes, (ii) if they were in close proximity to single-nucleotide polymorphisms, (iii) if more than 5% of the samples contained missing values and (iv) if they were not in a CpG context. Sites containing any missing values (between 0% and 5% missing values) were only used to aggregate sites into regions, they were excluded for all single site-based analyses. Unless indicated otherwise, we used methylation beta values which represent the methylated signal divided by the sum of the methylated and unmethylated signal at each CpG site. Sample sex prediction was carried out as described by Jung *et al.*[46] and implemented in the sEst package. Briefly, the X and Y chromosome beta value distributions of the test (ART) samples were combined with those of the reference male and female samples[46]. Subsequently, a principal component analysis (PCA) was conducted separately for each sex chromosome (referred to as PCA.X and PCA.Y). Then, k-means clustering (number of groups = 2) was conducted on the results from PCA.X and PCA.Y to determine if the test (ART) samples cluster with the female or male samples of the reference samples, respectively. When the k-means clustering for both sex chromosomes assigned the same sex, samples were labelled as male or female, all other samples were labelled 'not specified'. The X principal component (PC)1 threshold, to distinguishing between the presence of one or two X chromosomes, was set at 0.05. Principal component PC1 of the PCA.X and PCA.Y are shown in **Fig. 2A** and **Supplementary Fig. 1A**, without showing the reference samples that were analysed alongside the test (ART) samples.

Cellular deconvolution of saliva samples

Cell composition of the samples was estimated using the reference-based Houseman algorithm[47] implemented using the ewastools package[48]. Probes for cell-type deconvolution were identified using DNA methylation signatures from sorted saliva samples collected from children[49] (available at Gene Expression Omnibus GSE147318) yielding an estimate of the proportion of leucocytes and epithelial cells.

Figure 2 | Preprocessing of saliva methylome data

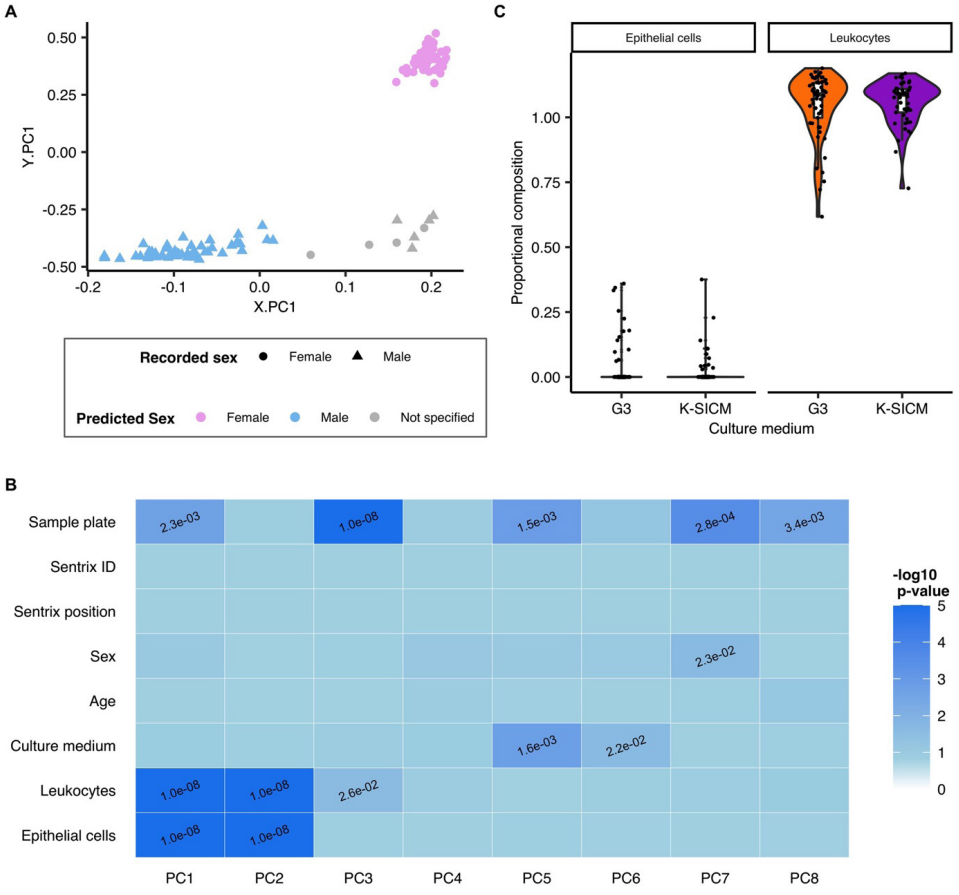

*(**A**) Scatter plot showing the projection of high-quality saliva samples (n = 106) into the principal component (PC) space generated using reference data for sex prediction. The shape of the dots represents the recorded sex of the participants (circles = female, triangle = male), while the colour shows the predicted sex based on results from sEst (blue = male, pink = female, grey = not specified). (**B**) Heatmap showing associations between the PCs and biological/technical aspects of the samples. The colour gradient represents the -log$_{10}$ of the P-values. P-values that are <0.05 are shown. (**C**) Violin plot showing the predicted cellular composition of the saliva samples, split by cell type (leucocytes and epithelial cells) and culture medium group (orange and purple represent G3 and Sydney IVF cleavage medium (K-SICM) respectively). The violin plots are overlaid with boxplots where the horizontal lines represent the 25th percentile, median and 75th percentile, respectively, while the whiskers extend to the farthest data points that are no more than 1.5 times the interquartile range (IQR) from the upper or lower quartile.*

Comparison of G3 and K-SICM children

We applied PCA on all high-quality CpG sites. The beta values were centred but not scaled for the PCA. Associations between the PCs and technical or demographic features of our samples were tested either (i) using permutation tests with 10000 permutations to

determine the significance of correlations (age, leucocytes, epithelial cells), (ii) using a two-sided Wilcoxon rank test for categorical variables creating two groups (sex, culture medium, sample plate) or (iii) using a Kruskal–Wallis one-way ANOVA for categorical variables generating three or more groups (Sentrix ID, Sentrix position—chip number and sample position, respectively).

Methylation *M*-values, representing the log2 ratio of the methylated probe intensity compared to the unmethylated probe intensity[50], were used to test for associations between DNA methylation and culture medium using mixed effects linear models implemented with the variancePartition package[51]. The models were adjusted for *a priori* chosen potential confounders: age at sample collection, sex and cell composition as fixed effects alongside batch correction (sample plate) as a random effect. They were applied to individual CpG sites or aggregate values of multiple CpG sites to identify differentially methylated positions (DMPs) and differentially methylated regions (DMRs), respectively. To aggregate sites into regions, we calculated the mean of all the beta values from probes attributed to the same gene, promoter or CpG island (CGI). For the targeted analyses, the aforementioned models were applied to (sites within) imprinted genes[52] and sites associated with birth weight[53]. The Benjamini–Hochberg[54] method was used to correct all analyses for multiple testing, and an adjusted *P*-value of <0.1 was considered significant.

DNA methylation outliers were defined as previously described by[55]. Briefly, hypomethylation outliers were defined as beta values more than three interquartile ranges (IQRs) below the 25th percentile, while hypermethylation outliers were defined as beta values more than three IQRs above the 75th percentile. The IQR and percentile thresholds were calculated across all saliva samples. We tested for associations between the log10 transformed number of outliers and culture medium using the mixed effects linear models described above. The significance of associations between the number of outliers per sample and various clinical and technical features were assessed using permutation tests with 10000 permutations for continuous variables (age and weight at sample collection, birth weight, leucocyte proportion, epithelial cell proportion) and with two-sided Wilcoxon rank tests for categorical variables (sample plate). To identify differentially variable sites, the improved epigenetic variable outliers for risk prediction analysis (iEVORA) algorithm[56] was applied using the matrixTests package[57]. In brief, iEVORA applies Bartlett's test, a parametric test for differential variance, and a Student's *t*-test to each CpG site. Subsequently, sites reaching significance after multiple testing correction (false discovery rate (FDR) corrected *P*-value < 0.05) of the Bartlett's test and reaching nominal significance (*P*-value < 0.05 without multiple testing correction) of the *t*-test are considered significant. This approach regularizes the result of the Bartlett's test which is usually overly sensitive to single outliers. The resulting

differentially variable sites were used for Gene ontology (GO) and Kyoto Encyclopedia of Genes and Genomes (KEGG) pathway enrichment analyses using functionality from the missMethyl package[58].

Comparison with naturally conceived children

Saliva methylome data were obtained from children enrolled in the longitudinal birth cohort FLEHS; the cohort has previously been described in detail[59,60]. From these children, saliva samples were collected at the age of 10–11 and the methylome was profiled using the 450K array (Illumina, CA, USA). Data preprocessing and the analysis procedures were largely the same as those described above, for more details see the **Supplementary materials and methods**.

Results

Of the 294 ART singletons from the culture medium study, 136 (48%) parent couples agreed for their child to participate. Three of the children failed or refused to provide 2 ml of saliva, a further 7 samples yielded insufficient DNA for processing and 6 samples did not meet quality criteria after bisulfite conversion. Therefore, methylome analysis by EPIC array was carried out on 120 saliva samples (n = 65 for G3, n = 55 for K-SICM). Quality control procedures on the generated data led to the exclusion of 5 poor quality samples (n = 3 for G3 and n = 2 for K-SICM) and 9 samples (n = 5 for G3 and n = 4 for K-SICM) with an undefined sex prediction (**Fig. 2A**). The characteristics of both groups were comparable (**Table 1**). Although the weight of G3 offspring at birth[21] and age 9[25] was reported to be higher than that of K-SICM offspring in the culture medium trial, these parameters were not significantly different in this sub-group of the original study. Nonetheless, the trend is the same.

Of ~850000 profiled CpG sites, 666262 were retained for analysis after the filtering procedures, of which 659708 sites contained no missing values and were used for downstream analysis.

Global analysis of DNA methylation

Global DNA methylation was first assessed by PCA (**Fig. 1B**), which did not show clear separation of the G3 and K-SICM groups within the first 4 PCs, which explain 49% of the variance in our data. Only PCs 5 and 6, representing 5.2% and 4.8% of the variance in our data, respectively, were significantly associated with the culture medium (**Fig. 2B**), thus suggesting that the culture medium is not the main source of variance within our data. Other significant associations were found between some of the first 8 PCs and certain technical or demographic factors, namely sample plate (PC1, PC3, PC5, PC7,

PC8), sex (PC7), leucocytes (PC1-3) and epithelial cells (PC1, 2) (**Fig. 2B and C**). These factors are therefore corrected for in the subsequent analyses. Similarly, the distribution of beta values was very similar in both culture medium groups (**Fig. 1C**).

Analysis of DNA methylation at individual CpG sites

We assessed the association of DNA methylation with culture medium at all individual CpG sites using mixed effects linear models corrected for potential confounders. We found no significant DMPs between the two culture medium groups after adjusting for multiple testing (adjusted *P*-value < 0.1) (**Fig. 3A, Supplementary Figs 2A, 3**). Additionally, the group mean differences at all sites were small, with <1% of sites (17 in total) having a group mean difference of more than 10% and the maximum group mean difference being 13.5% (**Supplementary Table 1**).

To reduce the number of comparisons in our analysis, we focused on genomic regions of potential relevance to our cohort, i.e. sites within imprinted genes[52] and sites associated with birth weight[53]. After our quality control and filtering procedure, 8940 sites within 207 imprinted genes were retained for the analysis. Among these sites, no significant DMPs were identified, and the maximum group mean was 7.4% (**Fig. 3A, Supplementary Fig. 2A**). Of the 914 previously identified birth weight-associated CpG sites[53] 726 passed our quality control (QC) criteria and none were significantly differentially methylated with a maximal group mean difference of 3.0% (**Fig. 3B, Supplementary Fig. 2B**).

Table 1 | Characteristics of the child, pregnancy and fertility treatment

	Culture medium		
Characteristic	**G3 (n = 57)**	**K-SICM (n = 49)**	***P*-value**
Characteristics of the child			
Sex (female)	29 (51)	26 (53)	0.977
Age at sample collection (years)	9.5 ± 0.3	9.5 ± 0.3	0.802
Weight (kg)	34.1 ± 6.7	31.8 ± 5.5	0.054
Height (cm)	139.0 ± 5.9	138.5 ± 7.5	0.706
Medical diagnoses			
Urological	3 (5)	2 (4)	1.000
Asthma/allergy	9 (16)	4 (8)	0.370
Autism	4 (7)	2 (4)	0.818
Pregnancy characteristics			
Maternal age (years)	32.8 ± 3.4	33.0 ± 3.4	0.772
Paternal age (years)	35.8 ± 4.5	35.6 ± 4.7	0.827
Gestational age	39.7 ± 1.5	39.5 ± 2.2	0.583
Birth weight (g)	3425.4 ± 486.4	3308.6 ± 537.0	0.247

Table 1 | Continued.

Characteristic		Culture medium		
		G3 (n = 57)	K-SICM (n = 49)	*P*-value
Fertility treatment				
Fertilization method				0.985
	IVF	18 (32)	17 (35)	
	ICSI	39 (68)	32 (65)	
Treatment indication				0.985
	Unknown	12 (21)	11 (22)	
	Male factor	38 (67)	32 (65)	
	Female factor	7 (12)	6 (12)	

Continuous variables shown as mean ± SD, categorical variables shown as n (%). Maternal and paternal age at time of ovum pick-up is shown.

Regional analysis of DNA methylation

We then analysed DNA methylation across larger regions of the genome, namely whole genes, promoters and CGIs. In total, 32564 genes were included in the analysis. Of these, the maximal group difference was found to be 9.4% and no significantly differentially methylated genes were identified between the culture medium groups. A targeted analysis of only the imprinted genes showed that these had even lower group mean differences (maximum group mean difference 1.2%) than the individual sites within these genes (**Fig. 3C, Supplementary Fig. 2C**). Furthermore, no imprinted genes were found to be significantly differentially methylated between the G3 and K-SICM groups. A total of 41519 promoters and 25224 CGIs were included in our analysis. The maximal group mean differences were 9.4% and 8.4% for promoters and CGIs, respectively, and no promoters or CGIs were found to be significantly differentially methylated between the culture medium groups (**Fig. 3D** and **E**, **Supplementary Fig. 2D** and **E**).

DNA-methylation variance in ART samples

To assess whether stochastic DNA methylation alterations contribute to the phenotypes observed in the culture medium trial, DNA methylation outliers were identified using previously defined thresholds[55] and differential variance was assessed using the iEVORA method[56]. Overall, we found a predominance of hypomethylation outliers compared to hypermethylation outliers (92238 hypomethylation outliers vs 33009 hypermethylation outliers). On average, we identified a total of 254 ± 485 (median ± IQR) outliers per G3 sample and 186 ± 153 (median ± IQR) outliers per K-SICM sample, which was not found to be significantly different ($p = 0.368$) (**Fig. 4**). Additionally, there was no significant difference between the culture medium groups when the numbers of hypomethylation outliers ($P = 0.86$) and hypermethylation outliers ($P = 0.238$) were analysed separately (**Fig. 4**). Outlier burden, i.e. the total number of outliers per sample, was not significantly associated with age at sample collection or weight at birth

or follow-up. On the other hand, technical features, specifically leucocyte proportion and sample plate, were significantly associated with outlier burden (**Supplementary Table II**). An association between the number of samples and the presence of common diseases (atopy, autism, urological problems) was not tested statistically, but one-third of the children with a diagnosis (8 out of 24) had a very high number of methylation outliers (more than the upper quartile).

Figure 3 | Analysis of systematic methylation differences between G3 and K-SICM children: differentially methylated positions and regions

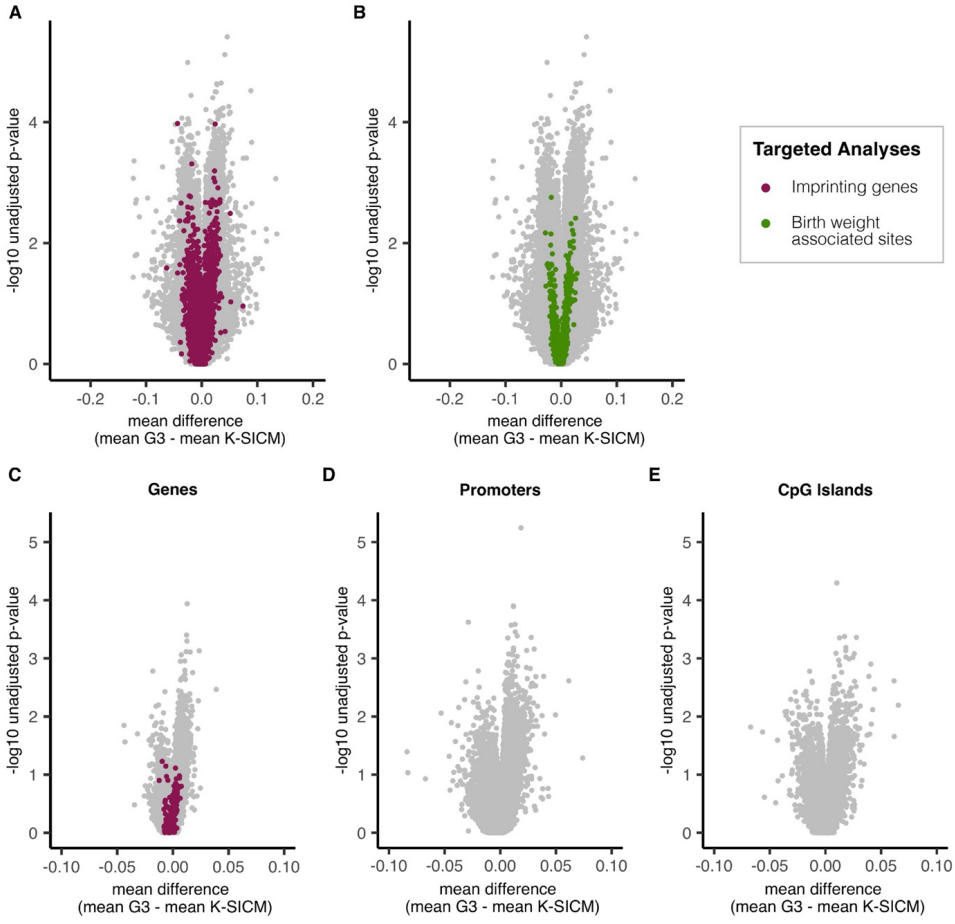

*Volcano plots showing differential methylation between G3 and Sydney IVF cleavage medium (K-SICM) children where the grey dots represent all individual cytosine-guanine dinucleotide (CpG) sites (**A, B**) or multiple CpG sites aggregated into genomic regions, namely genes (**C**), promoters (**D**), CpG islands (**E**). Imprinted genes (**C**) and sites within them (**A**) are highlighted in purple while CpG sites associated with birth weight are shown in green (**B**). Unadjusted P-values are shown. These were generated using M-values for mixed effects linear models, while the group mean differences are shown as beta values for interpretability. No significant differences were found between the culture medium groups (FDR adjusted P-value < 0.1) (see also **Supplementary Fig. S2**).*

Using iEVORA we identified 101 differentially variable CpG sites between the two groups, of which 94 sites were more variable in the G3 group than the K-SICM group. While 20 of the sites were unannotated, the remainder belonged to 80 unique genes. Two genes, *DOCK1* and *PDZRN3*, contained two differentially variable sites. Additionally, two of the sites were within imprinted genes, namely *KCNQ1* and *APBA1* (**Supplementary Table III, sheet 1**). The differentially methylated sites identified by iEVORA were not found to be significantly enriched (FDR < 0.05) in any pathways or ontologies according to the KEGG and GO analyses (**Supplementary Table III, sheets 2-3**).

Figure 4 | Methylation outliers

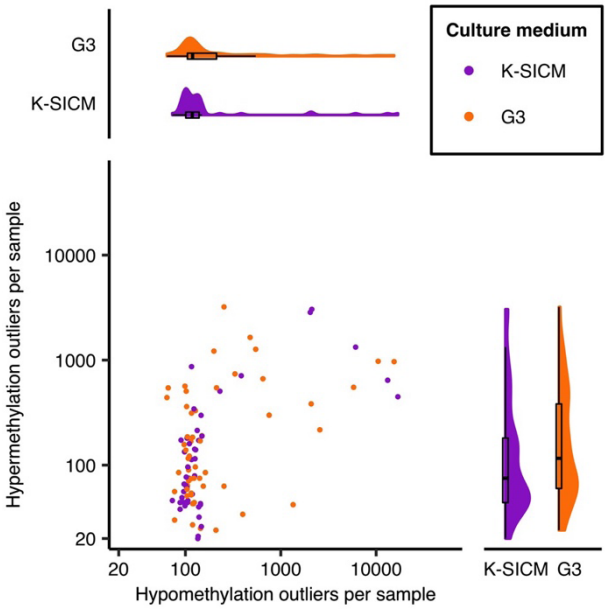

The main panel shows the number of hypomethylation (x-axis) and hypermethylation (y-axis) outliers per saliva sample (G3 = orange, Sydney IVF cleavage medium (K-SICM) = purple). Distribution summaries, in the form of a density plot and boxplot, are shown for hypomethylation outliers and hypermethylation outliers in the top and right side-panels, respectively. Lines of the boxplot represent the 25th percentile, median and 75th percentile, respectively, while the whiskers extend to the farthest data point that is no more than 1.5 times the interquartile range (IQR) from the upper or lower quartile. The axes are shown on a log10 scale. The groups were not found to be significantly different (P-value > 0.1).

Comparison of DNA methylation levels of ART children compared to naturally conceived individuals

All the saliva methylomes (n = 50) available from the FLEHS cohort passed our QC criteria (**Supplementary Fig. 1**) and the characteristics of these individuals are summarized in **Supplementary Table IV**. Of note is that saliva samples were collected from

significantly older naturally conceived children than ART children (ART age: 9.5 ± 0.3, naturally conceived age: 10.6 ± 0.3, mean ± SD, $P < 0.001$, Welch's two-sample *t*-test) with a higher incidence of asthma (12% vs 64% in the ART and naturally conceived cohorts, respectively). PCA showed significant separation of the ART and naturally conceived samples on PCs 1, 3, 4 and 5 (**Supplementary Fig. 4A** and **B**). Seventy-two percent of CpG sites were found to be significantly differentially methylated (adjusted *P*-value < 0.05) with a strong predominance of sites that were hypomethylated in the ART samples compared to the naturally conceived samples (**Supplementary Fig. 4C** and **D**). Such marked methylation differences in phenotypically similar individuals suggest systematic differences in the data that could be due to technical or cohort differences, such as the array type (EPIC or 450K) used, differences induced by the array scanner, laboratory environmental factors or minor pipetting or laboratory protocol deviations. When the sample groups of interest are processed separately, these features align perfectly with the groups of interest and therefore cannot be differentiated from meaningful biological variation. Further analyses were therefore not carried out.

Discussion

Here, we present the largest study to date of the saliva methylome of ART children that underwent embryo culture in different media, namely G3 or K-SICM. At age 9, we have found no significant DNA methylation differences between the culture medium groups when considering individual CpG sites, multiple CpG sites aggregated into genomic regions or when conducting a targeted analysis of (sites within) imprinted genes or birth weight associated CpG sites. The number of methylation outliers per sample was found to be comparable between the culture medium groups and was only significantly associated with technical features of the samples. Interestingly, iEVORA identified that the majority of differentially variable sites between the G3 and K-SICM groups were more variable in the G3 group.

Our findings are consistent with those from the only other ART culture medium cohort in which the saliva methylome was investigated during childhood (ages 7–8)[33,34]. Although the ART children included in that study underwent embryo culture in other media than those compared in the present work, no significant DNA methylation differences were found at any of the sites or regions[33,34]. The group mean differences that they observed between their culture medium groups were also similar to those observed in our cohort[33]. Due to the notably larger sample size of our study, we anticipate that we would have sufficient power (0.8) to detect smaller methylation differences compared to what was possible in the previously described cohort. The results from the current study were also comparable to those of the methylome studies conducted on placenta

or umbilical cord blood samples collected from ART neonates cultured in G5 or HTF media[31,32]. In addition to finding no significant DMPs or DMRs, these studies also reported that there was no difference in the number of outliers per sample between the culture medium groups[31,32].

Interestingly, in the recent umbilical cord blood methylome study[32], 90% of the differentially variable sites identified using iEVORA were more variable in the G5 group than in the HTF culture medium group. Although the effect was less striking once data from neonates that had experienced pregnancy complications had been excluded, 56% of the identified sites were still more variable in the G5 group. In both studies, the culture medium from Vitrolife was associated with a higher number of more variable CpG sites amongst the differentially variable sites[32]. Several explanations have been proposed for the relevance of differentially variable sites. For instance, low methylation variance could result from (environmental) selection pressures that only facilitate the survival of individuals of certain methylation signatures[61]. Alternatively, in oncological samples, sites with differential variability in pre-cancerous tissues are commonly found to be differentially methylated in tumours, when compared with healthy tissues, thus suggesting that these epimutations play a role in disease pathogenesis[56]. Therefore, in our study, less variability in DNA methylation, as seen in the K-SICM group, could indicate a greater environmental selection pressure which would be in concordance with the observed lower implantation and pregnancy rates in this group[21]. However, these sites with differentially variable methylation levels could also be indicative of (cardiometabolic) diseases that certain individuals may develop in later life, which would need to be investigated with further longitudinal follow-up studies of these individuals.

The main aim of the study was to compare the methylomes of ART children who had undergone embryo culture in different media, therefore saliva samples from naturally conceived children were not collected and processed alongside the ART samples. Although a comparison with children from the FLEHS cohort was attempted, the results indicate a large contribution of technical or cohort differences that cannot be corrected in samples that are not processed simultaneously. As such, we recommend that future studies analysing the methylome of ART offspring also collect samples from naturally conceived individuals for simultaneous processing.

The strengths of our study lie in the use of a methylome analysis method that captures methylation status across the whole genome and the sample size which is the largest of any methylome study of ART children in the context of a culture medium study. Nonetheless, to reach sufficient power (0.8) to detect methylation differences of <10% between the culture medium groups a bigger sample size is likely required[62,63].

On the other hand, it is unclear whether such small differences would represent clinically meaningful differences. Since methylation is a binary state (methylated or unmethylated) a 5% methylation increase in any given individual signifies that 5% more of their cells are methylated at the given position. Whether this contributes to pathology or phenotypic variance remains to be determined.

Overall, the findings of this study are reassuring. Although phenotypic differences are observed, even at the age of 9, between ART offspring that had undergone embryo culture in G3 or K-SICM medium, there is no evidence that the epigenome of these individuals differs greatly. As the epigenome retains its plasticity throughout life it is possible that epigenetic dysregulation experienced during the pre-implantation period is no longer evident in ART offspring at the age of 9. Further research, profiling the epigenome of ART embryos, is required to understand how the ART culture environment modulates the epigenome during the period of *in vitro* culture and the significance of sites with differentially variable methylation for later life (disease) outcomes should be evaluated with longitudinal studies.

Data Availability

The raw and processed array data from this study have been uploaded to the Gene Expression Omnibus (GEO) database and are available under the accession number GSE196432 (https://www.ncbi.nlm.nih.gov/geo/query/acc.cgi?acc=GSE196432). The raw array data from the FLEHS study are available within the GEO database under the accession number GSE110128.

Acknowledgements

We thank the ART couples who have agreed for their children to participate in this study. We thank the FLEHS Supervisory Board for the provision of data. The FLEHS studies were commissioned, financed and steered by the Flemish Government (Department of Economy, Science and Innovations, Agency for Care and Health and Department of Environment).

Authors' roles

R.M.K., A.P.A.v.M. and M.Z.E. study design and conception. H.Z., R.v.G. and J.C.M.D. were involved in sample collection for the ART cohort. A.P.A.v.M. and F.B. carried out the lab work for the ART samples. S.R. and S.L. were involved in sample collection and processing for the naturally conceived cohorts. R.M.K., F.B., J.T., A.P.A.v.M. and M.Z.E were involved in the data analysis and interpretation. R.M.K. wrote the first draft of the manuscript. M.G., A.P.A.v.M. and M.Z.E. contributed to the writing of the manuscript. All authors provided textual comments and approved the manuscript. H.B., A.P.A.v.M. and M.Z.E supervised the study.

Funding
This study was funded by March of Dimes (6-FY13-153). Additionally, it was further supported by EVA (Erfelijkheid Voortplanting & Aanleg) specialty programme (grant no. KP111513) from Maastricht University Medical Centre (MUMC+) and the Horizon 2020 innovation (ERIN) (grant no. EU952516) from the European Commission. The FLEHS dataset has been generated by the Flemish Center of Expertise on Environment and Health (FLEHS 2016–2020), funded by the Environment, Nature and Energy Department of the Flemish government. The views expressed in this manuscript are those of the author(s) and are not necessarily endorsed by the Flemish government.

Conflict of interest
The authors do not report any conflicts of interest relevant to this study.

References

1 Adamson, G. D. *et al.* ICMART preliminary world report 2015. *Hum Reprod* **34** (2019). <https://academic.oup.com/humrep/article/34/Supplement_1/i1/5528444>.

2 Wyns, C. *et al.* ART in Europe, 2016: results generated from European registries by ESHRE. *Hum Reprod Open* **2020**, hoaa032 (2020). https://doi.org/10.1093/hropen/hoaa032

3 Bernsten, S. *et al.* The health of children conceived by ART: 'the chicken or the egg?'. *Hum Reprod update* **25**, 137-158 (2019).

4 Ceelen, M. *et al.* Growth during infancy and early childhood in relation to blood pressure and body fat measures at age 8-18 years of IVF children and spontaneously conceived controls born to subfertile parents. *Hum Reprod* **24**, 2788-2795 (2009). https://doi.org/10.1093/humrep/dep273

5 Hann, M. *et al.* The growth of assisted reproductive treatment-conceived children from birth to 5 years: a national cohort study. *BMC Med* **16**, 224 (2018). https://doi.org/10.1186/s12916-018-1203-7

6 Guo, X. Y. *et al.* Cardiovascular and metabolic profiles of offspring conceived by assisted reproductive technologies: a systematic review and meta-analysis. *Fertil Steril* **107**, 622-631.e625 (2017). https://doi.org/10.1016/j.fertnstert.2016.12.007

7 Bay, B., Lyngsø, J., Hohwü, L. & Kesmodel, U. S. Childhood growth of singletons conceived following in vitro fertilisation or intracytoplasmic sperm injection: a systematic review and meta-analysis. *BJOG* **126**, 158-166 (2019). https://doi.org/10.1111/1471-0528.15456

8 Wadhwa, P. D., Buss, C., Entringer, S. & Swanson, J. M. Developmental origins of health and disease: brief history of the approach and current focus on epigenetic mechanisms. *Semin Reprod Med* **27**, 358-368 (2009). https://doi.org/10.1055/s-0029-1237424

9 Mantikou, E. *et al.* Embryo culture media and IVF/ICSI success rates: a systematic review. *Hum Reprod Update* **19**, 210-220 (2013). https://doi.org/10.1093/humupd/dms061

10 Morbeck, D. E. *et al.* Composition of commercial media used for human embryo culture. *Fertil Steril* **102**, 759-766.e759 (2014). https://doi.org/10.1016/j.fertnstert.2014.05.043

11 Morbeck, D. E., Baumann, N. A. & Oglesbee, D. Composition of single-step media used for human embryo culture. *Fertil Steril* **107**, 1055-1060.e1051 (2017). https://doi.org/10.1016/j.fertnstert.2017.01.007

12 Sunde, A. *et al.* Time to take human embryo culture seriously. *Hum Reprod* **31**, 2174-2182 (2016). https://doi.org/10.1093/humrep/dew157

13 Fernández-Gonzalez, R. *et al.* Long-term effect of in vitro culture of mouse embryos with serum on mRNA expression of imprinting genes, development, and behavior. *Proc Natl Acad Sci U S A* **101**, 5880-5885 (2004). https://doi.org/10.1073/pnas.0308560101

14 Donjacour, A., Liu, X., Lin, W., Simbulan, R. & Rinaudo, P. F. In vitro fertilization affects growth and glucose metabolism in a sex-specific manner in an outbred mouse model. *Biol Reprod* **90**, 80 (2014). https://doi.org/10.1095/biolreprod.113.113134

15 Zandstra, H., Van Montfoort, A. P. & Dumoulin, J. C. Does the type of culture medium used influence birthweight of children born after IVF? *Hum Reprod* **30**, 530-542 (2015). https://doi.org/10.1093/humrep/deu346

16 Bouillon, C. *et al.* Does Embryo Culture Medium Influence the Health and Development of Children Born after In Vitro Fertilization? *PLoS One* **11**, e0150857 (2016). https://doi.org/10.1371/journal.pone.0150857

17 Velazquez, M. A. *et al.* Insulin and branched-chain amino acid depletion during mouse preimplantation embryo culture programmes body weight gain and raised blood pressure during early postnatal life. *Biochim Biophys Acta Mol Basis Dis* **1864**, 590-600 (2018). https://doi.org/10.1016/j.bbadis.2017.11.020

18 Kleijkers, S. H. *et al.* Influence of embryo culture medium (G5 and HTF) on pregnancy and perinatal outcome after IVF: a multicenter RCT. *Hum Reprod* **31**, 2219-2230 (2016). https://doi.org/10.1093/humrep/dew156

19 Virant-Klun, I. *et al.* Increased ammonium in culture medium reduces the development of human embryos to the blastocyst stage. *Fertil Steril* **85**, 526-528 (2006). https://doi.org/10.1016/j.fertnstert.2005.10.018

20 Hashimoto, S. *et al.* Medium without ammonium accumulation supports the developmental competence of human embryos. *J Reprod Dev* **54**, 370-374 (2008). https://doi.org/10.1262/jrd.20012

21 Dumoulin, J. C. *et al.* Effect of in vitro culture of human embryos on birthweight of newborns. *Hum Reprod* **25**, 605-612 (2010). https://doi.org/10.1093/humrep/dep456

22 Nelissen, E. C. *et al.* Placentas from pregnancies conceived by IVF/ICSI have a reduced DNA methylation level at the H19 and MEST differentially methylated regions. *Hum Reprod* **28**, 1117-1126 (2013). https://doi.org/10.1093/humrep/des459

23 Nelissen, E. C. *et al.* Further evidence that culture media affect perinatal outcome: findings after transfer

of fresh and cryopreserved embryos. *Hum Reprod* **27**, 1966-1976 (2012). https://doi.org/10.1093/humrep/des145
24 Kleijkers, S. H. *et al.* IVF culture medium affects post-natal weight in humans during the first 2 years of life. *Hum Reprod* **29**, 661-669 (2014). https://doi.org/10.1093/humrep/deu025
25 Zandstra, H. *et al.* Association of culture medium with growth, weight and cardiovascular development of IVF children at the age of 9 years. *Hum Reprod* **33**, 1645-1656 (2018). https://doi.org/10.1093/humrep/dey246
26 Zandstra, H. *et al.* No effect of IVF culture medium on cognitive development of 9-year-old children. *Hum Reprod Open* **2018**, hoy018 (2018). https://doi.org/10.1093/hropen/hoy018
27 Felix, J. F. & Cecil, C. A. M. Population DNA methylation studies in the Developmental Origins of Health and Disease (DOHaD) framework. *J Dev Orig Health Dis* **10**, 306-313 (2019). https://doi.org/10.1017/S2040174418000442
28 Li, L. *et al.* Single-cell multi-omics sequencing of human early embryos. *Nat Cell Biol* **20**, 847-858 (2018). https://doi.org/10.1038/s41556-018-0123-2
29 Hanna, C. W., Demond, H. & Kelsey, G. Epigenetic regulation in development: is the mouse a good model for the human? *Hum Reprod Update* **24**, 556-576 (2018). https://doi.org/10.1093/humupd/dmy021
30 DeAngelis, A. M., Martini, A. E. & Owen, C. M. Assisted Reproductive Technology and Epigenetics. *Semin Reprod Med* **36**, 221-232 (2018). https://doi.org/10.1055/s-0038-1675780
31 Mulder, C. L. *et al.* Comparison of DNA methylation patterns of parentally imprinted genes in placenta derived from IVF conceptions in two different culture media. *Hum Reprod* **35**, 516-528 (2020). https://doi.org/10.1093/humrep/deaa004
32 Koeck, R. M. *et al.* Methylome-wide analysis of IVF neonates that underwent embryo culture in different media revealed no significant differences. *NPJ Genom Med* **7**, 39 (2022). https://doi.org/10.1038/s41525-022-00310-3
33 Barberet, J. *et al.* Do assisted reproductive technologies and in vitro embryo culture influence the epigenetic control of imprinted genes and transposable elements in children? *Hum Reprod* **36**, 479-492 (2021). https://doi.org/10.1093/humrep/deaa310
34 Ducreux, B. *et al.* Genome-Wide Analysis of DNA Methylation in Buccal Cells of Children Conceived through IVF and ICSI. *Genes (Basel)* **12** (2021). https://doi.org/10.3390/genes12121912
35 Barberet, J. *et al.* DNA methylation profiles after ART during human lifespan: a systematic review and meta-analysis. *Hum Reprod Update* (2022). https://doi.org/10.1093/humupd/dmac010
36 El Hajj, N. & Haaf, T. Epigenetic disturbances in in vitro cultured gametes and embryos: implications for human assisted reproduction. *Fertil Steril* **99**, 632-641 (2013). https://doi.org/10.1016/j.fertnstert.2012.12.044
37 Melamed, N., Choufani, S., Wilkins-Haug, L. E., Koren, G. & Weksberg, R. Comparison of genome-wide and gene-specific DNA methylation between ART and naturally conceived pregnancies. *Epigenetics* **10**, 474-483 (2015). https://doi.org/10.4161/15592294.2014.988041
38 Håberg, S. E. *et al.* DNA methylation in newborns conceived by assisted reproductive technology. *Nat Commun* **13**, 1896 (2022). https://doi.org/10.1038/s41467-022-29540-w
39 Yeung, E. H. *et al.* Conception by fertility treatment and offspring deoxyribonucleic acid methylation. *Fertil Steril* **116**, 493-504 (2021). https://doi.org/10.1016/j.fertnstert.2021.03.011
40 Penova-Veselinovic, B. *et al.* DNA methylation patterns within whole blood of adolescents born from assisted reproductive technology are not different from adolescents born from natural conception. *Hum Reprod* **36**, 2035-2049 (2021). https://doi.org/10.1093/humrep/deab078
41 Novakovic, B. *et al.* Assisted reproductive technologies are associated with limited epigenetic variation at birth that largely resolves by adulthood. *Nat Commun* **10**, 3922 (2019). https://doi.org/10.1038/s41467-019-11929-9
42 *R Core Team. R: A language and environment for statistical computing. R Foundation for Statistical Computing, Vienna, Austria. https://www.R-project.org/*, <URL https://www.R-project.org/> (2021).
43 Gu, Z., Eils, R. & Schlesner, M. Complex heatmaps reveal patterns and correlations in multidimensional genomic data. *Bioinformatics* **32**, 2847-2849 (2016). https://doi.org/10.1093/bioinformatics/btw313
44 Müller, F. *et al.* RnBeads 2.0: comprehensive analysis of DNA methylation data. *Genome Biol* **20**, 55 (2019). https://doi.org/10.1186/s13059-019-1664-9
45 Maksimovic, J., Gordon, L. & Oshlack, A. SWAN: Subset-quantile within array normalization for illumina infinium HumanMethylation450 BeadChips. *Genome Biol* **13**, R44 (2012). https://doi.org/10.1186/gb-2012-13-6-r44
46 Jung, C. H. *et al.* sEst: Accurate Sex-Estimation and Abnormality Detection in Methylation Microarray Data. *Int J Mol Sci* **19** (2018). https://doi.org/10.3390/ijms19103172
47 Houseman, E. A., Molitor, J. & Marsit, C. J. Reference-free cell mixture adjustments in analysis of DNA

methylation data. *Bioinformatics* **30**, 1431-1439 (2014). https://doi.org/10.1093/bioinformatics/btu029
48 Just, A. C. & Heiss, J. A. (2018).
49 Middleton, L. Y. M. *et al.* Saliva cell type DNA methylation reference panel for epidemiological studies in children. *Epigenetics*, 1-17 (2021). https://doi.org/10.1080/15592294.2021.1890874
50 Du, P. *et al.* Comparison of Beta-value and M-value methods for quantifying methylation levels by microarray analysis. *BMC Bioinformatics* **11**, 587 (2010). https://doi.org/10.1186/1471-2105-11-587
51 Hoffman, G. E. & Schadt, E. E. variancePartition: interpreting drivers of variation in complex gene expression studies. *BMC Bioinformatics* **17**, 483 (2016). https://doi.org/10.1186/s12859-016-1323-z
52 Ginjala , V. Gene imprinting gateway. *Genome Biol* **2** (2001). https://doi.org/https://doi.org/10.1186/gb-2001-2-8-reports2009
53 Küpers, L. K. *et al.* Meta-analysis of epigenome-wide association studies in neonates reveals widespread differential DNA methylation associated with birthweight. *Nat Commun* **10**, 1893 (2019). https://doi.org/10.1038/s41467-019-09671-3
54 Benjamini, Y. & Hochberg, Y. Controlling the false discovery rate: a practical and powerful approach to multiple testing. *J. Roy. Statist. Soc.* **Ser. B57**, 289-300 (1995).
55 Gentilini, D. *et al.* Stochastic epigenetic mutations (DNA methylation) increase exponentially in human aging and correlate with X chromosome inactivation skewing in females. *Aging (Albany NY)* **7**, 568-578 (2015). https://doi.org/10.18632/aging.100792
56 Teschendorff, A. E., Jones, A. & Widschwendter, M. Stochastic epigenetic outliers can define field defects in cancer. *BMC Bioinformatics* **17**, 178 (2016). https://doi.org/10.1186/s12859-016-1056-z
57 Koncevičius, K. (2020).
58 Phipson, B., Maksimovic, J. & Oshlack, A. missMethyl: an R package for analyzing data from Illumina's HumanMethylation450 platform. *Bioinformatics* **32**, 286-288 (2016). https://doi.org/10.1093/bioinformatics/btv560
59 Langie, S. A. S. *et al.* GLI2 promoter hypermethylation in saliva of children with a respiratory allergy. *Clin Epigenetics* **10**, 50 (2018). https://doi.org/10.1186/s13148-018-0484-1
60 Van Den Heuvel, R. *et al.* Biobank@VITO: Biobanking the General Population in Flanders. *Front Med (Lausanne)* **7**, 37 (2020). https://doi.org/10.3389/fmed.2020.00037
61 Tobi, E. W. *et al.* Selective Survival of Embryos Can Explain DNA Methylation Signatures of Adverse Prenatal Environments. *Cell Rep* **25**, 2660-2667.e2664 (2018). https://doi.org/10.1016/j.celrep.2018.11.023
62 Tsai, P. C. & Bell, J. T. Power and sample size estimation for epigenome-wide association scans to detect differential DNA methylation. *Int J Epidemiol* **44**, 1429-1441 (2015). https://doi.org/10.1093/ije/dyv041
63 Saffari, A. *et al.* Estimation of a significance threshold for epigenome-wide association studies. *Genet Epidemiol* **42**, 20-33 (2018). https://doi.org/10.1002/gepi.22086

Supplementary Material

Supplementary materials and methods

ART and naturally conceived comparison

The raw saliva methylome data from the Flemish Environment Health Study (FLEHS) cohort were subjected to the same quality control (QC) and pre-processing procedure as described for the ART data. All 50 samples were deemed high quality and no sex mismatches were identified so all samples were included in the analyses. 391,619 of the 450K array sites passed our QC thresholds. Cellular composition of the samples was also calculated using the same method as the ART samples for inclusion as covariates. Within study batch effect, i.e. sample plate differences in the ART cohort, were corrected using ComBat before combining the data as these could not be corrected for in the statistical models. The data were then combined, retaining only sites that passed the QC in both studies and containing no missing values, resulting in a dataset containing 350,753 cytosine-guanine dinucleotide (CpG) sites. As for the culture medium comparison, empirical Bayes moderated linear models, implemented using Limma[1], were used to identify associations between DNA methylation M-values and the mode of conception. Age at sample collection, sex and cell composition were included as covariates in these models. Multiple testing correction was applied using the Benjamini-Hochberg method and adjusted p-values of <0.05 were considered significant.

References

1 Ritchie, M. E. *et al.* limma powers differential expression analyses for RNA-sequencing and microarray studies. *Nucleic Acids Res* **43**, e47 (2015). https://doi.org/10.1093/nar/gkv007

Supplementary figure 1 | Processing of saliva methylome data from naturally conceived children from the FLEHS cohort

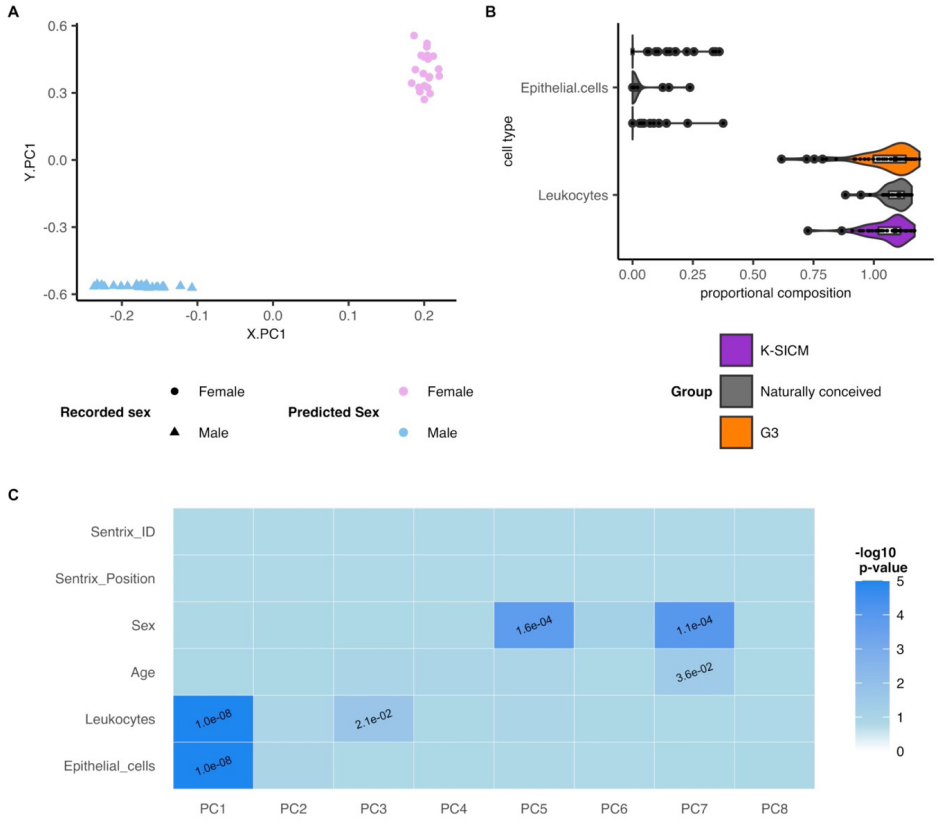

*(**A**) Scatter plot showing the projection of saliva samples from the FLEHS cohort (n = 50) into the principal component (PC) space generated using reference data for sex prediction. The shape of the dots represents the recorded sex of the participants (circles = female, triangle = male), while the colour shows the predicted sex based on results from sEST (blue = male, pink = female, grey = not specified). (**B**) Violin plot showing the predicted cellular composition of the saliva samples coloured by group (purple = ART K-SICM, grey = naturally conceived FLEHS, orange = ART G3). Overlaid is a boxplot in which the horizontal lines represent the 25th percentile, median and 75th percentile, respectively, while the whiskers extend to the farthest data point that is no more than 1.5 times the IQR from the upper or lower quartile. Data points lying outside of this range are represented by dots. (**C**) Heatmap showing associations between the principal components and biological/technical aspects of the FLEHS samples. The colour gradient represents the -log10 of the p-values. P-values that are <0.05 are shown. Significance of the correlation between continuous variables and the 8 principal components (PCs) was tested using a permutation test with 10,000 permutations. The associations of the PCs with variables creating 2 groups (and those creating 3 or more groups were tested using two-sided Wilcoxon rank tests and Kruskall-Wallis one-way analysis of variance, respectively.*

Supplementary figure 2 | Analysis of systematic methylation differences between G3 and K-SICM children: differentially methylation positions and regions (FDR adjusted)

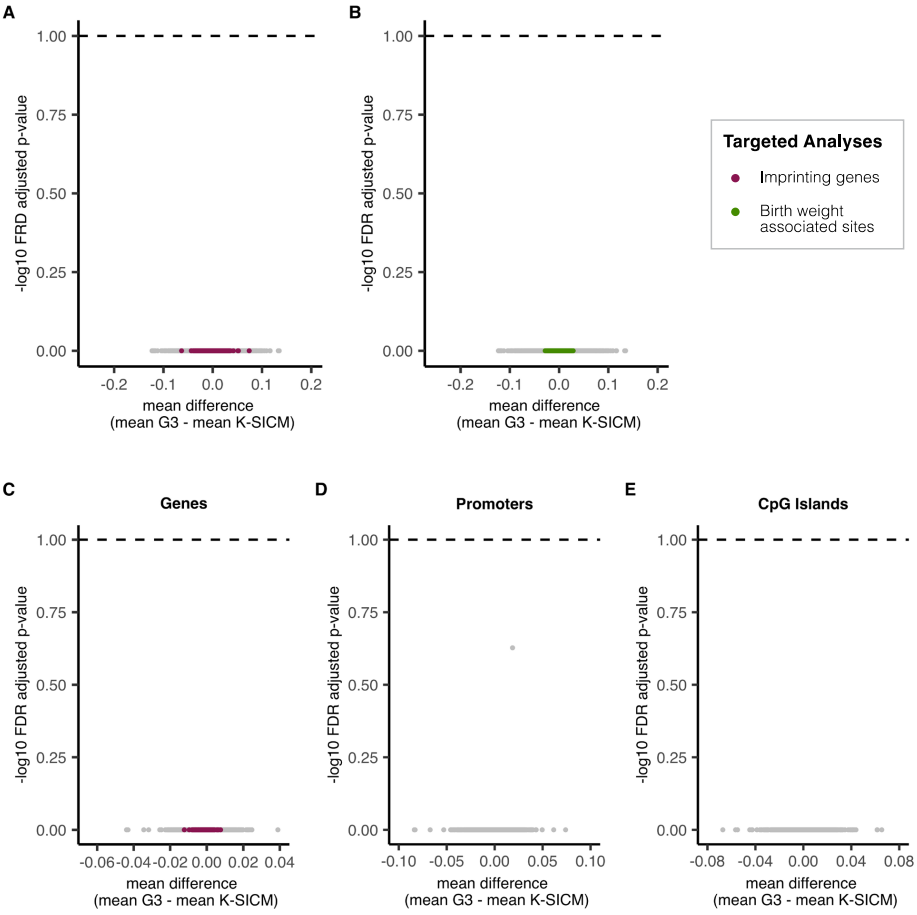

*Volcano plots showing differential methylation between G3 and K-SICM children where the grey dots represent all individual CpG sites (**A, B**) or multiple CpG sites aggregated into genomic regions, namely genes (**C**), promoters (**D**), CpG islands (**E**). Imprinted genes (**C**) and sites within them (**A**) are highlighted in purple while CpG sites associated with birth weight are shown in green (**B**). FDR adjusted p-values are shown. These were generated using M-values for mixed effects linear models while the group mean differences are shown as beta values for interpretability. The horizontal dashed line represents our FDR-adjusted p-value threshold of 0.01.*

Supplementary figure 3 | Genomic distribution of good quality CpG sites

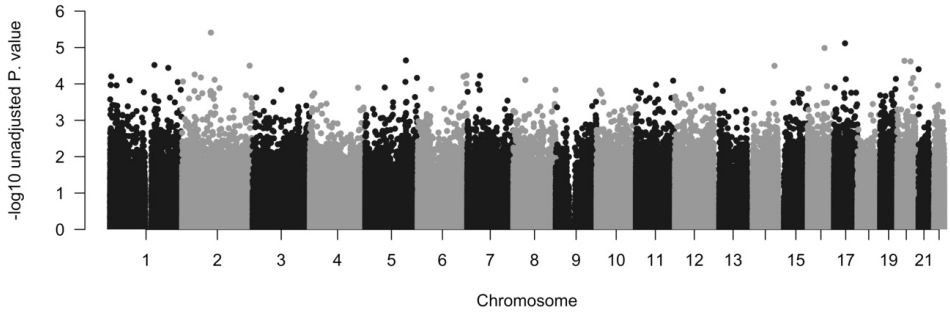

Manhattan plot showing the distribution of all high quality CpG sites with complete observations (n = 659,708). The sites are ordered by their genomic coordinates along the x-axis and the unadjusted p-values, obtained using M-values for mixed effects linear models, of the sites are shown on the y-axis. After multiple testing correction no significant differentially methylated sites were found (FDR adjusted p-value <0.1).

Supplementary figure 4| Comparison of ART and naturally conceived children

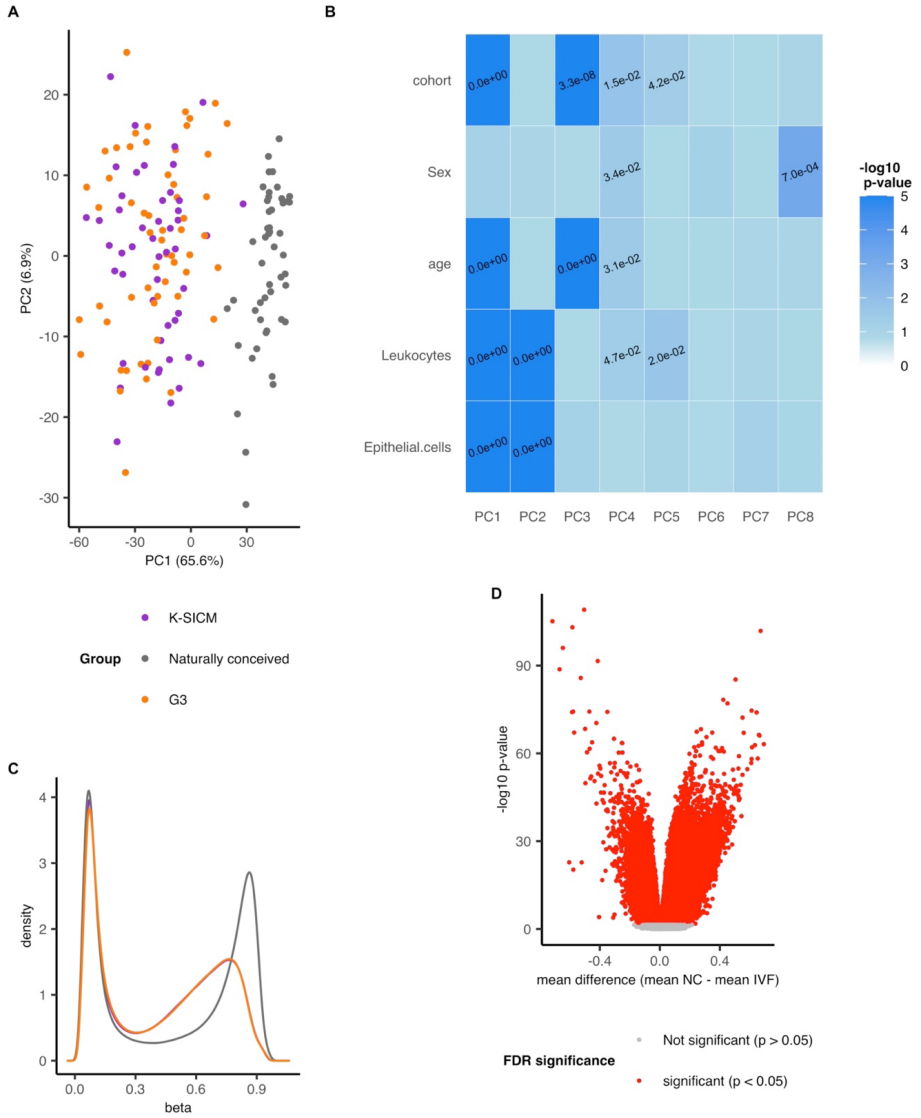

*(**A**) PCA including CpG sites that are present on the EPIC and 450K array and pass the QC criteria in the ART and naturally conceived samples: ART G3 = orange, ART K-SICM = purple, naturally conceived FLEHS = grey. The PCA plot shows the first two PCs, the variance explained by each is shown in brackets. (**B**) Heatmap showing associations between the principal components and biological/technical aspects of the samples (n = 50 naturally conceived, n = 106 ART). The colour gradient represents the -log10 of the p-values. P-values that are <0.05 are shown. Significance of the correlation between continuous variables and the 8 PCs was tested using a permutation test with 10,000 permutations. The associations of the PCs with variables creating 2 groups and those creating 3 or more groups were tested using two-sided Wilcoxon rank tests and Kruskall-Wallis one-way analysis of variance, respectively. (**C**) Density plot showing the distribution of beta values from all sites and samples within each group (ART G3 = orange, ART K-SICM = purple, naturally conceived FLEHS = grey). (**G**) Volcano plot showing differential methylation between naturally conceived (n = 50) and ART children (n = 106) at individual CpG sites (n = 350,753). The volcano*

plot shows significantly differentially methylated sites (FDR adjusted p-value <0.05) in red and all other sites in grey. The shown p-values were derived using methylation M-values while group mean differences are calculated from methylation beta values for interpretability.

Supplementary table I | CpG sites with a group mean difference (mean G3 – mean K-SICM) of more than 10%

ID	Chrom	Start	mean K-SICM	Std. Dev. K-SICM	mean G3	Std. Dev. G3	mean difference (G3 – K-SICM)	P. value	adjusted P. value	Gene Name	Genomic context
cg12602563	chr7	46172401	0.50484086	0.27357614	0.63979483	0.22172445	0.13495397	0.00708729	0.99998294		Body
cg23187802	chr10	81173663	0.53128076	0.24581127	0.6643036	0.17893084	0.13302283	0.00086271	0.99998294	ZCCHC24	
rs213028	chr1	21652177	0.36911638	0.32553015	0.24594672	0.26055949	-0.1231697	0.03685852	0.99998294		Body
cg07469168	chr19	41249427	0.68483403	0.13881745	0.56181141	0.20635569	-0.1230226	0.0008522	0.99998294	C19orf54	TSS1500
cg12776173	chr9	4726758	0.61063937	0.15689709	0.48893692	0.17154214	-0.1217025	0.00043832	0.99998294	AK3	Body
cg23803868	chr19	2340235	0.53221557	0.25453597	0.41247042	0.27451994	-0.1197451	0.01621846	0.99998294	SPPL2B	TSS1500
cg08477332	chr1	153590243	0.46572465	0.19611344	0.34666384	0.18240509	-0.1190608	0.00218423	0.99998294	S100A14	Body
cg07553030	chr20	61290360	0.78676215	0.14150482	0.66930668	0.23519024	-0.1174555	0.00192783	0.99998294	SLCO4A1	Body
cg03020684	chr15	71532066	0.57597679	0.22343915	0.45934161	0.22227078	-0.1166352	0.01544537	0.99998294	THSD4	TSS1500
cg18561199	chr14	95027379	0.3741927	0.21923792	0.49074978	0.21100027	0.11655708	0.00933182	0.99998294	SERPINA4	TSS1500
cg08210706	chr14	95046686	0.50453792	0.26346706	0.62042301	0.20060992	0.11588509	0.00587063	0.99998294	SERPINA5	
cg01282508	chr19	41319790	0.70366477	0.15111899	0.59159217	0.2000356	-0.1120726	0.00370241	0.99998294		Body
cg14599155	chr5	149575123	0.4642754	0.26140237	0.57328162	0.21562736	0.10900622	0.02653601	0.99998294	SLC6A7	Body
cg09281805	chr7	4751840	0.45678676	0.25661815	0.56138564	0.20502737	0.10459888	0.01815861	0.99998294	FOXK1	
cg20673407	chr10	31040939	0.49404179	0.23046727	0.38977754	0.19613997	-0.1042643	0.03428528	0.99998294		Body
cg18391209	chr1	223747670	0.50032881	0.29188218	0.39847304	0.28152066	-0.1018558	0.07561461	0.99998294	CAPN8	Body
cg06584796	chr19	3446107	0.27131586	0.23855204	0.37163596	0.25947522	0.1003201	0.02107894	0.99998294	NFIC	Body

Chrom = chromosome, Std. Dev. = standard deviation, body = gene body, TSS1500 = site within 1,500 base pairs of the transcription start site.
mean beta-values for each group (G3 or K-SICM) are presented. The mean difference is calculated by subtracting the mean of the K-SICM group from the mean of the G3 group, these values can be considered as a percentage by multiplying by 100 given that methylation beta values range from 0 (unmethylated) to 1 (fully methylated).

Supplementary table II | Association between number of outliers and sample features

	Hypomethylation outliers		Hypermethylation outliers		Total number of outliers	
Feature	**Correlation**	**Significance**	**Correlation**	**Significance**	**Correlation**	**Significance**
Age at sample collection	0.093	0.336	-0.069	0.473	0.074	0.450
Weight (9 years)	-0.091	0.331	-0.075	0.443	-0.099	0.297
Birth weight	-0.146	0.121	-0.090	0.341	-0.154	0.111
Leukocytes	**-0.280**	**0.010**	0.088	0.368	**-0.245**	**0.016**
Epithelial cells	0.119	0.127	0.002	0.987	0.112	0.212
Sample plate*		**0.000**		0.147		**0.018**

Correlations shown are Pearson correlations and significance was tested with permutation tests (1000 permutation)
* significance tested with two-sided Wilcoxon rank test.

S**upplementary Table III | Differentially variable sites identified by iEVORA** (see the excel file in the online version of the article)
Sheet 1) Differentially variable sites between the culture medium groups as identified by the iEVORA algorithm. Sheet 2) Ontologies reaching nominal significance after GO analysis on the differentially variable sites described in sheet 1. Sheet 3) Pathways reaching nominal significance after KEGG analysis on the differentially variable sites described in sheet 1.

Supplementary table SIV | Characteristics of naturally conceived children from the FLEHS cohort

Characteristic	**FLEHS** (naturally conceived)
	(*n* = 50)
Characteristics of the child	
Sex (female)	21 (42)
Age at sample collection (years)	10.6 ± 0.3
Medical diagnoses:	
t	32 (64)

Continuous variables shown as mean ± SD, categorical variables shown as n (%).

Chapter 4

Embryo tracking system for high-throughput sequencing-based preimplantation genetic testing

---

Wanwisa van Dijk*, Kasper Derks*, Marion Drüsedau, Jeroen Meekels, Rebekka M. Koeck, Rick Essers, Joseph Dreesen, Edith Coonen, Christine de Die-Smulders, Servi J. C. Stevens, Han G. Brunner, Arthur van den Wijngaard, Aimée D. C. Paulussen, Masoud Zamani Esteki
*** Joint first authors**

My contribution: analysis, visualisation and write-up of data quality control parameters as well as editing of the manuscript text.

Adapted from W. van Dijk, K. Derks, M. Drüsedau, J. Meekels, R. Koeck, R. Essers, J. Dreesen, E. Coonen, C. de Die-Smulders, S.J.C. Stevens, H.G. Brunner, A. van den Wijngaard, A.D.C. Paulussen, M. Zamani Esteki. Embryo tracking system for high-throughput sequencing-based preimplantation genetic testing. Hum Reprod. (2022) 37(11):2700-2708. https://doi.org/10.1093/humrep/deac208

Abstract

Study question

Can the embryo tracking system (ETS) increase safety, efficacy and scalability of massively parallel sequencing-based preimplantation genetic testing (PGT)?

Summary answer

Applying ETS-PGT, the chance of sample switching is decreased, while scalability and efficacy could easily be increased substantially.

What is known already

Although state-of-the-art sequencing-based PGT methods made a paradigm shift in PGT, they still require labor intensive library preparation steps that makes PGT cost prohibitive and poses risks of human errors. To increase the quality assurance, efficiency, robustness and throughput of the sequencing-based assays, barcoded DNA fragments have been used in several aspects of next-generation sequencing (NGS) approach.

Study design, size, duration

We developed an ETS that substantially alleviates the complexity of the current sequencing-based PGT. With (n = 693) and without (n = 192) ETS, the downstream PGT procedure was performed on both bulk DNA samples (n = 563) and whole-genome amplified (WGAed) few-cell DNA samples (n = 322). Subsequently, we compared full genome haplotype landscapes of both WGAed and bulk DNA samples containing ETS or no ETS.

Participants/materials, setting, methods

We have devised an ETS to track embryos right after whole-genome amplification (WGA) to full genome haplotype profiles. In this study, we recruited 322 WGAed DNA samples derived from IVF embryos as well as 563 bulk DNA isolated from peripheral blood of prospective parents. To determine possible interference of the ETS in the NGS-based PGT workflow, barcoded DNA fragments were added to DNA samples prior to library preparation and compared to samples without ETS. Coverages and variants were determined.

Main results and the role of chance

Current PGT protocols are quality sensitive and prone to sample switching. To avoid sample switching and increase throughput of PGT by sequencing-based haplotyping, six control steps should be carried out manually and checked by a second person in a clinical setting. Here, we developed an ETS approach in which one step only in the entire PGT procedure needs the four-eyes principal. We demonstrate that ETS not only

precludes error-prone manual checks but also has no effect on the genomic landscape of preimplantation embryos. Importantly, our approach increases efficacy and throughput of the state-of-the-art PGT methods.

Limitations, reasons for caution

Even though the ETS simplified sequencing-based PGT by avoiding potential errors in six steps in the protocol, if the initial assignment is not performed correctly, it could lead to cross-contamination. However, this can be detected in silico following downstream ETS analysis. Although we demonstrated an approach to evaluate purity of the ETS fragment, it is recommended to perform a pre-PGT quality control assay of the ETS amplicons with non-human DNA, such that the purity of each ETS molecule can be determined prior to ETS-PGT.

Wider implications of the findings

The ETS-PGT approach notably increases efficacy and scalability of PGT. ETS-PGT has broad applicative value, as it can be tailored to any single- and few-cell sequencing approach where the starting specimen is scarce, as opposed to other methods that require a large number of cells as the input. Moreover, ETS-PGT could easily be adapted to any sequencing-based diagnostic method, including PGT for structural rearrangements and aneuploidies by low-pass sequencing as well as non-invasive prenatal testing.

Study funding/competing interest(s)

M.Z.E. is supported by the EVA (Erfelijkheid Voortplanting & Aanleg) specialty program (grant no. KP111513) of Maastricht University Medical Centre (MUMC+), and the Horizon 2020 innovation (ERIN) (grant no. EU952516) of the European Commission.

Trial registration number

N/A.

Introduction

Since the birth of the first *in vitro* fertilized (IVF) baby in 1978[1], more than 8 million individuals have been conceived via IVF. This continues to increase due to various demographic factors, including advanced parental age. Preimplantation genetic testing (PGT) has evolved from locus- and family-specific genetic testing, e.g. PCR- and FISH-based PGT methods, to more sophisticated generic approaches, e.g. genome-wide haplotyping methods[2-4]. Currently, PGT is performed for monogenic disorders (PGT-M), structural rearrangements (PGT-SR) and aneuploidies (PGT-A). Over the last few years, the demand for PGT has increased rapidly due to the continuous discovery of new disease genes and pathogenic mutations[5], the development of massively parallel sequencing PGT (sequencing-based PGT) methods that have broadened the scope of PGT practice[6], increased public awareness of reproductive options, and the broader availability and accessibility of preconception carrier testing[7]. For instance, in our center, the number of PGT-M requests increased from 58 in 2009 to 432 in 2019, signifying that generic and scalable PGT is indispensable.

Whole-genome amplification (WGA) methods in combination with high-throughput single nucleotide polymorphism (SNP) profiling platforms, including SNP-array and massively parallel sequencing, have enabled PGT at the single-cell resolution[2,8-11]. Recently, we demonstrated sequencing-based haplarithmisis[9], allowing simultaneous haplotyping and copy-number typing, such that all forms of PGT (PGT-M, PGT-A and PGT-SR) can be performed in a single assay. As a result, the required time for a PGT work-up was reduced drastically. However, these sequencing-based PGT methods are still laborious and prone to specimen provenance errors, i.e. sample switching, cross-contamination or product carryover. This is due to the increased number of wet-lab steps of these methods as compared to the traditional locus-specific PCR-based approaches, which adds to the possibility of human error and misdiagnosis[12]. Although good laboratory practice in sample handling and laboratory automation is employed to minimize specimen provenance errors, multiple control steps are still essential. For instance, sample switching can affect 3% of samples in clinical laboratory testing[13,14]. Previously, several methods for sample tracking and the detection of cross-contamination and for single-cell DNA and RNA sequencing have been developed[15-18]. However, none have been proven to be suitable for tracing rare cells in a clinical setting, e.g. single- or few-cell DNA samples derived from human preimplantation embryos.

To minimize specimen provenance errors and increase the scalability of our sequencing-based PGT procedure, we developed an embryo tracking system (ETS)-PGT (**Fig. 1a**). We adapted sample tracking, using spiked-in short DNA probes[16], and developed an innovative, easy-to-use approach that makes sequencing-based PGT more robust with

higher throughput. ETS-PGT is unique due to its incorporation of the ETS fragments with (i) an extra 20-nucleotide sequence that allows the restriction enzyme to bind, (ii) an adjacent restriction site that is specific for the sequencing-based PGT procedure, (iii) an extra primer binding site that makes sample tracking universal for any sequencing-based wet-lab protocol and (iv) a complementary, integrative computational pipeline that automatically traces the embryos. Here, we show that the ETS eliminates the necessity of the four-eyes principal for six crucial control steps in sequencing-based PGT, allowing not only higher quality assurance but also increasing the scalability of the process by enabling a fully robotized comprehensive PGT.

Materials and methods

Patients with informed consent and embryo biopsies

All couples were counselled by clinical geneticists at Maastricht University Medical Centre (MUMC+) and enrolled in the diagnostic PGT procedure (licensed by the Dutch Ministry of Health, Welfare and Sport CZ-TSZ-291208) after signing an informed consent form. Couples suitable for the sequencing-based PGT procedure were included from December 2019 to December 2020 (**Table 1**). Oocytes were fertilized by means of ICSI and embryos that had developed to the blastocyst stage, showing a distinct inner cell mass and trophectoderm, underwent laser-assisted trophectoderm biopsy in G-MOPS PLUS (Vitrolife) at Day 5/6 post-fertilization[9]. Biopsy samples containing five to eight trophectoderm cells were further subjected to genetic analysis.

Table I | Samples used for clinical validation of the ETS-PGT approach

Inheritance mode[a]	Indication[b] (#)	PGT samples (#)			
		Without ETS		With ETS	
		Bulk	WGAed	Bulk	WGAed
AD	61	83	39	220	154
AR	47	47	1	149	94
XL	10	11	1	37	30
XL/AR	1	0	0	3	0
AD/AR	4	3	0	10	3
Total	**123**	**144**	**41**	**419**	**281**

ETS, embryo tracking system; PGT, preimplantation genetic testing; WGAed, whole-genome amplified few-cell DNA samples; Bulk, bulk DNA samples.

[a] AD, autosomal dominant disorders; AR, autosomal recessive disorders; XL, X-linked disorders; XL/AR, both autosomal recessive and X-Linked disorders; AD/AR, both autosomal recessive and dominant disorders.

[b] Genetic indications (genes) per inheritance mode.

Figure 1 | ETS-PGT design, mass production and implementation in PGT practice

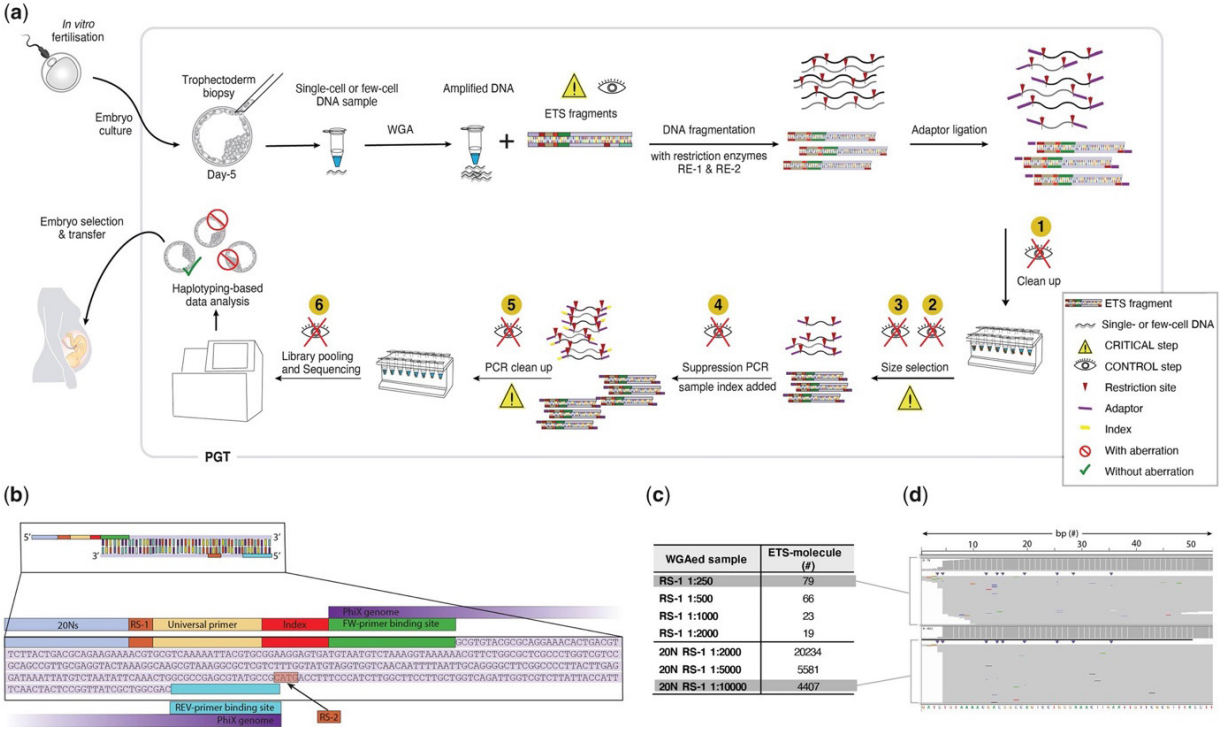

*(**a**) Implementation of the ETS in sequencing-based PGT procedure increases quality assurance and efficiency of sequencing-based PGT by avoiding controls in six crucial Control steps. (**b**) ETS fragments are based on the 429 nt amplicons of the PhiX 174 genome (purple) which contain the forward (FW, green) and reverse (REV, turquoise) primer binding site and the second restriction site (RS-2, brown). Added at the 3' end is a unique 11 nt Illumina index (red), an 18 nt universal primer binding site (yellow), the first restriction site (RS-1, brown) and a 20 nt random nucleotide sequence (blue). (**c**) Dilution and number of retrieved ETS fragment with and without 20 random nucleotides. (**d**) Low-yield (upper panel) and high-yield (lower panel) ETS without and with 20-nt, respectively. ETS, embryo tracking system; PGT, preimplantation genetic testing; RE-1, restriction enzyme one; RE-2, restriction enzyme two.*

PGT procedure and library preparation

The library preparation method for massively parallel sequencing, with an adapted form of the haplarithmisis algorithm, called OnePGT solution, has been previously described[9]. Surplus whole embryos were collected in a total of 2 µl washing buffer (Ca2+ and Mg2+ free phosphate-buffered saline with 0.2% polyvinylpyrrolidone (Sigma-Aldrich Chemie BV)). Bulk DNA samples of parents and phasing references were isolated from peripheral blood. All WGA products and genomic DNA from parents and references were then processed using OnePGT solution (Agilent Technologies) according to the manufacturer's instructions. Briefly, 500 ng of (whole-genome amplified (WGAed) or bulk) DNA was fragmented through restriction enzyme digestion, adapter-ligated, size-selected with PippinHT (Sage Science, USA) and PCR-amplified to yield a reduced representation library per sample. Per sequencing run, libraries of 24 samples were pooled equimolarly and sequenced on an Illumina NextSeq 500 using the High output (2 × 150 bp) kit (Illumina). The ETS is scalable as it has the capacity to pool 96 samples at a time using the 96 different ETS devised fragments (see **Supplementary Table S1**). A total of 885 samples (322 WGAed DNA from embryo biopsies and 563 peripheral blood DNA samples) were included in this study. Of the embryo trophectoderm biopsies, 308 were derived from '4–8 cells', 13 samples were from '9–15 cells' and 2 samples were from '16–25 cells'.

ETS amplicons preparation

The unique index sequence of the ETS amplicons was generated as described previously[16]. ETS amplicons were prepared by PCR using PhiX174 RF II DNA (New England Biolabs) as template DNA. In brief, each amplification reaction consisted of 200 ng of PhiX174 DNA (New England Biolabs), 0.5 µM of ETS-indexes forward primer, 0.5 µM ETS universal reverse primer and Q5 hot start high-fidelity 2× master mix (New England Biolabs). PCRs were performed on a Labcycler thermal cycler (Sensoquest GmbH) using the following conditions: 98°C for 30 s, 35 cycles of 98°C for 10 s, 60°C for 20 s, 72°C for 30 s and a final elongation step at 72°C for 30 s. A total of three PCR reactions were performed for each ETS amplicon. PCR products of each ETS amplicon were pooled and purified using the QIAquick PCR Purification Kit (Qiagen) and eluted in 30 µl of Qiagen elution buffer. Fragment concentration was measured using the Qubit™ dsDNA HS Assay Kit (Invitrogen). Each ETS amplicon was adjusted to a final concentration of 3 ng/µl, aliquoted and stored at −20°C as stock ETS plates. ETS amplicons were diluted further to 0.03 ng/µl. ETS fragments (**Fig. 1a**) and the entire ETS design (**Fig. 1, Supplementary Table SI**) were optimized and validated for sequencing-based PGT.

Haplarithmisis-based PGT

Demultiplexed sequencing data of both ETS indexes and sequencing-based PGT were mapped to the human reference genome, GRCh37/hg19, complemented with the

sequences of all ETS amplicons. Subsequently, the number and purity of the expected ETS fragments for each sample were computed. Purity (PUR) represents the percentage of an ETS fragment for a sample '*s*':

$$PUR_s = \frac{\sum_e eETS_{s,e}}{\sum_d dETS_{s,d}} x\ 100$$

where eETS is the number of expected ETS fragments and dETS is the number of detected ETS for sample '*s*', i.e. dETS is total number of both expected and unexpected ETS fragments. The index sequence of ETS amplicons was extracted using samtools (version 1.2)[19]. Data from sequencing-based PGT samples were analyzed using our analytical pipeline which includes a pre-PGT test and several quality control steps to ascertain genome-wide copy-number and haplotype profiles for each embryo. Briefly, we applied haplotypecaller from the GATK tool[20] to extract the genomic locations annotated in the dbSNP database (version 150). Using the R-function extract.gt (vcfR package bioconductor), the coverage of the genomic locations was calculated per sample. We then applied haplarithmisis as described previously[2].

4

***In silico* tracking of embryos**

The index sequence of ETS amplicons were extracted from the alignment (bam) files using samtools (version 1.2)[19]. Then, filtered for ETS amplicons with a minimal of 50 reads and the ETS amplicon with the highest number of reads was reported as a percentage of total ETS amplicons detected. The reported ETS amplicon is matched with the added ETS amplicon.

Other statistical analysis and visualization

The breadth and depth of coverage were compared per sample type (bulk or WGAed) using Welch's *t*-test which is robust to sample groups with unequal variances and sizes. Non-parametric allele drop out (ADO) and allele drop in (ADI) rates in WGAed samples were compared with ETS (n = 241) and without ETS (n = 51) using Wilcoxon signed-rank tests. Substandard samples (n = 5) were excluded based on QC-by-parents criteria[2] and the interquartile range above Q3 + 1.5 interquartile range (IQR). For genome haplarithm visualization, we applied adapted visualization modules of siCHILD.

Results

Embryo tracking system design

For the ETS fragments, we made use of the PhiX 174 DNA sequence as a template and amplified them with uniquely designed PCR primers that are specific to the PhiX genome, such that each restriction enzyme could cleave the DNA in only one location. PCR primer pairs with an optimal melting temperature and single restriction site, resulted in a PhiX amplicon length of 429 bp, including a forward primer at PhiX genome position 742 and a reverse primer at PhiX genome position 1138. The identification of a PhiX endogenous 3′ restriction site (RS-2) and the addition of a 5′ restriction site (RS-1) allowed us to make these fragments compatible with sequencing-based PGT. We further optimized the fragments by adding an 11 nt unique index[21-23] adjacent to the PhiX forward primer binding site as well as a universal primer (5′-GGCGTCCATCTCGAAG-3′) between RS-1 and the index. For optimal binding of the restriction enzyme, 20 random nucleotides were added at the 5′-end prior to RS-1 (**Fig. 1b**).

ETS fragment quantity and purity for next-generation sequencing-based PGT

The amount of ETS fragments added to the samples was optimized by making a dilution range in the WGAed DNA samples (**Fig. 1c**). The low yield of the ETS molecules indicated a suboptimal digestion when the molecule started directly with the restriction site RS-1 (**Fig. 1d**, upper panel). However, the incorporated 20-nucleotide fragment enabled optimal restriction enzyme binding (**Fig. 1d**, lower panel). Reducing to a 1:10000 dilution resulted in median of 2475 (IQR = 1378–4120) ETS molecules detected after sequencing (**Fig. 2a**). In addition, we calculated the purity of the ETS fragments for each sample and 689 out of 693 samples (99.42%) had a purity >98% (**Fig. 2b, Supplementary Fig. S1**). The small deviation from 100% purity could be due to amplification and/or sequencing errors. Overall, the ETS fragment purity in all the 693 samples had a median of 99.86% (IQR = 99.75–99.94%).

ETS implementation and clinical validation for PGT

Adding ETS fragments to WGAed or bulk DNA samples before sequencing-based PGT eliminates the necessity of the four-eyes principle at six Control steps (**Fig. 1a**), thus facilitating accurate and scalable PGT. The Critical steps indicate quality sensitive steps. At these steps, the DNA concentration is measured to detect if it falls within the QC-range of each specific step. The Control steps are the ones that four-eyes principle should be applied to avoid sample swap. In the process, both the DNA samples and ETS fragments are registered *in silico*. During the cleanup with magnetic beads, the purified product is removed from the wells with beads. At Control steps 2 and 3, the products are size selected and transferred back to new wells and after dilution suppression PCR is performed and indexes are added (Control step 4). Subsequently, the product is

cleaned (Control step 5), similar to Control step 2. At the last Control step 6, 24 samples are pooled and prepared for a sequencing run (see also **Table II**).

To clinically evaluate ETS-PGT, we analyzed WGAed DNA samples from IVF preimplantation embryos (n = 322) of couples (n = 162) who opted for PGT with 123 different genetic indications (**Table I** and **Supplementary Table SII**). The PGT procedure was performed on DNA samples with and without the ETS. By adding 0.06 ng of ETS fragments to 500 ng DNA samples, we observed comparable depth of coverage (bulk ETS: 12.76 ± 1.86 SD versus bulk without ETS: 12.47 ± 2.33 SD, $P = 0.176$ Welch's *t*-test, and WGAed ETS: 11.88 ± 1.63 SD versus WGAed without ETS: 11.55 ± 1.88 SD, $P = 0.283$ Welch's *t*-test) but slightly lower breadth of coverage in the WGAed ETS samples as compared to WGAed samples processed without ETS (bulk ETS: 13.70% ± 1.50% SD versus 13.65% ± 2.94% SD, $P = 0.846$ Welch's *t*-test, and WGAed ETS: 12.96 ± 1.24 SD versus WGAed without ETS: 13.96 ± 2.16 SD, $P = 0.005$ Welch's *t*-test) (**Fig. 2c**). The accuracy of the assayed SNP calls was measured by computation of WGA artifact using parental SNP calls to determine mendelian inconsistencies[2]. We found comparable ADO and ADI WGA artifacts ($P = 0.153$, Wilcoxon signed-rank test). Genome-wide ADO rates with and without ETS were 9.48% (±2.53% SD) and 8.05% (±1.36% SD), respectively. Genome-wide ADI rates with and without ETS were 3.86% (±1.73% SD) and 4.45% (±0.86% SD), respectively (**Fig. 2d**). Furthermore, the resulting genome-wide haplotype calls were 99.04% (±0.12% SD) concordant in embryos (n = 3) of one family for which we performed PGT with and without ETS on the same WGAed DNA samples (**Fig. 2e**).

Table II | Ruling out possible risks via ETS in a sequencing-based PGT haplotyping procedure

NGS-based PGT step (see Fig. 1a)	Without ETS				With ETS			
	Sample swap risk		Sample cross contamination		Sample swap risk		Sample cross contamination	
	presence	detected	presence	detected	presence	detected	presence	detected
DNA fragmentation	yes	no	yes	no	yes	yes	yes	yes
Adaptor ligation	no	n/a	no	n/a	no	n/a	no	n/a
PCR clean up #1	yes	no	yes	no	yes	yes	yes	yes
Size selection	yes	no	yes	no	yes	yes	yes	yes
Suppression PCR	yes	no	yes	no	yes	yes	yes	yes
PCR clean up #2	yes	yes	yes	yes	no	n/a	yes	yes

*During the NGS-based PGT, different types of risks can be introduced, but ETS can detect all those risks (see also **Fig. 1a**). Orange represents the possible risks or failure to detect those risks. Green represents no risk or ability to detect the risk. Grey represents steps with no risk introduced.*
ETS, embryo tracking system; PGT, preimplantation genetic testing; NGS, next-generation sequencing.

Figure 2 | Application of the embryo tracking system (ETS) for preimplantation genetic testing (PGT) from sequenced reads to reconstructed haplotypes

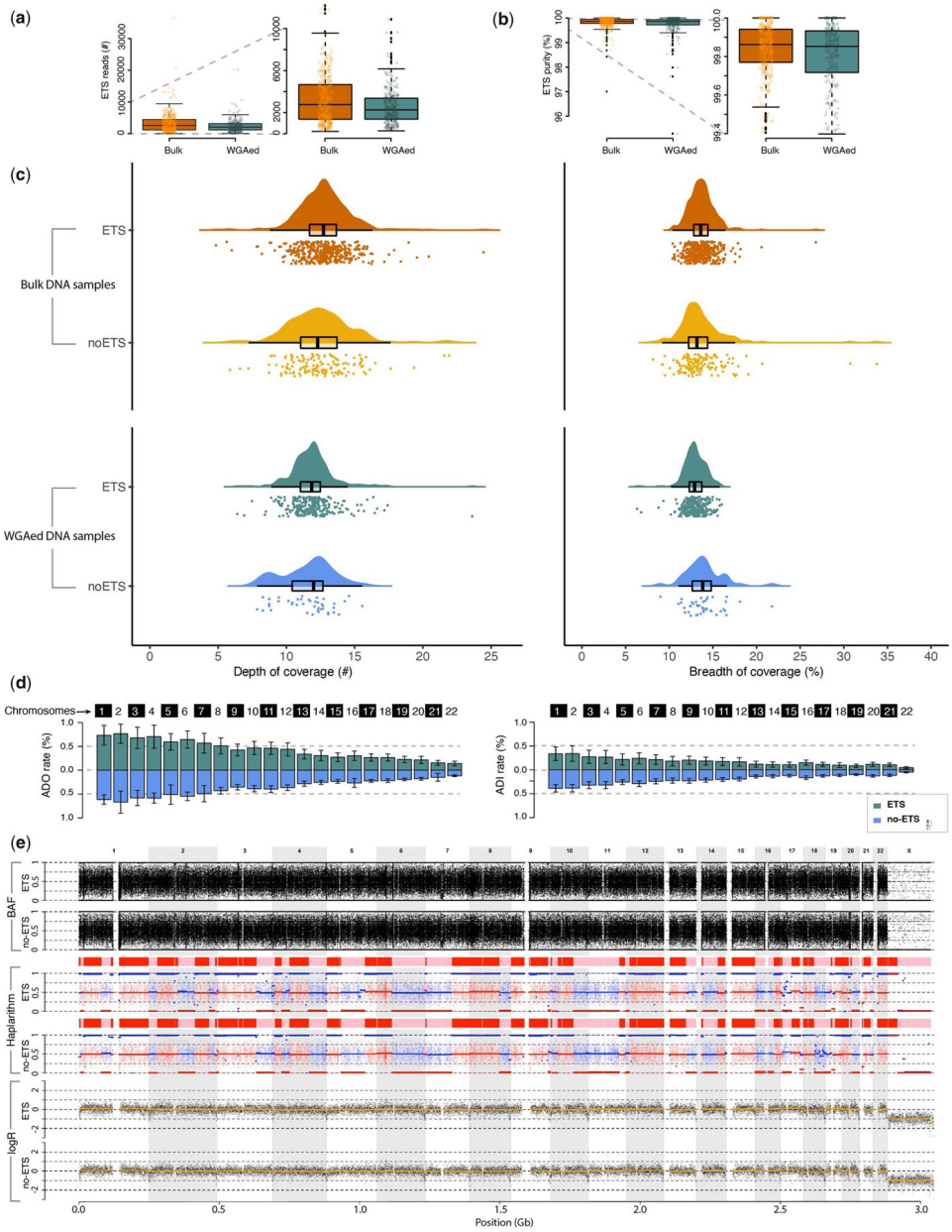

*(**a**) Number of ETS fragments and (**b**) their purity in all the samples (n = 885) that were processed by the ETS-PGT protocol. (**c**) Average depth and breadth of coverage with and without ETS for whole-genome amplified (WGAed) (n = 322) and bulk (n = 563) DNA samples. (**d**) Allelic dropout (ADO) and allelic drop in (ADI) rates following QC-by-parents analysis that computes mendelian inconsistencies across all WGAed samples (n = 241 with ETS and n = 51 without ETS). (**e**) Genome-wide profiles with and without ETS-PGT. From top to bottom, we show B allele frequency (BAF) profiles, maternal haplotypes and haplarithms and logR (relative copy number) values of embryo B2, each with and without ETS, respectively (see also Supplementary Fig. S1).*

ETS rules out the chance of sample switching during PGT procedure

Without the four-eyes principle at the six error-prone Control steps, it is not possible to detect sample switching. To test our system, we intentionally mixed samples with no, wrong or mixed ETS fragments in both WGAed and bulk DNA samples. Our computational pipeline could easily trace switched and mixed samples (**Supplementary Fig. S2**) such that by adding ETS fragments to DNA samples prior to the sequencing-based PGT process, all the possible sample switching or cross-contamination events could be detected (**Table II**), thereby, eliminating the necessity of controls at six critical steps.

To evaluate sensitivity of detecting contamination of WGAed DNA samples with other DNA samples without ETS, we made different admixtures of two sibling embryos (**Fig. 3**): one normal diploid embryo (Embryo1) and the other with trisomy Chr 22 (Embryo2). Since our approach is genome wide, this allowed us to examine admixtures of both (i) normal diploid and trisomy (**Fig. 3a**), as well as (ii) normal disomic chromosomes of Embryo1 and Embryo2 (**Fig. 3b**). This experiment revealed that contaminations <10% cannot be detected without ETS and that only contaminations >30% can be detected in discrete haplotypes with false haplotype blocks and false positive crossover sites, albeit distortion of B-allele frequency values in haplarithms is indicative of contaminations. The 50:50% admixture showed a combination of both embryos, indicating that PGT-M cannot be performed (**Fig. 3b**). Moreover, contaminations <10% with WGAed DNA sample of a trisomy cannot be accurately detected in the logR-values (**Fig. 3a**).

Figure 3 | Detection of sample contamination through admixing whole-genome amplified (WGAed) samples of two sibling embryos in different proportions (diploid Embryo1 and Embryo2 with Chromosome (Chr) 22 trisomy) without the embryo tracking system (ETS)

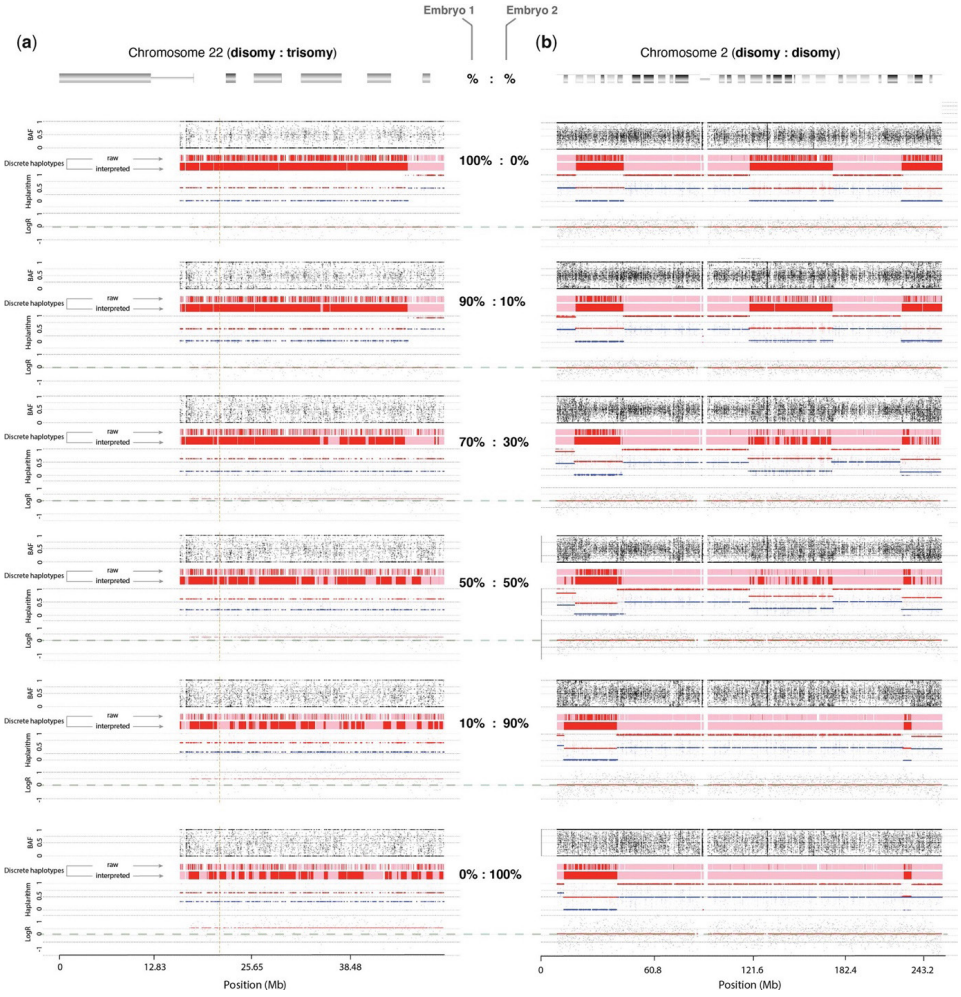

*(**a**) Normal disomic Chr22 of Embryo1 and Chr22 trisomy of Embryo2. (**b**) Normal Chr2 disomy of Embryo1 and Embryo2. Per mixture experiment (from top to bottom), we show B allele frequency (BAF) profile, raw and interpreted maternal haplotypes, maternal haplarithm and relative copy-number profile. Green dashed lines depict the baseline copy number 2 (logR = 0, i.e. disomic chromosome).*

Discussion

In the presence of PGT guidelines that provide best laboratory and clinical practice for traditional PGT approaches[24], misdiagnoses still occur with estimated rates of <1% and <5% for FISH- and PCR-based PGT, respectively[12]. The rate of misdiagnosis and adverse outcomes of sequencing-based PGT have not yet been reported. However, a number of laboratory errors, such as tube switching, could occur leading to a PGT-misdiagnosis with potentially devastating effects, such as the transfer of an affected embryo[12]. In the improved PGT international guidelines, to avoid misdiagnosis, it is currently recommended to have an extra observer during labeling and sample identification steps for PGT quality control and assurance[25]. Here, we demonstrate that ETS-PGT enables detection of very low contamination of DNA samples from two different embryos (<1%, **Fig. 2b**), even if the embryos are from the same couple (sibling embryos). Contaminations with unrelated (embryo) DNA samples can be detected with our rigorous QC-by-parents criteria[2], such that samples with >15% mendelian inconsistencies and <80% concordant SNP calls are labeled as substandard and diagnosis is not performed. When DNA sample mixing occurs, samples with more than 2% of unexpected ETS fragments will be excluded from the downstream PGT analysis. Without the ETS, however, <10% of contamination can go unnoticed when a euploid WGAed DNA sample is contaminated by an aneuploid one (**Fig. 3a**) and only >30% contamination can be detected with certainty when two euploid WGAed DNA samples are mixed (**Fig. 3b**). In the case of contamination during ETS index preparation, i.e. contamination of ETS molecules, the similar low purity percentage in all samples receiving the same contaminated ETS amplicons will be observed. While our purity determination approach would prevent misdiagnosis, it could lead to repetition of a PGT run, as library preparation and sequencing would have to be repeated with the new WGA aliquot of the same biopsy together with highly pure ETS fragments (>98%). Therefore, determining the purity of ETS amplicons prior to PGT implementation using a pre-PGT quality control assay with non-human DNA is recommended.

Clinical massively parallel sequencing increasingly leads to discovery of novel pathogenic variants[5] and therefore inherently increases PGT requests by couples with such mutations. PGT by sequencing-based haplotyping could alleviate this high demand, as genome-wide PGT methods are generic, i.e. they do not require family- and locus-specific designs. Although stringent laboratory procedures are effective to reduce the risk of sample switching and cross-contamination, they are cost-prohibitive and still subject to errors. Here, we developed and clinically implemented ETS-PGT that effectively increases sequencing-based PGT quality assurance and throughput. ETS can easily be utilized in any restriction enzyme-based protocol, including automated sequencing-based PGT to support increased PGT requests in the future with a shorter

turnaround time. ETS is not only suitable for PGT procedures but could also be implemented in other next-generation sequencing-based parallel procedures, such as non-invasive prenatal testing, single-molecule molecular inversion probes and whole-genome sequencing. We envision that ETS-PGT will rapidly be adopted in IVF clinics and will be incorporated into PGT best practice guidelines.

Data Availability

The data underlying in this article cannot be shared publicly in order to protect the privacy of the individuals who participated in the study. The anonymized data can be requested through the corresponding author.

Acknowledgements

We gratefully thank all the families who participated in this study. We thank Ping Cao and Darina Obukhova for critical reading of the manuscript.

Authors' roles

K.D., J.D., A.D.C.P., A.v.d.W. and M.Z.E. designed the study. W.v.D. and K.D. contributed to ETS fragment design. W.v.D., M.D. and J.M. performed the experiment. K.D., J.M., R.K., R.E., E.C. and M.Z.E. analyzed and interpreted the data. W.v.D. and M.Z.E. drafted the manuscript. W.v.D., M.D., C.d.D.-S., S.S., H.G.B., A.D.C.P. and M.Z.E. contributed to writing and critical revision of the manuscript.

Funding

M.Z.E. is supported by the EVA (Erfelijkheid Voortplanting & Aanleg) specialty program (grant no. KP111513) of Maastricht University Medical Centre (MUMC+) and the Horizon 2020 innovation (ERIN) (grant no. EU952516) of the European Commission.

Conflict of interest

M.Z.E is co-inventor on patent applications: ZL910050-PCT/EP2011/060211-WO/2011/157846 'Methods for haplotyping single cells' and ZL913096-PCT/EP2014/068315-WO/2015/028576 "Haplotyping and copy-number typing using polymorphic variant allelic frequencies".

References

1 Steptoe, P. C. & Edwards, R. G. Birth after the reimplantation of a human embryo. *Lancet* **2**, 366 (1978). https://doi.org/10.1016/s0140-6736(78)92957-4

2 Zamani Esteki, M. *et al.* Concurrent whole-genome haplotyping and copy-number profiling of single cells. *Am J Hum Genet* **96**, 894-912 (2015). https://doi.org/10.1016/j.ajhg.2015.04.011

3 Handyside, A. H., Kontogianni, E. H., Hardy, K. & Winston, R. M. Pregnancies from biopsied human preimplantation embryos sexed by Y-specific DNA amplification. *Nature* **344**, 768-770 (1990). https://doi.org/10.1038/344768a0

4 Backenroth, D. *et al.* Haploseek: a 24-hour all-in-one method for preimplantation genetic diagnosis (PGD) of monogenic disease and aneuploidy. *Genet Med* **21**, 1390-1399 (2019). https://doi.org/10.1038/s41436-018-0351-7

5 Gilissen, C. *et al.* Genome sequencing identifies major causes of severe intellectual disability. *Nature* **511**, 344-347 (2014). https://doi.org/10.1038/nature13394

6 Schobers, G. *et al.* Liquid biopsy: state of reproductive medicine and beyond. *Hum Reprod* **36**, 2824-2839 (2021). https://doi.org/10.1093/humrep/deab206

7 Sallevelt, S. C. E. H. *et al.* Diagnostic exome-based preconception carrier testing in consanguineous couples: results from the first 100 couples in clinical practice. *Genet Med* **23**, 1125-1136 (2021). https://doi.org/10.1038/s41436-021-01116-x

8 Vermeesch, J. R., Voet, T. & Devriendt, K. Prenatal and pre-implantation genetic diagnosis. *Nat Rev Genet* **17**, 643-656 (2016). https://doi.org/10.1038/nrg.2016.97

9 Masset, H. *et al.* Multi-centre evaluation of a comprehensive preimplantation genetic test through haplotyping-by-sequencing. *Hum Reprod* **34**, 1608-1619 (2019). https://doi.org/10.1093/humrep/dez106

10 Masset, H. *et al.* Single-cell genome-wide concurrent haplotyping and copy-number profiling through genotyping-by-sequencing. *Nucleic Acids Res* **50**, e63 (2022). https://doi.org/10.1093/nar/gkac134

11 De Witte, L. *et al.* GENType: all-in-one preimplantation genetic testing by pedigree haplotyping and copy number profiling suitable for third-party reproduction. *Hum Reprod* **37**, 1678-1691 (2022). https://doi.org/10.1093/humrep/deac088

12 Wilton, L., Thornhill, A., Traeger-Synodinos, J., Sermon, K. D. & Harper, J. C. The causes of misdiagnosis and adverse outcomes in PGD. *Hum Reprod* **24**, 1221-1228 (2009). https://doi.org/10.1093/humrep/den488

13 Pfeifer, J. D. & Liu, J. Rate of occult specimen provenance complications in routine clinical practice. *Am J Clin Pathol* **139**, 93-100 (2013). https://doi.org/10.1309/AJCP50WEZHWIFCIV

14 Sehn, J. K. *et al.* Occult Specimen Contamination in Routine Clinical Next-Generation Sequencing Testing. *Am J Clin Pathol* **144**, 667-674 (2015). https://doi.org/10.1309/AJCPR88WDJJLDMBN

15 Xu, W. *et al.* Coding SNPs as intrinsic markers for sample tracking in large-scale transcriptome studies. *Biotechniques* **52**, 386-388 (2012). https://doi.org/10.2144/0000113879

16 Quail, M. A. *et al.* SASI-Seq: sample assurance Spike-Ins, and highly differentiating 384 barcoding for Illumina sequencing. *BMC Genomics* **15**, 110 (2014). https://doi.org/10.1186/1471-2164-15-110

17 Cusanovich, D. A. *et al.* Multiplex single cell profiling of chromatin accessibility by combinatorial cellular indexing. *Science* **348**, 910-914 (2015). https://doi.org/10.1126/science.aab1601

18 Mulqueen, R. M. *et al.* High-content single-cell combinatorial indexing. *Nat Biotechnol* **39**, 1574-1580 (2021). https://doi.org/10.1038/s41587-021-00962-z

19 Li, H. *et al.* The Sequence Alignment/Map format and SAMtools. *Bioinformatics* **25**, 2078-2079 (2009). https://doi.org/10.1093/bioinformatics/btp352

20 McKenna, A. *et al.* The Genome Analysis Toolkit: a MapReduce framework for analyzing next-generation DNA sequencing data. *Genome Res* **20**, 1297-1303 (2010). https://doi.org/10.1101/gr.107524.110

21 Kozarewa, I. & Turner, D. J. 96-plex molecular barcoding for the Illumina Genome Analyzer. *Methods Mol Biol* **733**, 279-298 (2011). https://doi.org/10.1007/978-1-61779-089-8_20

22 Quail, M. A. *et al.* Optimal enzymes for amplifying sequencing libraries. *Nat Methods* **9**, 10-11 (2011). https://doi.org/10.1038/nmeth.1814

23 Bronner, I. F., Quail, M. A., Turner, D. J. & Swerdlow, H. Improved Protocols for Illumina Sequencing. *Curr Protoc Hum Genet* **80**, 18.12.11-42 (2014). https://doi.org/10.1002/0471142905.hg1802s80

24 Thornhill, A. R. *et al.* ESHRE PGD Consortium 'Best practice guidelines for clinical preimplantation genetic diagnosis (PGD) and preimplantation genetic screening (PGS)'. *Hum Reprod* **20**, 35-48 (2005). https://doi.org/10.1093/humrep/deh579

25 Carvalho, F. *et al.* ESHRE PGT Consortium good practice recommendations for the organisation of PGT. *Hum Reprod Open* **2020**, hoaa021 (2020). https://doi.org/10.1093/hropen/hoaa021

Supplementary Material

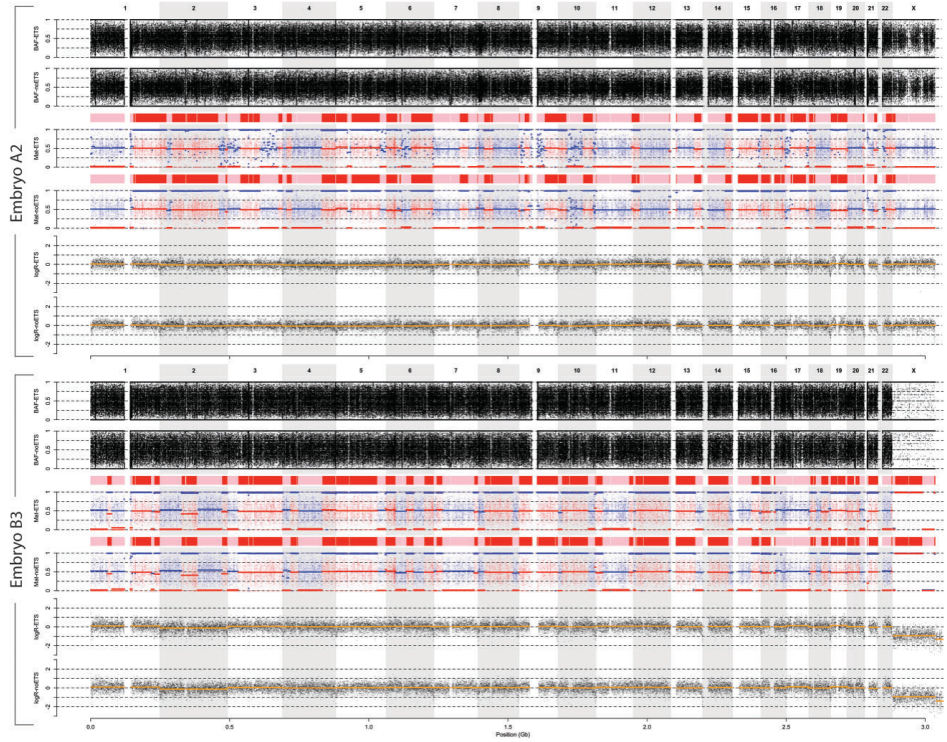

From top to bottom, we show B allele frequency (BAF) profiles, maternal haplotypes and haplarithms, and logR (relative copy number) values of embryos A2 and B3, each with and without the embryo tracking system (ETS). PGT, preimplantation genetic testing.

Supplementary Figure S2 | Embryo tracking system (ETS) assurance for next-generation sequencing-based PGT (NGS-PGT)

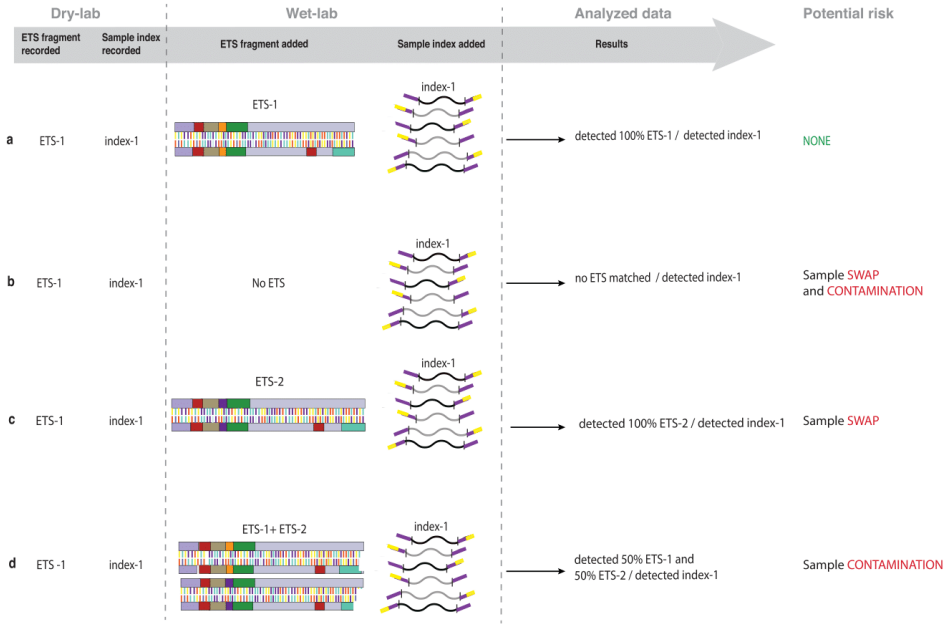

*Prior to the NGS-PGT procedure, ETS fragments and NGS-PGT indexes were recorded, such that switching and contamination could be detected in ETS-PGT. (**a**) An expected scenario where recorded ETS fragments and NGS-PGT indexes were identical. (**b**) Sample switching and contamination were introduced, i.e. in a wet-lab, no ETS was added. (**c**) The wrong ETS was added in the wet-lab to indicate a sample swap. (d) Sample contamination was introduced, by adding two different ETS prior to fragmentation, the first step in the NGS-based PGT.*

Supplementary Table SI |Sequences of ETS fragments including Illumina 11-mer indexes (see the excel file in the online version of the article)
Names and sequences (5' to 3') of the ETS fragments used in this study.

Supplementary Table SII | Detailed overview of the samples used for clinical validation of ETS-PGT approach (see the excel file in the online version of the article)
Detailed description of the samples included in this study for the clinical validation of the ETS-PGT approach. Included are the disease and gene names, inheritance patterns, OMIM identifiers, locations and characterisation of the variants and number of families / samples included for each indication.

Chapter 5

Clinical whole-genome sequencing-based haplarithmisis enables simple, scalable, and universal preimplantation genetic testing

---

Anouk Janssen*, Rebekka M. Koeck*, Rick Essers*, Wanwisa van Dijk, Marion Drüsedau, Jeroen Meekels, Burcu Yaldiz, Maartje van de Vorst, Bart de Koning, Debby Hellebrekers, Servi Stevens, Su Ming Sun, Malou Heijligers, Sonja de Munnik, Chris van Uum, Lisenka Vissers, Edith Coonen, Jos Dreesen, Christine de Die-Smulders, Han Brunner, Arthur van den Wijngaard, Aimee Paulussen, Masoud Zamani Esteki

***Joint first authors**

My contribution: processing, analysis, visualisation and write-up of i) the data quality control parameters, ii) the data generated to assess structural rearrangements and iii) the data generated to assess mitochondrial indications. Further contributions to the visualisation of haplarithmisis results for monogenic disorders and aneuploidy evaluation.

Manuscript in preparation

Abstract

Preimplantation genetic testing (PGT) is a widely used method to select *in vitro* fertilised embryos that do not harbour severe genetic abnormalities, thereby reducing the burden of heritable genetic disease. Growing demand for PGT has led to methodological advances and the testing scope has been expanded to include non-hereditary anomalies, such as aneuploidies, to aid embryo ranking and increase pregnancy rates. However, the clinical effectiveness of this approach has not been proven.

To address the limitations and challenges of current PGT methods, we introduce a whole-genome sequencing-based PGT approach (WGS-PGT) that is simplified, scalable and universally applicable. By applying WGS-PGT to 20 families (48 embryos) we showcase the method's i) reduced workflow time, ii) enhanced genome coverage, resulting in higher informative SNP counts and lower Mendelian error rates, iii) capacity for direct mutation analysis, iv) ability to determine the segregational origin and mosaicism level of aneuploidies, v) power to detect unbalanced and balanced structural rearrangements, and vi) capability to assess the mitochondrial genome.

Keywords

Pre-implantation genetic testing (PGT), whole genome sequencing (WGS), assisted reproductive technologies (ART), aneuploidy

Introduction

Preimplantation genetic testing (PGT) is an assisted reproductive technology (ART) that was developed to allow couples who are known carriers of heritable genetic disorders to prevent these from being passed on to their offspring and thereby reduce the burden of severe genetic disease[1]. Prior to the advent of PGT, the only option available to these couples was to undergo second trimester invasive diagnostic testing, i.e., amniocentesis or chorionic villus sampling, followed by a termination of pregnancy in cases where the fetus was proven to be affected. PGT on the other hand, is carried out on one or a few cells biopsied from *in vitro* fertilized embryos and facilitates the selection of unaffected embryos prior to intrauterine transfer and pregnancy. Due to the lower psychological burden associated with this approach[2], the demand for PGT has continually increased since its first application in 1990. In turn, this has driven tremendous advances in the field[3], including an expansion of the scope of testing to include non-hereditary genetic abnormalities that might impact an embryo's success potential or the health of the resulting child.

Data from the most recent ART and PGT reports, suggest that more than 70,000 PGT cycles are being carried out worldwide each year[4-7]. These statistics include PGT offered for monogenic disorders (PGT-M), including those affecting the mitochondrial genome (PGT-MT), structural rearrangements (PGT-SR), and chromosomal abnormalities such as aneuploidies (PGT-A). In Europe, more than half of PGT cycles are conducted for PGT-A[5]. The aim is to identify embryos without chromosomal copy number variations (CNVs), which are thought to have the highest chance of successfully establishing a viable pregnancy. PGT-A deems embryos harbouring any aneuploidies unsuitable for transfer. This practise remains popular despite recent randomised controlled trials (RCTs) casting doubt on the clinical utility of PGT-A, which was not shown to improve live birth rates or reduce pregnancy loss rates after IVF[8-12]. Furthermore, there is a growing body of literature demonstrating the birth of healthy, euploid children after the transfer of (mosaic) aneuploid embryos, and such the practise of discarding these embryos is increasingly criticised. The second most common PGT indication is PGT-M[5]. The Online Mendelian Inheritance in Man (OMIM) database lists more than 4,700 genes that are known to harbour phenotype-causing mutations[13]. Although not all of these are deemed severe enough to offer PGT-M, the number of identified disease-causing mutations, and therefore the number of indications for PGT-M, is expected to continue to rise as advances in sequencing technologies allow us to examine the human genome at an unprecedented level of detail. In addition to increasing demand from a growing list of approved indications, the offer of pre-conception genetic testing could be extended beyond consanguineous couples and high-risk populations (i.e., populations that share a limited, common ancestry) as genomic sequencing becomes cheaper and more

accessible. A population-wide offer of pre-conception carrier testing (PCT) has already been introduced in many countries and will likely contribute to increasing demand for PGT from couples who would have otherwise been unaware of their disease carrier status[14,15]. This clear, growing demand for PGT necessitates the continued development of more efficient, and scalable laboratory and analytical methods for PGT

Initially, PGT-M was carried out using indication-specific, PCR-based short tandem repeat (STR)-marker analysis that needed to be established and validated for each family. Due to the highly labour-intensive nature of this approach, more flexible methods were sought. Over the last decade we have seen the development of genome-spanning haplotyping methods that generate data which easily allow the region of interest (ROI) to be defined for any genetic indication. These methods include SNP array-based karyomapping[16], and sequencing-based methods such as GENType[17] and onePGT[18]. The latter two employ massively parallel, reduced representation genome sequencing, known as genotyping-by-sequencing (GBS), which also allows for concurrent copy number profiling. The reduced library complexity of GBS approaches, covering ~10% of the human genome, offers a cost-effective approach for embryonic genome-wide haplotyping for PGT[19,20]. In conjunction with sophisticated analysis methods such as haplarithmisis, which involves haplotyping and phasing of the embryonic genome by leveraging genetic information from the parents and related reference(s), GBS already offers a genome-wide solution for PGT[21]. Nonetheless, despite the inherent advantages of GBS approaches for PGT-M, in 2018 85% of PGT-M cases reported to the European Society of Human Reproduction and Embryology (ESHRE) PGT consortium were still carried out using PCR-based methods[5]. This may reflect the complexity of the GBS library preparation protocol, which is both time consuming and requires highly skilled laboratory technicians for tasks such as DNA fragment size selection. Furthermore, the need for specialised laboratory instruments is a barrier to automation. Incomplete genome coverage is another limitation of GBS-based PGT. To achieve reasonable diagnostic certainty, at least 8 informative SNPs, where one parent is heterozygous while the other is homozygous, are required in the 2Mb up- and downstream of the genetic indication. This threshold can be especially challenging to achieve in consanguineous couples; when the genetic indication is located in a difficult region of the genome (e.g.: telomeric or centromeric indications); or when there are homologous recombination events in close proximity to the genetic indication. Finally, PGT-A, PGT-SR and PGT-MT cases are not currently assessed using sequencing-based PGT approaches in conjunction with haplotyping, meaning that in cases with two or more different indications multiple laboratory protocols must be conducted on separate biopsies from the same embryo. These points highlight the need to develop a universal method for all forms of PGT that employs a simplified laboratory protocol and generates data with sufficient genome coverage to also resolve genetic indications at difficult locations.

Here, we present the first simple, scalable, and universal whole genome sequencing (WGS)-based method for PGT (WGS-PGT) that enables (simultaneous) (i) PGT for complex cases, including consanguineous couples, when an indication is located in a difficult genomic region, or when homologous recombination events occur in the vicinity of the genetic indication, (ii) direct detection of single base pair mutations and deletions, (iii) accurate determination of segregational origin of aneuploidies and their degree of mosaicism, (iv) PGT-SR with the ability to discern between normal embryos and embryos carrying balanced translocations, and (v) PGT for mitochondrial indications.

Results and Discussion

Whole genome sequencing for PGT

The WGS library preparation protocol depicted in **Figure 1A** can be completed in less than one third of the time taken for GBS-PGT library preparation, i.e., 2.8 vs. 8.5 hours respectively (**Fig. 1B**). Additionally, WGS-PGT eliminates the need for size selection using specialised gel electrophoresis machinery and therefore has the potential to be fully automated from end-to-end on a single liquid handling platform. The possibility of automation is vital for laboratories to be able to meet the continually growing demand for PGT[5,6] and would also eliminate the risk of sample switching that could theoretically lead to misdiagnosis[22]. Additionally, the incorporated embryo tracking system (ETS) already offers certainty that sample switching or mixing has not occurred[22]. Furthermore, considering that the WGS-PGT protocol can be implemented using only standard laboratory equipment, the set-up costs for laboratories wishing to upgrade from PCR-based PGT to sequencing-based PGT would be minimal.

Figure 1 | Study Overview

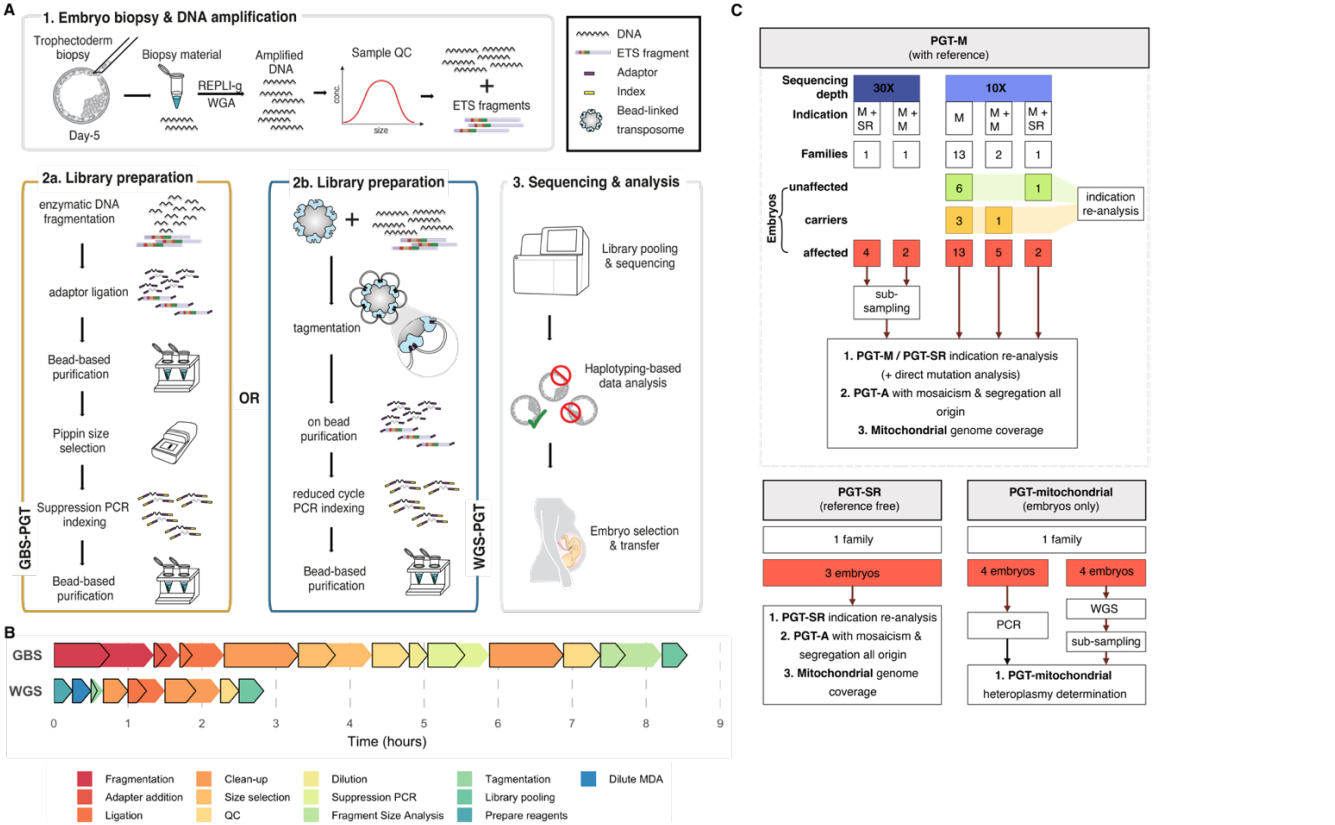

A) *The PGT protocol used for this study including the embryo biopsy procedure, DNA amplification, library preparation using GBS-PGT (2a) or WGS-PGT (2b), data generation and processing and clinical decision making.* ***B)*** *Time requirements for library preparation using GBS-PGT and WGS-PGT. The coloured arrows represent different steps of the protocol, while the black outlines depict the required hands-on time.* ***C)*** *Sample inclusion and analysis of this study.*

WGS-PGT generates higher resolution data than GBS-PGT

To assess the suitability of WGS for haplarithmisis-based PGT, and to ascertain the optimal depth of coverage for accurate diagnosis, we undertook deep sequencing (~30-40X) of two PGT families, including 6 embryos (**Fig. 1C**), and performed subsampling to simulate 5-30X depth of genome coverage. Using WGS we achieved a breadth of coverage exceeding 80%, while GBS covered less than 20% of the genome. This breadth of coverage was maintained for all simulated depths of coverage greater than or equal to 10X, with only 5X depth of coverage showing significantly lower breadth of coverage (**Fig. 2A**). Additionally, WGS-PGT yielded a significantly higher number of informative SNPs compared to GBS-PGT (**Supplementary Fig. 1B-D**) thereby increasing the accuracy and reliability of the haplotype inference. For example, at 10X depth of coverage, a ten-fold increase in the number of informative SNPs was seen compared to GBS, reaching, on average, a total of 2.5 million informative SNPs (**Supplementary Fig. 1B**). We also compared the haplotype results obtained by GBS and WGS at sites covered by both methods and found that these were more than 95% concordant regardless of simulated depth of coverage (**Supplementary Fig. 1E**) Furthermore, we observed lower Mendelian inconsistency rates in WGS-PGT (4.6% ± 1.35, mean ± SD, at 10X coverage) data compared to GBS-PGT (11.3% ±1.26, mean ± SD) data, except at 5X coverage (**Supplementary Fig. 2A**). It is noteworthy that one of the included embryos contained an aneuploid chromosome and four embryos harbour unbalanced translocations, without which the Mendelian inconsistency rate is expected to be lower for both methods. Based on these findings, we concluded that 10X sequencing provided sufficient data to reliably conduct Haplarithmisis-based PGT.

We further validated this by sequencing samples from 16 families (31 embryos) at 10X depth of coverage (**Fig. 1C, methods**). Specifically, we selected PGT families that were difficult to analyse using GBS-PGT due to, for example, telomeric indications, consanguinity, double indications, or homologous recombination events in close proximity to the indication (**Supplementary Table 1**). While we observed a disparity in the obtained depth of coverage between whole genome amplified (WGAed) and bulk samples for GBS, this was not seen after WGS library preparation (**Fig. 2B**). The difference in the GBS samples likely represents a loss of restriction enzyme sites during amplification leading to a lower library yield. WGS-PGT on the other hand, does not depend on restriction enzymes and therefore overcomes this amplification bias. Directly sequencing at a depth of coverage of 10X yielded comparable results to the sub-sampling simulation. Namely, per sample the mean number of informative SNPs was 4,737,652 and the mean Mendelian inconsistency rate was 2.42% (±2.23 SD) for WGS compared to 7.66% (±2.33 SD) for GBS (n = 29) (**Fig 2C, Supplementary Fig. 2B**). Moreover, the mean maternal haplotype concordance was 97.8% (±3.9 SD), and median paternal haplotype concordance was 99.0% (±1.6 SD) (**Fig 2D**). An outlier was observed for maternal haplotype concordance, at 81.0%, in an embryo with a triploid genome.

Given our selection of challenging indications, 12 of the 35 included indications were categorised as inconclusive after GBS-PGT, of these a further 5 could be resolved using WGS-PGT (**Fig. 3**). To verify reproducibility of the library preparation and sequencing, library preparation was performed twice for family 4 and showed comparable genomic coverage, and haplotype concordance (data not shown).

Figure 2 | Quality of WGS-PGT data compared to GBS-PGT data

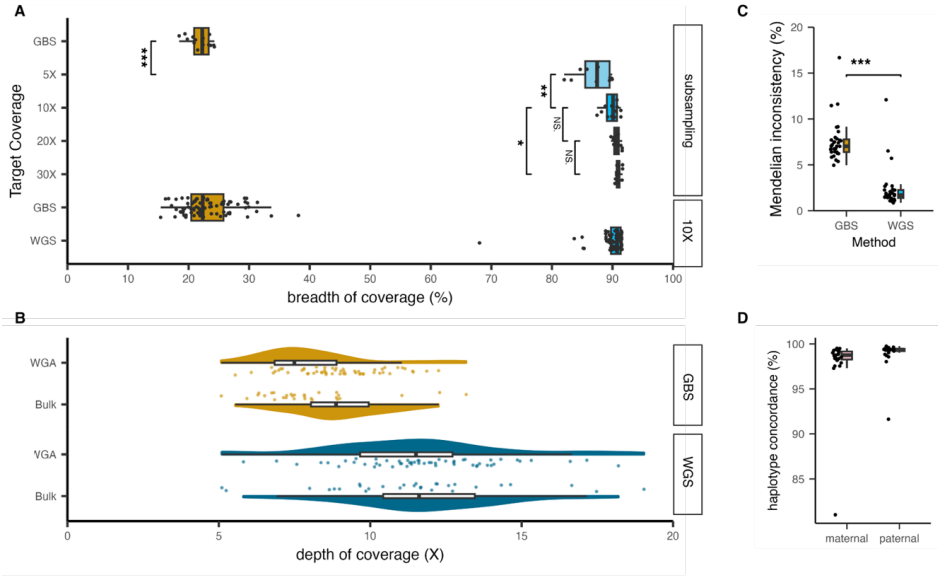

A) *Boxplots showing the breadth of coverage of deep sequenced and subsampled WGS-PGT samples (n = 12) as well as 10X sequenced WGS-PGT samples (n = 31) alongside their corresponding GBS-PGT data.* ***B)*** *Raincloud plots showing the depth of coverage of 10X sequenced WGS-PGT bulk (n = 58) and whole genome amplified (WGAed) embryo (n = 31) samples alongside their corresponding GBS-PGT data. C) Boxplot showing the WGS-PGT and GBS-PGT Mendelian inconsistency rate for 10X sequenced embryos (n = 31). D) Boxplot showing the maternal (pink) and paternal (blue) haplotype concordance between GBS-PGT and WGS-PGT for 10X sequenced embryos (n = 31). All boxplots show the 25th percentile, median and 75th percentile with whiskers extending to 1.5 times the interquartile range. The points represent individual samples with GBS-PGT samples shown in gold and WGS-PGT samples shown in blue.*

To the best of our knowledge, this study is the first comprehensive clinical validation of a WGS approach to PGT. We clearly demonstrate that the higher resolution data gained from WGS-PGT, compared to GBS-PGT, is beneficial to resolve challenging PGT-M indications. This highlights the clinical value of WGS-PGT, which would allow the offer of PGT-M to be extended to more couples for whom PGT is not possible with current methods, and by determining a diagnosis for previously inconclusive embryos, couples may have more embryos available for transfer.

Figure 3 | WGS-PGT generates higher resolution data for PGT-M

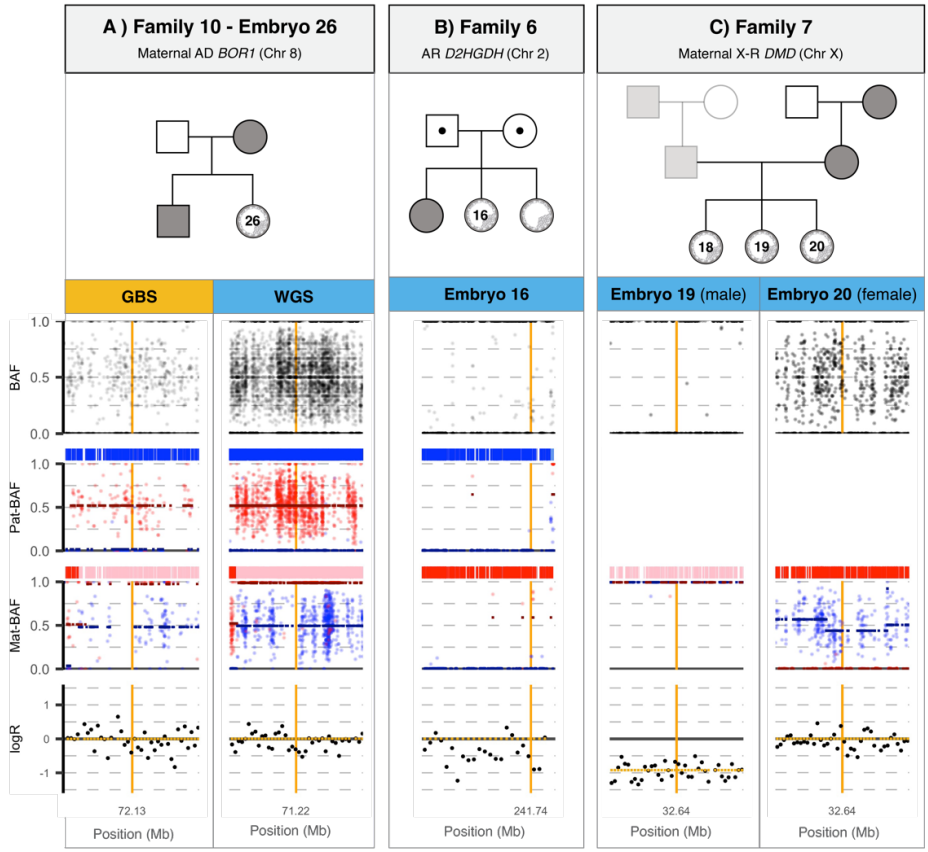

*Representative haplarithmisis plots showcasing the increased data resolution obtained using WGS-PGT vs. GBS-PGT (**A**) and the possibility to resolve all classes of genetic indications, i.e., autosomal dominant (**A**), autosomal recessive (**B**) and X-linked indications in both male and female embryos (**C**). Shown are the family pedigrees, (parentally informative) BAFs, inferred haplotypes and logRs. The data shown were generated with GBS (gold) or WGS (blue).*

Direct mutation analysis is possible with WGS-PGT

Currently, PGT faces challenges when a close relative is unavailable for phasing and in cases where prospective couples present with *de novo* mutations such that grandparents are non-informative for haplotype exclusion analysis. For these cases, direct mutation analysis represents a promising alternative which may facilitate a diagnosis. Unlike GBS approaches, which only cover 20% of the genome, our WGS approach covers > 80% of the genome (see above), thereby making direct mutations analysis possible. For the 22 single base substitution or deletion indications included in our cohort (**Supplementary Table 1**), we compared the genotypes and diagnoses ascertained from direct mutation analysis with those anticipated based on haplarithmisis. Direct mutation analysis yielded

the correct diagnosis in 90% (*n* = 20) of cases and the correct genotype in 82% (*n* = 18) of cases (**Fig. 4, Supplementary Fig. 3A, B**). For all incorrectly identified genotypes, the number of reads at the indication site was less than 5 (**Fig. 4**). Remarkably, direct mutation analysis showed promise in resolving cases where the haplarithmisis result was inconclusive. Specifically, embryo 23, which was tested for an autosomal dominant mutation, was deemed inconclusive after haplarithmisis due to the quality control (QC) thresholds for haplarithmisis (**Supplementary text 1**) not being met. Direct mutation analysis on the other hand, clearly showed the presence of the mutant variant, therefore allowing the embryo to be classified as "affected" (**Fig. 4**). All three cases where direct mutation analysis was unsuccessful in determining the correct genotype, were cases that were expected to be heterozygous based on the haplarithmisis results, however, only one allele was detected by direct mutation analysis (**Fig. 4**). This is likely due to the low coverage of the positions in question, which were only covered by two or three reads (**Fig. 4**). To examine whether this approach could also be applied to larger deletions, we visualised indications representing deletions of two or more base pairs (*n* = 11). While deletions spanning two or three base pairs (*n* = 2) could easily be identified (**Supplementary Fig. 3C**), deletions surpassing 50bp, classified as structural variants, posed visualization challenges in the integrated genomics viewer (IGV) and could therefore not be confirmed using our direct mutation analysis approach (data not shown).

Although it is conventionally recommended that 30-40X depth of coverage sequencing is conducted to identify single nucleotide variants (SNVs)[23], here we show that we can accurately describe an embryo's genotype when the position is covered by at least 5 reads. While validation of this approach, with a larger sample size is warranted to establish rigorous QC parameters, we could already showcase the method's potential to resolve cases that are inconclusive after haplarithmisis. Direct mutation analysis could also be offered in cases where a suitable reference individual is not available for haplotype phasing, thereby allowing the offer of PGT to be extended to more couples. Additionally, direct mutation analysis could plausibly be used to detect disease causing variants that are arising *de novo* in the embryo. Such variants are common causes for pathologies such as neurodevelopmental disorders[24] which could therefore be diagnosed prior to embryo transfer.

Figure 4 | Direct mutation analysis based on WGS-PGT data

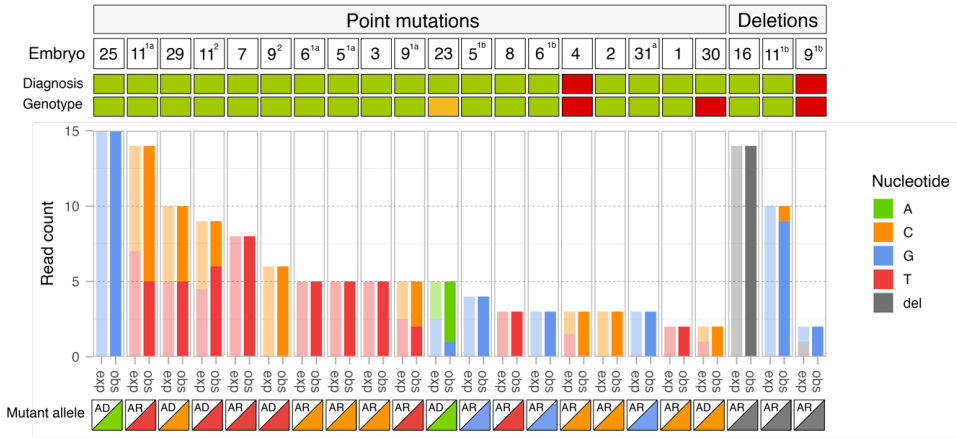

Shown are the number of reads supporting the genotype profile ascertained for each PGT-M indication, i.e., point mutations (left) and deletions (right). The expected genotype ("exp"), based on haplarithmisis results, is indicated in lighter colours to the left of the result from the direct mutation analysis ("obs"). The tracks above show whether the genotype and diagnosis are concordant with the haplarithmisis results (concordant = green, inconclusive = orange, discordant = red). For recessive indications results were considered inconclusive if the proportion of reads supporting the reference allele were <30% or >70%. The classification of the mutation (autosomal dominant = AD, autosomal recessive = AR) is described at the bottom. Superscript numbers are used to differentiate between indications if there are multiple indications or to link compound heterozygous mutations.

Haplarithmisis-based WGS-PGT can determine the mosaicism level and of segregational origin of aneuploidies

We investigated the chromosomal landscape of 20 embryos that underwent WGS-PGT for PGT-M (**Fig. 1B**). Using haplarithmisis we could identify chromosome-spanning copy number variants (CNVs) and further characterise them based on their degree of mosaicism (detection threshold > 10%) and segregational origin, i.e., meiosis 1, meiosis 2, or mitosis (**Fig. 5A**). In total, we identified at least one CNV in 50% (*n* = 10) of the analysed embryos. Of the identified aneuploidies, nine were trisomies, 4 were monosomies and one was a genome-wide (excluding chromosome 15) triploidy (**Supplementary Table 2**). The determined degrees of mosaicism ranged from 25% to 100%, with the majority (11 / 14) of aneuploidies having a mosaicism degree of 80% or more (**Fig. 5C, Supplementary Table 2**). While it is not possible to leverage parental haplotype information to determine the segregational origin of monosomies, we could identify the segregational origin of 9 of the 10 trisomies (**Fig. 5B, Supplementary table 2**). In the one case where this was not possible, the segregational origin could not be determined due to the lack of a cross-over event on the chromosome in question. As it has previously been shown using GENType, a haplotyping-based PGT method, that close relatives were not essential to conduct PGT-A[17], we explored whether

segregational origin detection was possible using only the parents and the embryo. In all nine cases the segregational origin detected by close-relative phasing could be replicated by parents-only phasing (**Fig. 5B**), showing that the sequencing of a close relative is not required when using WGS-PGT for PGT-A. Interestingly, we identified two embryos harbouring meiotic trisomies with a mosaicism degree of less than the expected 100%, specifically 80% and 90%, suggesting that a proportion of cells within these TE biopsies have undergone chromosomal rescue[25]. A similar phenomenon may have occurred in the triploid embryo where a post-zygotic mitotic event may have led to the loss of the extra chromosome 15, therefore making this chromosome diploid[25].

More sophisticated characterisation of aneuploidies, such as demonstrated here, may impact the clinical utility of PGT-A for embryo selection and ART success rate augmentation. PGT-A based embryo selection using crude mosaicism level cut-offs has thus far not proven beneficial for increasing pregnancy rates or reducing pregnancy losses after ART[8-12]. Furthermore, the relevance of PGT-A findings for the health of the resulting child is dubious considering that many euploid babies have been born after the transfer of embryos deemed abnormal by PGT-A[8-12]. In part, the discrepancy between PGT-A findings and clinical impact could relate to the lack of representativeness of a single TE biopsy as studies evaluating multiple biopsies from the same embryo by shallow sequencing, report variable results between the biopsies and also the inner cell mass (ICM)[26-28]. Potentially, cell free embryonic DNA (cfDNA) in spent embryo culture medium or blastocoel fluid would provide a more representative snapshot of the embryo's chromosomal composition[29], especially as epigenetic information could be leveraged to determine which embryonic compartment, i.e., ICM or TE, DNA fragments have originated from[30]. Furthermore, we have demonstrated that the mosaicism degree is not a good indicator for the segregational origin of trisomies, highlighting that mosaicism degree alone is likely insufficient for clinical decision making. We therefore advocate that the segregational origin and mosaicism degree, termed PGT for aneuploidy origin (PGT-AO), is carried out in place of conventional PGT-A. Although further research in this field is required to determine the true prevalence, developmental trajectory and clinical significance of meiotic and mitotic aneuploidies, it is currently thought that embryos harbouring mitotic abnormalities can safely be transferred while meiotic aneuploidies represent a risk to the health of the pregnancy and fetus and should therefore not be transferred[26-28].

Figure 5 | Haplarithmisis-based PGT-AO allows the segregational origin and degree of mosaicism of aneuploidies to be determined

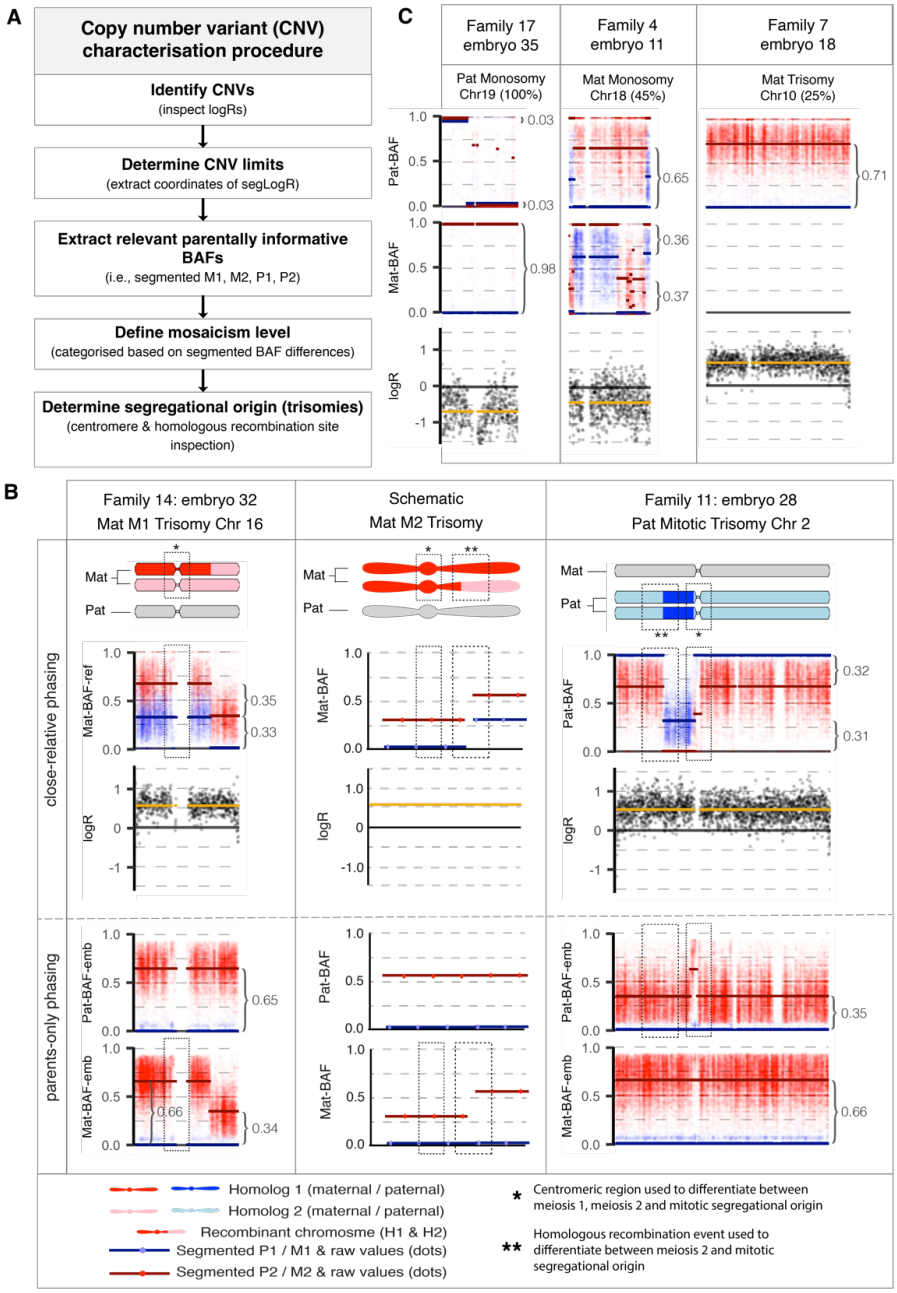

A) An overview of the procedure to identify and characterise copy number variants (CNVs) after haplarithmisis. B) Representative examples of trisomies with different segregational origins. A schematic representation of a maternal meiosis 2 trisomy is shown. Two analysis scenarios are shown, namely where the data are phased using a close-relative reference individual (top) and where the embryo itself is used as the reference individual (bottom). C) Representative examples of aneuploidies with different degrees of mosaicism. Haplarithmisis plots show the parentally informative BAFs, inferred haplotypes and logRs.

WGS-PGT can differentiate between balanced, unbalanced, and normal embryos for PGT-SR

Embryos from three families that underwent PGT-SR with VeriSeq-PGS were re-analysed using WGS-PGT (**Fig. 1B**). The copy number state of all embryos could be correctly determined with WGS-PGT and haplarithmisis purely by assessing the segmentation of the logR values (**Fig 6, Supplementary Fig 6**). Although small duplications, such as the 1.08 Mb segmental duplication of chromosome 16 in embryo 4 of family 1, were not segmented, such embryos could still be correctly diagnosed based on the presence of the reciprocal deletion (**Fig. 6**). The identification of these segmental deletions and duplications remained consistent across all subsampled sequencing depths, even at 5X coverage (**Supplementary Fig. 6**) and could be achieved when using an embryo as a referent for phasing instead of a sibling or grandparents (family 19, data not shown).

Embryos with no copy-number imbalances from these couples could either have inherited both normal homologs or both derivative chromosomes (balanced translocation) from the carrier parent. These cases cannot be distinguished using the shallow sequencing (VeriSeq) approach. On the other hand, if an embryo with the unbalanced translocation is identified by our haplotyping-based PGT, the flanking haplotypes of the duplication and deletion can be used to distinguish between the normal and derivative chromosomes in all other embryos (**Fig 6**). Alternatively, the paired-end sequencing data of the carrier parent and the embryos can be leveraged to identify breakpoint pairs between derivative chromosomes. In two of the three carrier parents included in this study we could identify a breakpoint pair, that closely corresponded to the expected translocation breakpoints ascertained using karyotyping (**Supplementary table 3, 4**). Unlike the karyotyping results, the breakpoints derived from paired-end sequencing data could be determined at base pair resolution allowing more precise regions of interest to be defined for haplarithmisis. Subsampled data from family 1 showed that a minimum genome-wide depth of coverage of 10X is required to accurately call these breakpoints (**Supplementary table 3**). We could identify corresponding breakpoint pairs in six of the eight unbalanced embryos from families 1 and 19 (**Supplementary table 3, 4**). The two embryos in which no breakpoints were identified both inherited a derivative chromosome 8 with the small, translocated segment of chromosome 16 (1.08Mb) (**Supplementary table 3**). Although paired-end sequencing analysis did not identify a breakpoint pair in the mother (carrier) of family 9, we could correctly identify the relevant breakpoint pair in the unbalanced embryo 25 (**Supplementary table 5**). The paternal ins(10;7) of family 19 could not be evaluated using the structural variant caller Manta, however leveraging information from haplarithmisis the chromosome 7 breakpoint lies at around 129135000 bp (data not shown).

The ability to differentiate between chromosomally normal and balanced carrier embryos is important for two reasons. Firstly, embryos appearing to have a balanced

chromosome composition may have gained or lost a number of nucleotides during an imprecise end-joining process involving non-homologous chromosomes which could lead to a disease phenotype[31]. Secondly, transferring embryos harbouring balanced translocations will necessitate future ART procedures as these individuals will carry the same reproductive risks as their carrier parent. Therefore, the transfer of chromosomally normal embryos should be priorities over the transfer of balanced translocation carrier embryos. While prior methods exist to differentiate between normal and balanced translocation carrier embryos, these were either based on shallow (0.1X)[31,32] or Nanopore sequencing[33] and are therefore difficult to integrate with PGT protocols for other indications.

Figure 6 | WGS-PGT for PGT-SR can differentiate between unbalanced, balanced, and normal embryos

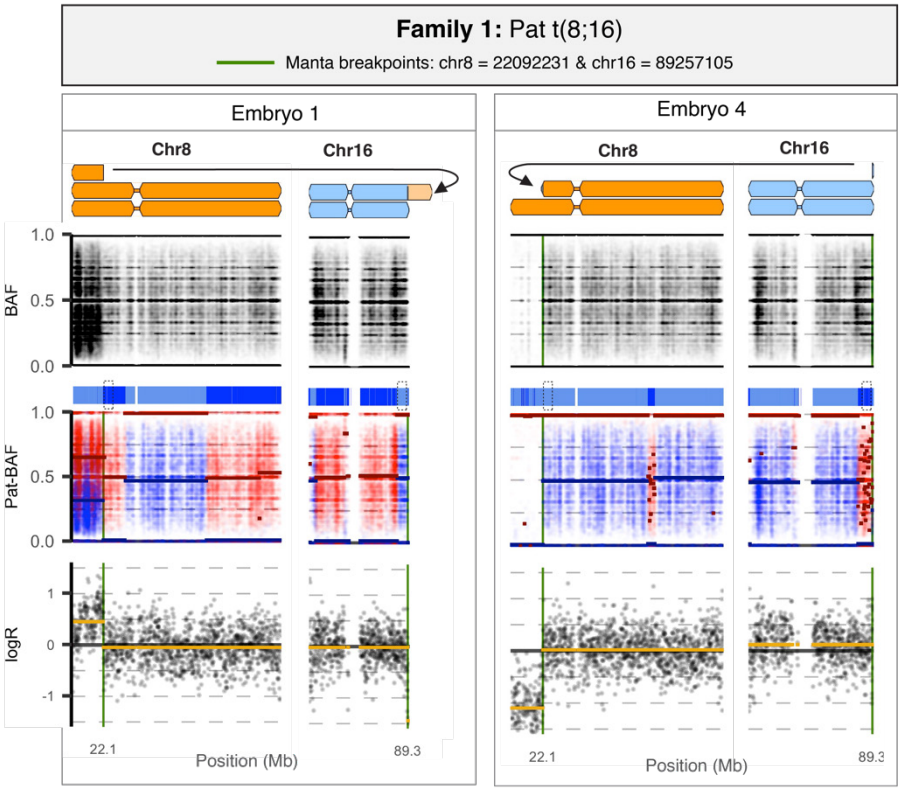

Structural rearrangement assessment of two representative embryos from family 1. Shown is a schematic of the chromosome constitution as well as the corresponding (paternally informative) BAFs, inferred haplotypes and logRs. The breakpoint identified by Manta in the carrier parent (father) is indicated by the green line and the flanking haplotypes are indicated by dashed boxes.

Substantial mitochondrial genome coverage allows accurate heteroplasmy level determination using WGS-PGT data

The current gold-standard for PGT-MT in our centre is a specialized restriction fragment length polymorphism (RFLP) PCR-based workflow carried out on a day-3 blastomere biopsy. We compared the results from the blastomere biopsy to results obtained by applying the same protocol to day-5 TE biopsies (*n* = 4) and found that the calculated heteroplasmy levels differed by 1 to 4% (**Fig. 1B, Fig. 7A**). Furthermore, the same protocol applied to the corresponding rest embryos yielded heteroplasmy levels that differed by 0 to 4 % and 1 to 3% to the day-3 and day-5 biopsy results, respectively (**Fig 7A**). We thereby show that a TE biopsy is an appropriate source of genetic material from which to determine mitochondrial heteroplasmy levels. Switching to TE-biopsy PGT-MT is likely to have a positive impact on ART success rates for these couples considering that TE biopsies have been shown to be less detrimental to embryo development than blastomere biopsies[34,35]. Furthermore, this finding is beneficial for ART laboratories who could streamline their embryo biopsy procedures to only collect TE biopsies for all PGT indications. This would reduce the time-consuming and laborious training requirements currently faced by new ART technicians and embryologists, who would then only need to become proficient in one of the two conceptually different, intricate procedures.

We then applied our WGS-PGT protocol to day-5 TE biopsy and rest embryo material (*n* = 4) with a target genome-wide sequencing depth of ~30-40X (**Fig. 1B**). The mitochondrial genome was highly covered at all levels of subsampling with only one site being covered less than 100 times in the TE-biopsy data after subsampling to 10X coverage (**Fig 7B**). Importantly, the mitochondrial sites with known pathological variants (*n* = 46) had a minimum coverage of 2,240X in the 10X subsampled TE-biopsy data (**Supplementary Fig 7**). The mitochondrial genome coverage of the samples sequenced at 10X for PGT-M and PGT-SR (*n* = 28) indications was comparable (two sites with coverage under 100X in any sample, minimum coverage of any pathological variant site 875X in any sample) (**Fig 7B, Supplementary Fig 7**). Compared to the heteroplasmy levels elucidated from the day-3 biopsies by RFLP-PCR the day-5 10X WGS-PGT results varied by 1.5 to 3.3% (**Fig 7A**). Subsampling the sequencing data had little effect on the calculated heteroplasmy levels with estimates varying up to a maximum of 1.6% in any sample at different levels of genome-wide coverage (**Supplementary Table 6, 7**). The 10X WGS-PGT heteroplasmy levels from the rest embryo differed by 0 to 3.6% compared to the day-3 biopsy-results and 0.3 to 1.6% to the day-5 biopsy results (**Fig 7A, Supplementary Table 6, 7**). Therefore, we could conclude that WGS-PGT conducted on TE biopsy material is a valid, accurate alternative to day-3 RFLP-PCR meaning that PGT laboratories would no longer need to maintain specialised workflows for PGT-MT. Although several studies have described the ability to achieve good mitochondrial genome coverage using sequencing based PGT protocols, this was

not previously been done in the context of PGT-MT. Instead, these studies focused on quantifying the mitochondrial DNA as a predictor of embryo quality[36-40]. Whether WGS-PGT data can predict outcomes based on mitochondrial DNA quantification remains to be determined and would necessitate larger studies in which clinical outcomes are recorded.

Figure 7 | Mitochondrial genome coverage allows accurate heteroplasmy level determination

A **PGT-MT** heteroplasmy

Embryo	Day-3 (PCR)	Day-5 Method	Day-5 (TE biopsy)	Day-5 (Rest embryo)
41	38%	PCR	35%	38%
42	58%		56%	57%
43	71%		70%	67%
44	78%		74%	77%
45	48%	WGS	49.6%	49.9%
46	64%		67.3%	67.6%
47	77%		75.5%	77.0%
48	-		41.0%	39.4%

B **PGT-MT** coverage

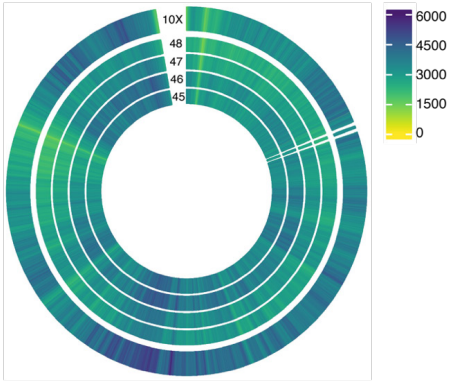

***A**) Heteroplasmy results of embryos from family 20. Day-3 results are from RFLP-PCR on blastomere biopsy material, day-5 results are from RFLP-PCR (embryos 41-44) or WGS-PGT (embryos 45-48) on TE-biopsy and rest embryo material. **B**) Depth of coverage per position of each embryo from family 20 and the mean depth of coverage per position of all embryos sequenced at 10X (V, n = 28). Position 0 is at the top counting in a clockwise fashion and colour represents the number of reads per position. The MELAS mutation position (m.3243) is highlighted as a separate segment and magnified 30x compared to all other positions.*

Conclusion

In conclusion, we have described the first comprehensive, clinical validation of a WGS-based approach for PGT. Our method has a shorter and simplified laboratory protocol that would be more straightforward to automate than existing GBS-based approaches for PGT, therefore allowing laboratories to process more samples to meet the growing demand for PGT. We also demonstrate the superior diagnostic power of WGS-PGT in terms of its ability to i) resolve challenging PGT-M indications, ii) ascertain the degree of mosaicism and segregational origin of aneuploidies, iii) differentiate between balanced and normal PGT-SR embryos, and iv) determine heteroplasmy levels for PGT-MT. Additionally, we showed that multiple analyses can be carried out simultaneously on material from a single biopsy, therefore eliminating the need for multiple embryo biopsies for different indications. Overall, WGS-PGT offers IVF and PGT laboratories a single streamlined workflow to accurately assess all PGT indications.

Methods

Study participants and ethical approval

Couples were counselled by clinical geneticists at Maastricht University Medical Centre (MUMC+) and enrolled in the diagnostic PGT procedure (licensed by the Dutch Ministry of Health, Welfare and Sport CZ-TSZ-291208) after signing an informed consent form. Couples who underwent PGT-M or PGT-SR, consented for the use of affected embryos for the development of PGT methods. We included 20 families who had undergone PGT for (double) monogenic, structural, or mitochondrial indications where spare (amplified) DNA from all samples was available. No additional biopsies were conducted for this study, except for PGT-MT (see section PGT for mitochondrial disorders) and one family with a PGT-SR indication (see section PGT for structural rearrangements).

GBS-PGT sample collection and processing

For PGT-M the standard clinical procedure in our facility involved genotyping-by sequencing (GBS), as described previously[41]. Briefly, peripheral blood samples were collected from prospective parents and reference individuals from which DNA was isolated using the QIAsymphony DSP DNA Midi kit (Qiagen, Germany). A trophectoderm (TE) biopsy was taken from sufficiently developed embryos on day-5 and the collected material was subjected to multiple displacement amplification (MDA) using the REPLI-g Single Cell kit (Qiagen, Germany), following the manufacturer's instructions. Library preparation, using the OnePGT solution (Agilent Technologies) was then carried out on genomic DNA samples from parents and references, along with MDA samples from embryos, following the manufacturer's instructions and as previously described[41]. The libraries were sequenced on a NextSeq 500 sequencing system. All excess DNA not used for library preparation was stored at -20 ° C, in accordance with clinical standards.

Whole genome sequencing sample processing

DNA from parents and references and whole genome amplified (WGAed) DNA from embryos, (see above), was subjected to WGS library preparation. Briefly, a minimum input of 20 □l, with a concentration of 30 ng/□l, was supplemented with 0.12 ng of embryo tracking system (ETS) fragments (concentration: 0.03 ng/□l)[22]. Subsequently, bead-linked transposome (BLT) PCR-free library preparation (Illumina, San Diego) was carried out according to the manufacturer's instructions for input quantities ranging from 300 to 2000 ng. The resulting libraries were purified using a double-sided bead purification process. Sequencing was performed using a NovaSeq 6000 to a target depth of coverage of ~30-40X or 10X.

Sequencing data processing and quality control

The raw sequencing data were demultiplexed and aligned to the human reference

genome (complemented with the sequences of all ETS amplicons) using bwa-mem2 (v. 2.2.1)[42]. The WGS data were aligned to Hg38 while the GBS data were aligned to Hg37, and positions were then converted to Hg38 using liftOver from the Rtracklayer package[43]. The quality of the resulting alignment was assessed using Qualimap (v.2.2.1.)[44] to determine breadth and depth of coverage as well as the purity of the expected ETS fragment.

Samples that underwent deep (~30-40X) sequencing, were subsampled using the "view" function from SAMtools (v. 1.15.1)[45]. The fraction of the original bam file required to generate different subsets was calculated by dividing the target coverage (5X, 10X, 20X and 30X) by the original coverage. Mann-Whitney U Tests / Wilcoxon Rank-Sum Tests were used to compare the GBS and WGS groups and Kruskal-Wallis test with Dunn's multiple comparisons test to compare the breadth of coverage in the different target coverage groups.

Haplarithmisis-based PGT

GBS and WGS data were analysed using a modified version of the siCHILD analytical pipeline that is equipped with haplarithmisis[21] and has been further adapted for sequencing data[22]. Initially, a preparatory test was conducted for the parents and references to assess whether the couple was eligible for PGT. Subsequently, an "embryo test" was run in which embryo haplotypes were reconstructed to ascertain a diagnosis. Using this pipeline, aligned sequencing data was processed using Joint HaplotypeCaller from GATK (v. 3.4-46)[46] to extract the genomic locations in the dbSNP database (v. 150). All subsequent processing was carried out in R (version 3.3.1)[47] as previously described[21,22]. Briefly, the GATK output was used to determine the genotype per position of each sample using vcfR (v. 1.8.0.9000)[48] R package. This was used to calculate B allele frequencies (BAFs), which were subsequently phased by leveraging information from the parents and a close relative. Segmentation of the parentally informative phased BAFs was used to determine the haplotypes. Copy number states for 100kb-sized genomic bins were assessed using the QDNAseq (v. 1.10.0)[49] R package and segmented using piecewise constant fitting (PCF)[50] with a gamma value of 50. The quality control thresholds applied for GBS-PGT were i) a minimum of eight informative SNPs available in the 2Mb either side of the region of interest (ROI) and ii) at least 80% of the informative SNPs in the 2Mb either side of the ROI support the same conclusion, i.e., show the same parental haplotype (**Supplementary text 1**).

Haplarithmisis comparison between GBS and WGS

We evaluated the haplarithmisis output from subsampled and data generated at ~10X depth of coverage by assessing mendelian inconsistency level, number of informative SNPs, and haplotype concordance. The QC threshold for preparatory and embryo

test are listed in **Supplementary text 1**. Mendelian inconsistency was defined as the proportion of inconsistent genotypes out of the total number of genotypes that were analysed. These rates were calculated for individual chromosomes and then the mean for all autosomes was summarised. Haplotype concordance between GBS and WGS was determined by comparing the inferred haplotypes per parent. Subsequently, the haplotype concordance of WGS-PGT with GBS-PGT was assessed for each target coverage using Kruskal-Wallis test followed by Dunn's multiple comparisons test.

Direct mutation analysis

Direct mutation analysis was carried out by direct examination of the nucleotides at the indicated position(s). We examined 19 single base substitutions and 11 deletions ranging from 2 base pairs to 398kb in size. Reads mapping the relevant genetic location were extracted from bam files by indicating the chromosome, start and end position of a genomic interval using the SAMtools "view" function[45]. The resulting bam files were visualized in the Integrated Genomics Viewer (IGV) (version 2.11.9) to examine the relevant nucleotides. We then compared the PGT results determined by haplarithmisis (affected, not affected, carrier, inconclusive) with the diagnosis and genotype based on direct mutation analysis.

PGT for aneuploidies

Copy number variants (CNV) were called by visual inspection of the haplarithmisis results. Specifically, deviations in the binned, normalised read intensities (logR) and BAFs were sought. Subsequently, the aberrations were characterised based on several criteria, namely i) the copy number aberration detected (gain or loss), ii) the size of the aberration (genome-wide, chromosomal, or sub-chromosomal), iii) the parental origin of the aberration (paternal or maternal), iv) the degree of mosaicism (categorised for mosaicism levels of >10%), and v) the segregational origin of the aberration (meiosis I, meiosis II, or mitosis) in cases of trisomies. To determine the degree of mosaicism, the genomic coordinates at the logR deviation were used to extract the relevant, parentally phased segmented BAF values. BAF values were then compared to the reference dataset by Conlin et al. 2010 to categorise the level of mosaicism[51]. In addition to conventional haplarithmisis, where phasing is carried out using a close relative of the parents, we performed "parents-only" phasing where the parental genome was phased using the embryo itself.

PGT for structural rearrangements

Three families with PGT-SR indications were included. Originally, these embryos were assessed for copy number variations using the Veriseq-PGS kit (Illumina Inc., Santa Clara, CA) according to the manufacturer's instructions. For embryos from families 1 and 9, who were analysed for dual PGT-M and PGT-SR indications, surplus WGAed

DNA from the GBS-PGT was used for WGS-PGT, as described above. For family 19, that only had a PGT-SR indication, a new TE biopsy was taken from affected embryos to carry out WGA using the REPLI-g single cell kit (Qiagen, Germany), as described above. The data for families with dual PGT-M and PGT-SR indications (family 1 and 9), for which reference individuals were also sequenced, were processed, and visualised as described for PGT-M cases. Where deep sequencing (~30-40X) was undertaken, the aforementioned subsampling strategy was also applied, and structural rearrangements were assessed at all target coverages. For one family (family 19) no close-relative was sequenced, in this case each embryo was used as a proxy sibling to phase the remaining embryos. Derivative chromosome breakpoints were ascertained using Manta (v1.6.0) with default settings[52]. The resulting variants were then filtered to include only break points ("BND") where pairs of "mates" were identified on the expected chromosomes. In cases where Manta did not identify identical breakpoints in the carrier parent and at least one of the embryos, breakpoints were estimated from the haplarithmisis output, specifically from the segmentation of the phased parental BAFs and the segmentation of the logRs.

PGT for mitochondrial disorders

Eight embryos deemed affected (> transfer threshold 15%) for mitochondrial encephalopathy, lactic acidosis and stroke-like episodes (MELAS, m.3243 A > G) based on results from the current gold-standard blastomere-biopsy (day-3) testing were included (**Fig 1B**). The embryos were re-biopsied on day-5 to obtain a TE biopsy sample and the remaining (rest-) embryo was also analysed to gain an accurate representation of the true heteroplasmy level. Four TE biopsies and their corresponding rest embryos were re-analysed using the restriction fragment length polymorphism (RFLP) PCR protocol that was also used to analyse the day-3 biopsy samples. The protocol was implemented as previously described by Sallevelt et al[53]. Briefly, the biopsy material was subjected to cell lysis followed by two rounds of PCR. The first amplification PCR was carried out with unlabelled primers for the MELAS mutation, after which a fluorescently labelled primer was added for the second PCR round. The resulting product was enzymatically digested, purified, and analysed by capillary electrophoresis. The mutation load was determined by dividing the area of the mutation peak by the sum of both the wild type and mutation peak. The remaining four embryos (TE biopsy and rest embryo) were processed with the WGS-PGT protocol described above. These samples underwent deep sequencing with a target sequencing depth of ~30-40X. The sequencing data were processed and subsampled as described above. Subsequently sequencing depth per position was determined using the "depth" function from SAMtools[45]. Known pathological variants in the mitochondrial genome were extracted from the MITOMAP database (MitoTIP = "Pathogenic")[54]. The "HaplotypeCaller" function form GATK was used to determine the number of reads supporting the reference and alternative alleles

at the indicated position[55], from which the heteroplasmy percentage was calculated.

Data visualization

Data were visualised using functionality from the ggplot2[56], circlize[57] and cowplot[58] R packages.

Funding

This study was funded by The EVA (Erfelijkheid Voortplanting & Aanleg) specialty program (grant no. KP111513), the Horizon Europe (NESTOR, grant no. 101120075) of the European Commission and the Horizon 2020 innovation (ERIN, grant no. EU952516) grants.

Competing Interests

The authors of this study declare no competing interests in relevance to this work.

Data Availability

The sequencing data analysed in this study represents clinical data that cannot be shared publicly to protect the privacy of the participants. Anonymised, processed data is available upon reasonable request by contacting the corresponding author.

References

1 Handyside, A. H. *et al.* Biopsy of human preimplantation embryos and sexing by DNA amplification. *Lancet* **1**, 347-349 (1989). https://doi.org/10.1016/s0140-6736(89)91723-6

2 Hughes, T. *et al.* A review on the motivations, decision-making factors, attitudes and experiences of couples using pre-implantation genetic testing for inherited conditions. *Hum Reprod Update* **27**, 944-966 (2021). https://doi.org/10.1093/humupd/dmab013

3 Handyside, A. H., Kontogianni, E. H., Hardy, K. & Winston, R. M. Pregnancies from biopsied human preimplantation embryos sexed by Y-specific DNA amplification. *Nature* **344**, 768-770 (1990). https://doi.org/10.1038/344768a0

4 Roche, K., Racowsky, C. & Harper, J. Utilization of preimplantation genetic testing in the USA. *J Assist Reprod Genet* **38**, 1045-1053 (2021). https://doi.org/10.1007/s10815-021-02078-4

5 Spinella, F. *et al.* ESHRE PGT Consortium data collection XXI: PGT analyses in 2018. *Hum Reprod Open* **2023**, hoad010 (2023). https://doi.org/10.1093/hropen/hoad010

6 van Montfoort, A. *et al.* ESHRE PGT Consortium data collection XIX-XX: PGT analyses from 2016 to 2017. *Hum Reprod Open* **2021**, hoab024 (2021). https://doi.org/10.1093/hropen/hoab024

7 Bai, F. *et al.* Assisted reproductive technology service availability, efficacy and safety in mainland China: 2016. *Hum Reprod* **35**, 446-452 (2020). https://doi.org/10.1093/humrep/dez245

8 Gleicher, N., Barad, D. H., Patrizio, P. & Orvieto, R. We have reached a dead end for preimplantation genetic testing for aneuploidy. *Hum Reprod* **37**, 2730-2734 (2022). https://doi.org/10.1093/humrep/deac052

9 Simopoulou, M. *et al.* PGT-A: who and when? A systematic review and network meta-analysis of RCTs. *J Assist Reprod Genet* **38**, 1939-1957 (2021). https://doi.org/10.1007/s10815-021-02227-9

10 Munné, S. *et al.* Preimplantation genetic testing for aneuploidy versus morphology as selection criteria for single frozen-thawed embryo transfer in good-prognosis patients: a multicenter randomized clinical trial. *Fertil Steril* **112**, 1071-1079.e1077 (2019). https://doi.org/10.1016/j.fertnstert.2019.07.1346

11 Yan, J. *et al.* Live Birth with or without Preimplantation Genetic Testing for Aneuploidy. *N Engl J Med* **385**, 2047-2058 (2021). https://doi.org/10.1056/NEJMoa2103613

12 Mastenbroek, S., de Wert, G. & Adashi, E. Y. The Imperative of Responsible Innovation in Reproductive Medicine. *N Engl J Med* **385**, 2096-2100 (2021). https://doi.org/10.1056/NEJMsb2101718

13 McKusick-Nathans Institute of Genetic Medicine, J. H. U. B., MD). (2022).

14 Van Steijvoort, E. *et al.* Interest in expanded carrier screening among individuals and couples in the general population: systematic review of the literature. *Hum Reprod Update* **26**, 335-355 (2020). https://doi.org/10.1093/humupd/dmaa001

15 Zhang, T. *et al.* Expanded Preconception Carrier Screening in Clinical Practice: Review of Technology, Guidelines, Implementation Challenges, and Ethical Quandaries. *Clin Obstet Gynecol* **62**, 217-227 (2019). https://doi.org/10.1097/GRF.0000000000000437

16 Handyside, A. H. *et al.* Karyomapping: a universal method for genome wide analysis of genetic disease based on mapping crossovers between parental haplotypes. *J Med Genet* **47**, 651-658 (2010). https://doi.org/10.1136/jmg.2009.069971

17 De Witte, L. *et al.* GENType: all-in-one preimplantation genetic testing by pedigree haplotyping and copy number profiling suitable for third-party reproduction. *Hum Reprod* **37**, 1678-1691 (2022). https://doi.org/10.1093/humrep/deac088

18 Esteki, M. Z. *et al.* Agilent Technologies OnePGT solution: External verification on both blastomere and trophectoderm biopsies. *Reproductive BioMedicine Online* **38**, e11-e12 (2019). https://doi.org/https://doi.org/10.1016/j.rbmo.2019.03.022

19 Esteki, M. Z. *et al.* HiVA: an integrative wet- and dry-lab platform for haplotype and copy number analysis of single-cell genomes. *bioRxiv*, 564914 (2019). https://doi.org/10.1101/564914

20 Masset, H. *et al.* Single-cell genome-wide concurrent haplotyping and copy-number profiling through genotyping-by-sequencing. *Nucleic Acids Res* **50**, e63 (2022). https://doi.org/10.1093/nar/gkac134

21 Zamani Esteki, M. *et al.* Concurrent whole-genome haplotyping and copy-number profiling of single cells. *Am J Hum Genet* **96**, 894-912 (2015). https://doi.org/10.1016/j.ajhg.2015.04.011

22 van Dijk, W. *et al.* Embryo tracking system for high-throughput sequencing-based preimplantation genetic testing. *Hum Reprod* **37**, 2700-2708 (2022). https://doi.org/10.1093/humrep/deac208

23 Souche, E. *et al.* Recommendations for whole genome sequencing in diagnostics for rare diseases. *Eur J Hum Genet* **30**, 1017-1021 (2022). https://doi.org/10.1038/s41431-022-01113-x

24 Brunet, T. *et al.* De novo variants in neurodevelopmental disorders-experiences from a tertiary care center. *Clin Genet* **100**, 14-28 (2021). https://doi.org/10.1111/cge.13946

25 Viotti, M. Preimplantation Genetic Testing for Chromosomal Abnormalities: Aneuploidy, Mosaicism, and

Structural Rearrangements. *Genes (Basel)* **11** (2020). https://doi.org/10.3390/genes11060602
26 Sachdev, N. M., McCulloh, D. H., Kramer, Y., Keefe, D. & Grifo, J. A. The reproducibility of trophectoderm biopsies in euploid, aneuploid, and mosaic embryos using independently verified next-generation sequencing (NGS): a pilot study. *J Assist Reprod Genet* **37**, 559-571 (2020). https://doi.org/10.1007/s10815-020-01720-x
27 Orvieto, R. The reproducibility of trophectoderm biopsies - The chaos behind preimplantation genetic testing for aneuploidy. *Eur J Obstet Gynecol Reprod Biol* **254**, 57-58 (2020). https://doi.org/10.1016/j.ejogrb.2020.07.052
28 Victor, A. R. *et al.* Assessment of aneuploidy concordance between clinical trophectoderm biopsy and blastocyst. *Hum Reprod* **34**, 181-192 (2019). https://doi.org/10.1093/humrep/dey327
29 Sousa, L. N. & Monteiro, P. B. Non-invasive preimplantation genetic testing: a literature review. *JBRA Assist Reprod* **26**, 554-558 (2022). https://doi.org/10.5935/1518-0557.20210102
30 Gao, Y., Chen, Y., Qiao, J., Huang, J. & Wen, L. DNA methylation protocol for analyzing cell-free DNA in the spent culture medium of human preimplantation embryos. *STAR Protoc* **4**, 102247 (2023). https://doi.org/10.1016/j.xpro.2023.102247
31 Zhai, F. *et al.* Preimplantation genetic testing for structural rearrangement based on low-coverage next-generation sequencing accurately discriminates between normal and carrier embryos for patients with translocations. *Reprod Biomed Online* **45**, 473-480 (2022). https://doi.org/10.1016/j.rbmo.2022.05.012
32 Xu, J. *et al.* Mapping allele with resolved carrier status of Robertsonian and reciprocal translocation in human preimplantation embryos. *Proc Natl Acad Sci U S A* **114**, E8695-E8702 (2017). https://doi.org/10.1073/pnas.1715053114
33 Xia, Q. *et al.* Nanopore sequencing for detecting reciprocal translocation carrier status in preimplantation genetic testing. *BMC Genomics* **24**, 1 (2023). https://doi.org/10.1186/s12864-022-09103-5
34 Scott, R. T., Upham, K. M., Forman, E. J., Zhao, T. & Treff, N. R. Cleavage-stage biopsy significantly impairs human embryonic implantation potential while blastocyst biopsy does not: a randomized and paired clinical trial. *Fertil Steril* **100**, 624-630 (2013). https://doi.org/10.1016/j.fertnstert.2013.04.039
35 Coll, L. *et al.* Transition from blastomere to trophectoderm biopsy: comparing two preimplantation genetic testing for aneuploidies strategies. *Zygote* **26**, 191-198 (2018). https://doi.org/10.1017/S0967199418000084
36 Luo, W. *et al.* Mitochondrial DNA quantification correlates with the developmental potential of human euploid blastocysts but not with that of mosaic blastocysts. *BMC Pregnancy Childbirth* **23**, 447 (2023). https://doi.org/10.1186/s12884-023-05760-w
37 Ritu, G. *et al.* Mitochondrial DNA Levels in Trophectodermal Cells Show No Association with Blastocyst Development and Pregnancy Outcomes. *J Hum Reprod Sci* **15**, 82-89 (2022). https://doi.org/10.4103/jhrs.jhrs_103_21
38 Wu, F. S. *et al.* Suboptimal trophectoderm mitochondrial DNA level is associated with delayed blastocyst development. *J Assist Reprod Genet* **38**, 587-594 (2021). https://doi.org/10.1007/s10815-020-02045-5
39 Chuang, T. H. *et al.* Reduced mitochondrial DNA content correlate with poor clinical outcomes in cryotransfers with day 6 single euploid embryos. *Front Endocrinol (Lausanne)* **13**, 1066530 (2022). https://doi.org/10.3389/fendo.2022.1066530
40 Podolak, A. *et al.* Mitochondrial DNA Copy Number in Cleavage Stage Human Embryos-Impact on Infertility Outcome. *Curr Issues Mol Biol* **44**, 273-287 (2022). https://doi.org/10.3390/cimb44010020
41 Masset, H. *et al.* Multi-centre evaluation of a comprehensive preimplantation genetic test through haplotyping-by-sequencing. *Hum Reprod* **34**, 1608-1619 (2019). https://doi.org/10.1093/humrep/dez106
42 Vasimuddin, M., Misra, S., Li, H. & Aluru, S. Efficient Architecture-Aware Acceleration of BWA-MEM for Multicore Systems. *2019 IEEE International Parallel and Distributed Processing Symposium (IPDPS), Rio de Janeiro, Brazil*, pp. 314-324 (2019). https://doi.org/10.1109/IPDPS.2019.00041
43 Lawrence, M., Gentleman, R. & Carey, V. rtracklayer: an R package for interfacing with genome browsers. *Bioinformatics* **25**, 1841-1842 (2009). https://doi.org/10.1093/bioinformatics/btp328
44 Okonechnikov, K., Conesa, A. & García-Alcalde, F. Qualimap 2: advanced multi-sample quality control for high-throughput sequencing data. *Bioinformatics* **32**, 292-294 (2016). https://doi.org/10.1093/bioinformatics/btv566
45 Danecek, P. *et al.* Twelve years of SAMtools and BCFtools. *Gigascience* **10** (2021). https://doi.org/10.1093/gigascience/giab008
46 Van der Auwera, G. A. & D., O. C. B. ***Genomics in the Cloud: Using Docker, GATK, and WDL in Terra 1st Edition*** edn, (O'Reilly Media, 2020).
47 *R Core Team. R: A language and environment for statistical computing. R Foundation for Statistical Computing, Vienna, Austria. https://www.R-project.org/*, <URL https://www.R-project.org/> (2021).

48 Knaus, B. J. & Grünwald, N. J. vcfr: a package to manipulate and visualize variant call format data in R. *Mol Ecol Resour* **17**, 44-53 (2017). https://doi.org/10.1111/1755-0998.12549
49 Scheinin, I. *et al.* DNA copy number analysis of fresh and formalin-fixed specimens by shallow whole-genome sequencing with identification and exclusion of problematic regions in the genome assembly. *Genome Res* **24**, 2022-2032 (2014). https://doi.org/10.1101/gr.175141.114
50 Nilsen, G. *et al.* Copynumber: Efficient algorithms for single- and multi-track copy number segmentation. *BMC Genomics* **13**, 591 (2012). https://doi.org/10.1186/1471-2164-13-591
51 Conlin, L. K. *et al.* Mechanisms of mosaicism, chimerism and uniparental disomy identified by single nucleotide polymorphism array analysis. *Hum Mol Genet* **19**, 1263-1275 (2010). https://doi.org/10.1093/hmg/ddq003
52 Chen, X. *et al.* Manta: rapid detection of structural variants and indels for germline and cancer sequencing applications. *Bioinformatics* **32**, 1220-1222 (2016). https://doi.org/10.1093/bioinformatics/btv710
53 Sallevelt, S. C. *et al.* Preimplantation genetic diagnosis in mitochondrial DNA disorders: challenge and success. *J Med Genet* **50**, 125-132 (2013). https://doi.org/10.1136/jmedgenet-2012-101172
54 Lott, M. T. *et al.* mtDNA Variation and Analysis Using Mitomap and Mitomaster. *Curr Protoc Bioinformatics* **44**, 1.23.21-26 (2013). https://doi.org/10.1002/0471250953.bi0123s44
55 McKenna, A. *et al.* The Genome Analysis Toolkit: a MapReduce framework for analyzing next-generation DNA sequencing data. *Genome Res* **20**, 1297-1303 (2010). https://doi.org/10.1101/gr.107524.110
56 Wickham, H. *ggplot2: Elegant Graphics for Data Analysis. Springer-Verlag New York. https://ggplot2.tidyverse.org*, <https://ggplot2.tidyverse.org> (2016).
57 Gu, Z., Gu, L., Eils, R., Schlesner, M. & Brors, B. circlize Implements and enhances circular visualization in R. *Bioinformatics* **30**, 2811-2812 (2014). https://doi.org/10.1093/bioinformatics/btu393
58 Wilke, C. O. cowplot: Streamlined Plot Theme and Plot Annotations for 'ggplot2'. (2020).

Supplementary Materials

Supplementary text 1 | Clinical quality control thresholds for GBS-PGT and WGS-PGT data

The criteria listed below are used to determine whether the data obtained for PGT are sufficient to make a make a diagnosis. First, a preparatory test is always carried out to determine whether the data available from parents and references are adequate to process embryo data. If so, data can be generated from embryo biopsies and if the quality control criteria are met a diagnosis can be assigned. The region of interest (ROI) is defined as 2Mb upstream and downstream of the indication. Concordance of informative SNPs (inf SNPs) refers to whether adjacent inf SNPs support the same parental haplotype. There are additional considerations if there is a homologous recombination (hom. recomb.) in close proximity to the indication. Due to the higher resolution of WGS generated data we recommend more stringent quality control parameters for this data.

Preparatory test quality control parameters:

Parameter	**Threshold GBS-PGT**	**Threshold WGS-PGT**
Number of reads per sample	≥ 26.000.000*	≥ 160.000.000*
Genome-wide inf SNPs	≥ 45.000	≥ 600.000
Inf SNP density in the ROI	≥ 4/Mb	≥ 40/Mb

*if the number of reads per sample does not meet the specified threshold in the preparatory test, but the inf SNP density in the ROI is sufficient, the preparatory test can still be approved. This only applies in cases where both grandparents are included as references and when the indication is not located in a challenging region (i.e., telomeric/centromeric, pseudogene, in close proximity to a homologous recombination site).

Embryo test quality control parameters:

Parameter	**Threshold GBS-PGT**	**Threshold WGS-PGT**
Total number of reads per embryo		≥ 90.000.000
Mendelian inconsistency rate	≤ 15%	≤ 6%
ROI inf SNP concordance	**Either** ≥ 70% upstream & ≥ 80% downstream **Or** ≥ 80% upstream & ≥ 70% downstream	**Either** ≥ 70% upstream & ≥ 80% downstream **Or** ≥ 80% upstream & ≥ 70% downstream
Number of consecutive corrected/discordant SNPs if <10 concordant SNPs adjacent to the indication	≤ 5 SNPs within ≤ 100 kb	-
Distance between indication and hom. recomb.	≥ 1 Mb	-
Number of inf SNPs between indication and hom. recomb.	≥ 10	≥ 10
Concordance of inf SNPs between indication and hom. recomb.	≥ 90%	≥ 90%

Supplementary Figure 1 | Quality of WGS-PGT data compared to GBS-PGT data

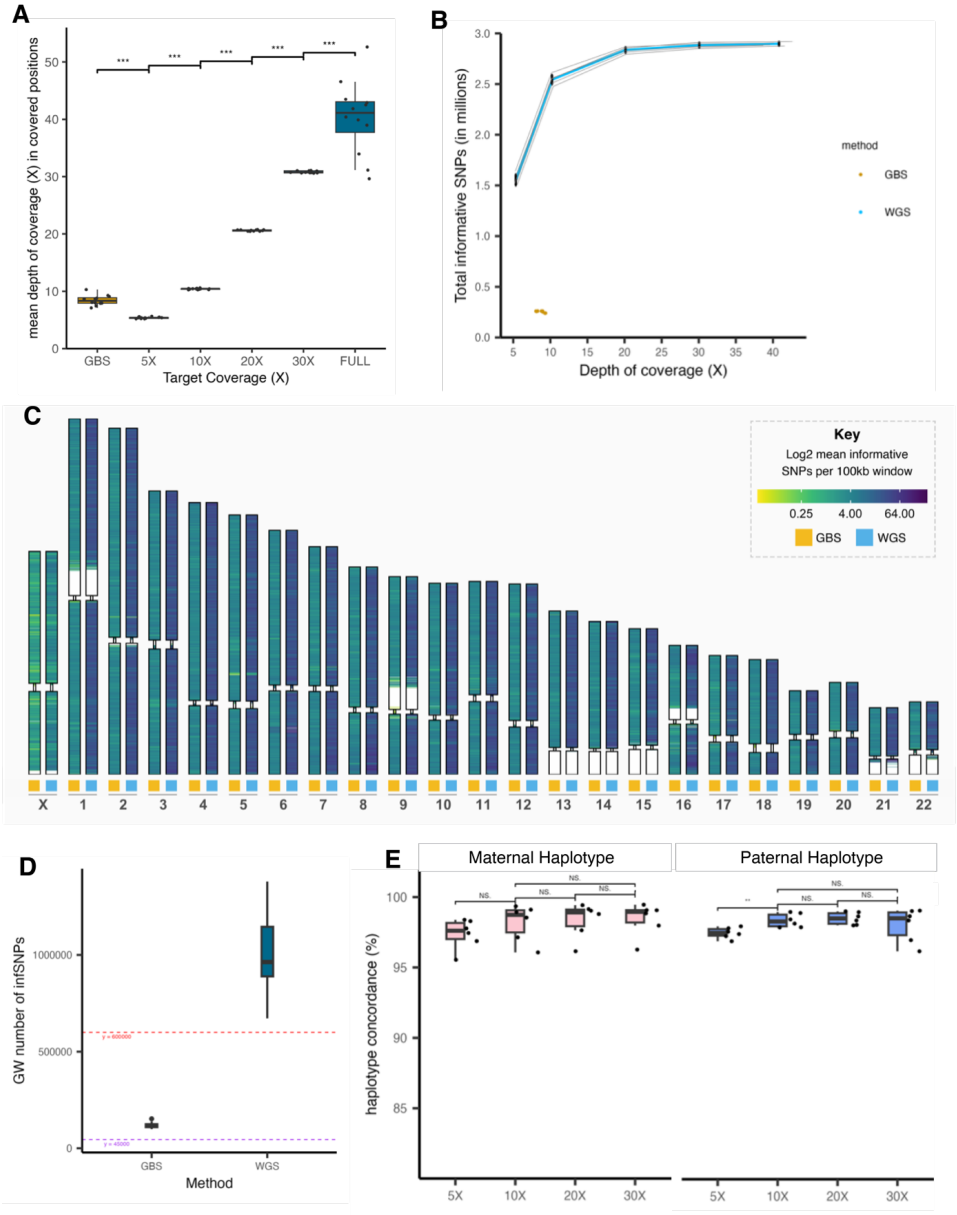

A) *Boxplot showing the effect of subsampling on mean depth of coverage (per position that is covered at least once). Shown are the original data (FULL), all target coverages from 5X to 30X and the corresponding GBS-PGT data from 12 samples (6 embryos, 6 bulk samples).* ***B)*** *Total number of informative SNPs per embryo (n = 6) at different simulated WGS-PGT depths of coverage and the corresponding GBS-PGT data.* ***C)*** *Heatmap showing the mean number of informative SNPs per phased parental haplotype in 100kb bins across chromosomes in data obtained by GBS or WGS. Mean number of informative SNPs was calculated*

from 47 phased parental (maternal or paternal) haplotypes from 29 embryos. ***D)*** *Genome-wide (GW) number of informative SNPs per embryo sequenced at 10X (n = 31). The dashed horizontal lines represent the minimum number of informative SNPs required according to our quality control criteria for GBS-PGT (purple) and WGS-PGT (pink).* ***E)*** *Haplotype concordance between GBS-PGT and WGS-PGT at different simulated depths of coverage (n = 6). Maternal haplotype concordance is shown in pink, paternal haplotype concordance is shown in blue. The horizontal lines of all boxplots represent the 25th percentile, median and 75th percentile with whiskers extending to 1.5 times the interquartile range. The points represent individual samples with GBS-PGT samples shown in gold and WGS-PGT samples shown in blue.*

Supplementary Figure 2 | Mendelian inconsistency

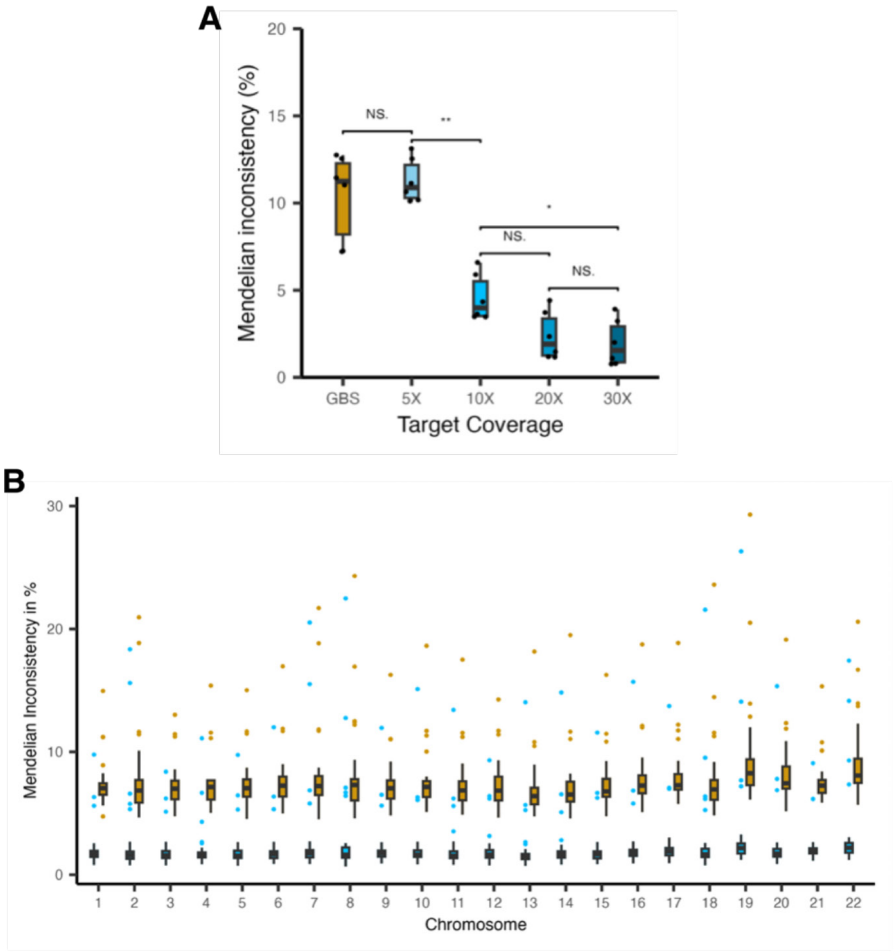

Mendelian inconsistencies represent sites at which the observed genotype violates Mendelian inheritance patterns, a percentage is calculated by dividing the number of inconsistent sites by the total number of sites evaluated. ***A)*** *Mendelian inconsistency rates of the autosomes at different simulated depths of coverage from WGS-PGT data and the corresponding rates from GBS-PGT data (n = 6).* ***B)*** *Mendelian inconsistency rates per chromosome of WGS-PGT samples sequenced at 10X and the Mendelian inconsistency rates from the corresponding GBS-PGT data (n = 31). The horizontal lines of all boxplots represent the 25th percentile, median and 75th percentile with whiskers extending to 1.5 times the interquartile range. The points represent individual samples with GBS-PGT samples shown in gold and WGS-PGT samples shown in blue.*

Supplementary Figure 3 | Direct mutation analysis: representative integrative genomics viewer (IGV) visualisations of point mutations / deletions

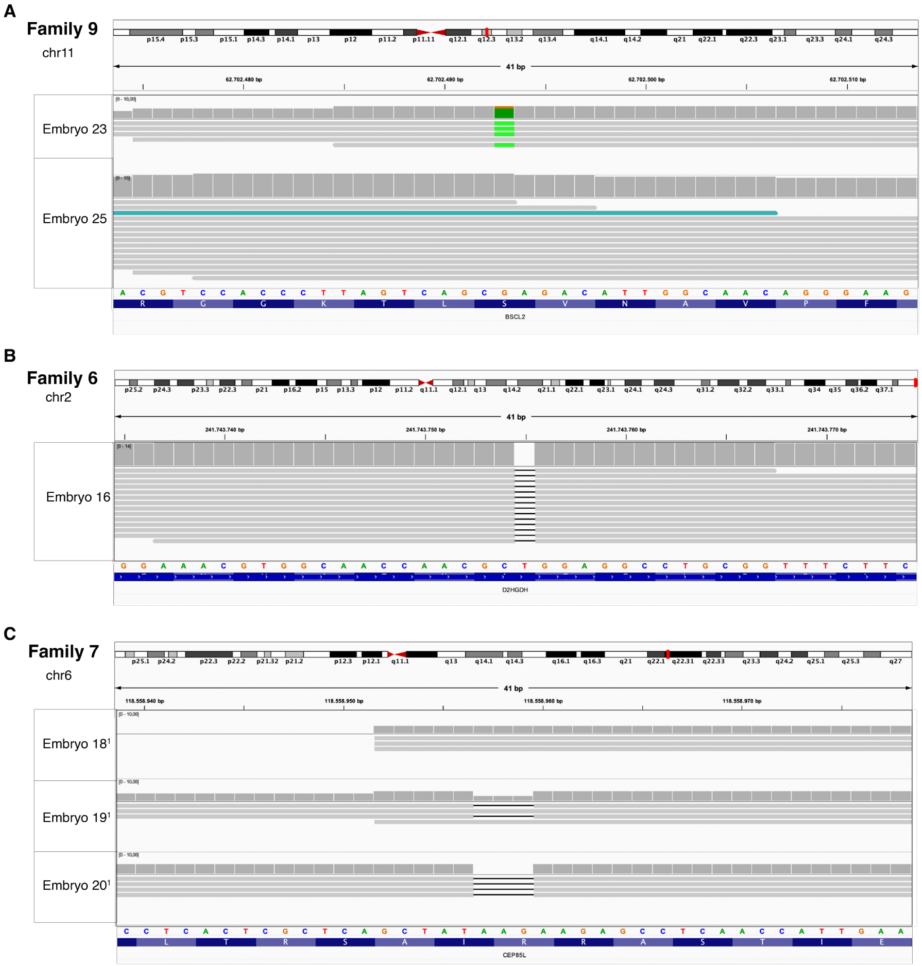

*Representative IGV visualisation of a **A**) single base pair substitution, **B**) single base pair deletion and **C**) larger deletion (3 bp). All embryos from the same family are viewed simultaneously. A total of 41 base pairs are shown in each visualisation with the indication position demonstrated by a vertical red line on the ideogram. The top track of each embryo represents the depth of coverage with the track thereunder displaying the identified nucleotides. Nucleotides deviating from the reference genome are coloured by base (A = green, C = blue, G = orange, T = red). The reference genotype according to the hg38 build is shown at the bottom.*

Supplementary Figure 6 | PGT-SR: segmental deletion and duplication detection at different depths of coverage

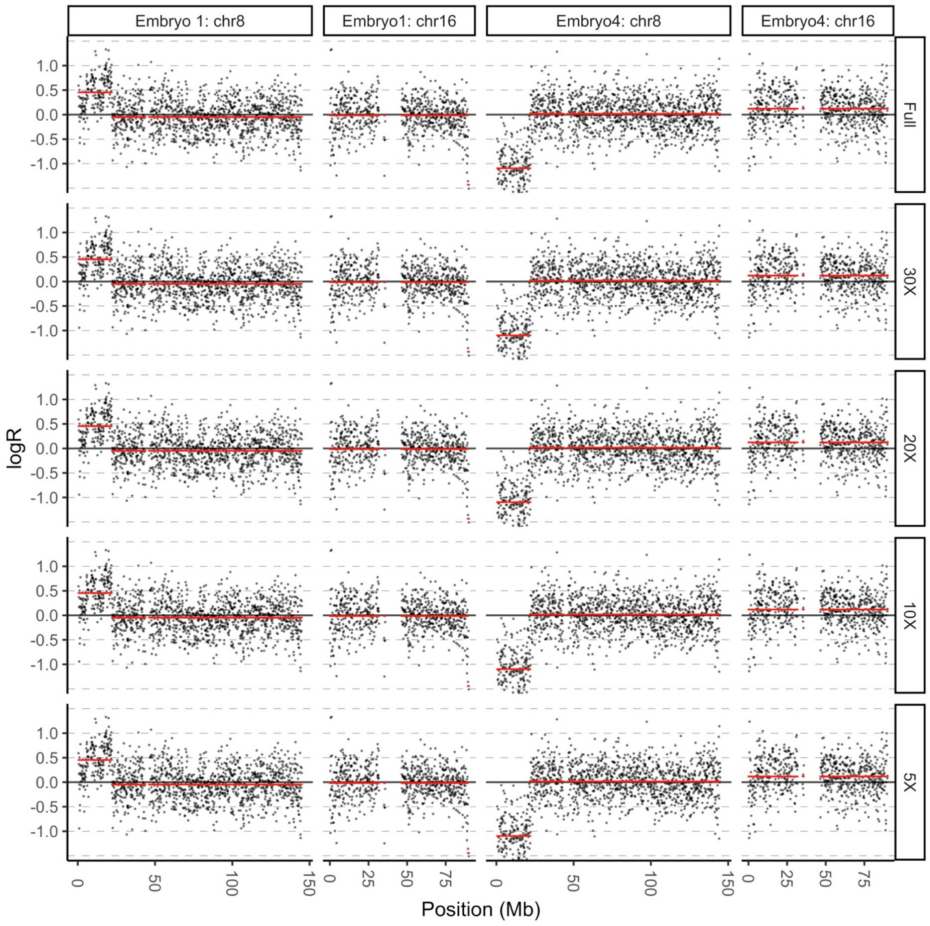

Raw logR values (black dots) and segmented logR values (red) derived from subsampled deep sequencing (~30-40X) data. Two representative embryos (embryos 1 and 4) from family 1 with a paternal translocation of chromosomes 8 and 16 are shown.

Supplementary Figure 7 | PGT-MT: depth of coverage at mitochondrial pathological mutation sites at different depths of coverage

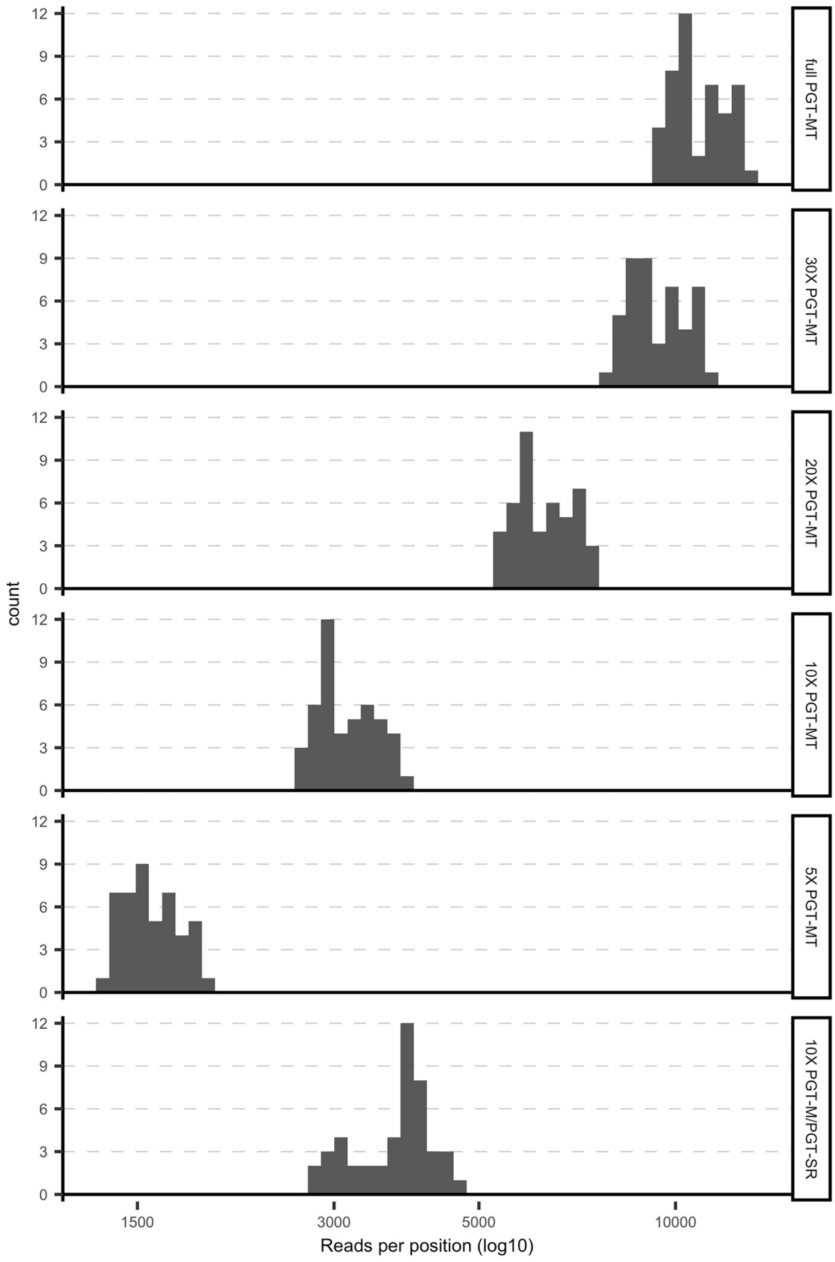

Histogram showing the mean number of reads per mitochondrial pathological mutation site (n = 46) at different (sub-sampled) levels of depths of coverage as indicated (right side labels). The mean is calculated based on four PGT-MT TE-biopsy samples (rows 1-5) or 28 embryos sequenced at 10X for PGT-M / PGT-SR indications (row 6).

Supplementary Table 1 | PGT indications of the included families

Family	PGT Type	Indication	Inheritance	Genetic Interval(s)	Notes
1	PGT-M	TGM1	AR	chr14: 24259813-24259814	Double indication
	PGT-SR	t(8;16)	-	-	
2	PGT-M	MEFV	AR	chr16: 3243407-3243408 chr16: 3243310-3243311	Double indication Consanguineous
	PGT-M	DMD	X-R	chrX: 31657989-31836820	
3	PGT-M	ARSA		chr22: 50626228-50626229	Consanguineous telomeric
4	PGT-M	BRCA1	AD	chr17: 43094569-43094570	Double indication
	PGT-M	OCA2	AR	chr15: 28081711-28081712 chr15: 27985101-27985102	
5	PGT-M	FSHD	AD	chr4: 189518883-189519279	Telomeric
6	PGT-M	D2HGDH	AR	chr2: 241743754-241743755	Consanguineous
7	PGT-M	PLN	AD	chr6: 118558961-118558963	Double indication
	PGT-M	DMD	X-R	chrX: 32644132-32645152	
8	PGT-M	GNAS	AD	chr20: 58910751-58910752	Homologous recombination at ROI
9	PGT-M	BSCL2	AD	chr11: 62702493-62702494	Double indication
	PGT-SR	t(2;11)	-	-	
10	PGT-M	BOR1	AD	chr8: 71215510-71215511	Homologous recombination at ROI
11	PGT-M	SCN9A	AD	chr2: 166195187-166375987	Trisomy at ROI
12	PGT-M	NF1	AD	chr17: 31261761-31261762	-
13	PGT-M	TMEM67	AR	chr8: 93786253-93786254 chr8: 93755039-93755044	Homologous recombination at ROI
14	PGT-M	TSC2	AD	chr16: 2080365-2080366	-
15	PGT-M	HemA	X-R	chrX: 155022473-155022474	Borderline sufficient data with GBS-PGT
16	PGT-M	GJB2	X-R	chr13: 20223037-20565037 chr13: 20189547-20189548	Homologous recombination at ROI
17	PGT-M	SLS	AR	chr17: 19543703-19751473	-
18	PGT-M	SHFM3	AD	chr10: 101227249-101624830	Triploid embryo
19	PGT-SR	t(3;13)	-	-	Double indication
	PGT-SR	ins(10;7)	-	-	Reference-free
20	PGT-MT	MELAS	-	chrMT: 3243	Mitochondrial

chr = chromosome, ROI = region of interest

Supplementary table 2 | PGT-AO: characterisation of identified chromosomal aberrations

Family	Embryo	Aberration	Chromosome	Parental origin	Segregational origin	Mosaicism level
1	1	Trisomy	2	Paternal	Mitosis	30%
1	4	Monosomy	19	Maternal	-	100%
4	11	Monosomy	18	Maternal	-	45%
7	18	Trisomy	10	Maternal	ND	25%
8	22	Trisomy	16	Maternal	Meiosis I	90%
		Trisomy	21	Maternal	Meiosis II	100%
11	28	Trisomy	2	Paternal	Mitosis	100%
		Monosomy	8	Maternal	-	100%
		Trisomy	14	Paternal	Meiosis I	100%
12	30	Trisomy	16	Maternal	Meiosis I	100%
14	32	Trisomy	4	Maternal	Meiosis I	80%
		Trisomy	16	Maternal	Meiosis I	100%
17	35	Monosomy	19	Paternal	-	100%
18	37	Triploidy	All (except 15)	Maternal	Meiosis II	100%

Sub-chromosomal aberrations associated with PGT-SR indications are not included.

Supplementary Table 3 | PGT-SR: Manta breakpoints identified for family 1

Sample	Simulated sequencing depth	Break point(s) Chr8	Corresponding break point Chr16	Filter	Qual	Imprecise
Father (carrier)	30X	**22092231**	**89257105**	PASS	840	FALSE
		22095311	89260346	PASS	607	FALSE
	20X	**22092231**	**89257105**	PASS	524	FALSE
		22095311	89260346	PASS	484	FALSE
	10X	**22092231**	**89257105**	PASS	275	FALSE
		22095311	89260346	PASS	119	FALSE
	5X	22095184	89260184	SampleFT	28	TRUE
Embryo 1	30X	**22092231**	**89257105**	PASS	466	FALSE
	20X	**22092231**	**89257105**	PASS	386	FALSE
	10X	**22092231**	**89257105**	PASS	243	FALSE
	5X	**22092231**	**89257105**	PASS	136	FALSE
Embryo 2	30X	**22092231**	**89257105**	PASS	999	FALSE
	20X	**22092231**	**89257105**	PASS	953	FALSE
	10X	**22092231**	**89257105**	PASS	302	FALSE
	5X	-	-	-	-	-
Embryo 3	-	-	-	-	-	-
Embryo 4	-	-	-	-	-	-

Consistently identified breakpoints are highlighted in green.

Supplementary Table 4 | PGT-SR: Manta breakpoints identified for family 19

Sample	Break point(s) Chr3	Corresponding break point Chr13	Filter	Qual	Imprecise
Father (Carrier)	180775646	105599571	PASS	643	FALSE
	180775646	105599573	PASS	643	FALSE
Embryo 38	56848461	86405296	Min QUAL		18
	58084818	54765142	PASS		22
	114753433	57765868	SampleFT		429
	149929733	97382114	MinQUAL; No Pair Support		19
	180775646	105599573	Max Depth		227
Embryo 39	180775646	105599571	PASS	443	FALSE
	7010416	25883379	PASS	94	FALSE
	33036326	110870500	Min QUAL	18	FALSE
Embryo 40	180775646	105599573	PASS	328	FALSE

Sample	Break point(s) Chr7	Corresponding break point Chr10	Filter	Qual	Imprecise
Father (Carrier)	139480299	19463401	PASS	122	FALSE
Embryo 38	124623421	105775111	PASS	47	FALSE
Embryo 39	81122896	60806560	PASS	51	FALSE
	115237501	50793538	PASS	89	FALSE
	117280169	51584626	PASS	44	FALSE
	143235835	30275090	MinQUAL; SampleFT	14	FALSE
Embryo 40	-	-	-	-	-

The matching breakpoints between the carrier parent (father) and the embryos are highlighted in yellow/orange.

Supplementary Table 5 | PGT-SR: Manta breakpoints identified for family 9

Sample	Break point(s) Chr2	Corresponding break point Chr11	Filter	Qual	Imprecise
Mother (carrier)	-	-	-	-	-
Embryo 25	4133636	100964344	50	PASS	FALSE
	41829506	74475192	24	PASS	FALSE
	53435892	115959442	200	PASS	FALSE
	139681038	2556247	999	MaxDepth	FALSE
	176261288	30432587	309	PASS	FALSE
	176634196	23969010	37	PASS	FALSE
	181982514	94227913	21	PASS	FALSE
	184738302	68369171	275	PASS	FALSE
	192082318	108048532	136	PASS	FALSE
	206427026	34855933	25	PASS	FALSE
	210554114	109595341	219	PASS	FALSE
	213084328	98088545	244	MaxDepth	FALSE
	227634802	99182224	999	MaxDepth	FALSE
	232608605	108575703	999	MaxDepth	FALSE

The break point presumed to be correct, based on the corresponding haplarithmisis result, is highlighted in orange.

Supplementary table 6 | PGT-MT: number of reads at the MELAS (m.3243 A > G) indication at different simulated depths of coverage

Depth	Embryo 45		Embryo 46		Embryo 47		Embryo 48	
	TE biopsy	Rest embryo	TE biopsy	Rest embryo	TE biopsy	Rest embryo	TE biopsy	Rest embryo
30X	4210	4634	4176	3996	3920	6952	3656	4333
	(2106)	(2283)	(2833)	(2743)	(2955)	(5303)	(1467)	(1742)
20X	3602	4191	3575	3346	3180	2956	2952	3776
	(1792)	(2076)	(2383)	(2301)	(2399)	(2228)	(1194)	(1473)
10X	2373	2965	2415	2231	2134	1972	1879	2472
	(1178)	(1481)	(1626)	(1509)	(1612)	(1518)	(771)	(974)
5X	1366	1831	1478	1288	1250	1135	1058	1488
	(675)	(910)	(977)	(885)	(936)	(872)	(436)	(586)

Numbers shown represent the total number of reads at the site and the number of reads with the mutation in brackets.

Supplementary table 7 | PGT-MT: heteroplasmy levels for the MELAS (m.3243 A > G) indication at different simulated depths of coverage

Depth	Embryo 45		Embryo 46		Embryo 47		Embryo 48	
	TE biopsy	Rest embryo	TE biopsy	Rest embryo	TE biopsy	Rest embryo	TE biopsy	Rest embryo
30X	50.0%	49.3%	67.8%	68.6%	75.4%	76.3%	40.2%	40.2%
20X	49.8%	49.6%	66.7%	68.85	75.4%	75.6%	40.4%	39.0%
10X	49.6%	49.9%	67.3%	67.6%	75.5%	77.0%	41.0%	39.4%
5X	49.5%	49.7%	66.1%	68.7%	74.9%	76.9%	41.2%	39.4%

Chapter 6

The nature and prevalence of chromosomal alterations in first-trimester spontaneous pregnancy loss

Rick Essers[#], Igor N. Lebedev[#], Ants Kurg[#], Elizaveta A. Fonova, Servi J. C. Stevens, Rebekka M. Koeck, Ulrike von Rango, Lloyd Brandts, Spyridon Panagiotis Deligiannis, Tatyana V. Nikitina, Elena A. Sazhenova, Ekaterina N. Tolmacheva, Anna A. Kashevarova, Dmitry A. Fedotov, Viktoria V. Demeneva, Daria I. Zhigalina, Gleb V. Drozdov, Salwan Al-Nasiry, Merryn V. E. Macville, Arthur van den Wijngaard, Jos Dreesen, Aimee Paulussen, Alexander Hoischen, Han G. Brunner, Andres Salumets[*], Masoud Zamani Esteki[*]

 # Joint first authors

*** Joint last authors**

My contribution: processing, analysis, visualisation, and write-up of the methylation data used for cell type deconvolution as well as editing the manuscript text.

Manuscript under review at Nature Medicine

Abstract

Pregnancy loss (PL) is often caused by chromosomal abnormalities of the conceptus. The prevalence of these abnormalities and the allocation of (ab)normal cells in embryonic and placental lineages during intrauterine development remain elusive. We analyzed 1,745 spontaneous PLs and found that roughly half (50.4%) of the products of conception (POC) were karyotypically abnormal, with maternal and paternal age independently contributing to the increased genomic aberration rate in PL. We applied genome haplarithmisis to a subset of 94 PLs with normal parental and POC karyotypes. Genotyping of parental DNA as well as POC extraembryonic mesoderm (EM) and chorionic villi (CV) DNA, representing embryonic and trophoblastic tissues, enabled characterization of the genomic landscape of both lineages. Of these PLs, 35.1% had chromosomal aberrations not previously detected by karyotyping, increasing the rate of aberrations of PLs to 67.8% by extrapolation. In contrast to viable pregnancies where mosaic chromosomal abnormalities are often restricted to CV, such as confined placental mosaicism, we found a higher degree of mosaic chromosomal imbalances in EM rather than CV in PLs. Our results stress the critical importance of scrutinizing the full allelic architecture of genomic abnormalities in PL to improve clinical management and basic research of this devastating condition.

Introduction

Worldwide, 23 million pregnancy losses (PLs) occur every year, with a high prevalence of 10-15% of all clinically recognized pregnancies[1]. PL primarily occurs prior to weeks 8-9 of gestation[1], and there is considerable additional loss in earlier stages of pregnancy that may go unnoticed. Overall, 10.8% of women experience at least one PL, and 1.9% and 0.7% have two or three PLs[1]. Identifying the cause of PL can provide important prognostic, diagnostic, and management recommendations to support future viable pregnancies[2]. Chromosomal abnormalities, in particular aneuploidy, defined as an incorrect number of chromosomes, in the conceptus are the leading causes of PLs. It has been established that aneuploidies commonly occur during oogenesis[3-5] and in early embryogenesis[6-8]. The incidence of chromosomal aneuploidies increases with maternal age, which contributes to age-related infertility[8]. This is due to the low fidelity of chromosome segregation in meiosis during oogenesis[3,8] and DNA replication stress[9] during mitotic cleavage divisions in preimplantation embryogenesis[6,7]. Previously, we and others demonstrated that although chromosome instability (CIN) is common in early embryogenesis[6,7], it is not present at birth[10]. This observation indicates that only embryos with sufficient genome integrity can survive to term and that both meiotic aneuploidies in oocytes and postzygotic chromosome abnormalities in early embryogenesis may lead to implantation failure and PLs[1].

CIN leads to mosaic embryos that contain both chromosomally normal and abnormal cells. It has been shown that aneuploid cells in mosaic embryos can be progressively depleted during preimplantation development[11]. Self-correction of human embryos may operate via cellular fragmentation and blastomere exclusion of abnormal cells [12] or by rescue mechanisms such as trisomy or monosomy rescue[13]. Spatiotemporal allocation of abnormal cells or aneuploidy rescue mechanisms can lead to confined placental mosaicism (CPM), the main biological cause for discordant abnormal non-invasive prenatal testing (NIPT) results, with normal fetus confirmed after invasive fetal testing[14]. For instance, previously, we showed that >70% of large (>100 kb) de novo copy-number variations (CNVs) are only present in the placental lineage[10].

Recently, the genomic landscape of second- and third-trimester PLs and elective terminations of fetuses with abnormal *in utero* phenotypes has been characterized[15]. However, little is known about the genomic landscape of first trimester spontaneous PLs. This knowledge is essential to understanding *in utero* mechanisms of CIN separately for fetal and placental lineages, and developing strategies for the early detection of high-risk pregnancies leading to PL. Here, we profiled the chromosomal landscape of the chorionic villi (CV) and the extraembryonic mesoderm (EM) of first trimester (~7 weeks of gestational age) spontaneous PLs, which are derived from the embryonic trophectoderm (TE) and the inner cell mass (ICM), respectively.

Results

Cohort characteristics and conventional cytogenetic tests

Following conventional karyotyping of the products of conception (POC) that were collected from 1,745 women over a course of 34 years (1987-2021), 866 (49.6%) and 879 (50.4%), PLs were classified as karyotypically normal and abnormal, respectively (**Fig. 1a, Table 1**). Of the 1,745 cases, 1,597 (91.5%) samples were karyotyped using conventional GTG banding after long-term extra-embryonic fibroblast culture, and 29 (1.7%) samples were karyotyped by direct preparations of the chorionic villi. If GTG banding was not possible, other traditional methods, including conventional comparative genomic hybridization (CGH) (3.4%, 59 samples) and interphase fluorescence in situ hybridization (FISH) with centromere-enumeration probes (3.4%, 60 samples) were performed.

In line with previous studies, abnormal fetal karyotypes were associated with higher parental age (maternal age; 29.0±6.4 SD and 27.8±5.9 SD, respectively, $P = 6.7 \times 10^{-5}$, paternal age; 31.3±6.8 SD and 30.3±6.3 SD, respectively, $P = 4.6 \times 10^{-3}$, two-sided Welch's T test) (**Fig. 1b**). Logistic regression was performed to further investigate whether maternal and paternal age were independently associated with abnormal POC karyotypes. Implementing both parental ages in the same regression model dissolved the statistically significant association for both factors, indicating that maternal and paternal age separately explain the same variance in the data and show high collinearity (**Supplementary Table 1**).

Table 1 | Clinical diagnosis of early pregnancy loss

Diagnosis	Conventional karyotyping		Genome haplarithmisis	
	n	%	n	%
Missed abortions	1,156	66.2	74	78.7
Anembryonic pregnancies	261	15.0	16	17.0
Spontaneous abortions	137	7.9	1	1.1
Fetus malformations	27	1.5	0	0
Hydatidiform mole	4	0.2	0	0
Inconclusive PL aetiology	160	9.2	3	3.2
Total POCs	**1, 745**	**100**	**94**	**100**

Figure 1 | Genome haplarithmisis reveals previously undetected chromosomal aberrations.

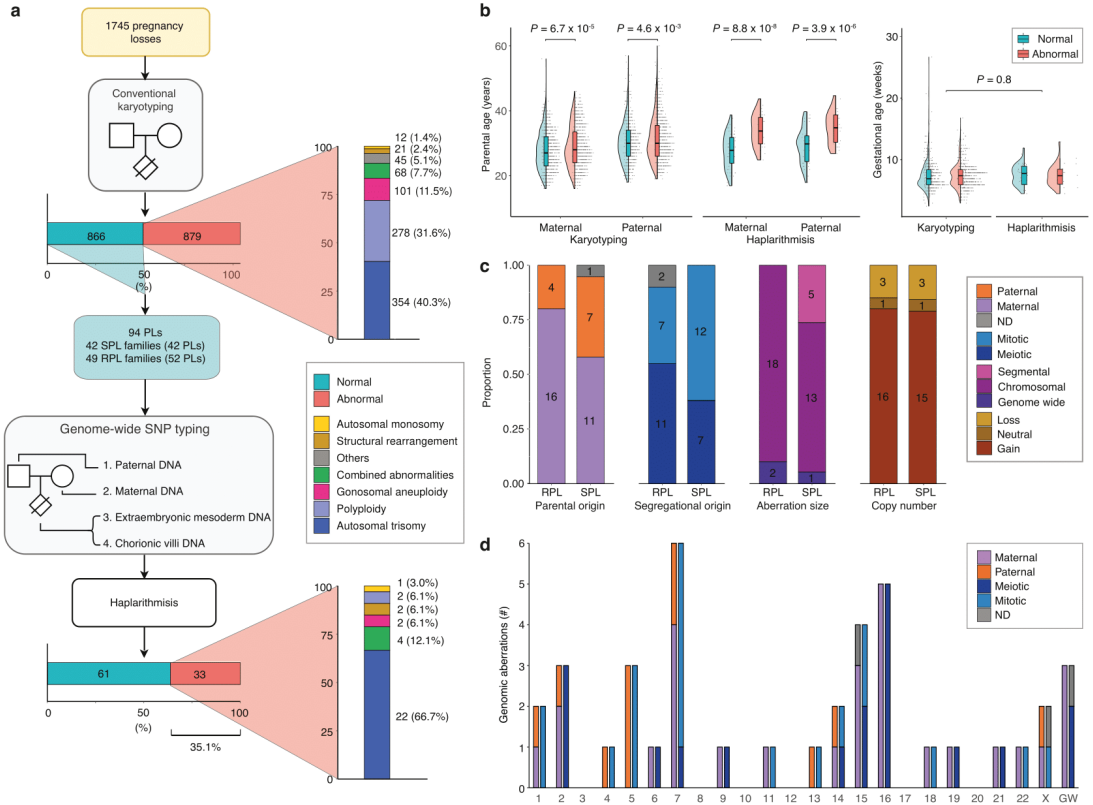

***a**) Study design and distribution of aberrations. **b**) Maternal, paternal, and gestational age in conventional karyotyping of POC samples with normal (n = 866) and abnormal (n = 879) karyotypes and in genome haplarithmisis POC samples with normal (n = 61) and abnormal (n = 33) genomes (two-sided Welch's T test). **c**) Parental and segregational origin of aberrations, aberration size (segmental, chromosomal, genome wide), and copy number (gain, loss, neutral) of unique aberrations per POC sample for the recurrent pregnancy loss (RPL) cohort (n = 20) and sporadic pregnancy loss (SPL) cohort (n = 19). **d**) Parental and segregational origin of genomic aberration per chromosome, including each unique aberration per POC sample.*

Genome haplarithmisis reveals genomic alterations in karyotypically normal POCs

We analysed 94 karyotypically normal PLs with good-quality DNA samples (**Methods**) from 91 families with similar gestational ages as the entire cohort (7.5±2.2 SD and 7.5±1.7 SD gestational weeks, respectively, P = 0.8, two-sided Welch's T test) (**Fig. 1b, Methods**). These samples were selected based on (i) their classification as "normal" by conventional karyotyping, (ii) the availability of POC EM and CV tissues, and parental DNA, and (iii) parents were karyotypically normal, without genetic predisposition for PL. To detect (mosaic) de novo genomic aberrations in POC undetected by conventional karyotyping, we performed genome-wide single nucleotide polymorphism (SNP-) genotyping of the parental as well as the EM and CV DNAs from POC followed by genome haplarithmisis[7,10]. Haplarithmisis is a conceptual method that transforms genotyping data to haplotypes and copy-number states, called parental haplarithms. When a copy-number change affects a combination of different homologous chromosomes of a parent, this represents meiotic error. If the centromere is from different homologous chromosomes this represents meiotic I error. If the centromere is not involved but a part of the chromosome derives from different homologous chromosomes, this specifies meiotic II error. In addition, distortion of B-allele frequency (BAF) values from expected $1_{maternal}$:$1_{paternal}$ allelic ratio indicates the degree (%) of abnormal cells, i.e. mosaicism. Here, we applied haplarithmisis on bulk DNA samples (i.e. derived from many cells) and made use of CV as a seed to phase the parental genomes, allowing the reconstruction of trio-based parental haplarithms (**Fig. 2a and Methods**). This allowed us to determine the prevalence and nature of different chromosomal abnormalities, including their parental and mechanistic origins (**Fig. 1c, d and 2a, b**) and their levels of mosaicism (**Fig. 2a, b and Extended Data Fig. 1**). The data showed that of 94 POCs (188 paired CV and EM DNA samples; 89 families with a single PL, one family with 2 PLs, and one family with 3 PLs), 65 DNA samples (34.6%; 33 CV and 32 EM DNA samples) had a genomic aberration (source data, not shown). Thus, out of 94 karyotypically normal POC samples as determined by conventional analysis, 33 POC samples (35.1%) had one or more genomic imbalances that were detected by genome haplarithmisis (**Fig. 1a and Supplementary Table 2**). If we consider these haplarithmisis-determined abnormal samples (35.1%) as well as the 50.4% abnormality rate reported through conventional karyotyping (n=879/1,745), the rate of genomic aberrations in POC samples reaches 67.8% by extrapolation (**Methods**). This is higher than what has been quoted previously by other studies that used karyotyping [13,16] or clinical-grade chromosomal microarrays[17-25] (**Supplementary Table 3**).

Figure 2 | Schematic representation of genome haplarithmisis and detection of various abnormalities

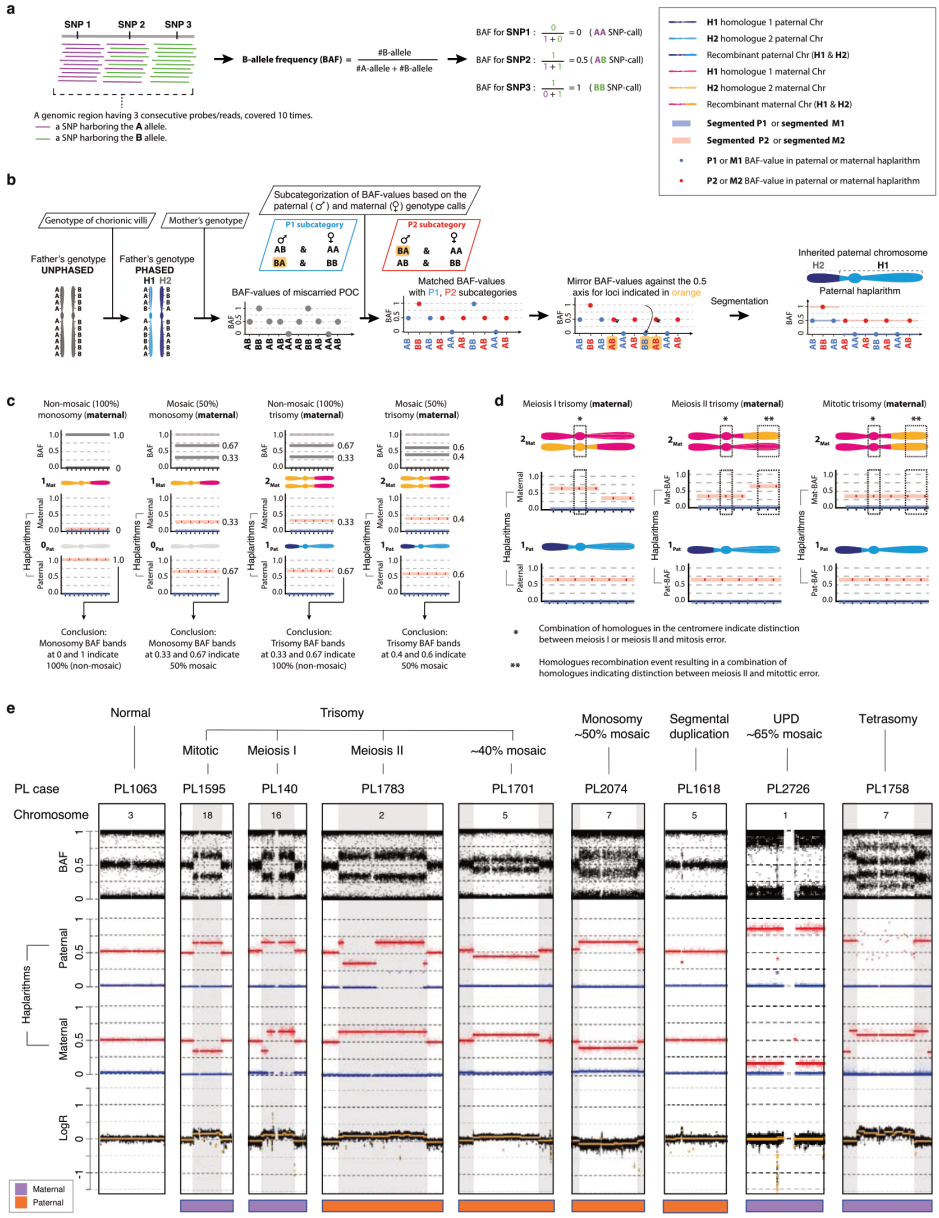

a) *A genomic region harbouring three consecutive single-nucleotide polymorphisms (SNPs), each with weighted signal intensity of 10, as well as equation for B-allele frequency (BAF) computation for those three SNPs.* ***b)*** *Schematic representation of the standard genome haplarithmisis workflow as demonstrated in Zamani Esteki et al. 2015,* ***c)*** *Detection of different level of mosaicism in trio-based haplarithmisis and* ***d)*** *parental and segregational origin of genomic anomalies in trio-based haplarithmisis (Methods).* ***e)*** *Haplarithms of several PLs with different types of abnormalities, parental and segregational origins and mosaicism degrees; only a single chromosome of interest is displayed per POC sample. PL1063 has a normal*

*diploid chromosome (Chr) 3, PL1595 has a nonmosaic trisomy 18 of maternal and mitotic error origin, PL140 has a nonmosaic trisomy 16 of maternal and meiosis I error origin, PL1783 has a nonmosaic trisomy 2 of paternal and meiosis II error origin, PL1701 has an ~40% mosaic trisomy 5 of paternal and mitotic error origin, PL2074 has ~50% mosaic monosomy 7 of paternal (maternal chromosome is left) and mitotic error origin, PL1618 has a (subchromosomal) ~2.7 Mb duplication in Chr 5 near the centromere (q11.1-q11.2) of paternal and mitotic error origin, PL2726 has an ~65% mosaic uniparental disomy (UPD) 1 of maternal and mitotic origin, and PL1758 has a tetrasomy 7 of maternal error origin (**Extended Data Fig. 7**).*

Profiling the genomic landscape of sporadic and recurrent PLs

To further characterize the genetic effect of the detected aberrations, we divided the 94 PLs into sporadic PL (SPL), defined as 1 PL (42 families and PLs, 84 DNA samples), and recurrent PL (RPL), defined as ≥2 consecutive PLs (49 families, 52 PLs, 104 DNA samples) (**Fig. 1a**). The SPL and RPL cohorts had 28 (33.3%, 19 unique copy number aberrations per POC) and 37 (35.6%, 20 unique copy number aberrations per POC) POC samples with genomic aberrations, respectively (**Extended Data Fig. 2**). The RPL and SPL cohorts did not show a significant difference in either segregational and parental origins of aberrations or in the total copy number or copy-neutral events (**Fig. 1c**). However, the SPL cohort contained more segmental aberrations, while the RPL cohort contained more numerical chromosomal aberrations (**Fig. 1c**, $P = 3.6 \times 10^{-2}$ Fisher's exact test).

Aberrations on Chr 7 and Chr 16 were most common in first trimester PL (**Fig. 1d**), as observed previously[1,26]. Aberrations on Chr 16 (n = 5) were all of maternal and meiotic in origin, and aberrations on Chr 7 were maternal and mitotic (n = 4), paternal and mitotic (n = 1), and paternal and meiotic (n = 1) in origin (**Fig. 1d**). Trisomy 16 impairs embryonic growth due to placental hyperplasia, potentially leading to first-trimester PL[26]. Trisomy Chr 16 is less prevalent in NIPT samples at 11-12 weeks of pregnancy[27,28] as compared to preimplantation embryos following preimplantation genetic testing (PGT)[29,30], indicating that pregnancies with trisomy Chr 16 have reduced capacity to reach to later gestational ages

Determining the level of mosaicism in CV and EM tissues

Comparing the haplarithm profiles of EM and CV allowed us to determine not only if these tissues carry different large CNVs (>100 kb) but also whether the level of mosaicism is different. The analysis of EM and CV DNA samples can be used to probe the spatiotemporal allocation of abnormal cells in early embryogenesis and to deduce whether this allocation affects the fate of early prenatal development and the risk of PL. To check for accurate dissection of EM and CV tissues, we performed methylome-wide analysis of 13 samples that generated good quality data (**Extended Data Fig. 3, Methods**). Principal component analysis of all methylation sites showed clear separation of CV and EM tissues (**Fig. 3b**). Subsequent cell composition deconvolution suggested that both CV and EM samples were of mixed, but different, cellular origin, with a significantly higher proportion of Hofbauer

cells as well as a significantly lower proportion of stromal cells in CV samples compared to the EM samples (**Extended Data Fig. 4**).

Figure 3 | Extraembryonic mesoderm and chorionic villi derive from inner call mass and trophectoderm, respectively

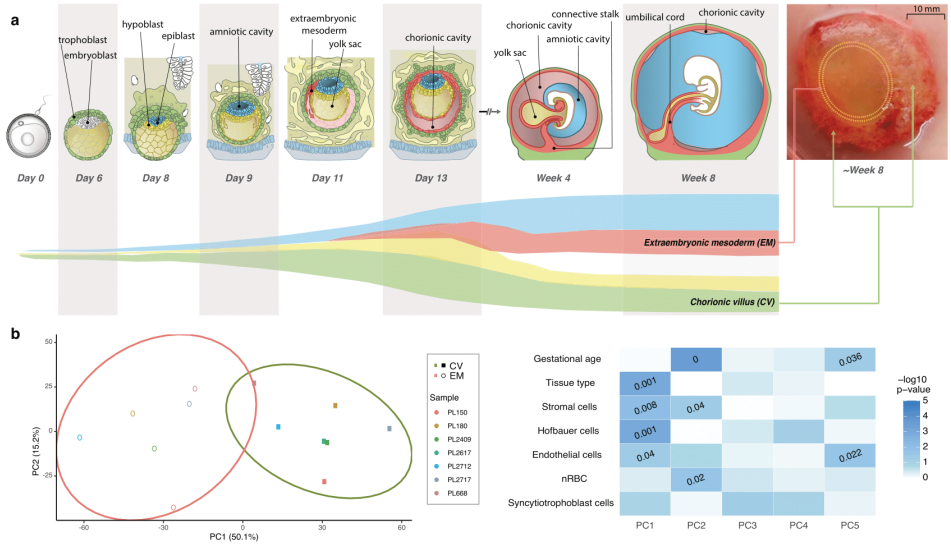

***a**) Schematic representation of early embryonic development. Extraembryonic mesoderm (EM) develops from the embryoblast lineage (hypo- and epiblast), while chorionic villi (CV) develop from the trophoblast lineage. EM and CV samples from PLs were collected at week 7.6 ± 1.7 SD. **b**) Principal component analysis of all CpG sites (n = 685,221) passing quality control criteria (**Methods**) in data from high DNA quality EM (n = 6) and CV (n = 7) samples. The ellipses represent the 90% confidence interval, and the percentage of variance explained by each principal component (PC) is shown in brackets. Heatmap showing associations between the first 5 principal components and biological aspects of the samples, including their predicted cell compositions (**Extended Data Fig. 6**). The color gradient shows the -log10 of the p values, and p values <0.05 are indicated. The significance of the correlation between the principal components and the continuous, numerical sample attributes was tested using a permutation test with 10,000 permutations. The association between the PCs and the binary variable tissue type was assessed using a two-sided Wilcoxon signed-rank test.*

While there is no doubt that the CV is derived from the TE[31,32], there is some uncertainty surrounding the developmental origin of EM[31,32]. A recent study proposed that the EM develops from the hypoblast-derived primary yolk sac supplemented by epiblast-derived mesoderm from the gastrulating embryo[31] (**Fig. 3a and Extended Data Fig. 5**). Hypoblasts and epiblasts are both derived from the ICM. Of the 33 genetically aberrant POC samples, a selection consisting of all tissues with a mitotic aberration or meiotic aberration with a >10% difference in the proportion of abnormal cells comparing EM and CV showed that the EM biopsies had a higher level of mosaicism relative to CV

(58.2% ± 30.1 SD and 43.4% ± 32.9 SD, respectively, P = 2.0 x 10^{-2} Wilcoxon signed rank test, **Fig. 4**). Of the nine POC samples (27.3%) with >10% difference in level of mosaicism, 8 samples (6 aberrations of mitotic origin, 2 of meiotic origin) had aberrations in autosomes and one sample (aberration of mitotic origin) in Chr X (**Fig. 5**). In all samples with autosomal aberrations, the level of mosaicism was higher in EM than in CV (**Fig. 4 and 5**). Strikingly, this contrasts with viable pregnancies where mosaic abnormalities are often restricted to the CV[31,32]. For two cases, copy number aberrations (trisomy 13 of PL2726 and monosomy 7 of PL2074, **Fig. 5 and Extended Data Fig. 6**) were detected only in EM, and haplarithmisis revealed the postzygotic mitotic origin of both of these aneuploidies, supporting the theoretical model for tissue-specific aneuploid cell line compartmentalization in early pregnancy loss[13].

Figure 4 | Genetic abnormalities in the embryoblast lineage are less tolerated and potentially lead to pregnancy loss (PL)

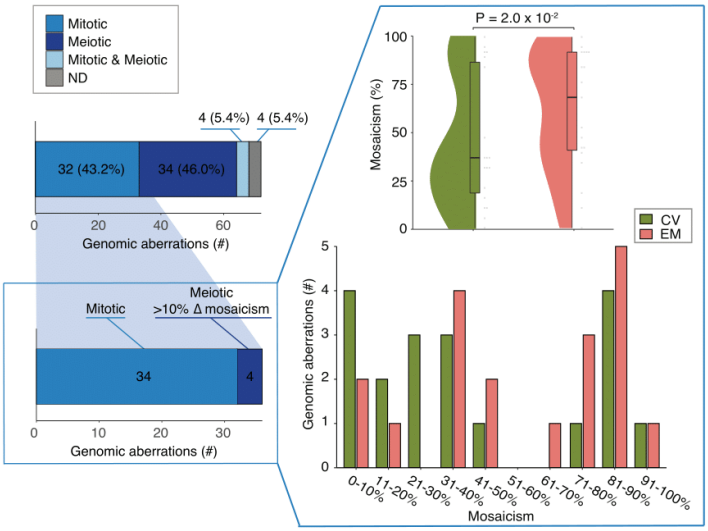

Segregational origin of each individual aberration in both EM and CV tissue per POC detected by genome haplarithmisis, while samples with aberrations of mitotic origin (n = 34; 17 EM; 17 CV) or meiotic origin with >10% mosaicism difference between EM and CV (n = 4; 2 EM; 2 CV) were selected for EM/CV plots and mosaicism statistics. The mosaicism degree in EM samples (n = 19) was significantly higher than that in CV samples (n = 19) (Wilcoxon signed-rank test).

Figure 5 | Higher degree of mosaicism (>10%) observed in extraembryonic mesoderm as compared to chorionic villi for pregnancy loss cases

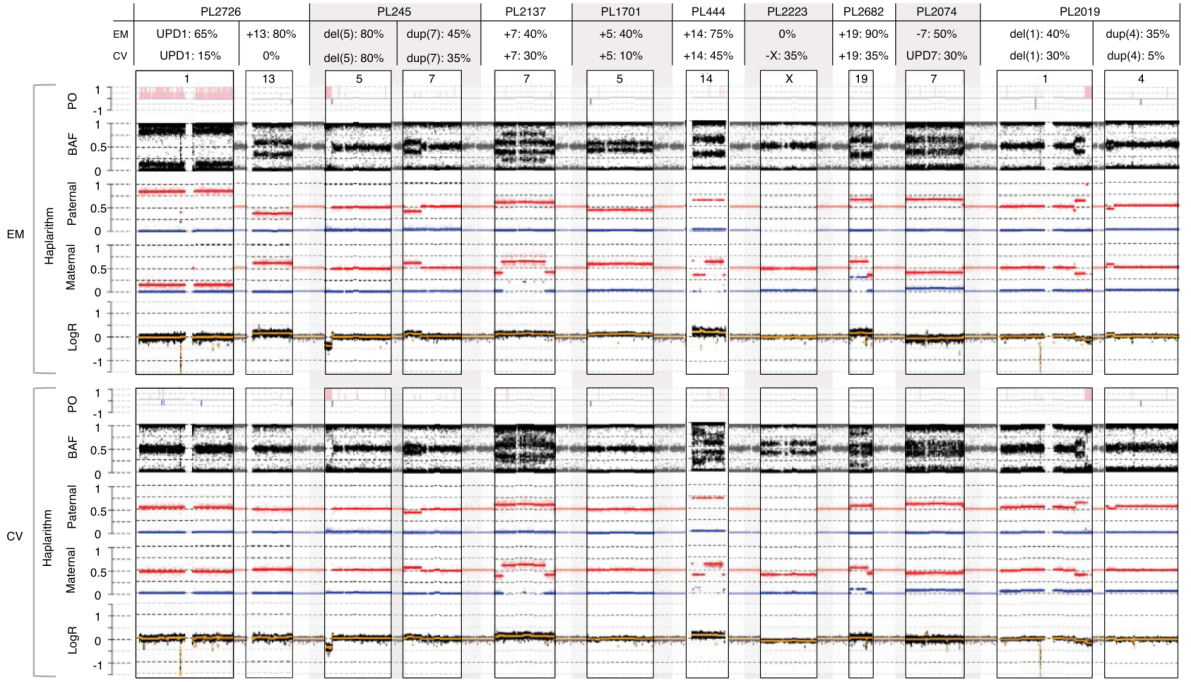

Haplarithms of 9 PL samples with differences between EM and CV of >10% mosaicism. PL2726 has a (EM ~65%, CV ~15%) mosaic uniparental disomy (UPD) 1 of maternal and mitotic origin, and an ~80% mosaic EM-only trisomy 13 of paternal and mitotic error origin. PL245 has a (EM ~80%, CV ~80%) mosaic (subchromosomal) ~16.7-Mb deletion in chromosome (Chr) 5 (p15.1-p15.33) of paternal and mitotic error origin, and a (EM ~45%, CV ~35%) mosaic ~43.2-Mb duplication in Chr 7 (p14.1-p22.3) of paternal and mitotic error origin. PL2137 has an (EM ~40%, CV ~30%) mosaic trisomy 7 of maternal and mitotic error origin, PL1701 has a (EM ~40%, CV ~10%) mosaic trisomy 5 of paternal and mitotic origin. PL444 has an (EM ~75%, CV ~45%) mosaic trisomy 14 of maternal and meiotic error origin. PL2223 has an ~35% mosaic CV only monosomy X of paternal error origin. PL2682 has an (EM ~90%, CV ~35%) mosaic trisomy 19 of maternal meiotic error origin. PL2074 has an ~50% mosaic EM only monosomy 7 of maternal and mitotic error origin, and an ~30% mosaic-CV-only UPD 7 of maternal and mitotic error origin. PL2019 has a (EM ~40%, CV ~30%) mosaic ~44.7-Mb deletion in Chr 1 (q32.1-q44) of paternal and mitotic error origin, and a (EM ~35%, CV ~5%) mosaic ~18.3-Mb duplication in Chr 4 (p15.32-p16.3) of paternal and mitotic error origin.

Discussion

Over 90% of PLs occur during the first trimester[33,34]. Chromosomal abnormalities in the fetus are recognized as a primary cause of PL. Previously, eight large studies (>1k POC sample size, in total 42,5k POCs) showed a combined yield of ~53.7% fetal chromosomal abnormalities[17-24] (**Supplementary Table 3**), which is in line with 53.1% reported rate in a recent meta-analysis[25]. The study that applied high-density SNP-arrays, gave a higher yield of 67%, which is similar to what we found here after genome haplarithmisis[22]. Thus, haplarithmisis gives a superior yield over karyotyping or standard microarray approach. In addition, six previous studies analyzed POCs that were classified as normal with conventional karyotyping[35-40] (**Supplementary Table 4**). The average frequency of additionally detected abnormalities found in these studies was 19.4%, which is nearly two-fold lower than 35.1% identified in this study. This difference can be explained by two major factors. Firstly, the previous studies relied on single POC tissue analysis, primarily CV or placenta. However, in this study, we carried out parallel analysis of EM and CV samples from the same POC, increasing the diagnostic yield of detecting the genomic aberrations. Strikingly, mosaicism tended to be higher in EM relative to CV, which again suggests persistent involvement of abnormal fetal cells in PL. Secondly, the conventional cytogenetic methods, including microarrays are unable to distinguish the meiotic and mitotic origins of genomic aberrations and detect low-level mosaicism. Here, we demonstrated that these shortcomings can be tackled via genome haplarithmisis.

The conventional karyotyping of POC that is being applied in routine care is limited by its low resolution, maternal contamination, high culture failure rates, and overgrowth of (maternal) normal cells compared to abnormal cells, leading to low diagnostic yield[41]. The quality also varies between samples and laboratories and is reliant on the expertise of technicians and cytogeneticists. Previously, we and others showed that low proliferative activity of extra-embryonic cells in vitro is a major limitation of conventional karyotyping of spontaneous abortions. Specifically, conventional cytogenetic analysis of miscarriages strongly depends on tissue culturing and is associated with a substantial culture failure rate, which varies from 5% to 42% in different laboratories[42-51]. This suggests that the use of sophisticated genome analysis methods that use DNA samples and do not require cell culturing in PL samples carry clear advantages. Genome haplarithmisis can detect low-grade mosaicism (>10%) from uncultured samples (**Fig. 2a and Extended Data Fig. 1, Methods**) with higher resolution and allows for the detection of smaller sub-chromosomal CNVs (>100 kilobase pairs (kb)) (**Fig. 2e and Extended Data Fig. 1b**)[10]. Additionally, it can detect the parental and segregational origins of aberrations and maternal cell contamination[7] (**Fig. 2d**). These features are well beyond the sensitivity of conventional methods such as karyotyping and standard

chromosomal microarray- or sequencing-based copy-number analyses that are being performed in routine care. There is an emerging need for prospective clinical studies comparing genome haplarithmisis with conventional methods to evaluate its clinical implementation and cost effectiveness for management of PL. The recent European Society of Human Reproduction and Embryology (ESHRE)'s guidelines in recurrent PL have restated the limitation of conventional karyotyping and suggested the usefulness of future studies on the role of next-generation sequencing techniques[52]. A strategy utilizing genetic analysis of miscarriage tissue could help patients to deal with the psychological impact of PL and would limit the need for further expensive and elaborate maternal investigations for other causes of recurrent PL[53].

Profiling the genomic landscape of PLs by carefully dissecting both the EM and CV tissues of the same POC and applying haplarithmisis, allowed us to detect 35.1% of karyotypically normal POCs as abnormal. Moreover, POCs with different level of mosaicism in EM and CV were found, with the prevalence of aberrations being higher in EM as compared to CV. This finding raises intriguing hypothesis about the origin of mosaic mutations in PL. While EM develops prior to gastrulation in primates, it develops during gastrulation in rodents. Therefore, EM cells are most likely derived from transient primary yolk sac, which is of embryoblast (ICM) and not trophoblastorigin[31]. It has previously been suggested that self-correction mechanisms for aneuploidy are active in the ICM during early embryogenesis and that there is a selective bottleneck in early embryogenesis when aneuploid cells are depleted[11,12]. Our data are compatible with a selective scenario in which chromosomal aberrations first emerge in the ICM of the blastocyst and persist at least in extraembryonic mesoderm, conferring a strong detrimental effect on the pregnancy outcome, and may result in PL.

We found that SPL and RPL cohorts have similar prevalence of genomic aberrations. However, these two groups had different types of genomic aberrations, such that the SPL cohort had significantly more segmental aberrations, while the RPL cohort carried more aneuploidies (**Fig. 1c**). Although our cohort is underpowered to draw firm conclusions, our POC analysis points to possible differences in the genetic aetiology of PLs which merits further study. We emphasize the importance of reaching an international consensus on the clinical definition of RPL, which is the topic of an ongoing debate and differs across guidelines and countries[1,52]. ESHRE's most recent guidelines define RPL as the loss of two or more pregnancies before 24 weeks of gestation[52], which was used in this study.

Our data inform discussions about the clinical importance of scrutinizing the full allelic architecture of genomic abnormalities and their segregational origin (meiotic vs. mitotic origin) in human embryos and pregnancies with relevance for the safety of transferring

in vitro fertilized (IVF) embryos with mosaic imbalances[54], as well as interpretation of NIPT results with mosaic aberration indications. In nation-wide NIPT studies[27,28] the rate of confirmed confined fetal mosaicism is very low as compared to CPM, indicating that abnormal cells in the fetus are less tolerated relative to the placenta. For instance, 94% of rare autosomal trisomies in NIPT were found to be most likely due to CPM[27]. The impact of chromosomal mosaicism is less clear due to current limitations for its detection. According to some rare cytogenetic studies on spontaneous abortions and confined placental chromosomal mosaicism, CPM is found in ~20% of the POCs, which is higher than the reported rate of 1-2% seen in viable pregnancies in chorionic villus sampling[49,55-57]. Additionally, when we compared the nature and prevalence of genomic aberrations along the gestational weeks of the first trimester, we observed that on average there may be a higher level of mosaicism in earlier POCs (**Supplementary Tables 2 and 5**). For instance, for mitotic aberrations in EM (n=14) the average level of mosaicism in POCs of gestational weeks 4-7 (n=7) was 67.9% ± 26.4%SD while in POCs of gestational weeks 8-13 (n=7) the average level of mosaicism was 48.9 ± 30.8 (*P=0.33,* 2-sided Mann Whitney U test, **Supplementary Table 5**). Our cohort is underpowered to draw firm conclusions regarding the comparison of different gestational ages. To reach a sufficient power of 0.8, a minimum sample size of 86, i.e. 43 POCs per time interval, would be required (**Methods**).

This study has practical implications, contributing to the emerging studies using NIPT in recurrent PL[58]. Specifically, in the case of detected copy number changes following NIPT, genome haplarithmisis can distinguish between meiotic and mitotic errors. NIPT with CPM can lead to false positive test results. These findings require fetal invasive genetic testing that could potentially be avoided by accurate detection of the segregational origin of the mutation as well as linking low abundant cell-free DNA (cfDNA) to the fetal or placental lineage, which is required to exclude the presence of aberrant cells in the fetus. Aberrations of meiotic origin, if occurring via rescue events into mosaic blastocysts, are likely affecting both fetal and placental lineages and predisposing for spontaneous miscarriage, while mitotic aberrations may be private to the placenta due to CPM[10] and are compatible with healthy pregnancies. This allows differentiating low risk of fetal involvement as in mitotic errors, from higher risk of a fetal (mosaic) abnormality with higher likelihood for severe clinical consequences as would be expected for meiotic errors. Additionally, epigenetic studies of cfDNA have suggested that fetal tissues other than the placenta-derived trophoblasts may also contribute to the cfDNA mixture of maternal blood[59]. This makes it possible to discriminate CPM, which is apparently safe for pregnancy, from a situation where (mosaic) aberration is present in both placental tissue and the fetus, with a higher risk for PL. This underlines the importance of developing technologies that can reliably identify placental and fetal origin when an aberration is found in early pregnancy. Moreover, haplotyping-based

NIPT methods enable a generic approach for detection of monogenic disorders[60].

Taken together, the detection of the segregational origin of chromosomal aberrations is of paramount importance for prognosing the successful completion of pregnancy. Although embryos with mosaic abnormalities can lead to the birth of healthy babies[61], the meiotic or mitotic origin of mosaicism has not always been determined in these successful cases. For instance, as in PGT of IVF embryos, the DNA sample is derived from a single trophectoderm biopsy, and the true extent of mosaicism in all embryo compartments, including the ICM, cannot be determined. However, the determination of the segregational origin of mosaic aberrations would help to avoid transferring meiotic (mosaic) IVF embryos, which confer a high risk for ICM aberrations and later PL. In contrast, we suggest that the rules for selecting mitotic mosaic embryos for uterine transfer could be more relaxed.

In conclusion, our study shows that as much as two-thirds of all pregnancy losses may be due to fetal chromosomal abnormalities. Further, the ability to accurately determine the segregational and lineage origins of fetal genomic aberrations may enhance the efficacy of human natural and assisted conception and thereby improve reproductive genetic care in general.

Data availability

All SNP array and methylation data generated in this study were deposited in the NCBI Gene Expression Omnibus (GEO) under accession number **GSE228151**. Source data for the figures and statistical analysis have been submitted with this manuscript.

Code availability

Custom code is available on GitHub: https://github.com/CellularGenomicMedicine/Pregnancy_loss_study

Acknowledgements

We are grateful to all families that participated in this study. We thank all the physicians and cytogeneticists who were involved in ultrasound examination of pregnant women, their genetic counselling, recruiting patients and collecting samples over 34 years. We would like to thank Greet Mommen for her contribution to embryo gastrulation illustrations. This study was supported by a Horizon 2020 innovation grant (ERIN, grant no. EU952516) and the Horizon Europe (NESTOR, grant no. 101120075) of the European Commission, the Estonian Research Council (grant no. PRG1076), Enterprise Estonia (grant no. EU48695), the Russian Science Foundation (grant no. 21-65-00017, in the part of cytogenetic analysis, aCGH, STR and RT-qPCR studies of POCs), and the EVA (Erfelijkheid Voortplanting & Aanleg) specialty program (grant no. KP111513) of

Maastricht University Medical Centre (MUMC+). We would like to thank the referees for their constructive remarks that helped increasing the quality of this work.

Author contributions

R.E., I.N.L., A.K., A.S., and M.Z.E. conceived the study and designed the experiments. R.E., I.N.L., A.K., S.J.C.S., R.K., U.V.R., S.A.N., M.V.E.M., A.V.D.W., A.H., H.G.B., A.S., M.Z.E contributed to manuscript writing and data interpretation. T.V.N., E.A.F., E.A.S., E.N.T carried out sample collection. T.V.N., E.A.S., E.N.T. carried out the conventional cytogenetic diagnosis of pregnancy loss. T.V.N., E.A.F., V.V.D. carried out dissection of CV and EM and DNA extraction from fetal tissues and parental blood samples. D.I.Z., G.V.D., V.V.D. performed conventional CGH, aCGH and interphase FISH. A.A.K., D.A.F., E.A.F. performed RT-qPCR and STR-analysis. A.K., and S.P.D. performed whole-genome SNP genotyping. R.E. and M.Z.E. performed genome haplarithmisis. R.E., S.J.C.S., J.D., A.P., A.H., H.G.B., and M.Z.E. analyzed and interpreted haplarithmisis data. R.E., L.B., and M.Z.E. applied and described statistical analysis. R.E., R.K., and M.Z.E. performed methylation profiling, processing, and analysis. A.S. and M.Z.E. oversaw and supervised the study. All the authors read and approved the manuscript for submission.

Competing Interests

M.Z.E. is co-inventor on patent applications: ZL910050-PCT/EP2011/ 060211-WO/2011/157846 'Methods for haplotyping single cells' and ZL913096-PCT/ EP2014/068315-WO/2015/028576 "Haplotyping and copy-number typing using polymorphic variant allelic frequencies".

References

1 Quenby, S. *et al.* Miscarriage matters: the epidemiological, physical, psychological, and economic costs of early pregnancy loss. *Lancet* **397**, 1658–1667 (2021). https://doi.org/10.1016/S0140-6736(21)00682-6

2 Coomarasamy, A. *et al.* Sporadic miscarriage: evidence to provide effective care. *Lancet* **397**, 1668–1674 (2021). https://doi.org/10.1016/S0140-6736(21)00683-8

3 Gruhn, J. R. *et al.* Chromosome errors in human eggs shape natural fertility over reproductive life span. *Science* **365**, 1466–1469 (2019). https://doi.org/10.1126/science.aav7321

4 Hassold, T. *et al.* Failure to recombine is a common feature of human oogenesis. *Am. J. Hum. Genet.* **108**, 16–24 (2021). https://doi.org/10.1016/j.ajhg.2020.11.010

5 Starostik, M. R., Sosina, O. A. & McCoy, R. C. Single-cell analysis of human embryos reveals diverse patterns of aneuploidy and mosaicism. *Genome Res.* **30**, 814–825 (2020). https://doi.org/10.1101/gr.262774.120

6 Vanneste, E. *et al.* Chromosome instability is common in human cleavage-stage embryos. *Nat. Med.* **15**, 577–583 (2009). https://doi.org/10.1038/nm.1924

7 Zamani Esteki, M. *et al.* Concurrent whole-genome haplotyping and copy-number profiling of single cells. *Am. J. Hum. Genet.* **96**, 894–912 (2015). https://doi.org/10.1016/j.ajhg.2015.04.011

8 Charalambous, C., Webster, A. & Schuh, M. Aneuploidy in mammalian oocytes and the impact of maternal ageing. *Nat. Rev. Mol. Cell Biol.* **24**, 27–44 (2023). https://doi.org/10.1038/s41580-022-00517-3

9 Palmerola, K. L. *et al.* Replication stress impairs chromosome segregation and preimplantation development in human embryos. *Cell* **185**, 2988–3007.e2920 (2022). https://doi.org/10.1016/j.cell.2022.06.028

10 Zamani Esteki, M. *et al.* In vitro fertilization does not increase the incidence of de novo copy number alterations in fetal and placental lineages. *Nat. Med.* **25**, 1699–1705 (2019). https://doi.org/10.1038/s41591-019-0620-2

11 Yang, M. *et al.* Depletion of aneuploid cells in human embryos and gastruloids. *Nat. Cell Biol.* **23**, 314–321 (2021). https://doi.org/10.1038/s41556-021-00660-7

12 Orvieto, R. *et al.* Do human embryos have the ability of self-correction? *Reprod. Biol. Endocrinol.* **18**, 98 (2020). https://doi.org/10.1186/s12958-020-00650-8

13 Lebedev, I. Mosaic aneuploidy in early fetal losses. *Cytogenet. Genome Res.* **133**, 169–183 (2011). https://doi.org/10.1159/000324120

14 Grati, F. R. *et al.* Fetoplacental mosaicism: potential implications for false-positive and false-negative noninvasive prenatal screening results. *Genet. Med.* **16**, 620–624 (2014). https://doi.org/10.1038/gim.2014.3

15 Byrne, A. B. *et al.* Genomic autopsy to identify underlying causes of pregnancy loss and perinatal death. *Nat. Med.* **29**, 180–189 (2023). https://doi.org/10.1038/s41591-022-02142-1

16 Hardy, K., Hardy, P. J., Jacobs, P. A., Lewallen, K. & Hassold, T. J. Temporal changes in chromosome abnormalities in human spontaneous abortions: results of 40 years of analysis. *Am. J. Med. Genet. A* **170**, 2671–2680 (2016). https://doi.org/10.1002/ajmg.a.37795

17 Levy, B. *et al.* Genomic imbalance in products of conception: single-nucleotide polymorphism chromosomal microarray analysis. *Obstet Gynecol* **124**, 202-209 (2014). https://doi.org/10.1097/AOG.0000000000000325

18 Zhou, Q., Wu, S. Y., Amato, K., DiAdamo, A. & Li, P. Spectrum of Cytogenomic Abnormalities Revealed by Array Comparative Genomic Hybridization on Products of Conception Culture Failure and Normal Karyotype Samples. *J Genet Genomics* **43**, 121-131 (2016). https://doi.org/10.1016/j.jgg.2016.02.002

19 Chen, Y. *et al.* Characterization of chromosomal abnormalities in pregnancy losses reveals critical genes and loci for human early development. *Hum Mutat* **38**, 669-677 (2017). https://doi.org/10.1002/humu.23207

20 Li, F. X. *et al.* Detection of chromosomal abnormalities in spontaneous miscarriage by low-coverage next-generation sequencing. *Mol Med Rep* **22**, 1269-1276 (2020). https://doi.org/10.3892/mmr.2020.11208

21 Peng, J. P. & Yuan, H. M. [Application of chromosomal microarray analysis for a cohort of 2600 Chinese patients with miscarriage]. *Yi Chuan* **40**, 779-788 (2018). https://doi.org/10.16288/j.yczz.18-120

22 Wang, Y. *et al.* Identification of Chromosomal Abnormalities in Early Pregnancy Loss Using a High-Throughput Ligation-Dependent Probe Amplification-Based Assay. *J Mol Diagn* **23**, 38-45 (2021). https://doi.org/10.1016/j.jmoldx.2020.10.002

23 Finley, J. *et al.* The genomic basis of sporadic and recurrent pregnancy loss: a comprehensive in-depth analysis of 24,900 miscarriages. *Reprod Biomed Online* **45**, 125-134 (2022). https://doi.org/10.1016/j.

rbmo.2022.03.014
24 Sahoo, T. *et al.* Comprehensive genetic analysis of pregnancy loss by chromosomal microarrays: outcomes, benefits, and challenges. *Genet Med* **19**, 83-89 (2017). https://doi.org/10.1038/gim.2016.69
25 Peng, G. *et al.* Estimation on risk of spontaneous abortions by genomic disorders from a meta-analysis of microarray results on large case series of pregnancy losses. *Mol Genet Genomic Med*, e2181 (2023). https://doi.org/10.1002/mgg3.2181
26 Van Prooyen Schuurman, L. *et al.* Clinical impact of additional findings detected by genome-wide non-invasive prenatal testing: follow-up results of the TRIDENT-2 study. *Am. J. Hum. Genet.* **109**, 1140–1152 (2022). https://doi.org/10.1016/j.ajhg.2022.04.018
27 van der Meij, K. R. M. *et al.* TRIDENT-2: National Implementation of Genome-wide Non-invasive Prenatal Testing as a First-Tier Screening Test in the Netherlands. *Am J Hum Genet* **105**, 1091-1101 (2019). https://doi.org/10.1016/j.ajhg.2019.10.005
28 Van Den Bogaert, K. *et al.* Outcome of publicly funded nationwide first-tier noninvasive prenatal screening. *Genet Med* **23**, 1137-1142 (2021). https://doi.org/10.1038/s41436-021-01101-4
29 Tsuiko, O. *et al.* Haplotyping-based preimplantation genetic testing reveals parent-of-origin specific mechanisms of aneuploidy formation. *NPJ Genom Med* **6**, 81 (2021). https://doi.org/10.1038/s41525-021-00246-0
30 Capalbo, A. *et al.* Mosaic human preimplantation embryos and their developmental potential in a prospective, non-selection clinical trial. *Am J Hum Genet* **108**, 2238-2247 (2021). https://doi.org/10.1016/j.ajhg.2021.11.002
31 Ross, C. & Boroviak, T. E. Origin and function of the yolk sac in primate embryogenesis. *Nat. Commun.* **11**, 3760 (2020). https://doi.org/10.1038/s41467-020-17575-w
32 Boss, A. L., Chamley, L. W. & James, J. L. Placental formation in early pregnancy: how is the centre of the placenta made? *Hum. Reprod. Update* **24**, 750–760 (2018). https://doi.org/10.1093/humupd/dmy030
33 Kolte, A. M., Westergaard, D., Lidegaard, O., Brunak, S. & Nielsen, H. S. Chance of live birth: a nationwide, registry-based cohort study. *Hum Reprod* **36**, 1065-1073 (2021). https://doi.org/10.1093/humrep/deaa326
34 Bortoletto, P. *et al.* Miscarriage syndrome: Linking early pregnancy loss to obstetric and age-related disorders. *EBioMedicine* **81**, 104134 (2022). https://doi.org/10.1016/j.ebiom.2022.104134
35 Shimokawa, O. *et al.* Array comparative genomic hybridization analysis in first-trimester spontaneous abortions with 'normal' karyotypes. *Am J Med Genet A* **140**, 1931-1935 (2006). https://doi.org/10.1002/ajmg.a.31421
36 Zhang, Y. X. *et al.* Genetic analysis of first-trimester miscarriages with a combination of cytogenetic karyotyping, microsatellite genotyping and arrayCGH. *Clin Genet* **75**, 133-140 (2009). https://doi.org/10.1111/j.1399-0004.2008.01131.x
37 Warren, J. E., Turok, D. K., Maxwell, T. M., Brothman, A. R. & Silver, R. M. Array comparative genomic hybridization for genetic evaluation of fetal loss between 10 and 20 weeks of gestation. *Obstet Gynecol* **114**, 1093-1102 (2009). https://doi.org/10.1097/AOG.0b013e3181bc6ab0
38 Rajcan-Separovic, E. *et al.* Identification of copy number variants in miscarriages from couples with idiopathic recurrent pregnancy loss. *Hum Reprod* **25**, 2913-2922 (2010). https://doi.org/10.1093/humrep/deq202
39 Kooper, A. J., Faas, B. H., Feenstra, I., de Leeuw, N. & Smeets, D. F. Best diagnostic approach for the genetic evaluation of fetuses after intrauterine death in first, second or third trimester: QF-PCR, karyotyping and/or genome wide SNP array analysis. *Mol Cytogenet* **7**, 6 (2014). https://doi.org/10.1186/1755-8166-7-6
40 Bug, S. *et al.* Diagnostic utility of novel combined arrays for genome-wide simultaneous detection of aneuploidy and uniparental isodisomy in losses of pregnancy. *Mol Cytogenet* **7**, 43 (2014). https://doi.org/10.1186/1755-8166-7-43
41 Robberecht, C., Schuddinck, V., Fryns, J. P. & Vermeesch, J. R. Diagnosis of miscarriages by molecular karyotyping: benefits and pitfalls. *Genet. Med.* **11**, 646–654 (2009). https://doi.org/10.1097/GIM.0b013e3181abc92a
42 Takahara, H., Ohama, K. & Fujiwara, A. Cytogenetic study in early spontaneous abortion. *Hiroshima J Med Sci* **26**, 291-296 (1977).
43 Hassold, T. *et al.* A cytogenetic study of 1000 spontaneous abortions. *Ann Hum Genet* **44**, 151-178 (1980). https://doi.org/10.1111/j.1469-1809.1980.tb00955.x
44 Kajii, T. *et al.* Anatomic and chromosomal anomalies in 639 spontaneous abortuses. *Hum Genet* **55**, 87-98 (1980). https://doi.org/10.1007/BF00329132
45 Byrne, J., Warburton, D., Kline, J., Blanc, W. & Stein, Z. Morphology of early fetal deaths and their

chromosomal characteristics. *Teratology* **32**, 297-315 (1985). https://doi.org/10.1002/tera.1420320218
46 Lin, C. C., De Braekeleer, M. & Jamro, H. Cytogenetic studies in spontaneous abortion: the Calgary experience. *Can J Genet Cytol* **27**, 565-570 (1985). https://doi.org/10.1139/g85-083
47 Dejmek, J., Vojtassak, J. & Malova, J. Cytogenetic analysis of 1508 spontaneous abortions originating from south Slovakia. *Eur J Obstet Gynecol Reprod Biol* **46**, 129-136 (1992). https://doi.org/10.1016/0028-2243(92)90257-y
48 Be, C., Velasquez, P. & Youlton, R. [Spontaneous abortion: cytogenetic study of 609 cases]. *Rev Med Chil* **125**, 317-322 (1997).
49 Griffin, D. K., Millie, E. A., Redline, R. W., Hassold, T. J. & Zaragoza, M. V. Cytogenetic analysis of spontaneous abortions: comparison of techniques and assessment of the incidence of confined placental mosaicism. *Am J Med Genet* **72**, 297-301 (1997). https://doi.org/10.1002/(sici)1096-8628(19971031)72:3<297::aid-ajmg9>3.0.co;2-o
50 Brajenovic-Milic, B., Petrovic, O., Krasevic, M., Ristic, S. & Kapovic, M. Chromosomal anomalies in abnormal human pregnancies. *Fetal Diagn Ther* **13**, 187-191 (1998). https://doi.org/10.1159/000020836
51 Qumsiyeh, M. B., Kim, K. R., Ahmed, M. N. & Bradford, W. Cytogenetics and mechanisms of spontaneous abortions: increased apoptosis and decreased cell proliferation in chromosomally abnormal villi. *Cytogenet Cell Genet* **88**, 230-235 (2000). https://doi.org/10.1159/000015557
52 European Society of Human Reproduction and Embryology. *Recurrent Pregnancy Loss Guideline of European Society of Human Reproduction and Embryology*. (European Society of Human Reproduction and Embryology, 2022).
53 Popescu, F., Jaslow, C. R. & Kutteh, W. H. Recurrent pregnancy loss evaluation combined with 24-chromosome microarray of miscarriage tissue provides a probable or definite cause of pregnancy loss in over 90% of patients. *Hum. Reprod.* **33**, 579–587 (2018). https://doi.org/10.1093/humrep/dey021
54 Mastenbroek, S., De Wert, G. & Adashi, E. Y. The imperative of responsible innovation in reproductive medicine. *N. Engl. J. Med.* **385**, 2096–2100 (2021). https://doi.org/10.1056/NEJMsb2101718
55 Kalousek, D. K., Barrett, I. J. & Gartner, A. B. Spontaneous abortion and confined chromosomal mosaicism. *Hum Genet* **88**, 642-646 (1992). https://doi.org/10.1007/BF02265289
56 Lebedev, I. N., Ostroverkhova, N. V., Nikitina, T. V., Sukhanova, N. N. & Nazarenko, S. A. Features of chromosomal abnormalities in spontaneous abortion cell culture failures detected by interphase FISH analysis. *Eur J Hum Genet* **12**, 513-520 (2004). https://doi.org/10.1038/sj.ejhg.5201178
57 Kalousek, D. K. Pathogenesis of chromosomal mosaicism and its effect on early human development. *Am J Med Genet* **91**, 39-45 (2000). https://doi.org/10.1002/(sici)1096-8628(20000306)91:1<39::aid-ajmg7>3.0.co;2-l
58 D'Ippolito, S. *et al.* Investigating the "Fetal Side" in Recurrent Pregnancy Loss: Reliability of Cell-Free DNA Testing in Detecting Chromosomal Abnormalities of Miscarriage Tissue. *J Clin Med* **12** (2023). https://doi.org/10.3390/jcm12123898
59 Gordevicius, J. *et al.* Identification of fetal unmodified and 5-hydroxymethylated CG sites in maternal cell-free DNA for non-invasive prenatal testing. *Clin Epigenetics* **12**, 153 (2020). https://doi.org/10.1186/s13148-020-00938-x
60 Che, H. *et al.* Noninvasive prenatal diagnosis by genome-wide haplotyping of cell-free plasma DNA. *Genet Med* **22**, 962-973 (2020). https://doi.org/10.1038/s41436-019-0748-y
61 Greco, E., Minasi, M. G. & Fiorentino, F. Healthy babies after intrauterine transfer of mosaic aneuploid blastocysts. *N. Engl. J. Med.* **373**, 2089–2090 (2015). https://doi.org/10.1056/NEJMc1500421

Methods

Ethical approval

Embryonic tissues and parental blood samples were obtained from the "Biobank of populations of Northern Eurasia", Research Institute of Medical Genetics, Tomsk National Research Medical Center. All couples signed an appropriate informed consent for the transfer of their samples to the biobank for scientific research. This study was approved by the local Ethics Committee of the Research Institute of Medical Genetics, Tomsk National Research Medical Center of the Russian Academy of Sciences (Protocol #10, February 15, 2021). Permission was given for the retrospective analysis of the anonymized biological samples of the biobank.

Ultrasound diagnosis of early pregnancy loss

The ultrasonography features of early pregnancy loss considered in this study were no cardiac activity or empty gestational sac with a diameter ≥ 25 mm, crown-rump lengths (CRL) ≥ 7 mm for embryos with no cardiac activity, the absence of an embryo and its cardiac activity 14 days after the detection of a gestational sac without a yolk sac, and the absence of an embryo and its cardiac activity 11 days after the detection of a gestational sac with a yolk sac[62]. Anembryonic pregnancy (AP) was diagnosed in the absence of an embryo in the gestational sac for a period of more than 7 weeks; in addition, ultrasound criteria for AP were a gestational sac ≥13 mm without a yolk sac or ≥18 mm without an embryo. Missed abortion (MA) was diagnosed for embryos with CRL ≥ 7 mm without cardiac activity or no cardiac activity upon the initial scan and post 7 days scan for embryos with a crown-rump length < 7 mm. Spontaneous abortion (SA) was diagnosed as a spontaneously terminated pregnancy without ultrasound examination. The most frequent clinical forms of early pregnancy loss in our study were missed abortions followed by anembryonic pregnancies and spontaneous abortions (**Table 1**). After ultrasonography diagnosis, women were admitted to gynecological clinics for curettage or medication abortion. Extraembryonic tissues or fragmented gestational sacs were collected in sterile saline and immediately transferred to the Laboratory of Cytogenetics, Research Institute of Medical Genetics, Tomsk National Research Medical Center (Tomsk, Russia) for cytogenetic analysis and cryopreservation.

Sampling of products of conception

The POC (products of conception), usually represented by fragments of the gestational sac, were delivered to the laboratory in sterile saline, thoroughly washed and separated from decidual tissues and blood clots under an inverted microscope. Part of each tissue sample was used for cell culture, and the remaining tissue sample was stored at -70°C for DNA extraction. Traditionally, cytogenetic studies of POC have used one of two methods to determine the karyotype[63]. The first involves long-term culture of extraembryonic

tissues; most often, cells that are cultured are derived from the stroma of the chorionic villi[64]. The second approach exploits spontaneously and rapidly dividing cells of the cytotrophoblast to obtain direct chromosome preparations without culturing[65,66]. Usually, the results of both techniques are similar. However, discordant results can be obtained in some cases due to tissue-specific placental mosaicism[13]. Therefore, when large fragments of fetal sac were present, the internal mesodermal layer of extraembryonic membrane was used for cell culture; otherwise, both extraembryonic mesoderm and chorionic villi were used (see **CV and EM dissection of the POCs and DNA extraction**). The tissues were chopped with scissors into small fragments, and long-term cultures were set up in 25 cm^2 flasks with 5 mL of DMEM/F12 (1:1) medium (Gibco) supplemented with 20% fetal bovine serum (HyClone), 1% MEM NEAA solution (Gibco), and 1% Pen-Strep (Gibco). Tissues were incubated at 37°C with once-weekly medium renewal. Extraembryonic fibroblasts were cultivated until sufficient mitotic cells for cytogenetic analysis were obtained. Demecolcine (Sigma) was added 4 hours before chromosome harvesting, and the samples were processed using standard techniques of hypotonic treatment with 0.55% sodium citrate and cell fixation with a 1:3 mixture of acetic acid:methanol. In some cases, direct preparations of the chorionic villi were used[67]. Slide preparations and GTG banding were performed by standard protocols in accordance with guidelines[68]. Subsequently, frozen tissues were used for DNA extraction and preparation of cell suspensions for interphase fluorescence in situ hybridization (FISH).

CV and EM dissection of the POCs and DNA extraction

Genomic DNA was extracted from blood samples of the parents and from two distinct locations in the POC: chorionic villi (CV) and extraembryonic mesoderm (EM). The dissection of CV and EM by experienced pathologist is possible from the 4th weeks of gestation onwards, while from the 6th week of gestation the separation of EM and CV almost always succeeds (the mean gestational week in this study is 7.5 ± 1.7 SD). Specifically, after thawing, chorionic villi were carefully scraped off under an Axiovert 200 inverted microscope (Carl Zeiss, Germany) from extraembryonic membranes based on their morphology, and DNA was extracted separately from these tissues of each sample. The main limitation for accurate dissection of CV and EM, however, is the way that POC are acquired after pregnancy termination. This is because different methods after pregnancy termination are used in medical practice, including curettage, vacuum aspiration or using specific drugs. Genomic DNA was extracted using a standard phenol‑chloroform extraction method that allows for the isolation of up to 900 ng DNA from the tissues. To isolate DNA from tissues, a small fragment of tissue (200-300 mg) was taken. Then, samples of CV or EM were placed in Eppendorf tubes, and 467 µl of buffer (1 ml of 1 M Tris-HCl, pH 7.4; 2 ml of 0.5 M EDTA; 200 µl of 5 M NaCI; 96.8 ml of H_2O) was added to them, 25 µl 20% SDS, 7.5 µl proteinase K (10 mg/ml).

The samples were incubated for 16 hours at 37°C. Then, 550 µl of phenol was added, mixed gently and centrifuged for 3 minutes at 12,000 rpm and room temperature. Next, 300 µl of phenol and 300 µl of a mixture (chloroform-isoamyl alcohol in a ratio of 24:1) were added to the supernatant liquid, mixed and centrifuged under the same conditions. Afterward, 550 µl of the mixture (chloroform-isoamyl alcohol) was added to the supernatant, mixed and centrifuged. The supernatant liquid was taken again, 30 µl of 10 M sodium acetate and 660 µl of ethanol were added, and the tube was inverted until DNA was visualized. The solution was removed, 100 µl of 70% ethanol was added to the DNA, the DNA was washed and centrifuged at 12,000 rpm for 3 min, the alcohol was removed, and the precipitate was dried at 37°C. DNA was dissolved in 100 µl of TE (Tris/EDTA) buffer. Likewise, genomic DNA was extracted from the peripheral blood of parents using the standard phenol–chloroform method.

Conventional CGH and interphase FISH

Conventional comparative genomic hybridization (CGH) and interphase FISH with centromere-enumeration probes were performed as described previously[56,69] for POC samples where traditional cytogenetic analysis failed. For interphase FISH, two tissues were mechanically separated, and the yield of chorionic cytotrophoblast cells was increased by maceration of chorionic villi under an Axiovert 200 inverted microscope (Carl Zeiss, Germany) and treatment with 70% acetic acid for 3-5 min followed by three washes of the obtained cell suspension with PBS according to a modified protocol[65]. The EM cells were obtained by digesting the extraembryonic membrane (**Fig. 3a**) with 125 U/ml collagenase type I (Sigma, USA) for 30–60 min at 37°C[56]. Cell suspensions were fixed and stored in 3:1 methanol/acetic acid at -20°C. For confirmation studies, interphase FISH was performed separately for thawed CV and EM cells using centromere-specific DNA probes for chromosomes 2, 15, X and Y as well as subtelomeric DNA probes for chromosome 16 (16p, 16q). From 100 to 400 interphase nuclei were scored for each sample using an Axio Imager Z2 microscope (Carl Zeiss, Germany) with Metafer and ISIS software (MetaSystems, Germany).

Selection criteria for the participating patients

From 1987 to 2021, a total of 1,745 spontaneous PLs were analyzed using karyotyping. The karyotypes of fetal tissue were determined by conventional metaphase analysis (n=1,745 and on average 10 metaphases) or additional testing by comparative genomic hybridization (CGH) and fluorescence *in situ* hybridization (FISH). All samples with abnormal karyotypes were excluded from downstream haplarithmisis. Of the karyotypically normal cases, 111 families (114 POC) were randomly selected for SNP haplotyping, given that fetal (EM and CV) and parental blood samples were available and that no genetic predisposition for PL had been identified in the couple. Twenty families were excluded due to the DNA of one or more family members being of insufficient

quantity or quality causing low SNP call rates or due to one or both parents not being the biological parent, making haplotyping analysis impossible (**Supplementary Table 6**). Ninety-one families (94 POCs) were successfully analyzed by haplarithmisis. Of those, 42 were categorized as SPL (loss of one pregnancy) and 49 as RPL (loss of two or more consecutive pregnancies).

Whole-genome SNP genotyping

SNP genotyping was performed on genomic DNA isolates using Illumina Infinium™ Global-Screening Array-24 v2.0 and v3.0 BeadChip Kit (Illumina, no. GEO: GLP28939), which contains approximately 665.000 SNP markers with a mean probe spacing of ~4.4 kb and a median probe spacing of ~2.3 kb. Genotype calls, SNP B-allele frequency values and logR values of all samples were computed using Illumina GenomeStudio software. Illumina genotyping was performed at the Core Facility of Genomics, Institute of Genomics, University of Tartu, Estonia.

Genome haplarithmisis

Haplarithmisis is a conceptual workflow that enables simultaneous genome wide haplotyping and copy number typing using genotyping information from offspring and parents[7]. This originally allowed tracing the inheritance of linked disease variants. Previously, we demonstrated that using Illumina's Global-Screening Array-24, haplarithmisis can detect low-grade mosaicism (>10%), sub-chromosomal copy number variants (>100 kb), the parental and segregational origin of aberrations, and maternal cell contamination in placenta[10].

Specifically, in this study, the parental genotypes are phased by using CV genotype of the POC as a seed for phasing. Subsequently, the BAF values, i.e. continues genotype values (**Fig. 2a**) of the EM and CV are deduced to parental haplarithms (**Fig. 2b**). Specifically, (i) informative SNP loci are defined when one parent is heterozygous and the other parent homozygous, (ii) these SNP loci are further categorized into maternal and paternal categories. A paternal category is all the SNP loci that have heterozygous SNP from the father and homozygous SNP from the mother. Similarly, a maternal category is all the SNP loci that have heterozygous SNP from the mother and homozygous SNP from the father. Subsequently, (iii) a subcategorization is made based on (phased) parental SNP genotype combinations, into paternal subcategories P1, P2 (shown in **Fig. 2b**), and maternal subcategories M1, M2 (not shown in **Fig. 2b**), (iv) this results in specific P1 and P2 in paternal haplarithm, depending on homologue inheritance, e.g. if homologue 1 (H1) is inherited from the father (and either H1 or H2 from the mother) P1 BAFs are either 0 or 1 (corresponding to homozygous AA and BB genotypes respectively) and P2 BAFs are 0.5 (corresponding to heterozygous AB genotype). In contrast when H2 is inherited from the father (and either H1 or H2 from the mother) P1 BAFs are 0.5

(corresponding to heterozygous AB genotype) and P2 BAFs either 0 or 1 (corresponding to homozygous AA and BB genotypes, respectively). M1 and M2 maternal subcategories are computed in the similar fashion. (v) BAF values are mirrored around the 0.5 axis for SNPs where either parent has a heterozygous SNP call BA after phasing. Thus, if H1 was inherited from the father (and either H1 or H2 from the mother), all P1 BAF values will now have a value of 0 and P2 BAF values will continue to have 0.5. In contrast, if H2 was inherited from the father (and either H1 or H2 from the mother), all P1 BAF values will continue to have a value of 0.5 and all P2 BAF values will now have a value of 1. The same computation applies to P2, M1, M2 BAFs. Mirroring of these specific values for P1 and P2 allows detection of homologous recombination between the paternal H1 and H2. Idem for M1 and M2 maternal subcategories. (vi) Per subcategory, consecutive parental BAF values are segmented by piecewise constant fitting (PCF, segmentation parameter gamma set to 14 in this study). (vii) The paternal (P1, P2) and maternal (M1, M2) segments are visualized into two separate haplarithm plots. Segmented paternal P1 and P2 BAFs are depicted in blue and red, respectively, as are maternal M1 and M2 BAFs in blue and red, respectively. (viii) Paternal and maternal haplarithms reveal haplotypes (imbalances) and their parental and segregational origin.

As described previously in detail[7], haplarithmisis has two features for detection of degree of mosaicism (**Fig. 2c**) and segregational origin (**Fig. 2d**). First, the parity within each parental haplarithm where the length of P1 and P2 segments should approximately correspond to breakpoints of homologues recombination (similarly for M1 and M2 segments). Second, the reciprocity between parental profiles where the difference between P1 and P2 BAFs (d_{pat}) in combination with the difference between M1 and M2 BAFs (d_{mat}) are characteristic for specific abnormalities and their specific pattern correlates to segregational origin. For example, if d_{pat} has a value of 0.67 and d_{mat} a value of 0.33 and the LogR value for this chromosome is raised above 0 as compared to the other chromosomes, this is indicative of a trisomy where the maternal chromosome has abnormal number of 2 copies, i.e. $1_{paternal}$:$2_{maternal}$ allelic ratio. Subsequently, segregational origin can be determined by the position of the M1 and M2 values around the centromere. These values around the centromere change depending on whether the centromere contains 3 different homologues (H1 maternal, H2 maternal, H1 paternal, indicating meiosis I) or 2 different homologues (H1 maternal, H1 paternal, indicating meiosis II or mitosis). To distinguish between meiosis II and mitotic errors, the M1 and M2 values effected by a recombination event are used. This depends on whether there are 3 different homologous (H1 maternal, H2 maternal, H1 paternal, indicating meiosis II) or 2 different homologues (H1 maternal, H1 paternal, indicating mitosis) at the recombination event. To determine the degree of mosaicism, the genomic coordinates at the logR distortion from the expected value, i.e. logR=0, were used to extract the BAFs and segmented P1, P2 or M1, M2 BAFs of the location of interest. BAF values

were then compared to the reference dataset for calculation of level of mosaicism as described previously[70].

Haplarithmisis was applied to each quartet DNA sample to delineate the allelic architecture of the fetal tissues. CV tissue was used as a reference to phase parental genotypes. Parental haplarithms were used to infer the DNA copy number state, parent-of-origin, and level of mosaicism of fetal tissues. In total, 450 DNA samples were analyzed. Levels of mosaicism were calculated as previously described[70]. Parent-of-origin haplotyping allows for the detection of maternal DNA contribution in fetal tissues as previously described[10]. In one DNA sample, complete maternal contamination was detected by genome haplarithmisis and validated by quantitative fluorescent polymerase chain reaction (QF-PCR). This DNA sample was excluded from the study.

Classification of (segmental) chromosomal abnormalities

Haplarithms of analyzed tissues were classified based on several factors: types of aberrations detected, size of aberrations (genome-wide/chromosomal/segmental), placental or embryonic origin based on tissue biopsy, parental (paternal, maternal) and segregational (mitotic, meiosis I, meiosis II) origin, and level (%) of mosaicism. Levels of mosaicism were calculated based on BAF values as previously described[70]. Extrapolation of the total abnormalities was calculated using the formula below:

$$\left((\mathrm{AK} + \left(\frac{\mathrm{NK} \times \mathrm{AH}}{\mathrm{TH}}\right)\right) \times 100) \,/\, \mathrm{TK} \;= 67.8\%$$

where AK is the number of abnormal cases by conventional karyotyping, NK is the number of normal cases by conventional karyotyping, AH is the number of abnormal cases by genome haplarithmisis, TH is the total number of cases by genome haplarithmisis, and TK is the total number of cases by conventional karyotyping.

Other statistical analyses

Comparisons between conventional karyotyping (n = 1,745) and genome haplarithmisis (n = 91 families, 94 POCs) concerning parental and gestational age were performed by two-sided Welch's T test. For dichotomous outcomes, the chi-squared test was applied to analyze parental and segregational origin outcomes of SPL and RPL. Due to low sample size (nonparametric) and paired samples (EM and CV from a single fetus), the Wilcoxon signed-rank test was applied to assess the difference in mosaicism degree between EM and CV. To calculate the required sample size for the Wilcoxon signed-rank test for matched pairs to test the difference in mosaicism between EM and CV, we assumed a normal parent distribution, a mean percentage of 43% mosaicism in the CV group, a standard deviation (SD) of 30 in both groups, and a correlation between the groups of 0.5. A total sample size of 35 participants was required to test a 15%

difference between the EM and CV group, performing a two-sided test using an alpha of 0.05 and a power (1-β) of 0.80. The sample size calculation was performed using G*power 3.1.9.7. In addition, power calculation was performed for mosaicism dynamics across gestational age bins. A total sample size of 86 samples was required to test a 15% difference between week bins 4-7 (n = 7) and 8-13 (n = 7) for EM tissues containing aberrations of mitotic origin, performing a two-sided test using an alpha of 0.05 and a power of (1-β) of 0.80, indicating that our study is underpowered concerning mosaicism dynamics across gestational age, with a power of (1-β) of 0.18 due to low sample size (**Supplementary Table 2** and **5**). To assess the relation between mosaicism and gestational age week bins (4-7 and 8-13), 2-sided Mann Whitney U test was performed (**Supplementary Table 5**).

Methylation profiling: sample selection and processing

For the methylome analysis, 7 POC (13 DNA samples) were randomly selected based on the following inclusion criteria: (1) availability of sufficient extracted DNA, (2) female sex (to eliminate potential sex differences from the analysis), and (3) absence of chromosomal abnormalities according to Haplarithmisis. Extracted DNA from both CV and EM tissues was processed as follows: 300 ng of DNA from each sample was bisulfite-converted using the EZ DNA Methylation Kit (Zymo Research) according to the manufacturer's instructions and analyzed using the Illumina Infinium™ MethylationEPIC v1.0 BeadChip (Illumina, no. GEO: GLP21145), therefore allowing us to examine DNA methylation at more than 850,000 CpG sites across the human genome. The Illumina methylation array was performed at the Core Facility of Genomics, Institute of Genomics, University of Tartu, Estonia.

Methylation data processing and analysis

Data preprocessing was carried out using the RnBeads R package as previously described[71,72]. Briefly, the data were normalized with subset-quantile within array normalization (SWAN)[73], and poor-quality sites/samples were removed based on the Greedycut algorithm (detection p value threshold: 0.05). Further sites were removed: (i) sites on the sex chromosomes, (ii) sites near SNPs, (iii) sites with missing values in more than 10% of samples, and (iv) sites not in a CpG context. Additional sample quality control, namely, sex prediction and SNP probe analysis, was carried out using the sEst[74] package and RnBeads, respectively. Methylation beta values, representing the methylated signal intensity divided by the sum of the methylated and unmethylated signal intensity, were used for all analyses. Cellular deconvolution of the samples was performed using the reference-based Houseman algorithm[75] on data preprocessed with the recommended preprocessNoob[76] method and implemented using the minfi[77] package. For this, the reference site and cell type data for stromal, Hofbauer, endothelial, trophoblast, syncytiotrophoblast and nucleated red blood cells (NRBCs) provided by

Yuan et al.[78] were used. Welch's T tests were applied for statistical comparison of the cellular proportions predicted in EM and CV samples. All high-quality samples and CpG sites were used to conduct a principal component analysis in which beta values were centered but not scaled. The significance of the associations between the principle components (PCs) and sample features was tested as follows: (i) permutation tests (with 10,000 permutations) for continuous numerical variables (gestational age, stromal cells, Hofbauer cells, endothelial cells, NRBCs, syncytiotrophoblast cells) and (ii) two-sided Wilcoxon rank tests for binary categorical variables (tissue type).

RT–qPCR validation of PL2074 monosomy and UPD

The haplarithm of PL2074 shows 50% mosaic monosomy 7 in the EM and 30% UPD in the CV. To validate these findings, RT–qPCR was performed with a diploid control, a hemizygous deletion case, two times diluted DNA from the hemizygous deletion case, and EM and CV from PL2074. Primers for exon 16 of the *WDR60* gene, which is located at 7q36.3, were used. The reference gene was *HEXB*, which encodes the β subunit of hexosaminidase and is located at 5q13. Reference genomic DNA was obtained from the peripheral blood lymphocytes of a healthy donor. The results confirmed the diploid genome in CV and the mosaic monosomy in EM (**Extended Data Fig. 6a** and **b**). The combination of monosomy and UPD may be indicative of monosomy rescue where the single homolog is duplicated (**Extended Data Fig. 6c**).

RT–qPCR validation of PL1758 and segregational origin of aberrations

The haplarithm of PL1758 shows a genome-wide triploidy of maternal error origin, with mosaic tetrasomy of Chr 2 and Chr 7. The segregational origin appears to be mitotic (Chrs 1, 4, 12), or meiotic II (Chrs 3, 5, 6, 8, 9, 10, 11, 13, 14, 15, 16, 17, 18, 19, 20, 21, 22). To validate whether haplotyping with CV as a reference for EM would yield accurate parent-of-origin results, additional haplotyping with 2 different siblings and grandparents from the maternal side as references was performed. The results from PL1758 confirm the segregational origin of the aberrations, even when CV is used as a reference (**Extended Data Fig. 7**). RT–qPCR with reference DNA from spontaneous PL with 69,XXX karyotype and primers for exon 12 of the *MBD5* gene (2q23.1), exon 12 of the *ASXL2* gene (2p23.3), and exon 1 of the *CHCHD2* gene (7p11.2) were used to confirm tetrasomy for Chr 2 and Chr 7 in DNA from CV of PL1758. The following calculations and formulas were used to determine the fold change between the copy number of the test loci in the PL and reference DNA: average value for three C_T; logQT test primer = (Ct test DNA – CT reference DNA)/slope; (logQT test primer – log QT control primer); fold change = $10^{\text{logQT test primer – logQT control primer}}$. Fold change values were used to build a chart (**Extended Data Fig. 7b-d**). Usually, fold change for reference DNA is 1, namely, there are two copies of the product for reference DNA. Variation from 0.8 to 1.2 in test DNA corresponds to two copies of DNA. Variation from 0.3 or lower to 0.7

(average 0.5–1 copy against 2 copies) indicates deletion, and variation from 1.3 to 1.7 (average 1.5–3 copies against 2 copies) indicates duplication. If both reference and test DNA are triploid and there is a tetrasomy for some chromosome in the test DNA then the fold change should be approximately 1.33 (i.e., 4 copies against 3).

Short tandem repeat analysis

To confirm relationships and exclude maternal cell contamination, the analysis of short tandem repeats (STR) was carried out using the "COrDIS Expert 26" kit for DNA identification of 26 STR markers (Gordis, Russia). The analysis included identification of 26 loci: *AMEL*, *SRY, D3S1358, TH01, D12S391, D5S818, TPOX, Yindel, D2S441, D7S820, D13S317, FGA, D22S1045, D18S51, D16S539, D8S1179, CSF1PO, D6S1043, VWA, D21S11, SE33, D10S1248, D1S1656, D19S433, D2S1338,* and *DYS391*. PCR products were fractionated using an ABI PRISM 3130 HID capillary electrophoresis system (Applied Biosystems, USA). Fragment length was determined using internal length standards (Size Standard GeneScan 550) and GeneMapper 4.1 software.

Comparative genomic hybridization array for aneuploidy detection

Chorionic villi DNA samples from spontaneous abortions and control male and female DNA samples were labeled by a SureTag Labeling Kit (#G9502A, Agilent, USA) and purified by SureTag Purification Columns (#5190-7730, Agilent USA). Labeled DNA samples were hybridized using the GenetiSure Pre-Screen Complete Kit (8×60) (#G5963A, Agilent, USA) at 67°C for 24 hours according to the manufacturer's protocol. Microarray images were obtained using a SureScan Microarray Scanner (Agilent, USA) and analyzed by Agilent Feature Extraction (v. 12.2.0.7) and CytoGenomics software (v. 5.2).

Methods references

62. Doubilet, P. M. et al. Diagnostic criteria for nonviable pregnancy early in the first trimester. *N. Engl. J. Med.* 369, 1443–1451 (2013).
63. Griffin, D. K., Millie, E. A., Redline, R. W., Hassold, T. J. & Zaragoza, M. V. Cytogenetic analysis of spontaneous abortions: comparison of techniques and assessment of the incidence of confined placental mosaicism. *Am. J. Hum. Genet.* 72, 297–301 (1997).
64. Hassold, T. et al. A cytogenetic study of 1000 spontaneous abortions. *Ann. Hum. Genet.* 44, 151–178 (1980).
65. Simoni, G. et al. Efficient direct chromosome analyses and enzyme determinations from chorionic villi samples in the first trimester of pregnancy. *Hum. Genet.* 63, 349–357 (1983).
66. Eiben, B. et al. Cytogenetic analysis of 750 spontaneous abortions with the direct-preparation method of chorionic villi and its implications for studying genetic causes of pregnancy wastage. *Am. J. Hum. Genet.* 47, 656–663 (1990).
67. Kuznetzova, T. V., Trofimova, I. L., Liapunov, M. S., Evdokimenko, E. V. & Baranov, V. S. Selective staining of pericentromeric heterochromatin regions in chromosomes of spontaneously dividing cells with the use of the acridine orange fluorochrome. *Genetika* 48, 451–456 (2012).
68. Silva, M. et al. European guidelines for constitutional cytogenomic analysis. *Eur. J. Hum. Genet.* 27, 1–16 (2019).
69. Ostroverkhova, N. V. et al. Detection of aneuploidy in spontaneous abortions using the comparative hybridization method. *Genetika* 38, 1690–1698 (2002).
70. Conlin, L. K. et al. Mechanisms of mosaicism, chimerism and uniparental disomy identified by single nucleotide polymorphism array analysis. *Hum. Mol. Genet.* 19, 1263–1275 (2010).
71. Muller, F. et al. RnBeads 2.0: comprehensive analysis of DNA methylation data. *Genome Biol.* 20, 55 (2019).
72. Koeck, R. M. et al. Methylome-wide analysis of IVF neonates that underwent embryo culture in different media revealed no significant differences. *NPJ Genom. Med.* 7, 39 (2022).
73. Maksimovic, J., Gordon, L. & Oshlack, A. SWAN: subset-quantile within array normalization for illumina infinium HumanMethylation450 BeadChips. *Genome Biol.* 13, R44 (2012).
74. Jung, C. H. et al. sEst: accurate sex-estimation and abnormality detection in methylation microarray data. *Int. J. Mol. Sci.* 19, 3172 (2018).
75. Houseman, E. A. et al. DNA methylation arrays as surrogate measures of cell mixture distribution. *BMC Bioinformatics* 13, 86 (2012).
76. Triche, T. J., Weisenberger, D. J., Van Den Berg, D., Laird, P. W. & Siegmund, K. D. Low-level processing of illumina infinium DNA methylation beadarrays. *Nucleic Acids Res.* 41, e90 (2013).
77. Aryee, M. J. et al. Minfi: a flexible and comprehensive bioconductor package for the analysis of Infinium DNA methylation microarrays. *Bioinformatics* 30, 1363–1369 (2014).
78. Yuan, V. et al. Cell-specific characterization of the placental methylome. *BMC Genomics* 22, 6 (2021).

Supplementary Material

Extended Data Figure 1 | Mosaicism of >10% and CNVs >100 kb are detected by genome haplarithmisis

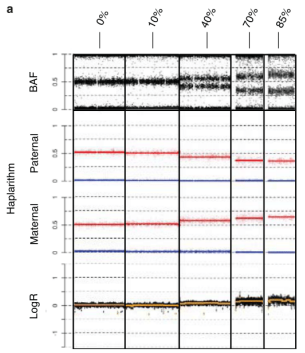

b

PL number	Group	Tissue	Aberration	Genome coordinates	Length	SNP probes
PL1618	SPL	EM	Duplication	Chr5:38166170-40845121	2678951	399
		CV	Duplication	Chr5:38265653-40851369	2585716	370
PL245	SPL	EM	Deletion	Chr5:58814-16708741	16649927	2918
		CV	Deletion	Chr5:58814-16708741	16649927	2918
		EM	Duplication	Chr7:58814-43206934	43148120	7187
		CV	Duplication	Chr7:58814-43216201	432010387	7190
PL2019	SPL	EM	Deletion	Chr1:204215542-248928328	44712786	7353
		CV	Deletion	Chr1:204219033- 248928328	44709295	7351
		EM	Duplication	Chr4:58814-18387778	18328964	3274
		CV	Duplication	Chr4:58814-18443081	18384267	3278

***a**) Different mosaicism degrees for chromosomal trisomy of paternal origin of several PLs. **b**) Detected CNVs for 3 PLs including genome coordinates, length, and number of SNP probes.*

Extended Data Figure 2 | Abnormality rate per tissue between SPL and RPL with parental and segregational origin

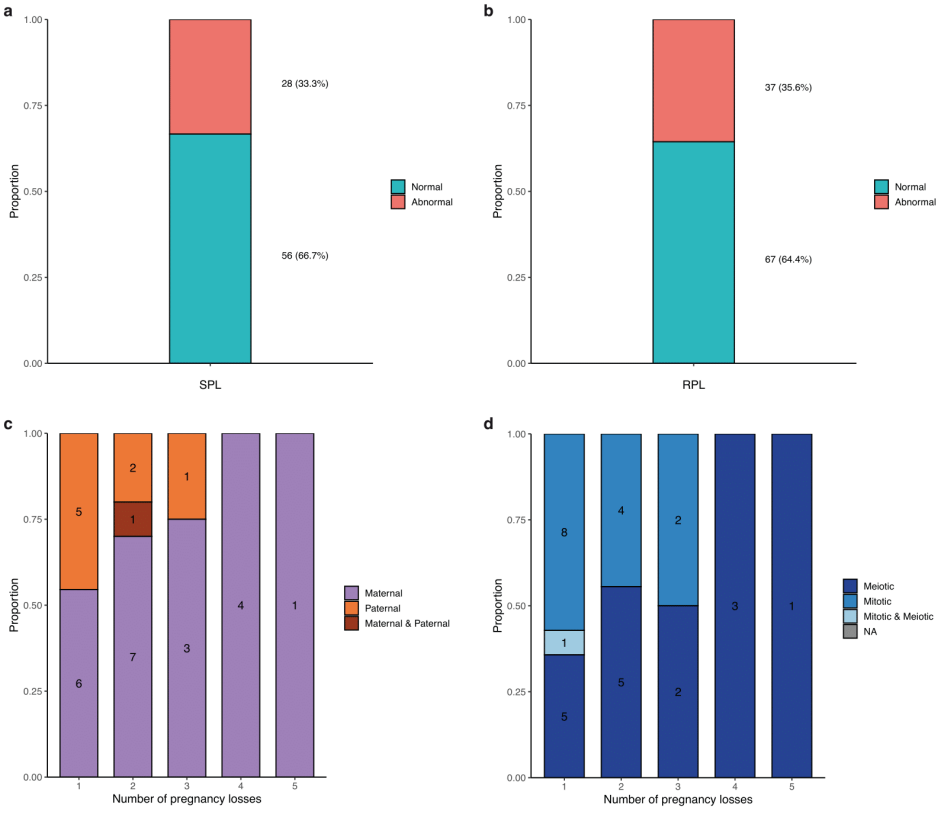

***a**) Abnormality rate SPL DNA samples (n = 84). **b**) Abnormality rate RPL DNA samples (n = 104). **c**) Parental origin and number of PLs per family (n = 30). **d**) Segregational origin and number of PLs per family (n = 32).*

Extended Data Figure 3 | Heatmap and PCA of EM and CV tissue samples

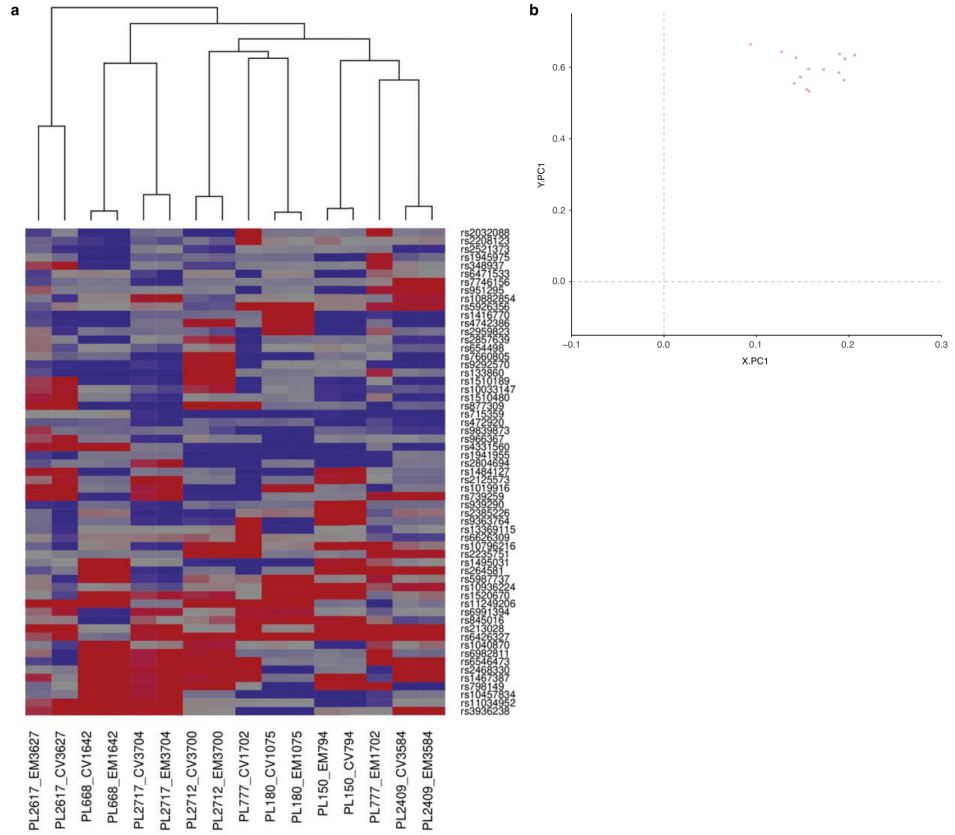

***a**) Heatmap of EPIC array SNP probes (n = 59) of all paired EM and CV tissue samples (n = 13). Hierarchical clustering of the samples was constructed using Euclidian distance and complete linkage and is shown as a dendrogram. **b**) Scatter plot showing the projection of all EM and CV tissue samples (n = 13) into the principal component space generated using reference data for sex prediction (not shown). All chosen samples were female according to the haplotyping analysis and the methylation sex prediction. Grey dashed lines separate the quadrants where male (XY) samples are expected to map to the lower left quadrant and female (XX) samples to the upper right quadrant.*

Extended Data Figure 4 | Predicted cell composition of EM and CV samples based on methylation data

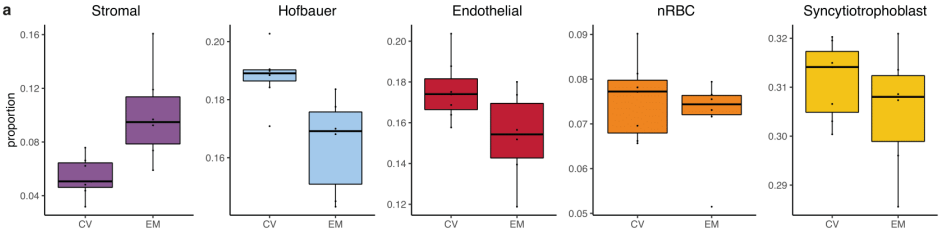

b

Cell type	Mean (CV)	Mean (EM)	Welch's t-test p-value
Stromal	0.054	*0.100*	***0.024***
Hofbauer	0.188	*0.165*	***0.018***
Endothelial	0.176	*0.154*	*0.070*
nRBC	0.076	0.071	0.451
Syncytiotrophoblast	0.311	0.305	0.350

***a**) Boxplots showing the predicted cellular composition of the high DNA quality EM (n = 6) and CV (n = 7) samples for each cell type: stromal cells, Hofbauer cells, Endothelial cells, nucleated red blood cells (nRBCs) and syncytiotrophoblast cells. The horizontal lines of the of the boxplot represent the 25th percentile, median and 75th percentile respectively while the whiskers extend to the farthest data point that is no more than 1.5 times the interquartile range (IQR) from the upper or lower quartile. The dots represent individual samples. **b**) Table with mean values of each cell type, P values were calculated with two-sided Welch's T-test.*

Extended Data Figure 5 | Detailed schematic representation of early embryonic development

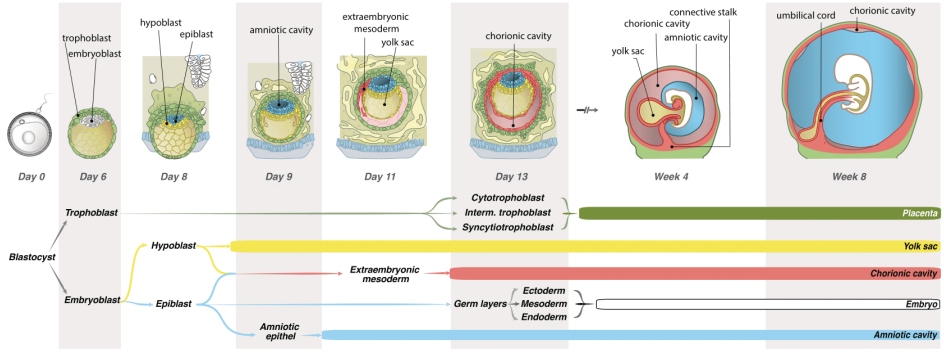

*Trophoblast and embryoblast lineages develop at day 6, hypoblast and epiblast develop from the embryoblast at day 8, hypoblast develops into the yolk sac, while epiblast develops into the different embryonic germ layers and the embryo and into the amnionic cavity. Extraembryonic mesoderm develops around day 11 from the hypo- and epiblast. The trophoblast cells become the placenta including cytotrophoblast, intermediate trophoblast, and syncytiotrophoblast cells, chorionic villi develop around day 13 from the trophoblast lineage (see also **Fig. 2a**).*

Extended Data Figure 6 | Validation of chromosome 7 copy number in PL2074

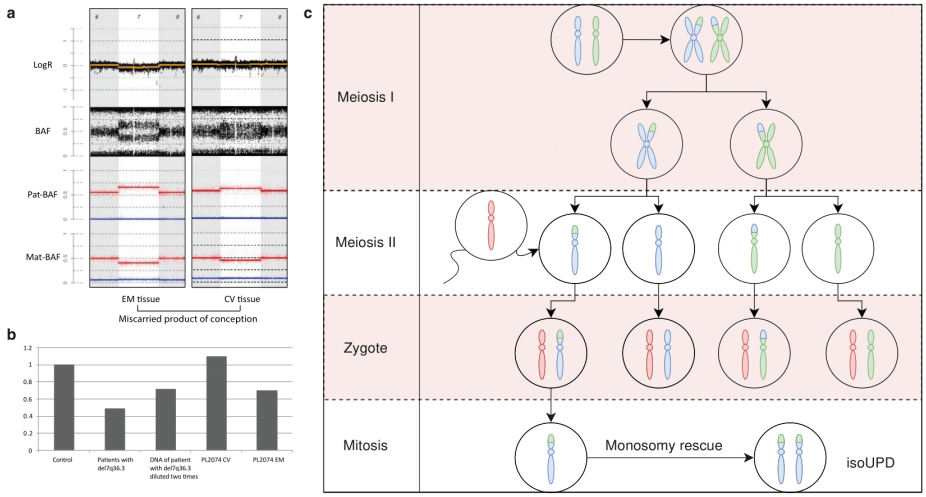

a) *Haplarithm of EM and CV tissue of PL2074, EM shows a 50% mosaic monosomy 7 while CV shows a 30% UPD (copy-neutral).* ***b)*** *RT-qPCR results with a diploid control, patient with a 7q36.3 deletion and two times diluted, PL2074 CV (UPD, copy neutral), and PL2074 (50% mosaic monosomy 7).* ***c)*** *Schematic representation of proposed chromosomal mechanism leading to uniparental disomy (UPD).*

Extended Data Figure 7 | Validation of segregational origin of aberrations in PL1758 CV DNA sample

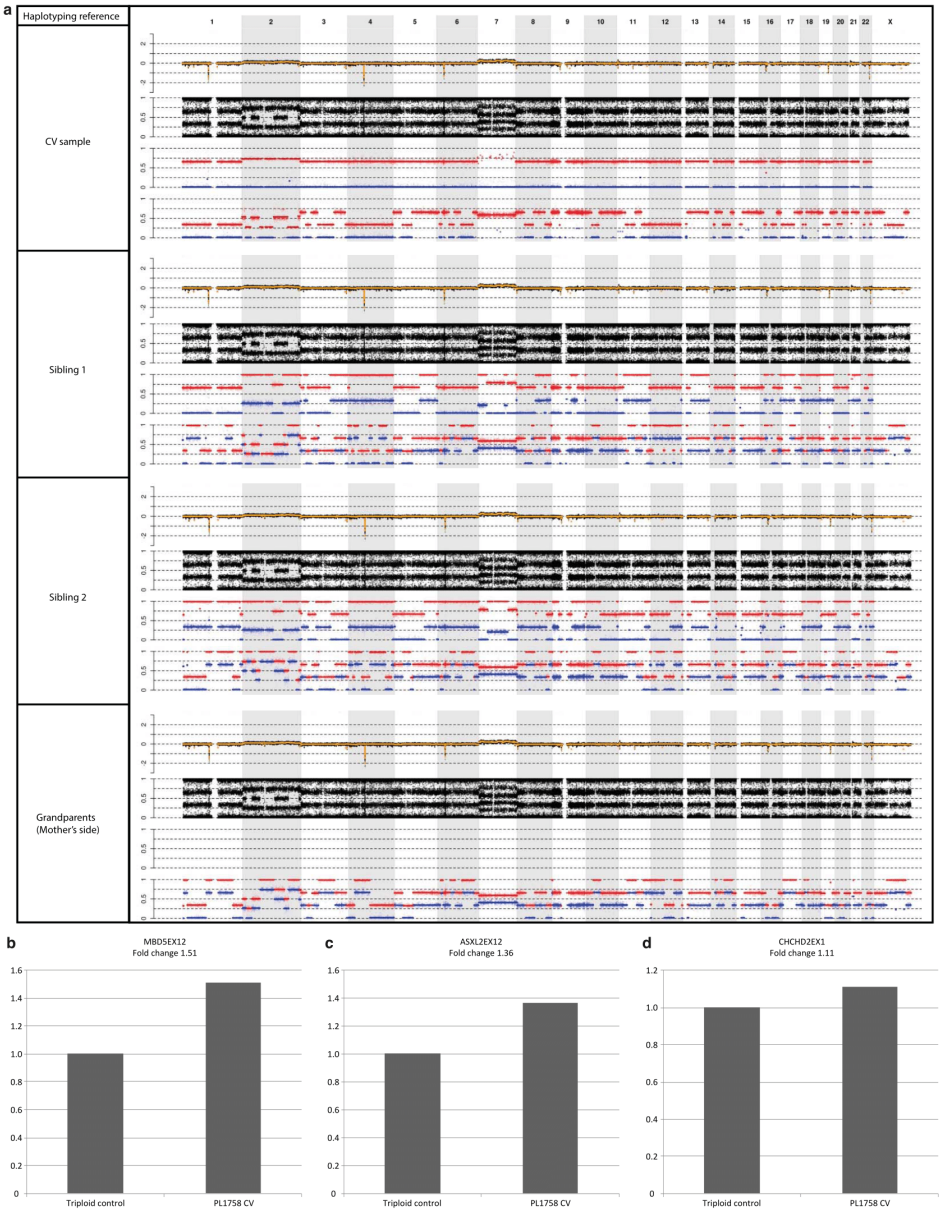

***a**) Haplarithms of fetal EM of PL1758, produced with different references for phasing, namely CV of the same fetus, 2 different siblings, and maternal grandparents. PL1758 shows complex abnormalities with genome-wide triploidy of maternal error origin, and mosaic tetrasomy of Chr 2 and Chr 7, segregational origin appear to be mitotic (Chrs 1, 4, 12), or meiotic II (Chrs 3, 5, 6, 8, 9, 10, 11, 13, 14, 15, 16, 17, 18, 19, 20, 21, 22). Haplarithmisis can accurately determine segregational origin with CV as reference compared to siblings or grandparents as a reference. Validation of PL1758 by RT-qPCR using DNA from spontaneous PL with 69,XXX karyotype and primers for **b**) exon 12 of the MBD5 gene (2q23.1), **c**) exon 12 of the ASXL2 gene (2p23.3), and **d**) exon 1 of the CHCHD2 gene (7p11.2) were used to confirm tetrasomy for Chr 2 and Chr 7 in DNA from CV of PL1758.*

Supplementary Table 1 | Logistic regression analysis of parental, gestational age and abnormality status

Maternal, paternal and gestational age on genomic status of tissue samples (normal, abnormal)

	Estimate	Std. Error	Z value	Pr(>|z|)	2.5 %	97.5 %
(Intercept)	-0.44421	0.40332	-1.101	0.271	0,28993311	1,41106131
Paternal age	0.01244	0.01346	0.924	0.356	0,98624736	1,0397907
Maternal age	0.00842	0.01477	0.570	0.569	0,9796628	1,03814665
Gestational age	0.01627	0.02902	0.561	0.575	0,96049016	1,07655417

Maternal and paternal age on genomic status of tissue samples (normal, abnormal)

	Estimate	Std. Error	Z value	Pr(>|z|)	2.5 %	97.5 %
(Intercept)	-0.59236	0.28226	-2.099	0.0358	0,3173412	0,96013088
Paternal age	0.01410	0.01191	1.184	0.2365	0,99087323	1,03829935
Maternal age	0.01381	0.01277	1.081	0.2795	0,98885307	1,03967305

Paternal age on genomic status of tissue samples (normal, abnormal)

	Estimate	Std. Error	Z value	Pr(>|z|)	2.5 %	97.5 %
(Intercept)	-0.478889	0.262114	-1.827	0.06770	0,36967328	1,03356382
Paternal age	0.023349	0.008339	2.800	**0.00511**	1,00711936	1,04061187

Maternal age on genomic status of tissue samples (normal, abnormal)

	Estimate	Std. Error	Z value	Pr(>|z|)	2.5 %	97.5 %
(Intercept)	-0.856824	0.229770	-3.729	**0.000192**	0,27010982	0,66507459
Maternal age	0.031344	0.007919	3.958	**7. 55e-05**	1,01600643	1,04805353

Supplementary Table 2 | Aberrations detected in POCs after PL by genome haplarithmisis

Sample	Gestational age by ultrasound (week)	Tissue	Aberration	Chr.	Size (Mb)	Mosaicism (%)
PL2650	4.5	CV	Trisomy	16	88.7	90
		EM	Trisomy		88.7	97.5
PL140	4.5	CV	Trisomy	16	88.7	87.5
		EM	Trisomy		88.7	85
PL2074	5.5	CV	UPD	7	160.6	30
		EM	Monosomy		160.6	50
PL2682	5.5	CV	Trisomy	19	61.7	35
		EM	Trisomy		61.7	90
PL1618	6.0	CV	Duplication	5	~2.7	20
		EM	Duplication		~2.7	17.5
PL2660	6.0	CV	Trisomy	14	101.2	85
		EM	Trisomy		101.2	87.5
PL2678	6.0	CV	Trisomy	16	88.7	97.5
		EM	Trisomy		88.7	97.5
PL1400	6.1	CV	Trisomy	16	88.7	85
		EM	Trisomy		88.7	87.5
PL1783	6.1	CV	Trisomy	2	242.7	97.5
		EM	Trisomy		242.7	85
PL2733	6.2	CV	Trisomy	16	88.7	90
		EM	Trisomy		88.7	90
PL2726	6.4	CV	Normal	GW	-	0
		EM	Trisomy	13	113.6	80
		CV	UPD	1	248.4	15
		EM	UPD		248.4	65
PL2727	6.5	CV	Trisomy	9	150.6	100
		EM	Trisomy		150.6	97.5
PL2653	6.7	CV	Trisomy	2	242.7	100
		EM	Trisomy		242.7	100
PL2087	7.0	CV	Trisomy	15	99.8	90
		EM	Trisomy		99.8	85
PL1744	7.0	CV	Trisomy	22	51.3	87.5
		EM	Trisomy		51.3	87.5
PL2621	7.4	CV	Trisomy	7	160.6	97.5
		EM	Trisomy		160.6	100
PL1595	7.5	CV	Trisomy	18	80.5	87.5
		EM	Trisomy		80.5	87.5
PL2016	7.5	CV	Polyploidy	GW	-	NA
		EM	Polyploidy		-	NA
PL1359	8.0	CV	Trisomy	6	172.1	87.5
EM	Trisomy	172.1	87.5			
PL2019	8.0	CV	Deletion	1	~44.7	30
EM	Deletion	~44.7	40			
CV	Duplication	4	~18.3	5		
EM	Duplication	~18.3	32.5			

Supplementary Table 2 | Continued.

Sample	Gestational age by ultrasound (week)	Tissue	Aberration	Chr.	Size (Mb)	Mosaicism (%)
PL401	8.0	CV	Monosomy	11	135.1	10
EM	Monosomy	135.1	10			
PL2728	8.1	CV	Trisomy	15	99.8	90
EM	Trisomy	99.8	90			
PL1701	8.4	CV	Trisomy	5	182.0	10
EM	Trisomy	182.0	37.5			
PL2702	8.5	CV	Trisomy	15	99.8	90
EM	Trisomy	99.8	87.5			
PL444	8.5	CV	Trisomy	14	101.2	45
EM	Trisomy	101.2	72.5			
PL1896	8.6	CV	Monosomy	X	154.3	100
EM	Monosomy	154.3	100			
PL2452	8.6	EM	Trisomy	21	45.1	100
CV	Trisomy	45.1	100			
PL2451	9.5	CV	Polyploidy	GW	-	100
EM	Polyploidy	-	95			
PL2701	10.3	CV	Trisomy	15	99.8	95
EM	Trisomy	99.8	95			
PL2137	13.0	CV	Trisomy	7	160.6	30
EM	Trisomy	160.6	40			
PL1758	NA	CV	Tetrasomy	2	242.7	NA
EM	Tetrasomy	242.7	NA			
CV	Tetrasomy	7	160.6	45		
EM	Tetrasomy	160.6	40			
CV	Polyploidy	GW	-	100		
EM	Polyploidy	-	90			
PL2223	NA	CV	Monosomy	X	154.3	35
EM	Normal	GW	-	0		
PL245	NA	CV	Deletion	5	~16.7	80
EM	Deletion	~16.7	80			
CV	Duplication	7	~43.2	35		
EM	Duplication	~43.2	45			

EM = extraembryonic mesoderm; CV = chorionic villi; GW = genome wide

Supplementary Table 3 | Chromosomal microarray studies of PLs with >1000 samples, without previous karyotyping

№	Study	Clinical specimen	Microarray technology	Total cases (#)	Cases with chromosomal abnormalities (#)	Prevalence (%)
1	Levy et al., 2014 (PMID: 25004334)	Miscarriages (<20 weeks of gestation)	Illumina CytoSNP-12	1861	1118	60.1
2	Zhou et al., 2016 (PMID: 27020032)	POC from PL	Agilent 60K aCGH	1235	507	41.1
3	Chen et al., 2017 (PMID: 28247551)	POC from PL	Version 7.6 Oligo, Baylor, WGS	2186	975	44.6
4	Peng and Yuan, 2018 (PMID: 30369481)	POC from PL	Affymetrix CytoScan 750K	2505	959	38.3
5	Li et al., 2020 (PMID: 32626971)	Miscarriages	Agilent aCGH, 60K, lc-NGS	1401	693	49.5
6	Wang et al., 2021 (PMID: 33069876)	Miscarriages (<13 weeks of gestation)	Affymetrix CytoScan 750K, QF-PCR, HLPA	1042	698	67.0
7	Finley et al., 2022 (PMID: 35523710)	POC (fresh/FFPE) from PL	Illumina CytoSNP-12	24900	13909	55.9
8	Sahoo et al., 2017 (PMID: 35523710)	RPL	CMA or SNP-array (3520 clones, BAC-clone-based array-CGH (CombiMatrix), 180334 oligonucleotide probes oligonucleotide array (Agilent) or CytoSNP-850 K array (Illumina))	7396	3975	53.7
Total				**42526**	**22834**	**53.7**

POC = product of conception, RPL = recurrent pregnancy loss, PL = pregnancy loss

Supplementary Table 4 | Chromosomal microarray studies of PLs, where karyotyping was performed previously by conventional karyotyping techniques.

№	Study	Clinical specimens	Methods	Total cases with normal karyotype	Additionally detected chromosomal abnormalities	%
1	Shimokawa et al., 2006 (PMID: 16906550)	PLs with normal karyotype	BAC Array – 1 Mb System, Spectral Genomics, Houston. TX. USA	20	2	10.0
2	Zhang et al., 2009 (PMID: 19215247)	First-trimester PLs	oligonucleotide-based array-CGH with a 244K chip (Agilent Technologies))	58	13	22.4
3	Warren et al., 2009 (PMID: 20168112)	Fetal loss at 10–20 weeks	Spectral 2600 whole genome BAC array (PerkinElmer) and Agilent 244 K oligonucleotide array to confirm it)	30	4	13.3
4	Rajcan-Separovic et al., 2010 (PMID: 20847186)	RPL	Agilent 105 K oligonucleotides array-CGH	26	11	42.3
5	Kooper et al., 2014 (PMID: 24428858)	Intrauterine fetal death	Affymetrix GeneChip 250 k (NspI) SNP-array) for 71 samples and CytoScan HD, 2.6 M for 97 samples	167	31	18.6
6	Bug et al., 2014 (PMID: 25013457)	POCs	CGH + SNP8×60K microarrays (BlueGnome Ltd., Cambridge, UK) (customized)	34	4	11.8
Total				**335**	**65**	**19.4**
	Present study	POCs	SNP-array + Genome haplarithmisis	94	33	35.1
Total				**429**	**98**	**22.8**

PLs = pregnancy losses; RPL = recurrent pregnancy loss; POCs = products of conception

Supplementary Table 5 | Degree of mosaicism and gestational age in week bins

Segregational origin	Tissue	Mosaicism % (mean ± sd)				*P* value*
		Weeks 4-7	n	Weeks 8-13	n	
Mitotic	CV	46.4 ± 38.7	7	38.6 ± 38.2	7	1.00
	EM	67.9 ± 26.4		48.9 ± 30.8		0.33
Meiotic	CV	88.2 ± 18.4	11	84.5 ± 22.8	5	1.00
	EM	92.3 ± 6.30		89.0 ± 10.4		0.77
Mitotic and meiotic	CV	71.9 ± 34.1	18	61.0 ± 39.4	13	0.81
	EM	82.8 ± 20.5		68.3 ± 31.5		0.43

**2-sided Mann Whitney U test*
EM = extraembryonic mesoderm; CV = chorionic villi.

Supplementary Table 6 | Excluded samples

ID	Group	Maternal age	Paternal age	Gestational age	Total PLs	Exclusion reason	Affected member
PL137	SPL	24	25	NA	1	Bad quality DNA	Father
PL142	SPL	34	NA	NA	1	Bad quality DNA	EM & CV
PL158	SPL	25	24	NA	1	Mix up	Mother & father
PL167	SPL	19	22	NA	1	Bad quality DNA	Mother
PL228	SPL	34	34	NA	1	Bad quality DNA	Mother & father & EM & CV
PL241	SPL	30	43	NA	1	Mix up	Father
PL246	SPL	30	30	NA	1	Bad quality DNA	EM & CV
PL250	RPL	29	29	NA	4	Bad quality DNA	Mother & father & EM & CV
PL278	SPL	33	37	NA	1	Bad quality DNA	Mother
PL379	SPL	22	22	10	1	Bad quality DNA	EM & CV
PL384	RPL	24	25	13	2	Bad quality DNA	EM
PL588	RPL	27	27	10	3	Bad quality DNA	Father
PL714	RPL	23	25	6	3	Bad quality DNA	Mother
PL822	SPL	31	26	7	1	Mix up	Mother & father
PL915	SPL	25	33	6	1	Bad quality DNA	EM
PL920	SPL	28	33	5,5	1	Bad quality DNA	Mother
PL1362	RPL	24	23	6	2	Bad quality DNA	EM & CV
PL2178	RPL	25	31	8	3	Bad quality DNA	Mother
PL2730	RPL	30	28	7,4	3	Bad quality DNA	CV
PL2734	RPL	43	37	8,2	7	Mix up	Mother

SPL = sporadic pregnancy loss; RPL = recurrent pregnancy loss; EM = extraembryonic mesoderm; CV = chorionic villi.

Chapter 7

Liquid biopsy: state of reproductive medicine and beyond

Gaby Schobers*, Rebekka M. Koeck*, Dominique Pellaers, Servi J. C. Stevens, Merryn V. E. Macville, Aimée D. C. Paulussen, Edith Coonen, Arthur van den Wijngaard, Christine de Die-Smulders, Guido de Wert, Han G. Brunner, Masoud Zamani Esteki
*** Joint first authors**

My contribution: reviewing references, editing the text, and generating figures.

Adapted from G. Schobers*, R. Koeck*, D. Pellaers, S.J.C. Stevens, M.V.E. Macville, A.D.C. Paulussen, E. Coonen, A. van den Wijngaard, C. de Die-Smulders, G. de Wert, H.G. Brunner, M. Zamani Esteki. Liquid biopsy: state of reproductive medicine and beyond. Hum Reprod. (2021) 36(11):2824-2839.
https://doi.org/10.1093/humrep/deab206

Abstract

Liquid biopsy is the process of sampling and analyzing body fluids, which enables non-invasive monitoring of complex biological systems in vivo. Liquid biopsy has myriad applications in health and disease as a wide variety of components, ranging from circulating cells to cell-free nucleic acid molecules, can be analyzed. Here, we review different components of liquid biopsy, survey state-of-the-art, non-invasive methods for detecting those components, demonstrate their clinical applications and discuss ethical considerations. Furthermore, we emphasize the importance of artificial intelligence in analyzing liquid biopsy data with the aim of developing ethically-responsible non-invasive technologies that can enhance individualized healthcare. While previous reviews have mainly focused on cancer, this review primarily highlights applications of liquid biopsy in reproductive medicine.

Introduction

Traditionally, studying pathogenesis commences with the sampling of a tissue or cytological specimen from the affected site of the human body. Such sampling usually requires invasive procedures, posing possible serious complications to the patient. Additionally, these procedures are inherently prone to incomplete representation of the affected tissue or cells[1] and require prior knowledge of the anatomical site of disease presentation. A promising alternative to invasive sampling are liquid biopsy techniques, which make use of circulating components in the body. Due to their non-invasive nature and representation of the tissue of origin, these emerging techniques offer a promising alternative to detect health- and disease-specific markers (**Fig. 1**).

Figure 1 | Dissecting the liquid biopsy

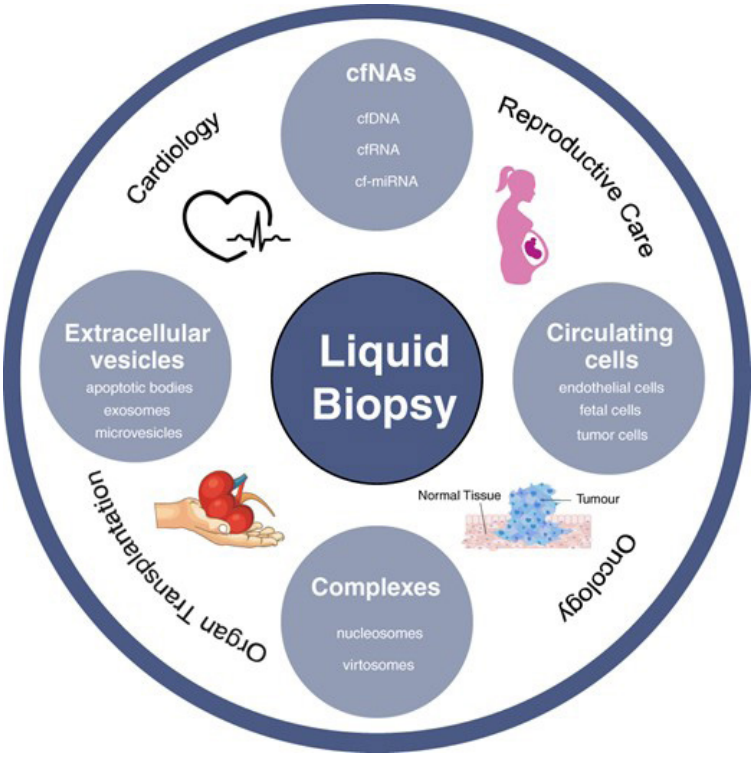

Analysis of circulating components within body fluids can be used for non-invasive disease detection and monitoring in several medical disciplines including cardiology, oncology, transplant and reproductive medicine. Different circulating components, such as cells, cell-free nucleic acids (cfNAs) and extracellular vesicles (EVs), are utilized for different tests. cfDNA, cell-free DNA; cfRNA, cell-free RNA; cf-miRNA, cell-free micro RNA.

Not all circulating components are equally abundant in body fluids, nor are they equivalent with respect to their size and biological properties. They range from rare, large circulating cells, e.g. circulating tumor cells (CTCs) and circulating trophoblastic cells, to more abundant, short cell-free nucleic acids (cfNAs), such as cell-free DNA (cfDNA), cell-free RNA (cfRNA) and circulating microRNA (miRNA). Furthermore, cfNAs do not only circulate in isolation, they can also be associated with protective protein complexes or encapsulated within extracellular vesicles (EVs). The accurate detection and characterization of low abundant circulating components in liquid biopsy still poses a challenge, especially as they are often dispersed among material originating from multiple tissues[2]. Therefore, sufficient sampling and sophisticated computational approaches are required to generate reliable results for clinical reports.

While previous reviews about liquid biopsy have primarily focused on cancer, here we highlight its importance and potential in reproductive medicine by: describing past liquid biopsy component discoveries; summarizing technological advances in the field; showcasing potential applications of those technologies in reproductive medicine; highlighting the importance of artificial intelligence (AI); and discussing the ethical principles that these novel possibilities may engender.

Detection of different liquid biopsy components

Circulating cells

CTCs, which were first described 151 years ago[3] (**Fig. 2**), can be characterized based on their size and cell-surface marker expression using size-based membrane filters and cell-sorting techniques, such as CellSearch[4], the size of epithelial tumor cells (ISET) method[5], CellSieve[4], ScreenCell[6] and other microfluidic systems (**Fig. 3**, **Table I**). In principle, microfluidic systems perform electric charge-, density-, or size-based separation[7]. For instance, size-sorting microfluidic chips are designed to capture CTCs, which are larger (~17–52 μm) than leukocytes (~7–15 μm) and erythrocytes (~6–8 μm)[8]. Similarly, circulating fetal trophoblastic cells, which were first discovered in the maternal circulation in 1893[9], can be isolated by the ISET method, differentiating cytotrophoblast-like cells (~14.3–30 μm) and syncytiotrophoblast-like cells (~44–60 μm)[10]. In addition, other circulating fetal cells (CFCs) such as fetal erythroblasts, lymphocytes and granulocytes have been found in maternal blood[11,12]. Efficient isolation of CFCs from maternal blood can be achieved by their enrichment using a panel of selective cell expression markers (**Fig. 3Fi**), such as CD105 and CD141[13] or GB17, GB21 and GB25[14], or by depleting their trophoblast-marker negative maternal counterparts (**Fig. 3Fii**). CFCs can be used for cell-based non-invasive prenatal testing (NIPT)[15]. Upon isolation, these cells provide a pure source of fetal genomic DNA.

However, the main challenge is that CFCs are exceedingly rare, approximately 1–2 cell(s) per ml of maternal blood[12], requiring a large volume of the maternal blood to perform this test. Even though cell-based NIPT enables enrichment of fetal cells and pure fetal copy number variation (CNV) detection[15-17], the extracted DNA from those fetal cells should be whole-genome amplified before genome sequencing; a process that introduces many artifacts, including allelic drop out and preferential amplification (see Sequencing section). Nevertheless, single-cell sequencing methods could alleviate this problem and are now validated for clinical use[15].

Circulating cell-free nucleic acids

cfNAs, including cfDNA and RNA, were first described in 1948[18]). They originate from cultivated cells, non-malignant somatic tissues, tumors and embryos or fetuses and are released when cells undergo necrosis or apoptosis. cfNAs can be characterized based on their length, physical size, surface molecules, electric charge and density (**Fig. 3**).

Table I | Methods used in liquid biopsy processing

Compartment		enumeration	genomics	transcriptomics	epigenomics	single cell
Cells	CTC	+	+	+	+	+
	CFC	+	+	+	+	+
cfNAs	cfDNA	-	+	-	+	-
	cffDNA	-	+	-	+	-
	cfRNA	-	+	+	-	-
	cffRNA	-	+	+	-	-
	miRNA	-	+	+	+	-
Extracellular vesicles and other complexes	exosome	-	+	+	-	-
	small vesicles	-	+	-	-	-
	ABs	-	-	-	-	-
	nucleosomes	-	-	-	+	-
Methods		CellSearch[4]	ddPCR[19]	qRT-PCR[20]	RRBS[21]	MALBAC[22,23]
		ISET[5]	BEAMing[19]	microarray[20]	targeted BS[21]	MDA[24]
		CellSieve[4]	Tam-Seq[25]	RNA-seq[26]	WGBS[21]	DOP-PCR[27]
		ScreenCell[6]	WGS[28]			DR-seq[29]
						G&T-seq[30]
						scNMT-seq[31] scCOOL-seq[32]

AB, apoptotic bodies; BEAMing, bead, emulsion, amplification and magnetics; CFC, circulating fetal cell; cfDNA, cell-free DNA; cffDNA, cell-free fetal DNA; cffRNA, cell-free fetal RNA; cfRNA, cell-free RNA; CTC, circulating tumor cell; ddPCR, droplet digital PCR; DOP-PCR, degenerate oligonucleotide-primed PCR; DR-seq, gDNA and mRNA sequencing; G&T-seq, genome and transcriptome sequencing; MALBAC, multiple annealing and looping-based amplification cycles; MDA, multiple displacement amplification; miRNA, microRNA; qRT-PCR, quantitative reverse transcription PCR; RRBS, reduced representation bisulfite sequencing; scCOOL, single cell chromatin overall omic-scale landscape sequencing; scNMT, single cell nucleosome, methylation and transcription sequencing; Tam-Seq, tagged-amplicon deep sequencing; WGBS, whole-genome bisulfite sequencing; WGS, whole genome sequencing.

Figure 2 | A timeline capturing the discovery of liquid biopsy components

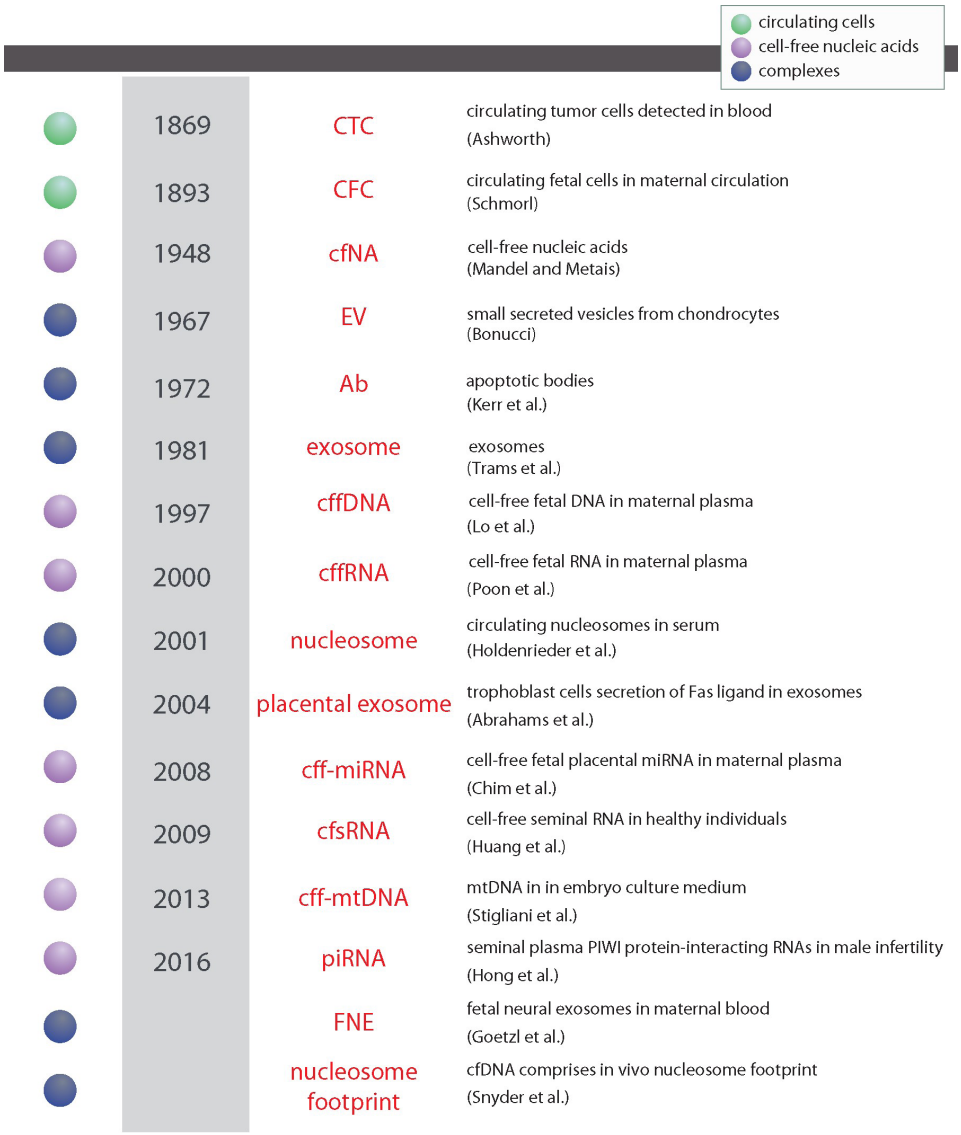

About a century after the discovery of circulating cells (green), cell-free nucleic acids (cfNAs) (purple) were observed. Their clinical application was not established until decades later but sparked many further discoveries relating to cfNAs, as well as extracellular vesicles (EVs) and other complexes (blue) that can carry them, in rapid succession. CTC, circulating tumor cells; CFC, circulating fetal cells; Ab, apoptotic bodies; cffDNA, cell-free fetal DNA; cffRNA, cell-free fetal RNA; cff-miRNA, cell-free fetal micro RNA; cfsRNA, cell-free seminal RNA; cff-mtDNA, cell-free fetal mitochondrial DNA; piRNA, PIWI-interacting RNA; FNE, fetal neural exosomes.

Figure 3 | Enrichment of liquid biopsy components

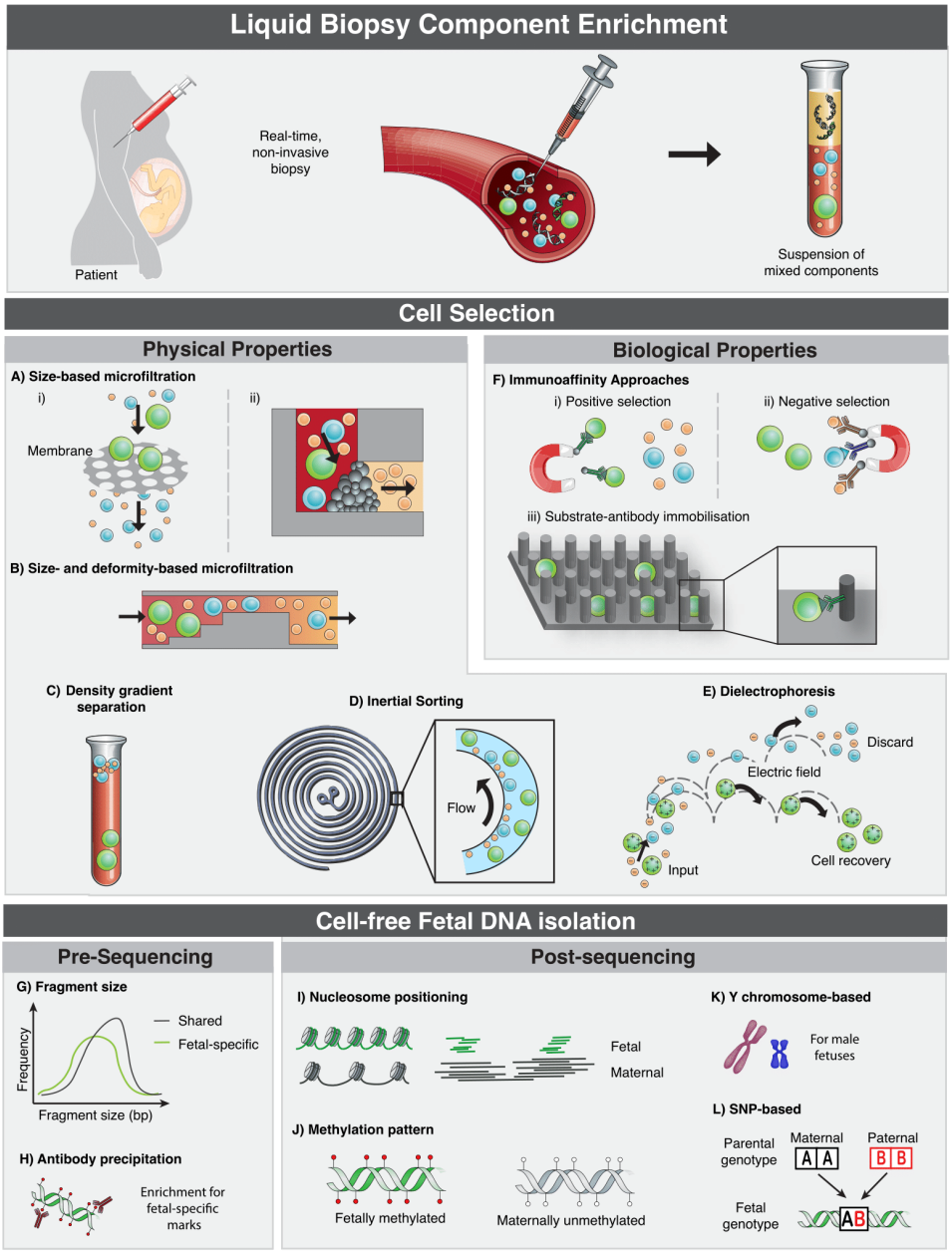

*To isolate a component of interest from the mixed liquid biopsy suspension, a variety of techniques are employed. Methods used to enrich for specific cell populations, such as epithelial, tumor, or fetal cells, are based on either, or both, physical or biological characteristics of the cells of interest. Enrichment of cells of interest or depletion of unwanted cells using physical properties is achieved by size-based microfiltration, using membranes (**Ai**) or packed beads (**Aii**), size- and deformity-based microfiltration (**B**), density gradient centrifugation (**C**), inertial sorting, based on cell size and hydrodynamics (**D**), or dielectrophoresis (**E**). Other common enrichment methods use cell-specific markers to separate cells based on their biological*

*properties (**Fi**). By negative selection, a sample can be depleted of unwanted cells using the same approach (**Fii**). These capture agents can, for instance, be bound by magnetic particles or located on microchips (**Fiii**). The characteristics of cffDNA are used to enable enrichment for cffDNA before sequencing or determination of the fetal fraction after the maternal blood sample has been sequenced. Pre-sequencing (NGS library preparation), cfDNA fragment sizes can be used for size selection to discriminate cffDNA from the maternal cfDNA (**G**). Fetal-specific marks can also be used for affinity-based enrichment (**H**). Post-sequencing, the proportion of cffDNA sized fragments, nucleosome positioning (**I**) and methylation patterns (**J**) are correlated with the fetal fraction. Additionally, using parental genotype information, fetal specific alleles can be detected and used for the estimation of the fetal fraction (**K** and **L**). NGS; next generation sequencing, SNP; single nucleotide polymorphism.*

Cell-free DNA

In 1997, the presence of cell-free fetal DNA (cffDNA), originating from the placental trophoblast[33], was reported in the maternal circulation[34]. cffDNA that are released by apoptotic trophoblast cells within the fetal compartment of the placenta can be used for nucleic acid-based NIPT[35], representing the fetus but not completely. This is due to confined placenta mosaicism (CPM), i.e. the presence of chromosomally abnormal cells in the placenta but not in the fetus. CPM can lead to false-positive cfDNA-based NIPT, which is now widely used. In contrast to pure fetal DNA from CFCs, cffDNA is fragmented and mixed with maternal DNA, which makes it even more challenging to identify true submicroscopic CNVs. A recent study showed that >70% of large CNVs (>10 kb) are confined to the placenta[36], this is well below the detection limit of cfDNA-based approaches and may be misinterpreted with maternal CNVs[37], including malignancies (see Application section). The size distribution of maternal serum cfDNA can be used for size- and origin-based diagnostic approaches (**Fig. 3G**), as maternal cfDNA fragments are, on average, longer (166 bp) than cffDNA fragments (143 bp)[38]. cfDNA is also detectable in blastocoel fluid (BF) of human embryos and in spent IVF culture medium, enabling minimally- and non-invasive genetic testing, respectively[39]. Furthermore, the presence of mitochondrial DNA (mtDNA) in the embryo's culture medium has been associated with fragmentation of the embryo caused by apoptosis or necrosis[40] (**see Application section**).

Cell-free RNA

Since the detection of cell-free fetal RNAs in the blood stream of pregnant women in 2000[41], most studies have focused on placental small non-coding RNAs, such as miRNAs[42] and especially those contained within protective exosomes[43]. This is because of their relatively greater stability and abundance as compared with mRNA. Placental miRNAs can serve as potential biomarkers for pregnancy complications such as preeclampsia and intra-uterine growth retardation, by influencing gene expression levels related to placental development[44]. However, characterizing miRNAs is challenging due to their short length (~22 nucleotides) and high level of homology, which complicates the use of primers. This obstacle has been overcome by the detection of several recognition

elements that can be employed in electrochemical- or optical-based miRNA detection[45]. To characterize male-factor infertility, cfRNA[46] and piwi-interacting RNA[47] can be isolated from semen.

Extracellular vesicles and other complexes

In 1967, small secreted vesicles were first reported[48]. EVs, such as apoptotic bodies (ABs) and exosomes, can be distinguished by their distinct characteristics. For example, exosomes[49], which arise upon fusion of internal multivesicular endosomes with the plasma membrane, are the smallest EVs (~30–200 nm diameter)[50]. Placental-derived exosomes[51] identified in maternal plasma could serve as biomarkers for the diagnosis and prognosis of preeclampsia as they are elevated in pre-symptomatic pregnancies, which subsequently may develop preeclampsia. Recently, specific fetal neural exosomes (FNEs) have been isolated from maternal plasma during pregnancy[52]. FNEs can potentially be used as a diagnostic tool to detect early signs of fetal neurological disease and are correlated with fetal exposure to alcohol[53].

ABs[54], containing degraded DNA, generated during apoptosis, are the largest EVs (4000–5000 nm diameter)[55]. Alternatively, cfNAs can circulate in association with protective protein complexes, such as nucleosomes[56] Importantly, from the exact spacing of nucleosomes, the tissue of origin of a cfNA fragment can be determined[57]. For instance, maternal cfDNA is predominantly cleaved with the linker region intact while cffDNA is cleaved at the border with or within the nucleosome[58] (**Fig. 3I**). Different EV types can be detected by centrifugation, (agglutination-)precipitation, or ultracentrifugation after size-exclusion. Exosomes can also be captured by immunoaffinity-beads and microfluidic chip methods and can be enriched using antibody-based label or label-free exosome arrays[59].

Sequencing of liquid biopsy components

Sequencing cell-free nucleic acids

The introduction of next-generation sequencing (NGS) has enabled the detection of genomic variants, such as point mutations, CNVs and structural aberrations[60] across the fetal genome. Furthermore, NGS offers a reliable platform for multi-faceted analysis of cfNAs, including exome[61], (epi)genome[21,28] and transcriptome[26] analyses (**Table I**).

One NGS approach, to detect mutant alleles that are present in at least 2% of circulating tumor DNA fragments, is tagged-amplicon deep sequencing[25], which is based on targeted resequencing of a panel of specific low-frequency mutations. Rarer mutant alleles can be detected with other targeted approaches, such as droplet digital PCR or

parallel beads, emulsion, amplification and magnetics PCR[19].

A challenge in NGS data analysis is tackling background error noise, which can occur when 'jackpot' mutations arise after errors in the first PCR cycle and by preferential amplification. This can be solved by computational approaches that correct for GC content or by assuming a diploid genome as a baseline, e.g. GC and median corrections, respectively[62]. Molecular barcoding, unique molecular identifiers (UMIs) and circle sequencing can also reduce these errors. For instance, UMIs facilitate the grouping of sequence reads according to DNA molecule, thereby distinguishing between true variants and artifacts. Similarly, circle sequencing reduces sequencing error rates by circularization of single-stranded DNA fragments, followed by inverse PCR or rolling circle amplification[63]. Thus, both robust computational pipelines and wet-lab protocols are key to produce accurate results.

NGS-based methods can also be applied to study the epigenome of cfNAs and to characterize cfRNAs. The epigenome, and specifically DNA methylation, can be used to ascertain the tissue-of-origin of cfDNA[64]. DNA methylation is most commonly examined using bisulfite treatment of DNA, which converts unmethylated cytosine residues to uracil. Subsequent methylome profiling can be performed in three forms[21]: (i) reduced representation bisulfite sequencing, which is untargeted but enriches for CpG-rich fragments; (ii) targeted capture of bisulfite-converted DNA, either by array or padlock capture; and (iii) whole-genome bisulphite sequencing (WGBS). WGBS, for instance, has been used on cfDNA to uncover placenta hypomethylation, which might aid in cffDNA enrichment[65]. The transcriptome can be profiled by technologies such as quantitative reverse transcription-PCR, microarray and RNA sequencing[20]. Improved NGS techniques have facilitated the isolation of nanogram quantities of cfRNA from serum and plasma. Plasma- and serum-specific profiles can then be discerned by probing different RNA forms, such as miRNAs, mRNA and tRNAs[26].

Sequencing circulating (single) cells

Advances in cell isolation, whole-genome amplification (WGA) and NGS have contributed to the emergence of single-cell genomics. DNA sequencing of scarce circulating cells requires WGA as they only possess a small amount of DNA (~7 picogram). Multiple annealing and looping-based amplification cycles, multiple displacement amplification and degenerate oligonucleotide-primed PCR are the most commonly used WGA methods[24]. Recently, techniques for simultaneous analysis of multiple omic layers in single cells, e.g. genomic DNA and mRNA in DR-seq[29], the genome and transcriptome in G&T-seq[30], single-cell Nucleosome, Methylation and Transcription in scNMT-seq[31] and (improved) single-cell Chromatin Overall Omic-scale Landscape Sequencing in (i) scCOOL-seq[66] that can detect chromatin state, nucleosome positioning, methylation,

CNV and ploidy, have emerged. Such bi- or multi-layer omic assays are of paramount importance to establish the interplay and connectivity (a.k.a. molecular circuitry) between different molecular layers by facilitating their direct side-by-side comparison.

Robust analysis of any single-cell omic-layer requires highly efficient capture and enrichment techniques to reduce technical artifacts. Specifically, WGA is prone to technical errors, such as non-linear amplification and insufficient coverage[67]. Analysis of the single-cell transcriptome further introduces the challenge of recovering the full-length cDNA, quantification of translational activity and sense and antisense transcript discrimination[68].

Applications of liquid biopsy in reproductive medicine

Liquid biopsy has potential and already realized applications in different fields. It is now evident that cfDNA is highly representative of genomic DNA as it shares many of its features[69,70]. Interestingly, cfDNA has a short half-life (4 min to 2.5 h), as it is rapidly filtered out of the circulation by the liver, spleen and kidney[71]. Caution is warranted using quantitative analysis methods as suboptimal extraction processes can affect the quantity of isolated cfDNA. Serum contains a relatively high concentration of cfDNA, but is less informative, as a greater proportion of serum cfDNA originates from leucocyte lysis. For this reason, DNA is preferentially extracted from plasma[72]. Importantly, cfNAs can be traced to their tissue of origin, which makes them informative biomarkers for assisted reproductive technology (ART)[57,73,74].

Assisted reproductive technology

In-vitro fertilization

Embryo selection procedures in IVF aim to identify good quality embryos with the highest implantation potential. Follicular fluid (FF), which influences maturation of follicles and oocyte growth *in vivo*, contains cfDNA of apoptotic granulosa cells and is sampled as part of the IVF oocyte retrieval process. Low levels of cfDNA in FF samples are significantly correlated with low embryo fragmentation rate and are indicative of high-quality embryos[75]. FF also contains cell-free mitochondrial DNA (cf-mtDNA), which can be quantified to predict embryo viability[76]. Cumulus cells (CCs), surrounding the oocyte during its development, have been shown to increase the quantities of cf-mtDNA in the IVF culture medium if mitochondrial dysfunction is present[77]. The effect of mitochondrial dysfunction is being studied with the hope of gaining further insights into embryo quality and being able to predict the developmental competence and implantation potential of the embryo. CC gene expression is also a valid biomarker of oocyte quality, as the expression of specific genes in CCs correlates with embryo potential

and pregnancy outcome[78]. In addition, a novel non-invasive metabolomics approach for embryo selection has been established, which identified 60 metabolomic biomarkers of euploidy and aneuploidy in spent IVF culture medium (SCM)[79], demonstrating the power of metabolomics in IVF as a non-invasive selection approach.

Male infertility

Presence of higher levels of cell-free seminal DNA (cfs-DNA) is associated with azoospermia[80], i.e. absence of sperm in the semen. In these cases, testicular sperm can be utilized for ICSI during IVF. cfs-DNA is detectable in both normal and azoospermic semen samples. Epigenetic analysis of the same cfs-DNA also identifies differences, such as hypermethylation, that are associated with hypospermatogenesis[81]. Additionally, cf-RNA can be isolated from semen[46], such that analysis of cfs-mRNA accurately distinguishes between non-obstructive and obstructive azoospermia[82].

Preimplantation genetic testing

Preimplantation genetic testing (PGT) is an ART that prevents transmission of genetic disorders to the offspring[83]. Currently, testing is primarily either conducted on a single blastomere taken from a cleavage-stage embryo, or on a few trophectoderm (TE) cells taken from a blastocyst, both of which are obtained through invasive biopsy methods that may be harmful to the embryo[84]. PGT is offered for monogenic disorders[73,74], structural rearrangements and aneuploidies (PGT-A)[74,84]. However, the clinical utility of PGT-A in its current form, i.e. only determining the number of chromosomes, is still under debate[85,86].

Minimally and non-invasive preimplantation genetic testing

Following *in vitro* culture, the transfer of embryos can be postponed by cryopreservation using vitrification[87], a process that requires collapse of the expanded blastocyst. If not occurring spontaneously, artificial shrinkage can be induced by BF microsuction[88]. A BF biopsy is a minimally invasive procedure as it does not involve removal of cells from the embryo and thus should be less harmful to the embryo as compared with standard cell-biopsy-based PGT methods. The non-invasive alternative would be embryonic-derived cfDNA in SCM[89-92]. cfDNA shed into the blastocyst cavity and SCM has been proposed to be derived from apoptotic cells[93,94]. However, current studies suggest that other mechanisms, besides apoptosis and necrosis, may be involved in DNA release from the inner cell mass and TE in BF and SCM. Recently, it was demonstrated that the amount of cffDNA in BF and SCM or the concordance rates of NGS results were similar for both moderate/low and good quality blastocysts[95]. Nevertheless, current media-based non-invasive PGT methods remain inferior to standard cell-biopsy-based invasive PGT methods, reaching a maximum of 80–90% concordances between non-invasive PGT and standard PGT[96,97], thus leaving ~10% of samples of which no informative results could be given. Recently, the combination of cffDNA from BF and SCM was shown to reach

an overall concordance rate of 88/90 (97.8%) for euploidy/aneuploidy status between minimally invasive PGT-A and TE biopsy samples[95]. This implies that the combination of BF and SCM shows promise for the clinical application of minimally invasive PGT. One of the remaining challenges is maternal cfDNA contamination in the culture medium that arises from the presence of, for instance, maternal CCs[98,99]. It has been suggested that maternal contamination can be minimized by omitting the cell lysis step recommended in the procedure of WGA[95].

Next-generation preimplantation genetic testing

Traditional PGT methods are based on targeted multiplex PCR or fluorescent *in situ* hybridization[100]. However, high throughput genomic technologies, such as single-nucleotide polymorphism (SNP)-array and NGS-based haplotyping, are revolutionizing PGT[101-105]. The addition of parental haplotyping can offer further valuable insights for PGT-A[103]. A haplotype represents consecutive alleles that are inherited together on a stretch of DNA, indicating which parts of homologous parental chromosomes are transmitted to the embryo. As such, the mechanistic origin of aneuploidies, i.e. meiotic or mitotic, can be determined. This is vital information, because aneuploidies originating during meiosis are likely to affect all the cells of an embryo, and hence the fetus, leading to the aneuploidy-associated phenotype or miscarriage. On the other hand, aneuploidies with a mitotic origin are only present in a fraction of embryonic cells and can therefore be outgrown by euploid cells, leading to successful pregnancies with genetically normal infants[36]. Such mitotic aneuploidies may arise because of chromosome instability, which is commonly seen in preimplantation human embryos[103,106].

Prenatal genetic testing

Traditionally, prenatal genetic testing involves invasive chorionic villus or amniotic fluid sampling. However, the non-negligible risk of pregnancy loss associated with these techniques urged the need for non-invasive alternatives. Although plasma levels of cffDNA increase during pregnancy, its isolation remains challenging due to its relative low abundance[107]. The presence of fetal DNA can be confirmed by Y-chromosome markers[108] (**Fig. 3K**). However, this is only the case in pregnancies with male fetuses and is unreliable due to false negatives caused by insufficient sampling. Alternatively, cffDNA can be recognized by the presence of paternally inherited short tandem repeats[109] (**Fig. 3L**). Furthermore, distinct DNA methylation patterns of placental and maternal genes can be used to establish the cellular origin of cfDNA fragments[64] (**Fig. 3J**). Stable mRNA transcripts from placenta-expressed genes have also been used as markers to detect pregnancy pathologies and for non-invasive fetal sex determination[110].

Despite challenges relating to isolation and characterization of cffDNA from the maternal circulation, NIPT has been introduced into clinical practice[86,111], not just for high-risk

pregnancies but also as part of a screening program for all pregnancies[112]. Currently, three forms of NIPT can be carried out, including NIPT for aneuploidy, structural rearrangements and monogenic disorders (NIPT-M)[113-116]. Initially, the median increase of fetal DNA concentration was used as a marker of trisomy 21[108]. Subsequently, chromosome-specific markers have been introduced, allowing the detection of chromosomal anomalies using either the allelic ratios from SNP genotyping[117], e.g. CNV detection in alpha-thalassemia[118], or the transcriptome unique to the fetus[119]. Advances in the technology even permit the detection of fetal single-gene defects from maternal plasma. In most instances, NIPT-M involves targeted sequencing of genes of interest[116]. For example, targeted enrichment by solution-based hybridization followed by sequencing and haplotyping of the β-globin gene region can detect mutations and diagnose β-thalassemia[113], and targeted massively parallel sequencing provides early prenatal diagnosis of fetuses at risk for congenital adrenal hyperplasia[120]. Further improvements have come from the introduction of single-molecule amplification and resequencing technology[114] and new algorithmic methods[115,121] in combination with isolating circulating cells.

NIPT samples are typically processed using shallow sequencing protocols, such as WISECONDOR[62,122,123], which can detect aneuploidies and large CNVs using inter-chromosomal read count comparison. While these methods have high analytical accuracy, detected chromosomal abnormalities still need to be confirmed by invasive testing[62,111,112]. This is a biological rather than a technical problem, as CPM is observed in 1–2% of pregnancies[124]. Besides CPM-related false positive trisomies of autosomes, NIPT has limited utilities for sex chromosome aneuploidies, for instance low-level mosaicism of chromosome X that is due to age-related loss of chromosome X in women[125] can lead to false positive Turner syndrome (45, X) diagnoses[126]. Thus, the use of CFCs can solve misdiagnoses that are caused by fetal (e.g. CPM) or maternal (e.g. loss of chromosome X) mosaicisms. For NIPT-M, haplotyping-based analysis methods, e.g. relative haplotype dosage analysis[38], have been implemented to trace allelic inheritance. However, current haplotyping methods require high-coverage NGS, and necessitate parental samples to define heterozygous parental SNPs whose relative representation can be sought in the fetal genome[127]. Haplarithmisis is a more sophisticated genome-wide haplotyping method that makes use of continuous B-allele fractions, instead of error-prone discrete SNP genotypes, to determine copy number states[103] alongside the parental and segregation origin of genomic alterations in cffDNA[128].

It is now evident that NIPT has the potential to detect maternal malignancies. cfDNA from malignant cells can be shed into the blood stream[129]. As such, it provided proof-of-principle of liquid biopsy for cancer screening in large populations[130]. Given the fact that the population screened in NIPT is relatively young, the incidence of

maternal malignancies is low. Large cohort studies estimate the frequency with which malignancies can be detected with the current NIPT protocol is in the range of about 1:10 000[112,131,132]. The malignancies in NIPT as reported in literature include (amongst others) leukemia or lymphoma, breast and cervical carcinoma[133]. However, it may be difficult to pinpoint where a putative tumor may be located based solely on genomic aberrations. Furthermore, a substantial number of suspicious NIPT findings are not confirmed by subsequent diagnostic tests or physical examinations. This may be due to occult malignancies or benign proliferations that are below the level of detection of current diagnostic techniques or due to placenta abnormalities. In addition, the aberrant NIPT signals may be derived from benign clonal proliferations, e.g. leiomyoma[131] for which it is questionable whether detection during pregnancy is beneficial[129].

As data are scarce, there are currently no evidence-based guidelines for counseling and clinical follow-up after a NIPT result putatively indicating a malignancy. A multidisciplinary collaboration that includes genetic counselors, oncologists, clinical laboratory geneticists and gynecologists is deemed crucial for accurate patient management[129,134,135]. Although studies thus far look promising, they did not investigate the assumed clinical benefits of earlier detection versus the burden that a NIPT finding may impose on the woman, and there has been no follow-up of women screened negative[129]. As with all screening programs, the question that remains is whether earlier detection of malignancy in a pregnant population ultimately leads to better clinical outcomes for both mother and child.

Future directions

Diagnostic, prognostic and therapeutic values

Liquid biopsy is an emerging field with numerous important applications (**Table II**). In particular, these techniques are invaluable for screening practices. For example, NIPT can be used in place of conventional invasive testing procedures that are associated with a risk of miscarriage[136]. Additionally, liquid biopsies can be used for risk-free screening of asymptomatic individuals, promising reduced morbidity and mortality associated with conditions where treatment success diminishes with disease progression. For instance, earlier diagnosis and more accurate monitoring of preeclampsia[137] and other pregnancy-related pathologies[138] may be possible using liquid biopsies, thereby facilitating the timely initiation of appropriate treatment and a reduction of complications. Liquid biopsy may also be implemented to predict progression in other diseases, as is the case in heart failure where the circulating long non-coding RNA LIPCAR can be used to predict survival[139]. Similarly, treatment response could be assessed using cfDNA monitoring as already illustrated in transplantation medicine[140].

Circulating components have even shown promise for therapeutic applications. For instance, EVs have been developed as highly biocompatible, stable, tissue-targeted drug delivery systems[141].

Table II | The clinical utilities of liquid biopsy in reproductive genetics

	COMPARTMENT	ORIGIN	BIOMARKER FUNCTION	TECHNIQUE	TARGET	REF
NIPT-A	cfDNA	blood	prediction of fetal trisomy 21	qPCR	quantification	101
NIPT-A	cfDNA	blood	prenatal detection of pathogenic CNVs in alpha thalassemia	qPCR	quantification	111
NIPT-A	cfDNA	blood	detection of fetal chromosomal aneuploidy	NGS	Methylation	112
NIPT-A	cfDNA	blood	detection of fetal chromosomal aneuploidy	NGS	expression profile	110
NIPT-M	cfDNA	blood	prenatal detection of pathogenic mutations	qPCR	quantification	107
NIPT-M	cfDNA	blood	prenatal diagnosis of monogenic diseases	qPCR	quantification	108
NIPT-M	cfDNA	blood	prenatal diagnosis of monogenic diseases	NGS	quantification	109
NIPT-M	cfDNA	blood	prenatal diagnosis of congenital adrenal hyperplasia	NGS	quantification	113
PGT-M	cfDNA	medium	preimplantation diagnosis of a-thalassemia	qPCR	quantification	71
PGT-A/M	cfDNA	medium	preimplantation diagnosis of aneuploidy and beta thalassemia	NGS	Methylation	70
embryo quality	cfDNA	medium	prediction of embryo quality	NGS	quantification	72
embryo quality	cfRNA	ff	prediction of implantation rate	NGS	quantification	73
male infertility	cfRNA	semen	identification the presence of germ cells or complete obstruction in azoospermia	array	SNP detect / quantify	79
male infertility	cfRNA	semen	assessing diseases of semen secreting organs	array	SNP detect / quantify	77
male infertility	cfRNA	semen	prediction of successful testicular sperm retrieval in non-obstructive azoospermia patients	NGS	Methylation	78
fetal neurodevelopment	exosomes	medium	non-invasive prenatal diagnosis of fetal central nervous system insult	ELISA	amplicon detect / quantify	39

Key	Compartment	Origin	Technique	Target
	cfDNA	blood	qPCR	quantification
	cfRNA	semen	NGS	Methylation
	cf-mtDNA	ff	ddPCR	expression profile
	cells	medium	array	SNP detect / quantify
	exosomes		PCR	amplicon detect / quantify
			ELISA	

cf-mtDNA, cell-free mitochondrial DNA; ddPCR, droplet digital PCR; ELISA, enzyme-linked immuno sorbent assay; ff, follicular fluid; NGS, next-generation sequencing; NIPT-A, non-invasive prenatal testing for aneuploidies; NIPT-M, non-invasive testing for monogenic disorders; PCR, polymerase chain reaction; PGT, prenatal genetic testing; qPCR, quantitative polymerase chain reaction; SNP, single-nucleotide polymorphism.

Artificial intelligence

Emerging (ultra-)sensitive technologies and their introduction in healthcare systems

generate extensive datasets, necessitating standardization of the produced data and development of secure data sharing platforms. Subsequently, sophisticated AI-based analysis methods can be used on different data sources that are being collected along the continuum of early development, from newly emerging preconception carrier testing[142] to preimplantation and prenatal testing. AI can then avoid potential human errors and shorten long waiting lists, e.g. for PGT. The use of machine learning (ML), which is a branch of AI, in medicine offers an exciting prospect for disease diagnosis, monitoring and therapy. ML algorithms range from simple methods, e.g. regression and clustering, to more sophisticated approaches, e.g. artificial neural networks and deep learning. ML algorithms can be categorized into supervised or unsupervised learning. Classification is a supervised learning approach which requires labeled data, e.g. classification of PGT or NIPT results that are well annotated by specialists previously. While unsupervised learning primarily looks for patterns, e.g. clustering. The real-life example that makes use of ML in medicine more prominent is semi-supervised learning, where the clinical data are partly labeled. Semi-supervised ML systems would save enormous time and energy. ML systems that are based on multiple data sources (e.g. genomic and radiomic data) can be trained *via* deep learning. Deep learning is an approach that builds upon a cascade of several (i.e. deep) complex information layers to obtain prediction or classification models. Each layer uses the output of the preceding layer as its input, before applying different transformations to the input[143]. These cascades of data processing are trained with labeled test data to optimize (hyper-) parameters of the model, eventually leading to the most accurate model possible[143]. Well-trained deep-learning algorithms could, for instance, be used to identify very low abundance genetically aberrant cells and link them to their tissue of origin using WGS of cfDNA[144]. The process of embryo ranking during IVF treatment is another potential application that could benefit from these techniques. However, more data collection, technology development and validation are required before robust, diagnostically valuable techniques can be brought from bench to bedside[145]. Nonetheless, it is clear that AI has the potential to enhance the decision-making of healthcare professionals by allowing them to harness the power of vast data resources generated and stored by all healthcare systems.

Ethical exploration

Ethical aspects of applying liquid biopsy in the context of (reproductive) screening, where screening is defined as the unsolicited offer of testing to asymptomatic individuals, need to be scrutinized. Here, we discuss two criteria for sound screening, namely proportionality and respect for autonomy[146]. The principle of proportionality requires that the possible benefits of screening clearly outweigh any potential risks. The autonomy requirement underlines the importance of informed and voluntary consent. The proportionality and autonomy requirements raise complex issues in the context of different types of reproductive screening, including the rapidly evolving NIPT and PGT procedures.

Given that the aim of NIPT is to facilitate well-informed, personal decision making of prospective parents about possible serious reproductive risks, the question is how to achieve this. This challenge is compounded by the prospect of whole fetal genome sequencing and analysis that could easily result in information overload. Furthermore, such broad-scope prenatal screening could violate future children's right to informational self-determination. Moreover, the morality of future NIPT-linked (research on) 'fetal personalized medicine' requires ongoing scrutiny[147].

In principle, non-invasive PGT to predict embryo viability would be welcome. However, as stressed in comments critical toward PGT[85], an important prerequisite for introducing a new test is a strong evidence base demonstrating its effectiveness and reliability. Difficult normative issues could arise if non-invasive PGT also endeavors to generate information about genetic risk factors for disorders, alone or in combination with invasive PGT methods. How then, to balance, higher/lower scores for viability and risk factors for (often complex) genetic characteristics with a lower positive predictive value? Furthermore, this may cause tension between the decision-making authority of prospective parents on one hand and of reproductive doctors on the other hand when it comes to the selection of 'the best embryo' for transfer[148].

Finally, even though ML may help to integrate the huge amount of data generated by multiparametric assays, the implicit morality of the algorithms involved require the development of ethics frameworks bridging AI and assisted reproduction. Clearly, the prospects of and progress in liquid biopsy-based reproductive screening require multidisciplinary research and reflection for responsible innovation.

Conclusions

Here, we described different circulating components, state-of-the-art methods to detect them, and their implications in health and disease. Specifically, we reviewed how liquid biopsy can be used to monitor patients as a whole, because the sampled components themselves are informative for their type and origin. Advanced computational methods and single-cell multi-omics will ultimately overcome some of the challenges that are associated with liquid biopsy, including the low-frequency and fragmentation of circulating components, background error rates and haplotyping phasing following NGS. AI-based interpretation of liquid biopsy profiles paves the way for individualized medicine and a much greater repertoire of non-invasive tests, which will greatly benefit patient care.

Data availability

No new data were generated in this research.

Authors' roles

G.S. and R.K.: First draft, literature search, writing, revision and display items. D.P.: Literature review, writing, revision and display items. S.J.C.S., G.W. and H.G.B.: Literature review, writing and revision. M.V.E.M, A.D.C.P., E.C., A.W., C.D.-S.: Literature review and revision. M.Z.E.: Supervision, first draft, literature search, writing and revision of all components of this manuscript.

Funding

EVA (Erfelijkheid Voortplanting & Aanleg) specialty program (grant no. KP111513) of Maastricht University Medical Centre (MUMC+) and the Horizon 2020 innovation (ERIN; grant no. EU952516) of the European Commission to M.Z.E.

Conflict of interest

M.Z.E. is co-inventor on patent applications: ZL910050-PCT/EP2011/060211-WO/2011/157846 Methods for haplotyping single cells' and ZL913096-PCT/EP2014/068315-WO/2015/028576 "Haplotyping and copy-number typing using polymorphic variant allelic frequencies".

References

1 Gerlinger, M. *et al.* Intratumor heterogeneity and branched evolution revealed by multiregion sequencing. *N Engl J Med* **366**, 883-892 (2012). https://doi.org/10.1056/NEJMoa1113205

2 Sun, K. *et al.* Plasma DNA tissue mapping by genome-wide methylation sequencing for noninvasive prenatal, cancer, and transplantation assessments. *Proc Natl Acad Sci U S A* **112**, E5503-5512 (2015). https://doi.org/10.1073/pnas.1508736112

3 Ashworth, T. R. A case of cancer in which cells similar to those in the tumours were seen in the blood after death. *Aust Med J* **14**, 146-147 (1869).

4 Adams, D. L. *et al.* Cytometric characterization of circulating tumor cells captured by microfiltration and their correlation to the CellSearch(®) CTC test. *Cytometry A* **87**, 137-144 (2015). https://doi.org/10.1002/cyto.a.22613

5 Mazzini, C. *et al.* Circulating tumor cells detection and counting in uveal melanomas by a filtration-based method. *Cancers (Basel)* **6**, 323-332 (2014). https://doi.org/10.3390/cancers6010323

6 Freidin, M. B. *et al.* An assessment of diagnostic performance of a filter-based antibody-independent peripheral blood circulating tumour cell capture paired with cytomorphologic criteria for the diagnosis of cancer. *Lung Cancer* **85**, 182-185 (2014). https://doi.org/10.1016/j.lungcan.2014.05.017

7 Warkiani, M. E. *et al.* Ultra-fast, label-free isolation of circulating tumor cells from blood using spiral microfluidics. *Nat Protoc* **11**, 134-148 (2016). https://doi.org/10.1038/nprot.2016.003

8 Neoh, K. H. *et al.* Rethinking liquid biopsy: Microfluidic assays for mobile tumor cells in human body fluids. *Biomaterials* **150**, 112-124 (2018). https://doi.org/10.1016/j.biomaterials.2017.10.006

9 Schmorl & G. Pathologisch-Anatomische Untersuchungen Über Puerperal-Eklampsie. *Vogel* (1893).

10 Vona, G. *et al.* Enrichment, immunomorphological, and genetic characterization of fetal cells circulating in maternal blood. *Am J Pathol* **160**, 51-58 (2002). https://doi.org/10.1016/S0002-9440(10)64348-9

11 ZIPURSKY, A., HULL, A., WHITE, F. D. & ISRAELS, L. G. Foetal erythrocytes in the maternal circulation. *Lancet* **1**, 451-452 (1959). https://doi.org/10.1016/s0140-6736(59)92264-0

12 Krabchi, K. *et al.* Quantification of all fetal nucleated cells in maternal blood between the 18th and 22nd weeks of pregnancy using molecular cytogenetic techniques. *Clin Genet* **60**, 145-150 (2001). https://doi.org/10.1034/j.1399-0004.2001.600209.x

13 Hatt, L. *et al.* A new marker set that identifies fetal cells in maternal circulation with high specificity. *Prenat Diagn* **34**, 1066-1072 (2014). https://doi.org/10.1002/pd.4429

14 Bruch, J. F. *et al.* Trophoblast-like cells sorted from peripheral maternal blood using flow cytometry: a multiparametric study involving transmission electron microscopy and fetal DNA amplification. *Prenat Diagn* **11**, 787-798 (1991). https://doi.org/10.1002/pd.1970111007

15 Vossaert, L. *et al.* Validation Studies for Single Circulating Trophoblast Genetic Testing as a Form of Noninvasive Prenatal Diagnosis. *Am J Hum Genet* **105**, 1262-1273 (2019). https://doi.org/10.1016/j.ajhg.2019.11.004

16 Breman, A. M. *et al.* Evidence for feasibility of fetal trophoblastic cell-based noninvasive prenatal testing. *Prenat Diagn* **36**, 1009-1019 (2016). https://doi.org/10.1002/pd.4924

17 Kølvraa, S. *et al.* Genome-wide copy number analysis on DNA from fetal cells isolated from the blood of pregnant women. *Prenat Diagn* **36**, 1127-1134 (2016). https://doi.org/10.1002/pd.4948

18 Mandel, P, Metais & P. Les acides nucléiques du plasma sanguin chez l'homme. *C R Seances Soc Biol Fil* **142**, 241-243 (1948).

19 Chen, W. W. *et al.* BEAMing and Droplet Digital PCR Analysis of Mutant IDH1 mRNA in Glioma Patient Serum and Cerebrospinal Fluid Extracellular Vesicles. *Mol Ther Nucleic Acids* **2**, e109 (2013). https://doi.org/10.1038/mtna.2013.28

20 Byron, S. A., Van Keuren-Jensen, K. R., Engelthaler, D. M., Carpten, J. D. & Craig, D. W. Translating RNA sequencing into clinical diagnostics: opportunities and challenges. *Nat Rev Genet* **17**, 257-271 (2016). https://doi.org/10.1038/nrg.2016.10

21 Laird, P. W. Principles and challenges of genomewide DNA methylation analysis. *Nat Rev Genet* **11**, 191-203 (2010). https://doi.org/10.1038/nrg2732

22 Hou, Y. *et al.* Genome analyses of single human oocytes. *Cell* **155**, 1492-1506 (2013). https://doi.org/10.1016/j.cell.2013.11.040

23 Huang, J. *et al.* Validation of multiple annealing and looping-based amplification cycle sequencing for 24-chromosome aneuploidy screening of cleavage-stage embryos. *Fertil Steril* **102**, 1685-1691 (2014). https://doi.org/10.1016/j.fertnstert.2014.08.015

24 Huang, L., Ma, F., Chapman, A., Lu, S. & Xie, X. S. Single-Cell Whole-Genome Amplification and Sequencing: Methodology and Applications. *Annu Rev Genomics Hum Genet* **16**, 79-102 (2015). https://doi.

org/10.1146/annurev-genom-090413-025352
25 Forshew, T. *et al.* Noninvasive identification and monitoring of cancer mutations by targeted deep sequencing of plasma DNA. *Sci Transl Med* **4**, 136ra168 (2012). https://doi.org/10.1126/scitranslmed.3003726
26 Max, K. E. A. *et al.* Human plasma and serum extracellular small RNA reference profiles and their clinical utility. *Proc Natl Acad Sci U S A* **115**, E5334-E5343 (2018). https://doi.org/10.1073/pnas.1714397115
27 Chappell, L., Russell, A. J. C. & Voet, T. Single-Cell (Multi)omics Technologies. *Annu Rev Genomics Hum Genet* **19**, 15-41 (2018). https://doi.org/10.1146/annurev-genom-091416-035324
28 Leary, R. J. *et al.* Detection of chromosomal alterations in the circulation of cancer patients with whole-genome sequencing. *Sci Transl Med* **4**, 162ra154 (2012). https://doi.org/10.1126/scitranslmed.3004742
29 Dey, S. S., Kester, L., Spanjaard, B., Bienko, M. & van Oudenaarden, A. Integrated genome and transcriptome sequencing of the same cell. *Nat Biotechnol* **33**, 285-289 (2015). https://doi.org/10.1038/nbt.3129
30 Macaulay, I. C. *et al.* G&T-seq: parallel sequencing of single-cell genomes and transcriptomes. *Nat Methods* **12**, 519-522 (2015). https://doi.org/10.1038/nmeth.3370
31 Clark, S. J. *et al.* scNMT-seq enables joint profiling of chromatin accessibility DNA methylation and transcription in single cells. *Nat Commun* **9**, 781 (2018). https://doi.org/10.1038/s41467-018-03149-4
32 Li, L. *et al.* Single-cell multi-omics sequencing of human early embryos. *Nat Cell Biol* **20**, 847-858 (2018). https://doi.org/10.1038/s41556-018-0123-2
33 Alberry, M. *et al.* Free fetal DNA in maternal plasma in anembryonic pregnancies: confirmation that the origin is the trophoblast. *Prenat Diagn* **27**, 415-418 (2007). https://doi.org/10.1002/pd.1700
34 Lo, Y. M. *et al.* Presence of fetal DNA in maternal plasma and serum. *Lancet* **350**, 485-487 (1997). https://doi.org/10.1016/S0140-6736(97)02174-0
35 Tjoa, M. L., Cindrova-Davies, T., Spasic-Boskovic, O., Bianchi, D. W. & Burton, G. J. Trophoblastic oxidative stress and the release of cell-free feto-placental DNA. *Am J Pathol* **169**, 400-404 (2006). https://doi.org/10.2353/ajpath.2006.060161
36 Zamani Esteki, M. *et al.* In vitro fertilization does not increase the incidence of de novo copy number alterations in fetal and placental lineages. *Nat Med* **25**, 1699-1705 (2019). https://doi.org/10.1038/s41591-019-0620-2
37 Kotsopoulou, I., Tsoplou, P., Mavrommatis, K. & Kroupis, C. Non-invasive prenatal testing (NIPT): limitations on the way to become diagnosis. *Diagnosis (Berl)* **2**, 141-158 (2015). https://doi.org/10.1515/dx-2015-0002
38 Lo, Y. M. *et al.* Maternal plasma DNA sequencing reveals the genome-wide genetic and mutational profile of the fetus. *Sci Transl Med* **2**, 61ra91 (2010). https://doi.org/10.1126/scitranslmed.3001720
39 Assou, S., Aït-Ahmed, O., El Messaoudi, S., Thierry, A. R. & Hamamah, S. Non-invasive pre-implantation genetic diagnosis of X-linked disorders. *Med Hypotheses* **83**, 506-508 (2014). https://doi.org/10.1016/j.mehy.2014.08.019
40 Stigliani, S., Anserini, P., Venturini, P. L. & Scaruffi, P. Mitochondrial DNA content in embryo culture medium is significantly associated with human embryo fragmentation. *Hum Reprod* **28**, 2652-2660 (2013). https://doi.org/10.1093/humrep/det314
41 Poon, L. L., Leung, T. N., Lau, T. K. & Lo, Y. M. Presence of fetal RNA in maternal plasma. *Clin Chem* **46**, 1832-1834 (2000).
42 Chim, S. S. *et al.* Detection and characterization of placental microRNAs in maternal plasma. *Clin Chem* **54**, 482-490 (2008). https://doi.org/10.1373/clinchem.2007.097972
43 Huang, X. *et al.* Characterization of human plasma-derived exosomal RNAs by deep sequencing. *BMC Genomics* **14**, 319 (2013). https://doi.org/10.1186/1471-2164-14-319
44 Awamleh, Z., Gloor, G. B. & Han, V. K. M. Placental microRNAs in pregnancies with early onset intrauterine growth restriction and preeclampsia: potential impact on gene expression and pathophysiology. *BMC Med Genomics* **12**, 91 (2019). https://doi.org/10.1186/s12920-019-0548-x
45 Tian, T., Wang, J. & Zhou, X. A review: microRNA detection methods. *Org Biomol Chem* **13**, 2226-2238 (2015). https://doi.org/10.1039/c4ob02104e
46 Huang, S., Li, H., Ding, X. & Xiong, C. Presence and characterization of cell-free seminal RNA in healthy individuals: implications for noninvasive disease diagnosis and gene expression studies of the male reproductive system. *Clin Chem* **55**, 1967-1976 (2009). https://doi.org/10.1373/clinchem.2009.131128
47 Hong, Y. *et al.* Systematic characterization of seminal plasma piRNAs as molecular biomarkers for male infertility. *Sci Rep* **6**, 24229 (2016). https://doi.org/10.1038/srep24229
48 Bonucci & E. Fine structure of early cartilage calcification. *J Ultrastruct Res* **20**, 33-50 (1967).
49 Trams, E. G., Lauter, C. J., Salem, N. & Heine, U. Exfoliation of membrane ecto-enzymes in the form of micro-vesicles. *Biochim Biophys Acta* **645**, 63-70 (1981). https://doi.org/10.1016/0005-2736(81)90512-5

50 Pegtel, D. M. & Gould, S. J. Exosomes. *Annu Rev Biochem* **88**, 487-514 (2019). https://doi.org/10.1146/annurev-biochem-013118-111902
51 Abrahams, V. M., Straszewski-Chavez, S. L., Guller, S. & Mor, G. First trimester trophoblast cells secrete Fas ligand which induces immune cell apoptosis. *Mol Hum Reprod* **10**, 55-63 (2004). https://doi.org/10.1093/molehr/gah006
52 Goetzl, L., Darbinian, N. & Goetzl, E. J. Novel window on early human neurodevelopment via fetal exosomes in maternal blood. *Ann Clin Transl Neurol* **3**, 381-385 (2016). https://doi.org/10.1002/acn3.296
53 Goetzl, L., Darbinian, N. & Merabova, N. Noninvasive assessment of fetal central nervous system insult: Potential application to prenatal diagnosis. *Prenat Diagn* **39**, 609-615 (2019). https://doi.org/10.1002/pd.5474
54 Kerr, J. F., Wyllie, A. H. & Currie, A. R. Apoptosis: a basic biological phenomenon with wide-ranging implications in tissue kinetics. *Br J Cancer* **26**, 239-257 (1972). https://doi.org/10.1038/bjc.1972.33
55 Tixeira, R. *et al.* Defining the morphologic features and products of cell disassembly during apoptosis. *Apoptosis* **22**, 475-477 (2017). https://doi.org/10.1007/s10495-017-1345-7
56 Holdenrieder, S. *et al.* Circulating nucleosomes in serum. *Ann N Y Acad Sci* **945**, 93-102 (2001). https://doi.org/10.1111/j.1749-6632.2001.tb03869.x
57 Snyder, M. W., Kircher, M., Hill, A. J., Daza, R. M. & Shendure, J. Cell-free DNA Comprises an In Vivo Nucleosome Footprint that Informs Its Tissues-Of-Origin. *Cell* **164**, 57-68 (2016). https://doi.org/10.1016/j.cell.2015.11.050
58 Shi, J., Zhang, R. & Li, J. Size profile of cell-free DNA: A beacon guiding the practice and innovation of clinical testing. *Theranostics* **10**, 4737-4748 (2020). https://doi.org/10.7150/thno.42565
59 Ko, J., Carpenter, E. & Issadore, D. Detection and isolation of circulating exosomes and microvesicles for cancer monitoring and diagnostics using micro-/nano-based devices. *Analyst* **141**, 450-460 (2016). https://doi.org/10.1039/c5an01610j
60 Goodwin, S., McPherson, J. D. & McCombie, W. R. Coming of age: ten years of next-generation sequencing technologies. *Nat Rev Genet* **17**, 333-351 (2016). https://doi.org/10.1038/nrg.2016.49
61 Butler, T. M. *et al.* Exome Sequencing of Cell-Free DNA from Metastatic Cancer Patients Identifies Clinically Actionable Mutations Distinct from Primary Disease. *PLoS One* **10**, e0136407 (2015). https://doi.org/10.1371/journal.pone.0136407
62 Bayindir, B. *et al.* Noninvasive prenatal testing using a novel analysis pipeline to screen for all autosomal fetal aneuploidies improves pregnancy management. *Eur J Hum Genet* **23**, 1286-1293 (2015). https://doi.org/10.1038/ejhg.2014.282
63 Lou, D. I. *et al.* High-throughput DNA sequencing errors are reduced by orders of magnitude using circle sequencing. *Proc Natl Acad Sci U S A* **110**, 19872-19877 (2013). https://doi.org/10.1073/pnas.1319590110
64 Chim, S. S. *et al.* Detection of the placental epigenetic signature of the maspin gene in maternal plasma. *Proc Natl Acad Sci U S A* **102**, 14753-14758 (2005). https://doi.org/10.1073/pnas.0503335102
65 Jensen, T. J. *et al.* Whole genome bisulfite sequencing of cell-free DNA and its cellular contributors uncovers placenta hypomethylated domains. *Genome Biol* **16**, 78 (2015). https://doi.org/10.1186/s13059-015-0645-x
66 Gu, C., Liu, S., Wu, Q., Zhang, L. & Guo, F. Integrative single-cell analysis of transcriptome, DNA methylome and chromatin accessibility in mouse oocytes. *Cell Res* **29**, 110-123 (2019). https://doi.org/10.1038/s41422-018-0125-4
67 Navin, N. E. The first five years of single-cell cancer genomics and beyond. *Genome Res* **25**, 1499-1507 (2015). https://doi.org/10.1101/gr.191098.115
68 Tang, F., Lao, K. & Surani, M. A. Development and applications of single-cell transcriptome analysis. *Nat Methods* **8**, S6-11 (2011). https://doi.org/10.1038/nmeth.1557
69 Beck, J., Urnovitz, H. B., Riggert, J., Clerici, M. & Schütz, E. Profile of the circulating DNA in apparently healthy individuals. *Clin Chem* **55**, 730-738 (2009). https://doi.org/10.1373/clinchem.2008.113597
70 van der Vaart, M., Semenov, D. V., Kuligina, E. V., Richter, V. A. & Pretorius, P. J. Characterisation of circulating DNA by parallel tagged sequencing on the 454 platform. *Clin Chim Acta* **409**, 21-27 (2009). https://doi.org/10.1016/j.cca.2009.08.011
71 Khier, S. & Lohan, L. Kinetics of circulating cell-free DNA for biomedical applications: critical appraisal of the literature. *Future Sci OA* **4**, FSO295 (2018). https://doi.org/10.4155/fsoa-2017-0140
72 Lee, T. H., Montalvo, L., Chrebtow, V. & Busch, M. P. Quantitation of genomic DNA in plasma and serum samples: higher concentrations of genomic DNA found in serum than in plasma. *Transfusion* **41**, 276-282 (2001). https://doi.org/10.1046/j.1537-2995.2001.41020276.x
73 Wu, H. *et al.* Medium-based noninvasive preimplantation genetic diagnosis for human α-thalassemias-SEA. *Medicine (Baltimore)* **94**, e669 (2015). https://doi.org/10.1097/MD.0000000000000669

74 Liu, W. *et al.* Non-invasive pre-implantation aneuploidy screening and diagnosis of beta thalassemia IVSII654 mutation using spent embryo culture medium. *Ann Med* **49**, 319-328 (2017). https://doi.org/10.1080/07853890.2016.1254816
75 Scalici, E. *et al.* Cell-free DNA in human follicular fluid as a biomarker of embryo quality. *Hum Reprod* **29**, 2661-2669 (2014). https://doi.org/10.1093/humrep/deu238
76 Stigliani, S. *et al.* Mitochondrial DNA in Day 3 embryo culture medium is a novel, non-invasive biomarker of blastocyst potential and implantation outcome. *Mol Hum Reprod* **20**, 1238-1246 (2014). https://doi.org/10.1093/molehr/gau086
77 Kansaku, K. *et al.* Mitochondrial dysfunction in cumulus-oocyte complexes increases cell-free mitochondrial DNA. *J Reprod Dev* **64**, 261-266 (2018). https://doi.org/10.1262/jrd.2018-012
78 Assou, S. *et al.* A non-invasive test for assessing embryo potential by gene expression profiles of human cumulus cells: a proof of concept study. *Mol Hum Reprod* **14**, 711-719 (2008). https://doi.org/10.1093/molehr/gan067
79 Cabello-Pinedo *et al.* A novel non-invasive metabolomics approach to screen embryos for aneuploidy. *Fertil Steril* **114**, e5-e6 (2020).
80 Li, H. G., Huang, S. Y., Zhou, H., Liao, A. H. & Xiong, C. L. Quick recovery and characterization of cell-free DNA in seminal plasma of normozoospermia and azoospermia: implications for non-invasive genetic utilities. *Asian J Androl* **11**, 703-709 (2009). https://doi.org/10.1038/aja.2009.65
81 Wu, W. *et al.* Genome-wide microRNA expression profiling in idiopathic non-obstructive azoospermia: significant up-regulation of miR-141, miR-429 and miR-7-1-3p. *Hum Reprod* **28**, 1827-1836 (2013). https://doi.org/10.1093/humrep/det099
82 Li, H., Wu, C., Gu, X. & Xiong, C. A novel application of cell-free seminal mRNA: non-invasive identification of the presence of germ cells or complete obstruction in men with azoospermia. *Hum Reprod* **27**, 991-997 (2012). https://doi.org/10.1093/humrep/der481
83 Handyside, A. H., Kontogianni, E. H., Hardy, K. & Winston, R. M. Pregnancies from biopsied human preimplantation embryos sexed by Y-specific DNA amplification. *Nature* **344**, 768-770 (1990). https://doi.org/10.1038/344768a0
84 Kuliev, A. & Rechitsky, S. Preimplantation genetic testing: current challenges and future prospects. *Expert Rev Mol Diagn* **17**, 1071-1088 (2017). https://doi.org/10.1080/14737159.2017.1394186
85 Mastenbroek, S. & Repping, S. Preimplantation genetic screening: back to the future. *Hum Reprod* **29**, 1846-1850 (2014). https://doi.org/10.1093/humrep/deu163
86 Vermeesch, J. R., Voet, T. & Devriendt, K. Prenatal and pre-implantation genetic diagnosis. *Nat Rev Genet* **17**, 643-656 (2016). https://doi.org/10.1038/nrg.2016.97
87 Zhu, D. *et al.* Vitrified-warmed blastocyst transfer cycles yield higher pregnancy and implantation rates compared with fresh blastocyst transfer cycles--time for a new embryo transfer strategy? *Fertil Steril* **95**, 1691-1695 (2011). https://doi.org/10.1016/j.fertnstert.2011.01.022
88 Chen, S. U. *et al.* Microsuction of blastocoelic fluid before vitrification increased survival and pregnancy of mouse expanded blastocysts, but pretreatment with the cytoskeletal stabilizer did not increase blastocyst survival. *Fertil Steril* **84 Suppl 2**, 1156-1162 (2005). https://doi.org/10.1016/j.fertnstert.2005.03.074
89 Galluzzi, L. *et al.* Extracellular embryo genomic DNA and its potential for genotyping applications. *Future Sci OA* **1**, FSO62 (2015). https://doi.org/10.4155/fso.15.62
90 Shamonki, M. I., Jin, H., Haimowitz, Z. & Liu, L. Proof of concept: preimplantation genetic screening without embryo biopsy through analysis of cell-free DNA in spent embryo culture media. *Fertil Steril* **106**, 1312-1318 (2016). https://doi.org/10.1016/j.fertnstert.2016.07.1112
91 Xu, J. *et al.* Noninvasive chromosome screening of human embryos by genome sequencing of embryo culture medium for in vitro fertilization. *Proc Natl Acad Sci U S A* **113**, 11907-11912 (2016). https://doi.org/10.1073/pnas.1613294113
92 Feichtinger, M. *et al.* Non-invasive preimplantation genetic screening using array comparative genomic hybridization on spent culture media: a proof-of-concept pilot study. *Reprod Biomed Online* **34**, 583-589 (2017). https://doi.org/10.1016/j.rbmo.2017.03.015
93 Palini, S. *et al.* Genomic DNA in human blastocoele fluid. *Reprod Biomed Online* **26**, 603-610 (2013). https://doi.org/10.1016/j.rbmo.2013.02.012
94 Gianaroli, L. *et al.* Blastocentesis: a source of DNA for preimplantation genetic testing. Results from a pilot study. *Fertil Steril* **102**, 1692-1699.e1696 (2014). https://doi.org/10.1016/j.fertnstert.2014.08.021
95 Kuznyetsov, V. *et al.* Minimally Invasive Cell-Free Human Embryo Aneuploidy Testing (miPGT-A) Utilizing Combined Spent Embryo Culture Medium and Blastocoel Fluid -Towards Development of a Clinical Assay. *Sci Rep* **10**, 7244 (2020). https://doi.org/10.1038/s41598-020-64335-3
96 Lane *et al.* Ability to detect aneuploidy from cell free DNA collected from media is dependent on the stage of development of the embryo. e61 (2017).

97 Ho, J. R. *et al.* Pushing the limits of detection: investigation of cell-free DNA for aneuploidy screening in embryos. *Fertil Steril* **110**, 467-475.e462 (2018). https://doi.org/10.1016/j.fertnstert.2018.03.036
98 Hammond, E. R. *et al.* Characterizing nuclear and mitochondrial DNA in spent embryo culture media: genetic contamination identified. *Fertil Steril* **107**, 220-228.e225 (2017). https://doi.org/10.1016/j.fertnstert.2016.10.015
99 Vera-Rodriguez, M. *et al.* Origin and composition of cell-free DNA in spent medium from human embryo culture during preimplantation development. *Hum Reprod* **33**, 745-756 (2018). https://doi.org/10.1093/humrep/dey028
100 Sermon, K., Van Steirteghem, A. & Liebaers, I. Preimplantation genetic diagnosis. *Lancet* **363**, 1633-1641 (2004). https://doi.org/10.1016/S0140-6736(04)16209-0
101 Handyside, A. H. *et al.* Karyomapping: a universal method for genome wide analysis of genetic disease based on mapping crossovers between parental haplotypes. *J Med Genet* **47**, 651-658 (2010). https://doi.org/10.1136/jmg.2009.069971
102 Natesan, S. A. *et al.* Genome-wide karyomapping accurately identifies the inheritance of single-gene defects in human preimplantation embryos in vitro. *Genet Med* **16**, 838-845 (2014). https://doi.org/10.1038/gim.2014.45
103 Zamani Esteki, M. *et al.* Concurrent whole-genome haplotyping and copy-number profiling of single cells. *Am J Hum Genet* **96**, 894-912 (2015). https://doi.org/10.1016/j.ajhg.2015.04.011
104 Backenroth, D. *et al.* Haploseek: a 24-hour all-in-one method for preimplantation genetic diagnosis (PGD) of monogenic disease and aneuploidy. *Genet Med* **21**, 1390-1399 (2019). https://doi.org/10.1038/s41436-018-0351-7
105 Masset, H. *et al.* Multi-centre evaluation of a comprehensive preimplantation genetic test through haplotyping-by-sequencing. *Hum Reprod* **34**, 1608-1619 (2019). https://doi.org/10.1093/humrep/dez106
106 Vanneste, E. *et al.* Chromosome instability is common in human cleavage-stage embryos. *Nat Med* **15**, 577-583 (2009). https://doi.org/10.1038/nm.1924
107 Lo, Y. M. *et al.* Quantitative analysis of fetal DNA in maternal plasma and serum: implications for noninvasive prenatal diagnosis. *Am J Hum Genet* **62**, 768-775 (1998). https://doi.org/10.1086/301800
108 Lo, Y. M. *et al.* Increased fetal DNA concentrations in the plasma of pregnant women carrying fetuses with trisomy 21. *Clin Chem* **45**, 1747-1751 (1999).
109 Pertl, B. *et al.* Detection of male and female fetal DNA in maternal plasma by multiplex fluorescent polymerase chain reaction amplification of short tandem repeats. *Hum Genet* **106**, 45-49 (2000). https://doi.org/10.1007/s004390051008
110 Mersy, E. *et al.* Cell-Free RNA Is a Reliable Fetoplacental Marker in Noninvasive Fetal Sex Determination. *Clin Chem* **61**, 1515-1523 (2015). https://doi.org/10.1373/clinchem.2015.244962
111 Bianchi, D. W., Rava, R. P. & Sehnert, A. J. DNA sequencing versus standard prenatal aneuploidy screening. *N Engl J Med* **371**, 578 (2014). https://doi.org/10.1056/NEJMc1405486
112 van der Meij, K. R. M. *et al.* TRIDENT-2: National Implementation of Genome-wide Non-invasive Prenatal Testing as a First-Tier Screening Test in the Netherlands. *Am J Hum Genet* **105**, 1091-1101 (2019). https://doi.org/10.1016/j.ajhg.2019.10.005
113 Lam, K. W. *et al.* Noninvasive prenatal diagnosis of monogenic diseases by targeted massively parallel sequencing of maternal plasma: application to β-thalassemia. *Clin Chem* **58**, 1467-1475 (2012). https://doi.org/10.1373/clinchem.2012.189589
114 Lv, W. *et al.* Noninvasive prenatal testing for Wilson disease by use of circulating single-molecule amplification and resequencing technology (cSMART). *Clin Chem* **61**, 172-181 (2015). https://doi.org/10.1373/clinchem.2014.229328
115 Yin, X. *et al.* Identification of a de novo fetal variant in osteogenesis imperfecta by targeted sequencing-based noninvasive prenatal testing. *J Hum Genet* **63**, 1129-1137 (2018). https://doi.org/10.1038/s10038-018-0489-9
116 Zhang, J. *et al.* Non-invasive prenatal sequencing for multiple Mendelian monogenic disorders using circulating cell-free fetal DNA. *Nat Med* **25**, 439-447 (2019). https://doi.org/10.1038/s41591-018-0334-x
117 Lo, Y. M. *et al.* Digital PCR for the molecular detection of fetal chromosomal aneuploidy. *Proc Natl Acad Sci U S A* **104**, 13116-13121 (2007). https://doi.org/10.1073/pnas.0705765104
118 Ge, H. *et al.* Noninvasive prenatal detection for pathogenic CNVs: the application in α-thalassemia. *PLoS One* **8**, e67464 (2013). https://doi.org/10.1371/journal.pone.0067464
119 Lo, Y. M. *et al.* Plasma placental RNA allelic ratio permits noninvasive prenatal chromosomal aneuploidy detection. *Nat Med* **13**, 218-223 (2007). https://doi.org/10.1038/nm1530
120 New, M. I. *et al.* Noninvasive prenatal diagnosis of congenital adrenal hyperplasia using cell-free fetal DNA

in maternal plasma. *J Clin Endocrinol Metab* **99**, E1022-1030 (2014). https://doi.org/10.1210/jc.2014-1118
121 Rabinowitz, T. *et al.* Bayesian-based noninvasive prenatal diagnosis of single-gene disorders. *Genome Res* **29**, 428-438 (2019). https://doi.org/10.1101/gr.235796.118
122 Straver, R. *et al.* WISECONDOR: detection of fetal aberrations from shallow sequencing maternal plasma based on a within-sample comparison scheme. *Nucleic Acids Res* **42**, e31 (2014). https://doi.org/10.1093/nar/gkt992
123 Raman, L., Dheedene, A., De Smet, M., Van Dorpe, J. & Menten, B. WisecondorX: improved copy number detection for routine shallow whole-genome sequencing. *Nucleic Acids Res* **47**, 1605-1614 (2019). https://doi.org/10.1093/nar/gky1263
124 Kalousek, D. K. & Vekemans, M. Confined placental mosaicism. *J Med Genet* **33**, 529-533 (1996). https://doi.org/10.1136/jmg.33.7.529
125 Russell, L. M., Strike, P., Browne, C. E. & Jacobs, P. A. X chromosome loss and ageing. *Cytogenet Genome Res* **116**, 181-185 (2007). https://doi.org/10.1159/000098184
126 Wang, Y. *et al.* Cell-free DNA screening for sex chromosome aneuploidies by non-invasive prenatal testing in maternal plasma. *Mol Cytogenet* **13**, 10 (2020). https://doi.org/10.1186/s13039-020-0478-5
127 Fan, H. C. *et al.* Non-invasive prenatal measurement of the fetal genome. *Nature* **487**, 320-324 (2012). https://doi.org/10.1038/nature11251
128 Che, H. *et al.* Noninvasive prenatal diagnosis by genome-wide haplotyping of cell-free plasma DNA. *Genet Med* **22**, 962-973 (2020). https://doi.org/10.1038/s41436-019-0748-y
129 Bianchi, D. W. Unusual Prenatal Genomic Results Provide Proof-of-Principle of the Liquid Biopsy for Cancer Screening. *Clin Chem* **64**, 254-256 (2018). https://doi.org/10.1373/clinchem.2017.282459
130 Lenaerts, L. *et al.* Comprehensive genome-wide analysis of routine non-invasive test data allows cancer prediction: A single-center retrospective analysis of over 85,000 pregnancies. *EClinicalMedicine* **35**, 100856 (2021). https://doi.org/10.1016/j.eclinm.2021.100856
131 Dharajiya, N. G. *et al.* Incidental Detection of Maternal Neoplasia in Noninvasive Prenatal Testing. *Clin Chem* **64**, 329-335 (2018). https://doi.org/10.1373/clinchem.2017.277517
132 Bianchi, D. W. *et al.* Noninvasive Prenatal Testing and Incidental Detection of Occult Maternal Malignancies. *JAMA* **314**, 162-169 (2015). https://doi.org/10.1001/jama.2015.7120
133 Ji, X. *et al.* Copy number variation profile in noninvasive prenatal testing (NIPT) can identify co-existing maternal malignancies: Case reports and a literature review. *Taiwan J Obstet Gynecol* **57**, 871-877 (2018). https://doi.org/10.1016/j.tjog.2018.10.032
134 Giles, M. E. *et al.* Prenatal cfDNA screening results indicative of maternal neoplasm: survey of current practice and management needs. *Prenat Diagn* **37**, 126-132 (2017). https://doi.org/10.1002/pd.4973
135 Smith, J. *et al.* Cell-free DNA results lead to unexpected diagnosis. *Clin Case Rep* **5**, 1323-1326 (2017). https://doi.org/10.1002/ccr3.1051
136 van Schendel *et al.* For the Dutch NIPT Consortium. Women's experience with non-invasive prenatal testing and emotional well-being and satisfaction after test-results . . *J Genet Counsel* 1348 – 1356 (2017).
137 Wahid, B. *et al.* Biomarkers for diagnosis of pre-eclampsia and endometriosis. *Biomark Med* **12**, 1161-1173 (2018). https://doi.org/10.2217/bmm-2018-0058
138 Pernemalm, M. *et al.* In-depth human plasma proteome analysis captures tissue proteins and transfer of protein variants across the placenta. *Elife* **8** (2019). https://doi.org/10.7554/eLife.41608
139 Kumarswamy, R. *et al.* Circulating long noncoding RNA, LIPCAR, predicts survival in patients with heart failure. *Circ Res* **114**, 1569-1575 (2014). https://doi.org/10.1161/CIRCRESAHA.114.303915
140 Burnham, P., Khush, K. & De Vlaminck, I. Myriad Applications of Circulating Cell-Free DNA in Precision Organ Transplant Monitoring. *Ann Am Thorac Soc* **14**, *S*237-S241 (2017). https://doi.org/10.1513/AnnalsATS.201608-634MG
141 Meng, W. *et al.* Prospects and challenges of extracellular vesicle-based drug delivery system: considering cell source. *Drug Deliv* **27**, 585-598 (2020). https://doi.org/10.1080/10717544.2020.1748758
142 Sallevelt, S. C. E. H. *et al.* Diagnostic exome-based preconception carrier testing in consanguineous couples: results from the first 100 couples in clinical practice. *Genet Med* **23**, 1125-1136 (2021). https://doi.org/10.1038/s41436-021-01116-x
143 Eraslan, G., Avsec, Ž., Gagneur, J. & Theis, F. J. Deep learning: new computational modelling techniques for genomics. *Nat Rev Genet* **20**, 389-403 (2019). https://doi.org/10.1038/s41576-019-0122-6
144 Wan, N. *et al.* Machine learning enables detection of early-stage colorectal cancer by whole-genome sequencing of plasma cell-free DNA. *BMC Cancer* **19**, 832 (2019). https://doi.org/10.1186/s12885-019-6003-8
145 Topol, E. J. High-performance medicine: the convergence of human and artificial intelligence. *Nat Med* **25**, 44-56 (2019). https://doi.org/10.1038/s41591-018-0300-7

146 Council, N. H. *Screening: Between Hope and Hype* . <https://www.healthcouncil.nl/documents/advisory-reports/2008/04/01/screening-between-hope-and-hype> (2008).
147 Dondorp, W. *et al.* Non-invasive prenatal testing for aneuploidy and beyond: challenges of responsible innovation in prenatal screening. *Eur J Hum Genet* **23**, 1438-1450 (2015). https://doi.org/10.1038/ejhg.2015.57
148 Wert & D, G. in *Preimplantation genetic diagnosis* (ed Harper J) Ch. 17, 259 – 273 (Cambridge University Press, 2009).

Chapter 8

General discussion & summary

Glossary of abbreviated terms

ART	Assisted reproductive technology
cfDNA	Cell free DNA
G3	Culture medium from Vitrolife
G5	Culture medium from Vitrolife
GEM	Genome scale metabolic model
HTF	Human tubal fluid (culture medium from Lonza)
ICM	Inner cell mass
ICSI	Intracytoplasmic sperm injection
IVF	*In vitro* fertilisation
K-SICM	Sydney IVF cleavage medium (culture medium from Cook)
NC	Naturally conceived
NIPT	Non-invasive prenatal testing
PGT	Preimplantation genetic testing
PGT-A	PGT for aneuploidies
TE	Trophectoderm
ZGA	Zygotic genome activation

The use of assisted reproductive technologies (ART), including *in vitro* fertilisation (IVF), intracytoplasmic sperm injection (ICSI) and preimplantation genetic testing (PGT), has increased dramatically since the first successful implementation of IVF in 1978[1] and PGT in 1990[2]. At present in Europe, more than 1 million cycles of IVF and almost 50,000 PGT procedures are carried out annually[3,4] and these numbers are expected to continue to rise in the future. This is due to the fact that ART represent the mainstay of infertility treatment[5] and that PGT offers couples who are known carriers of heritable genetic disorders an option to prevent these from being passed on to the next generation[6]. Yet, despite our growing reliance on these procedures, we still lack fundamental insights into the interplay between the pre-implantation environment and the molecular regulation of embryonic development and the significance of commonly observed genomic abnormalities for pregnancy establishment or success. Further, to ensure that the growing demand for these treatments can be met, innovations in the field are required to reduce the complexity, time requirement and cost of the interventions. This could be achieved through a combination of improving ART success rates, thereby the reducing time to pregnancy, and PGT innovations. To this end, my thesis aimed to i) ascertain whether there was an epigenetic signature associated with IVF embryo culture in compositionally different culture media, ii) showcase advances in PGT practises that offer a simplified, scalable, safe, and universally applicable approach, and iii) elucidate the genomic abnormalities associated with pregnancy loss.

This general discussion will mainly focus on the early embryonic environment and the use of different embryo culture systems. The other aims will be briefly discussed in the context of future perspectives.

The role of embryo culture media in ART success

Human pre-implantation embryo development is a highly dynamic process where extensive molecular changes, including zygotic genome activation[7] (ZGA), epigenetic reprogramming[8,9], and lineage differentiation[10], are accompanied by changes in metabolism[11]. For successful *in vitro* embryo culture, metabolic demands must be met by components from the culture medium and therefore much attention has been awarded to optimising ART culture media to improve treatment success rates[12]. However, our understanding of the *in vivo* pre-implantation environment, i.e. the intra-fallopian and the intra-uterine environment, is incomplete[13], and therefore a multitude of different embryo culture systems have been developed and used over the years[12,14-17]. While the full composition of these commercially available options has rarely been fully disclosed, it is known that they differ in their composition in terms of amino acids, energy substrates and electrolytes[14,15,18]. Furthermore, conceptually different culture

systems have been developed, namely single-step systems that are used continuously from fertilisation until embryo transfer and sequential systems where a medium change is carried out 3 days post-fertilisation[19] to coincide with ZGA and the embryo's major energy substrate switch from pyruvate to glucose[11]. A growing number of studies have highlighted the need to carefully evaluate the different ART culture media that are available. For example, it has been shown that compositionally different culture media have the capacity to influence embryo development (e.g. embryo quality and cell number), ART treatment outcomes (e.g. pregnancy and live birth rates) as well as the antenatal and childhood growth of the resulting children[16,20-28]. However, few studies have tried to elucidate the molecular mechanisms underlying these observed differences[29,30] and in turn no molecular parameters are available against which to test further culture medium composition modifications.

In **chapter 2** and **chapter 3** we profiled the methylomes of neonates and 9-year-old children, respectively, who had undergone embryo culture in one of four compositionally different ART culture media. We chose to examine DNA methylation as epigenetic reprogramming involves virtually complete erasure and re-establishment of DNA methylation marks[8,9]. Furthermore, evidence suggests that this process can be modulated by environmental factors which bears significance for the long-term health and development of the individual[9,31,32].

In these two studies, we did not observe any significant methylation differences when comparing the respective culture medium pairs. This is in line with findings from other studies comparing the methylomes of ART offspring that experienced embryo culture in different media[30,33,34]. It is plausible that any epigenetic differences induced by these media during the first 3-5 days post-fertilisation do not persist until the time points at which we collected samples, i.e., birth or 9 years of age. This hypothesis is supported by studies that compared DNA methylation profiles between ART and naturally conceived (NC) individuals. Although these studies find modest but significant methylation differences between the two groups at birth, they largely fade by adolescence[35,36]. Furthermore, it is known that developmental programs, environmental factors, and disease processes modulate DNA methylation patterns throughout life[37]. These could potentially have a greater impact on DNA methylation levels than the ART culture media to which the embryo is only exposed for a very limited period of time. Alternatively, the lack of CpG sites or genes that have significantly different DNA methylation levels between the culture medium groups could indicate that the phenotypic differences are modulated by different molecular mechanisms which could include other epigenetic marks, such as histone modifications, or post-transcriptional modification of gene expression.

Interestingly, we did observe differences in the variability of methylation levels at certain CpG sites when comparing the respective culture medium pairs. Specifically, in both studies, the culture medium from Vitrolife, i.e., either G3 or G5, was associated with a greater number of hypervariable sites compared to the other medium (i.e., K-SICM or HTF, respectively). While the significance of these sites remains to be fully characterised, oncological studies have suggested that such sites may be involved in disease pathogenesis because differentially variable sites identified in pre-malignant tissues are frequently found to be significantly differentially methylated in cancerous tissues[38]. In our studies, the sites could also represent signatures associated with pregnancy pathologies, such as gestational diabetes and pre-eclampsia, that were only experienced by some individuals[39-42]. Alternatively, *in silico* studies suggest that applying a selection pressure during development would result in a group of individuals with diminished DNA methylation variance[43]. This theory would fit with the clinical outcomes of our cohorts, where both Vitrolife media resulted in a greater number of usable embryos and higher pregnancy rates compared to either K-SICM or HTF[20,24].

In these studies, we also highlighted the need to recruit NC controls alongside ART-conceived neonates/children to serve as a baseline against which comparisons can be made. We showed that integration of methylation data across studies is not possible unless comparable individuals from the same study group are processed in each batch to allow for the correction of technical effects without removing biological variation. This is an increasingly relevant consideration for study design as novel assays generating big (sequencing) data are typically not normalised to standardised controls. Therefore, integration of data from different sample batches generated separately in-house, in different laboratories, or in different studies, is not possible unless all batches contain samples that can be used to normalise the data.

Future perspectives for ART culture systems

Considering that the lack of DNA methylation differences identified in the ART neonates and children described in **chapter 2** and **chapter 3**, could be due to continued modulation of the methylome between embryo transfer and the studied timepoints, future studies should evaluate the impact of culture media on the epigenome at earlier time points, either during or at the end of the culture period or antenatally. Until recently, it has been challenging to conduct such studies as few human embryos are available for research and the minimum input for many molecular assays exceeded the number of cells of an individual embryo. Emerging single-cell technologies are however enabling us to understand the molecular workings of organisms at an unprecedented level[44]. For embryo research this means that studies can be conducted with smaller

numbers of embryos and at a much higher resolution, meaning for instance, that the effects of different culture media could now be ascertained per cell lineage of each included embryo. Furthermore, employing assays that probe multiple molecular layers, such as the epigenome and transcriptome, simultaneously would allow the functional relevance of identified differences to be directly evaluated[44]. Increasingly, methods such as those described in **chapter 7**, are being developed to leverage information from cell-free DNA (cfDNA) in place of analysing intracellular DNA[45]. These methods do not lead to the destruction of the sample material and could therefore be hugely beneficial for embryo research. Assaying cfDNA from spent embryo culture medium would allow the molecular impact of the culture medium to be studied at the time of clinical trials, rather than waiting until couples have completed their treatments and choose to donate their spare embryos to research. Additionally, embryos sampled with this strategy could still be transferred to establish a pregnancy, therefore likely increasing the number of couples who would be willing to participate, and also for the first time allow molecular findings to be related to clinical outcomes beyond the *in vitro* culture period. Furthermore, recent advances in non-invasive prenatal testing (NIPT), also described in **chapter 7**, have provided us with the tools to track the methylome throughout the antenatal period[46]. In combination such studies would provide us with a comprehensive DNA methylation timeline from which it can be ascertained whether, and to what extent, different ART culture media modulate the human epigenome.

The phenotypic, e.g.: birth weight, differences between the culture medium groups described in **chapter 2** and **chapter 3** and the observed differences in DNA methylation variance warrant long-term follow-up. In general, little is known about the health of ART offspring in adulthood as the oldest IVF-conceived individuals are in their 40s. Ideally, the ART-conceived individuals should be compared to NC individuals to determine whether they have greater than baseline risks for any diseases such as cardiometabolic disease which is known to be related to birth weight[47].

Ultimately, to generate an optimal culture medium for ART procedures, concentration gradients of individual components should be tested both as single-step and sequential culture systems. Due to the aforementioned challenges relating to the number of embryos available for research and the nature of the available molecular assays, such detailed research examining culture medium composition has not yet been possible. However, recent methodological advances offer some potential solutions to this bottleneck. Firstly, the invention of sophisticated computational modelling methods, such as genome scale metabolic models (GEM)[48], could be used to reduce the number metabolites that need to be considered. An embryo-specific GEM could be constructed from (existing) transcriptome data that is generated from a limited number of embryos. Subsequently, such models could be used to simulate the addition or removal of specific

metabolites to the culture medium and the effect thereof, thereby identifying potentially beneficial compounds that should be further validated. Secondly, in recent years human embryo-like structures, referred to as blastoids, have successfully been assembled from simple cell cultures[49-54]. These blastoids can easily be produced in large numbers and therefore represent a viable option to carry out testing of a vast array of culture medium components. Furthermore, blastoids can be used for both molecular and functional characterisation, as they have been shown to be transcriptionally similar to *in vitro* generated human embryos[49-54] and have the capacity to mimic implantation in *in vitro* assays[51,53,54]. Finally, the already mentioned non-invasive, cfDNA-based approaches for molecular characterisation of human embryos could facilitate culture medium testing on a larger scale without the need to generate surplus embryos that can be used for research.

In the future, increasingly sophisticated culture systems and microfluidics devices could allow the *in vivo* pre-implantation embryo environment to be mimicked with ever greater accuracy[55]. Such systems could potentially allow continuous media adjustments, to match the metabolic requirements of the embryo at different developmental stages, without needing to remove the embryo from the light, temperature, and gas-controlled environment of the incubator. By using such highly adjustable culture systems in combination with the artificial intelligence (AI)-based methods that are being developed to track embryo development dynamics[56], a fully automated, personalised (per embryo), culture system could be created. The expectation would be that providing more refined developmental support would allow more embryos to develop into good quality blastocysts that have a high chance of establishing a successful pregnancy.

Future perspectives for PGT

In **chapter 4** and **chapter 5,** we describe innovations in PGT that offer a number of benefits over existing methods. Specifically, with these methods i) we achieve greater diagnostic certainty by being able to identify sample switching errors and generating more data on which to base our conclusions, ii) we can resolve a greater proportion of complex cases, iii) we reduce the complexity of the required laboratory protocols by reducing the reliance on the four-eyes principle and by using a simplified library preparation protocol, and iii) we offer a universal solution for PGT that can be used to simultaneously assess monogenic indications, chromosomal copy number aberrations (including their segregational origin and mosaicism level), structural rearrangements and mitochondrial heteroplasmy levels. These innovations already represent significant progress in the field, allowing laboratories to process more samples with same resources and thereby improve patient access to PGT.

However, the described PGT protocols process genomic material from embryos that is collected by means of an invasive trophectoderm (TE) biopsy. This removal of cellular material from the growing embryo may be detrimental to its ongoing development[57] and therefore alternatives to this practise are being sought. One potential alternative is to conduct PGT on cfDNA aspirated from the blastocoel cavity during vitrification or cfDNA obtained from the spent culture medium. This possible minimally- and non-invasive approach to PGT, as well as other applications of liquid biopsy in the field of reproductive medicine are described in **chapter 7**. While it has been repeatedly demonstrated that the extraction and analysis of cfDNA from embryo culture medium and blastocoel fluid is possible, most studies were conducted in the context of PGT for aneuploidies (PGT-A) with the aim of determining which embryos had the highest chance of a successful outcome[58]. In these studies, discordant results were often obtained when comparing the PGT-A results from TE biopsies and the spent culture medium[58]. More generally, the practice of PGT-A based embryo selection has been questioned in light of recent meta-analyses that show no improvement in pregnancy rates after PGT-A[59-63]. We therefore advocate for further studies to better understand the significance of aneuploidy in early human development so that potentially viable embryos are not unnecessarily discarded. In **chapter 6** we describe one such study, where we have profiled the chromosomal landscape of first trimester pregnancy losses to better understand the abnormalities that are not compatible with ongoing pregnancies. This study and prior studies clearly showed that embryos often harbour multiple lineages with different chromosomal copy number compositions, i.e., they are mosaic, and therefore a single TE biopsy is frequently not fully representative of the whole embryo[64-66]. Whether cfDNA in spent culture medium provides a more representative view of the ploidy status of embryos remains to be determined. However, cfDNA-based PGT can potentially be augmented by leveraging epigenetic information to determine which embryonic compartment (TE or inner cell mass) the DNA arose from and could therefore provide more comprehensive representation of the different lineages[45].

Conclusion

Over the last decades societal attitudes towards reproduction have been changing, leading to advancing parental ages and a greater desire for reproductive autonomy. In turn, ART has become ever more important to overcome (age-related) infertility and to facilitate the selection of embryos free from severe genetic disease. Since, ART procedures represent a substantial medical intervention, it is imperative that innovations are introduced responsibly to ensure that the treatments are safe and psychologically tolerable to the couples and to safeguard the health of the resulting children. To this end, we have tried to determine the molecular mechanisms underlying

phenotypic differences observed in ART offspring after embryo culture in different media; described current innovations and future potentials for PGT protocols; and analysed the genomic landscape of pregnancy loss tissues. More research is still needed to generate an optimal ART culture system and to reduce the invasiveness PGT procedures. Additionally, the health outcomes of ART offspring should be studied throughout their lifespan.

References

1 Steptoe, P. C. & Edwards, R. G. Birth after the reimplantation of a human embryo. *Lancet* **2**, 366 (1978). https://doi.org/10.1016/s0140-6736(78)92957-4

2 Handyside, A. H. *et al.* Biopsy of human preimplantation embryos and sexing by DNA amplification. *Lancet* **1**, 347-349 (1989). https://doi.org/10.1016/s0140-6736(89)91723-6

3 Spinella, F. *et al.* ESHRE PGT Consortium data collection XXI: PGT analyses in 2018. *Hum Reprod Open* **2023**, hoad010 (2023). https://doi.org/10.1093/hropen/hoad010

4 Wyns, C. *et al.* ART in Europe, 2018: results generated from European registries by ESHRE. *Hum Reprod Open* **2022**, hoac022 (2022). https://doi.org/10.1093/hropen/hoac022

5 The Unexplained Infertility guideline group, Romualdi D, Ata B, Bhattacharya S, Bosch E, Costello M, Gersak K, Homburg R, Le Clef N, Mincheva M et al. Evidence-based guideline: Unexplained Infertility. 2023. ESHRE, https://www.eshre.eu/guideline/UI.

6 Hughes, T. *et al.* A review on the motivations, decision-making factors, attitudes and experiences of couples using pre-implantation genetic testing for inherited conditions. *Hum Reprod Update* **27**, 944-966 (2021). https://doi.org/10.1093/humupd/dmab013

7 Yuan, S. *et al.* Human zygotic genome activation is initiated from paternal genome. *Cell Discov* **9**, 13 (2023). https://doi.org/10.1038/s41421-022-00494-z

8 Li, L. *et al.* Single-cell multi-omics sequencing of human early embryos. *Nat Cell Biol* **20**, 847-858 (2018). https://doi.org/10.1038/s41556-018-0123-2

9 Hanna, C. W., Demond, H. & Kelsey, G. Epigenetic regulation in development: is the mouse a good model for the human? *Hum Reprod Update* **24**, 556-576 (2018). https://doi.org/10.1093/humupd/dmy021

10 De Paepe, C., Krivega, M., Cauffman, G., Geens, M. & Van de Velde, H. Totipotency and lineage segregation in the human embryo. *Mol Hum Reprod* **20**, 599-618 (2014). https://doi.org/10.1093/molehr/gau027

11 Leese, H. J. Metabolism of the preimplantation embryo: 40 years on. *Reproduction* **143**, 417-427 (2012). https://doi.org/10.1530/REP-11-0484

12 Sunde, A. *et al.* Time to take human embryo culture seriously. *Hum Reprod* **31**, 2174-2182 (2016). https://doi.org/10.1093/humrep/dew157

13 Saint-Dizier, M., Schoen, J., Chen, S., Banliat, C. & Mermillod, P. Composing the Early Embryonic Microenvironment: Physiology and Regulation of Oviductal Secretions. *Int J Mol Sci* **21** (2019). https://doi.org/10.3390/ijms21010223

14 Morbeck, D. E. *et al.* Composition of commercial media used for human embryo culture. *Fertil Steril* **102**, 759-766.e759 (2014). https://doi.org/10.1016/j.fertnstert.2014.05.043

15 Morbeck, D. E., Baumann, N. A. & Oglesbee, D. Composition of single-step media used for human embryo culture. *Fertil Steril* **107**, 1055-1060.e1051 (2017). https://doi.org/10.1016/j.fertnstert.2017.01.007

16 Mantikou, E. *et al.* Embryo culture media and IVF/ICSI success rates: a systematic review. *Hum Reprod Update* **19**, 210-220 (2013). https://doi.org/10.1093/humupd/dms061

17 Youssef, M. M. *et al.* Culture media for human pre-implantation embryos in assisted reproductive technology cycles. *Cochrane Database Syst Rev*, Cd007876 (2015). https://doi.org/10.1002/14651858.CD007876.pub2

18 Tarahomi, M. *et al.* The composition of human preimplantation embryo culture media and their stability during storage and culture. *Hum Reprod* **34**, 1450-1461 (2019). https://doi.org/10.1093/humrep/dez102

19 Dieamant, F. *et al.* Single versus sequential culture medium: which is better at improving ongoing pregnancy rates? A systematic review and meta-analysis. *JBRA Assist Reprod* **21**, 240-246 (2017). https://doi.org/10.5935/1518-0557.20170045

20 Dumoulin, J. C. *et al.* Effect of in vitro culture of human embryos on birthweight of newborns. *Hum Reprod* **25**, 605-612 (2010). https://doi.org/10.1093/humrep/dep456

21 Zandstra, H., Van Montfoort, A. P. & Dumoulin, J. C. Does the type of culture medium used influence birthweight of children born after IVF? *Hum Reprod* **30**, 530-542 (2015). https://doi.org/10.1093/humrep/deu346

22 Zandstra, H. *et al.* Association of culture medium with growth, weight and cardiovascular development of IVF children at the age of 9 years. *Hum Reprod* **33**, 1645-1656 (2018). https://doi.org/10.1093/humrep/dey246

23 Kleijkers, S. H. *et al.* IVF culture medium affects post-natal weight in humans during the first 2 years of life. *Hum Reprod* **29**, 661-669 (2014). https://doi.org/10.1093/humrep/deu025

24 Kleijkers, S. H. *et al.* Influence of embryo culture medium (G5 and HTF) on pregnancy and perinatal outcome after IVF: a multicenter RCT. *Hum Reprod* **31**, 2219-2230 (2016). https://doi.org/10.1093/

humrep/dew156
25 Bouillon, C. *et al.* Does Embryo Culture Medium Influence the Health and Development of Children Born after In Vitro Fertilization? *PLoS One* **11**, e0150857 (2016). https://doi.org/10.1371/journal.pone.0150857
26 Nelissen, E. C. *et al.* IVF culture medium affects human intrauterine growth as early as the second trimester of pregnancy. *Hum Reprod* **28**, 2067-2074 (2013). https://doi.org/10.1093/humrep/det131
27 Nelissen, E. C. *et al.* Further evidence that culture media affect perinatal outcome: findings after transfer of fresh and cryopreserved embryos. *Hum Reprod* **27**, 1966-1976 (2012). https://doi.org/10.1093/humrep/des145
28 Castillo, C. M. *et al.* The impact of selected embryo culture conditions on ART treatment cycle outcomes: a UK national study. *Hum Reprod Open* **2020**, hoz031 (2020). https://doi.org/10.1093/hropen/hoz031
29 Kleijkers, S. H. *et al.* Differences in gene expression profiles between human preimplantation embryos cultured in two different IVF culture media. *Hum Reprod* **30**, 2303-2311 (2015). https://doi.org/10.1093/humrep/dev179
30 Mulder, C. L. *et al.* Comparison of DNA methylation patterns of parentally imprinted genes in placenta derived from IVF conceptions in two different culture media. *Hum Reprod* **35**, 516-528 (2020). https://doi.org/10.1093/humrep/deaa004
31 Wadhwa, P. D., Buss, C., Entringer, S. & Swanson, J. M. Developmental origins of health and disease: brief history of the approach and current focus on epigenetic mechanisms. *Semin Reprod Med* **27**, 358-368 (2009). https://doi.org/10.1055/s-0029-1237424
32 Felix, J. F. & Cecil, C. A. M. Population DNA methylation studies in the Developmental Origins of Health and Disease (DOHaD) framework. *J Dev Orig Health Dis* **10**, 306-313 (2019). https://doi.org/10.1017/S2040174418000442
33 Barberet, J. *et al.* Do assisted reproductive technologies and in vitro embryo culture influence the epigenetic control of imprinted genes and transposable elements in children? *Hum Reprod* **36**, 479-492 (2021). https://doi.org/10.1093/humrep/deaa310
34 Ducreux, B. *et al.* Genome-Wide Analysis of DNA Methylation in Buccal Cells of Children Conceived through IVF and ICSI. *Genes (Basel)* **12** (2021). https://doi.org/10.3390/genes12121912
35 Barberet, J. *et al.* DNA methylation profiles after ART during human lifespan: a systematic review and meta-analysis. *Hum Reprod Update* (2022). https://doi.org/10.1093/humupd/dmac010
36 Penova-Veselinovic, B. *et al.* DNA methylation patterns within whole blood of adolescents born from assisted reproductive technology are not different from adolescents born from natural conception. *Hum Reprod* **36**, 2035-2049 (2021). https://doi.org/10.1093/humrep/deab078
37 Mitchell, C., Schneper, L. M. & Notterman, D. A. DNA methylation, early life environment, and health outcomes. *Pediatr Res* **79**, 212-219 (2016). https://doi.org/10.1038/pr.2015.193
38 Teschendorff, A. E., Jones, A. & Widschwendter, M. Stochastic epigenetic outliers can define field defects in cancer. *BMC Bioinformatics* **17**, 178 (2016). https://doi.org/10.1186/s12859-016-1056-z
39 Cirkovic, A. *et al.* Systematic review supports the role of DNA methylation in the pathophysiology of preeclampsia: a call for analytical and methodological standardization. *Biol Sex Differ* **11**, 36 (2020). https://doi.org/10.1186/s13293-020-00313-8
40 Elliott, H. R., Sharp, G. C., Relton, C. L. & Lawlor, D. A. Epigenetics and gestational diabetes: a review of epigenetic epidemiology studies and their use to explore epigenetic mediation and improve prediction. *Diabetologia* **62**, 2171-2178 (2019). https://doi.org/10.1007/s00125-019-05011-8
41 Awamleh, Z. *et al.* Exposure to Gestational Diabetes Mellitus (GDM) alters DNA methylation in placenta and fetal cord blood. *Diabetes Res Clin Pract* **174**, 108690 (2021). https://doi.org/10.1016/j.diabres.2021.108690
42 Howe, C. G. *et al.* Maternal Gestational Diabetes Mellitus and Newborn DNA Methylation: Findings From the Pregnancy and Childhood Epigenetics Consortium. *Diabetes Care* **43**, 98-105 (2020). https://doi.org/10.2337/dc19-0524
43 Tobi, E. W. *et al.* Selective Survival of Embryos Can Explain DNA Methylation Signatures of Adverse Prenatal Environments. *Cell Rep* **25**, 2660-2667.e2664 (2018). https://doi.org/10.1016/j.celrep.2018.11.023
44 Vandereyken, K., Sifrim, A., Thienpont, B. & Voet, T. Methods and applications for single-cell and spatial multi-omics. *Nat Rev Genet* **24**, 494-515 (2023). https://doi.org/10.1038/s41576-023-00580-2
45 Gao, Y., Chen, Y., Qiao, J., Huang, J. & Wen, L. DNA methylation protocol for analyzing cell-free DNA in the spent culture medium of human preimplantation embryos. *STAR Protoc* **4**, 102247 (2023). https://doi.org/10.1016/j.xpro.2023.102247
46 Wang, H. D. *et al.* Detection of fetal epigenetic biomarkers through genome-wide DNA methylation study for non-invasive prenatal diagnosis. *Mol Med Rep* **15**, 3989-3998 (2017). https://doi.org/10.3892/mmr.2017.6506

47 Risnes, K. R. *et al.* Birthweight and mortality in adulthood: a systematic review and meta-analysis. *Int J Epidemiol* **40**, 647-661 (2011). https://doi.org/10.1093/ije/dyq267
48 Passi, A. *et al.* Genome-Scale Metabolic Modeling Enables In-Depth Understanding of Big Data. *Metabolites* **12** (2021). https://doi.org/10.3390/metabo12010014
49 Yu, L. *et al.* Blastocyst-like structures generated from human pluripotent stem cells. *Nature* **591**, 620-626 (2021). https://doi.org/10.1038/s41586-021-03356-y
50 Yanagida, A. *et al.* Naive stem cell blastocyst model captures human embryo lineage segregation. *Cell Stem Cell* **28**, 1016-1022.e1014 (2021). https://doi.org/10.1016/j.stem.2021.04.031
51 Kagawa, H. *et al.* Human blastoids model blastocyst development and implantation. *Nature* **601**, 600-605 (2022). https://doi.org/10.1038/s41586-021-04267-8
52 Sozen, B. *et al.* Reconstructing aspects of human embryogenesis with pluripotent stem cells. *Nat Commun* **12**, 5550 (2021). https://doi.org/10.1038/s41467-021-25853-4
53 Liu, X. *et al.* Modelling human blastocysts by reprogramming fibroblasts into iBlastoids. *Nature* **591**, 627-632 (2021). https://doi.org/10.1038/s41586-021-03372-y
54 Fan, Y. *et al.* Generation of human blastocyst-like structures from pluripotent stem cells. *Cell Discov* **7**, 81 (2021). https://doi.org/10.1038/s41421-021-00316-8
55 Ferraz, M. A. M. M. *et al.* An oviduct-on-a-chip provides an enhanced in vitro environment for zygote genome reprogramming. *Nat Commun* **9**, 4934 (2018). https://doi.org/10.1038/s41467-018-07119-8
56 Jiang, V. S. & Bormann, C. L. Artificial intelligence in the in vitro fertilization laboratory: a review of advancements over the last decade. *Fertil Steril* **120**, 17-23 (2023). https://doi.org/10.1016/j.fertnstert.2023.05.149
57 Alteri, A. *et al.* Obstetric, neonatal, and child health outcomes following embryo biopsy for preimplantation genetic testing. *Hum Reprod Update* **29**, 291-306 (2023). https://doi.org/10.1093/humupd/dmad001
58 Brouillet, S., Martinez, G., Coutton, C. & Hamamah, S. Is cell-free DNA in spent embryo culture medium an alternative to embryo biopsy for preimplantation genetic testing? A systematic review. *Reprod Biomed Online* **40**, 779-796 (2020). https://doi.org/10.1016/j.rbmo.2020.02.002
59 Gleicher, N., Barad, D. H., Patrizio, P. & Orvieto, R. We have reached a dead end for preimplantation genetic testing for aneuploidy. *Hum Reprod* **37**, 2730-2734 (2022). https://doi.org/10.1093/humrep/deac052
60 Simopoulou, M. *et al.* PGT-A: who and when? A systematic review and network meta-analysis of RCTs. *J Assist Reprod Genet* **38**, 1939-1957 (2021). https://doi.org/10.1007/s10815-021-02227-9
61 Munné, S. *et al.* Preimplantation genetic testing for aneuploidy versus morphology as selection criteria for single frozen-thawed embryo transfer in good-prognosis patients: a multicenter randomized clinical trial. *Fertil Steril* **112**, 1071-1079.e1077 (2019). https://doi.org/10.1016/j.fertnstert.2019.07.1346
62 Yan, J. *et al.* Live Birth with or without Preimplantation Genetic Testing for Aneuploidy. *N Engl J Med* **385**, 2047-2058 (2021). https://doi.org/10.1056/NEJMoa2103613
63 Mastenbroek, S., de Wert, G. & Adashi, E. Y. The Imperative of Responsible Innovation in Reproductive Medicine. *N Engl J Med* **385**, 2096-2100 (2021). https://doi.org/10.1056/NEJMsb2101718
64 Orvieto, R. The reproducibility of trophectoderm biopsies - The chaos behind preimplantation genetic testing for aneuploidy. *Eur J Obstet Gynecol Reprod Biol* **254**, 57-58 (2020). https://doi.org/10.1016/j.ejogrb.2020.07.052
65 Victor, A. R. *et al.* Assessment of aneuploidy concordance between clinical trophectoderm biopsy and blastocyst. *Hum Reprod* **34**, 181-192 (2019). https://doi.org/10.1093/humrep/dey327
66 Sachdev, N. M., McCulloh, D. H., Kramer, Y., Keefe, D. & Grifo, J. A. The reproducibility of trophectoderm biopsies in euploid, aneuploid, and mosaic embryos using independently verified next-generation sequencing (NGS): a pilot study. *J Assist Reprod Genet* **37**, 559-571 (2020). https://doi.org/10.1007/s10815-020-01720-x

Appendices

Nederlandse samenvatting
Impact Statement
Acknowledgements
About the author
List of manuscripts

Nederlandse samenvatting

Genomische en epigenomische benaderingen voor kunstmatige voortplantingstechnieken (ART) bij mensen

In de 45 jaar sinds de geboorte van de allereerste 'reageerbuisbaby' in 1978 zijn kunstmatige voortplantingstechnieken (artifical reproductive technologies, ART in het Engels), zoals in-vitrofertilisatie (IVF), uitgegroeid tot speerpunt van de behandeling van onvruchtbaarheid. Jaar op jaar is er een stijging van het aantal ART-cycli. Wereldwijd worden er nu meer dan 3 miljoen behandelingen uitgevoerd. In landen als Nederland wordt tegenwoordig 2.5% van de baby's geboren door middel van ART. Deze cijfers weerspiegelen verschuivingen in maatschappelijke opvattingen over voortplanting, waarbij een toenemende leeftijd van ouders en een groter verlangen naar reproductieve autonomie (inclusief de wens om een gezond kind te krijgen) kernwaarden zijn.

Het vergroten van ons inzicht in de dynamiek van het genoom en het epigenoom, evenals hun interactie met de omgeving van het embryo tijdens de vroege embryogenese kan nieuwe inzichten opleveren. Deze inzichten kunnen op hun beurt de optimalisatie van ART-procedures en embryoselectie bevorderen. Het uiteindelijke doel is om de succespercentages van ART te verbeteren. Een praktische uitdaging is om de nieuwste omics (DNA, RNA, eiwit) methoden te integreren en te ontwikkelen voor toepassingen bij laboratorium- en bioinformatische en bioinformatische analyses van pre-implantatie genetische testen (PGT). Dit vergemakkelijkt het karakteriseren van het embryonale genoom en waarborgt betrouwbare en gemakkelijke toegang tot PGT.

In **hoofdstukken 2 en 3** onderzoeken we de invloed van het gebruik van verschillende ART-kweekmedia op het methyloom van de resulterende kinderen (neonaten en 9-jarigen). Klinisch onderzoek heeft aangetoond dat het gebruik van de vier kweekmedia in kwestie zowel de uitkomsten van de ART-behandeling als de groei van de daaruit voortvloeiende kinderen beïnvloedde. Het onderliggende mechanisme van dit verband was nog niet vastgesteld. De twee onderzoeken die in dit proefschrift worden gepresenteerd, hebben geen verschillen in de hoeveelheid DNA-methylatie gevonden in de kinderen uit de respectievelijke kweekmediumgroepen. In beide onderzoeken werden echter wel verschillen in variantie van de DNA-methylatie waargenomen. De betekenis van verschillen in variantie van de DNA-methylatie moet nog worden bepaald, maar het zou kunnen wijzen op selectiedruk uit de omgeving of prenatale blootstelling die een subgroep van de onderzoeksgroep ervaart. Omdat deze studies geen licht werpen op de moleculaire mechanismen die verantwoordelijk zijn voor de groeiverschillen die worden waargenomen bij de ART-kinderen die zijn verwerkt na IVF met verschillende kweekmedia, zouden toekomstige onderzoeken kunnen overwegen om het methyloom op een eerder tijdstip te onderzoeken, bijvoorbeeld tijdens de in vitro pre-implantatie ontwikkeling van het embryo. Daarbij kan ook worden gekeken

naar andere epigenetische kenmerken, zoals histon-modificaties.

In **hoofdstukken 4 en 5** wordt de implementatie en validatie van verbeteringen aan de huidige PGT methoden uiteengezet. Deze genetische testen, uitgevoerd op embryobiopsie-materiaal verzameld tijdens een IVF cyclus, zijn essentieel voor de selectie van een embryo zonder ernstige genetische afwijkingen voor terugplaatsing. **Hoofdstuk 4** belicht de ontwikkeling van een innovatief monstervolgsysteem dat unieke barcode-oligonucleotiden gebruikt. Deze oligonucleotiden, samen met gangbare genotyping-by-sequencing (GBS) protocollen, worden aan elk monster toegevoegd bij aanvang van de verwerking in het laboratorium. De oligonucleotiden kunnen worden getraceerd en garanderen daarmee de zuiverheid van sequentiegegevens en voorkomen monsterverwisselingen. We hebben aangetoond dat het monstervolgsysteem veilig kan worden geïmplementeerd om de afhankelijkheid van het 4-ogenprincipe (er kijkt altijd iemand mee bij het werk als controleur) te verminderen en om verkeerde diagnosen gerelateerd aan monsterverwisseling of monstercontaminatie te voorkomen, terwijl de kwaliteit van de gegeneerde diagnostische gegevens behouden blijft. In **hoofdstuk 5** wordt de PGT methode gebaseerd op Whole Genome Sequencing (WGS) geïntroduceerd. Deze methode, onderscheidt zich door zijn vermogen om meer gegevens van hogere kwaliteit te genereren, wat leidt tot een verhoogde diagnostische nauwkeurigheid. In tegenstelling tot eerdere methoden, biedt WGS-PGT een veelzijdige en generieke benadering. Het is geschikt voor alle bestaande vormen van PGT: (i) PGT voor monogene aandoeningen, (ii) PGT voor structurele aandoeningen, en (iii) PGT voor aneuploïdeën (met oorsprong), (iv) daarnaast is deze methode ook toepasbaar voor PGT voor paren met een risico op een mitochondriale ziekte.

In **hoofdstuk 6** wordt een diepgaande karakterisering van het chromosomale landschap van vroege miskramen gepresenteerd. Dit werd gedaan door een bioinformatica-methode (genoombrede haplarithmisis) toe te passen op vlokkenweefels en op extra-embryonale mesodermweefsels afkomstig van miskramen. Hiermee werd inzicht verkregen in de chromosomale samenstelling van de weefsels die respectievelijk verwant zijn aan de placenta en aan de foetus. Deze geavanceerde karakterisering toonde aan dat aneuploïdieën vaker voorkomen in weefsel van miskramen dan dat voorheen werd gedacht. Dit heeft gevolgen voor de klinische behadeling van zwangerschapsverlies, evenals de interpretatie van PGT-resultaten waar deze aneuploïdieën ook kunnen worden gedetecteerd.

In **hoofdstuk 7** worden de beschikbare methoden voor niet-invasieve, vloeibare biopsieën ("liquid biopsy" in het Engels), gebaseerde diagnostiek besproken evenals de huidige toepassingen in de reproductieve geneeskunde. Het artikel bespreekt hoe de huidige methodologische beperkingen kunnen worden overwonnen en hoe deze methoden in de toekomst kunnen worden benut voor pre-implantatie en prenatale genetische testen.

Impact Statement

Infertility is an important global health issue that one in six people will experience at some point in their lives indiscriminately of their income-status or geographic location[1]. Nonetheless, our understanding of the underlying pathophysiology remains primitive and for 30% of couples presenting with infertility no cause is identified[2]. Even when a cause is identified, very few evidence-based disease-specific treatments are available[3] and therefore assisted reproductive technology (ART) procedures, such as *in vitro* fertilisation (IVF) and intracytoplasmic sperm injection (ICSI), persist as the mainstay of fertility treatment. Access to ART varies widely from country to country and often poses a significant financial burden for couples who are obligated to shoulder treatment cost themselves[4,5]. Additionally, the limited availability of ART treatments can, in part, be attributed to their relatively low success rate, which has plateaued at approximately 30% per embryo transferred[6]. In turn, many couples face multiple rounds of treatment that make ART both a time consuming and resource intensive endeavour. As such, innovations that improve the success rates or reduce the complexity or cost of ART procedures are urgently needed.

The first part of this thesis focused on the *in vitro* embryo culture environment (ART culture media), not only as an avenue to improve ART success rates, but also as a potential strategy to ameliorate the increased perinatal and childhood cardiometabolic morbidity seen in children conceived through ART[7]. We focused specifically on the methylome of neonates and children born after embryo culture in different culture media as a potential mechanism underlying their phenotypic differences because periconception environmental factors are thought to modulate the epigenome with potential implications for future disease development[8]. Reassuringly, we did not find large methylation differences between children conceived after embryo culture in the media that we studied. This suggests that the culture media either did not differentially module the methylome, or if they did that the differences did not persist until the studied time points and as such, we would not expect differences in the occurrence of DNA methylation-mediated disease in these individuals. Importantly, we also excluded DNA methylation at imprinting regions. This is of relevance, as a marginally increased rate of imprinting disorders is observed in ART offspring compared to their naturally conceived counterparts[9]. Our studies imply that the culture media we investigated would not differentially affect the incidence of imprinting disorders.

Next, we focused on innovations in preimplantation genetic testing (PGT). Although PGT was initially developed to allow couples with heritable genetic disorders to prevent these from being passed to their offspring, it has since attracted substantial interest as a tool for embryo ranking and selection with the aim of improving ART success rates[6].

Firstly, we described the development and validation of barcoded oligonucleotides for sample tracking as part of an embryo tracking system (ETS). Implementation of the ETS positively impacted the laboratory workflow by eliminating the need for the four-eyes principle, previously employed during error-prone steps, thereby directly reducing the time requirement of highly skilled laboratory technicians, and in turn the associated labour cost. Furthermore, the ETS could identify switched or mixed samples and therefore prevent associated misdiagnoses that could have devastating consequences for patients undergoing PGT with the aim of preventing disease in their offspring. Secondly, we described a whole-genome sequencing (WGS)-based approach for PGT. Compared to our prior reduced-representation genotyping by sequencing protocol, WGS library preparation could be carried out in less than half of the time and yielded vastly more relevant data. With this approach a greater number of embryos surpassed the minimum diagnostic threshold for PGT for monogenic disorders (PGT-M), especially in cases with challenging indications, such as consanguineous couples, couples with indications in difficult to sequence genomic locations and couples with multiple indications. The improved diagnostic capacity of this approach will increase the number of unaffected embryos available to couples and therefore reduce the number of ovarian stimulation and ovum pick-up procedures that are needed. Not only does this save time and resources, but it also reduces the number of times patients are exposed to procedures that carry a risk of complications. Furthermore, we demonstrated that the WGS-PGT approach could be applied (simultaneously) for all forms of PGT, including PGT for (multiple) monogenic disorders, structural re-arrangements, (meiotic) aneuploidies (PGT-A) and mitochondrial disorders. Developing PGT protocols with robust but simplified laboratory and analytical protocols will allow more centres to adopt these approaches and move away from commonly used time-consuming patient specific PGT protocols. Ultimately, universally applicable PGT methods will reduce the processing time per couple, therefore reducing waiting lists and increasing the availability of PGT without the need for more highly specialised clinical and laboratory staff.

In this thesis we have also looked at the genomic landscape of (recurrent) pregnancy loss. Furthering our understanding of the genetic factors underlying pregnancy loss is useful to guide which patients would likely benefit from IVF/ICSI and whether PGT, for aneuploidies or other genetic indications, should be conducted as part of their treatment. Additionally, gaining insights into the genome dynamics of early *in vivo* human development is beneficial to interpret the significance of PGT-A results and may contribute to more accurate embryo ranking/selection practises in the future.

Finally, we have explored the potential of liquid biopsy in reproductive medicine. We highlighted the potential of liquid biopsy for PGT where a non-invasive test analysing cell-free DNA in spent embryo culture medium could supersede embryo biopsies.

Replacing invasive embryo biopsies, that are potentially detrimental to the ongoing development of an embryo, could increase the number of well-developed embryos that are available to couples for transfer. Furthermore, collection of spent culture medium can be achieved without specialised equipment and with minimal training so it could be easily implemented in many IVF clinics. We also consider how non-invasive prenatal testing (NIPT), which is currently used to identify common chromosomal abnormalities, could be expanded to detect other genetic abnormalities thereby eliminating the need for invasive pre-natal diagnostic testing and the associated risk of miscarriage. Additionally, NIPT samples could be analysed for biomarkers of pregnancy-related conditions such as pre-eclampsia that benefit greatly from timely diagnosis, surveillance, and management and could therefore be implemented to reduce the morbidity and mortality associated with such conditions.

References

1 Infertility prevalence estimates, 1990–2021. Geneva: World Health Organization; 2023. Licence: CC BY-NC-SA 3.0 IGO.

2 Abdallah, K. S., Hunt, S., Abdullah, S. A., Mol, B. W. J. & Youssef, M. A. How and Why to Define Unexplained Infertility? *Semin Reprod Med* **38**, 55-60 (2020). https://doi.org:10.1055/s-0040-1718709

3 The Unexplained Infertility guideline group, Romualdi D, Ata B, Bhattacharya S, Bosch E, Costello M, Gersak K, Homburg R, Le Clef N, Mincheva M et al. Evidence-based guideline: Unexplained Infertility. 2023. ESHRE, https://www.eshre.eu/guideline/UI.

4 Njagi, P. *et al.* Financial costs of assisted reproductive technology for patients in low- and middle-income countries: a systematic review. *Hum Reprod Open* **2023**, hoad007 (2023). https://doi.org:10.1093/hropen/hoad007

5 Messinis, I. E., Messini, C. I., Daponte, A., Garas, A. & Mahmood, T. The current situation of infertility services provision in Europe. *Eur J Obstet Gynecol Reprod Biol* (2016). https://doi.org:10.1016/j.ejogrb.2016.10.004

6 Wyns, C. *et al.* ART in Europe, 2018: results generated from European registries by ESHRE. *Hum Reprod Open* **2022**, hoac022 (2022). https://doi.org:10.1093/hropen/hoac022

7 Bernsten, S. *et al.* The health of children conceived by ART: 'the chicken or the egg?'. *Hum Reprod update* **25**, 137-158 (2019).

8 Wadhwa, P. D., Buss, C., Entringer, S. & Swanson, J. M. Developmental origins of health and disease: brief history of the approach and current focus on epigenetic mechanisms. *Semin Reprod Med* **27**, 358-368 (2009). https://doi.org:10.1055/s-0029-1237424

9 DeAngelis, A. M., Martini, A. E. & Owen, C. M. Assisted Reproductive Technology and Epigenetics. *Semin Reprod Med* **36**, 221-232 (2018). https://doi.org:10.1055/s-0038-1675780

Acknowledgements

First and foremost, I would like to thank my supervisors **Han, Masoud, Aafke** and **Marij** for the privilege of working on a project that aligns so closely with my passions. I am very grateful that even in the difficult circumstances posed by the covid pandemic, you found a way for me to be able to continue working on projects that piqued my interest. The valuable skills I learned under your supervision and guidance are ones I cherish and am excited to apply in the next chapters of my professional journey.

Throughout my PhD journey I have had the privilege of working a myriad of inspirational people whose contributions have been invaluable to the completion of this thesis. I would like to express my gratitude to:

My paranymphs **Darina** and **Anouk** – thank you for your enthusiastic collaboration on our joint ventures. Your scientific curiosity and probing questions have often led me to gain a better understanding of my own work and have also broadened my awareness of the field. And thank you for always humouring my eclectic suggestions for data visualisation!

Ping, Alvin, **Marjan**, **Maryn**, **Rick** and all the interns that have been a part of the CGM team – thank you for many insightful scientific discussions.

Everybody who has helped me with lab work – your unwavering willingness to assist and mentor enabled me to work on a multitude of diverse projects and to acquire numerous new skills. A special note of thanks to **Wanwisa** - thank you for lighting up the windowless lab with your positivity on long days of repetitive pipetting!

The **PGT group** - thank you for making me feel at home at clinical genetics from my very first day. I found your unlimited enthusiasm for work (parties) motivating and uplifting and I am deeply grateful for the time you devoted sharing your single-cell expertise with me.

The **bioinformaticians** at clinical genetics – I was truly inspired by the work that you do. Thank you for always being there to help me troubleshoot.

All **co-authors** on my publications – thank you for your insightful suggestions that have improved my research output.

The **participants** of the studies included in this thesis without whom this work would not have been possible - thank you for your selfless contribution to science.

Equally important to this PhD journey has been the support of my friends and family who have been there for me every step of the way.

To the **coffee club** – thank you for ensuring I am equipped with a “dad joke” for every scenario and enough food recommendations for a lifetime of travel!

Jeroen – thank you for always making sure my blood sugar levels were sufficiently topped up!
To the **moeflon crew** – thank you for the many rejuvenating mini-getaways from PhD life.

Balazs and **Petra** – thank you for the many culinary adventures together.

Mama, Papa, Elissa und Thomas - vergelt’s Gott, für aia Geduld und dass iaz eich oiwei Zeit gnumma habt’s, um meine Sorg’n anzuhör’n.

And last but by no means least, to **David** – thank you! (for everything)

About the author

Rebekka Koeck was born 8th of February 1993 in Karlsruhe, Germany. After completing her A-levels at Barton Peveril College (Eastleigh, England) in 2011, she went on to study Medicine at Brighton and Sussex Medical School (England). She undertook an intercalated master's degree in medical science research with a focus on maternal and fetal health at the University of Manchester (England). For the thesis of this research Master, she examined the impact of hyperosmolar stress on mouse embryo implantation using an *in vitro* model. After obtaining her master's degree with a distinction grade in 2015, she returned to medical school where she undertook an independent research project investigating microRNA expression in differentiating CG4 oligodendrocyte cells in response to erythropoietin (EPO) and leukaemia inhibitory factor (LIF). She completed medical school in 2017, obtaining several subject distinctions in her final year, and went on to work as a trainee doctor in Milton Keynes and Oxford (England) where she completed rotations in geriatrics, respiratory medicine, urology, emergency surgery, orthopaedics, and general practise. In 2019, she started her PhD project at the department of Genetics and Cell biology at Maastricht University (The Netherlands). During her project she studied genome and epigenome dynamics during human preimplantation embryo development in the context of assisted reproduction, under the supervision of Prof. Han Brunner, Dr. Masoud Zamani Esteki, Dr. Aafke van Montfoort and Dr. Marij Gielen. In addition, she gave several oral presentations at national and international conferences for which she was awarded two prizes.

List of manuscripts

Published

Koeck RM, Busato F, Tost J, Zandstra H, Remy S, et al. At age 9, the methylome of assisted reproductive technology children that underwent embryo culture in different media is not significantly different on a genome-wide scale. Hum Reprod. 2022 Oct 31. https://doi.org/10.1093/humrep/deac213

van Dijk W, Derks K, Drüsedau M, Meekels J, Koeck R, et al. Embryo tracking system for high-throughput sequencing-based preimplantation genetic testing. Hum Reprod. 2022 Oct 31. https://doi.org/10.1093/humrep/deac208

Koeck RM, Busato F, Tost J, Consten D, van Echten-Arends J, et al. Methylome-wide analysis of IVF neonates that underwent embryo culture in different media revealed no significant differences. NPJ Genom Med. 2022 Jun 29. https://doi.org/10.1038/s41525-022-00310-3

Schobers G*, Koeck R*, Pellaers D, Stevens SJC, Macville MVE, et al. Liquid biopsy: state of reproductive medicine and beyond. Hum Reprod. 2021 Oct 18. https://doi.org/10.1093/humrep/deab206

***Joint first authors**

Ruane PT, Koeck R, Berneau SC, Kimber SJ, Westwood M, et al. Osmotic stress induces JNK-dependent embryo invasion in a model of implantation. Reproduction. 2018 Aug 21. https://doi.org/10.1530/REP-18-0154

Ruane PT, Berneau SC, Koeck R, Watts J, Kimber SJ, et al. Apposition to endometrial epithelial cells activates mouse blastocysts for implantation. MHR: Basic science of reproductive medicine. 2017 Sep 01. https://doi.org/10.1093/molehr/gax043

In preparation / under review

Essers R#, Lebedev IN#, Kurg A#, Fonova EA, Stevens SJC, Koeck RM, von Rango U, Brandts L, Panagiotis Deligiannis S, Nikitina TV, Sazhenova EA, Tolmacheva EN, Kashevarova AA, Fedotov DA, Demeneva VV, Zhigalina DI, Drozdov GV, Al-Nasiry S, Macville MVE, van den Wijngaard A, Dreesen J, Paulussen A, Hoischen A, Brunner HG, Salumets A*, Zamani Esteki M*. The nature and prevalence of chromosomal alterations in first-trimester spontaneous pregnancy loss. *(Under review at Nature Medicine)*

 # Joint first authors, * Joint last authors

Janssen A*, Koeck RM*, Essers R*, van Dijk W, Drüsedau M, Meekels J, Yaldiz B, van der Vorst M, de Koning B, Hellebrekers D, Stevens S, Heijligers M, de Munnik S, van den Wijngaard A, Coonen E, Dreesen J, de Die-Smulders C, Brunner H, Paulussen A, Zamani Esteki M. Clinical whole-genome sequencing-based haplarithmisis enables simple, scalable, and universal preimplantation genetic testing (PGT). *(In preparation)*

*** Joint first authors**